Optimization of thermodynamic systems

Von Der Fakultät für Physik und Geowissenschaften

der Universität Leipzig

genehmigte

D I S S E R T A T I O N

zur Erlangung des akademischen Grades

doctor rerum naturalium

Dr. rer. nat.

vorgelegt

von M.Sc. Zhuolin Ye

geboren am Juni 29, 1994 in Stadt Yichun, China

Gutachter:

Prof. Dr. Klaus Kroy, Universität Leipzig

Prof. Dr. Antonio Calvo Hernández, Universität Salamanca

Tag der Verleihung Dezember 11, 2023

Declaration of Independence

I hereby formally declare that I have written the submitted thesis independently. I did not use it any outside support except for the quoted literature and other sources mentioned in the thesis. I clearly marked and separately listed all of the literature and all of the other sources which I employed when producing this academic work, either literally or in content. Apart from the persons named in the acknowledgments and under author contributions, no other persons were involved in the intellectual production of the present work. Benefits in kind were not awarded to third parties, either directly or indirectly. This thesis has not been handed in or published before in the same or similar form.

Leipzig, January 12, 2024

Zhuolin Ye

Zusammenfassung der Dissertation

Titel: Optimierung thermodynamischer Systeme

Author: M.Sc. Zhuolin Ye, Institut für Theoretische Physik, Universität Leipzig

Supervisor:
Prof. Dr. Klaus Kroy, Institut für Theoretische Physik, Universität Leipzig
Dr. Viktor Holubec, Abteilung für Makromolekulare Physik, Karls-Universität

---

Diese Dissertation fasst die von mir während meines Promotionsstudiums an der Universität Leipzig verfassten Veröffentlichungen zum Thema Optimierung thermodynamischer Systeme zusammen. Dabei konzentriere ich mich auf drei Optimierungsperspektiven: maximale Effizienz, maximale Leistung und maximale Effizienz bei gegebener Leistung. Wir betrachten zwei derzeit intensiv untersuchte Modelle der Finite-Zeit-Thermodynamik, nämlich Modelle mit geringer Dissipation und Brown'sche Systeme. Das Modell mit geringer Dissipation wird verwendet, um allgemeine Grenzen für die Leistungsfähigkeit realer Maschinen abzuleiten, während uns Brown'sche Systeme helfen, die praktischen Grenzen und Eigenschaften kleiner Systeme besser zu verstehen. Zunächst leiten wir die maximale Effizienz bei gegebener Leistung für verschiedene Aufbauten mit geringer Dissipation ab, wobei wir uns besonders auf das Verhalten in der Nähe der maximalen Leistung konzentrieren. Dies hilft uns festzustellen, ob es vorteilhafter ist, das System bei maximaler Leistung, nahe maximaler Leistung oder in einem anderen Regime zu betreiben. Anschließend gehen wir zur Gestaltung von Protokollen für maximale Effizienz und maximale Leistung bei Brown'schen Systemen unter verschiedenen Randbedingungen über. Insbesondere präsentieren wir eine geometrische Methode, die maximal-effiziente und maximal-leistungsstarke Protokolle liefert, die für Systeme mit periodisch skaliertem Energiespektrum und sonst beliebiger Dynamik gültig sind, wenn die Beschränkungen für die Steuerungsparameter experimentell motiviert sind. Jedes Kapitel enthält eine kurze informelle Einführung in das Thema sowie einen Ausblick, der die Richtung unserer zukünftigen Forschung aufzeigt.

Summary of the dissertation

Title: Optimization of thermodynamic systems

Author: M.Sc. Zhuolin Ye, Institute for Theoretical Physics, University of Leipzig

Supervisor:
Prof. Dr. Klaus Kroy, Institute for Theoretical Physics, University of Leipzig
Dr. Viktor Holubec, Department of Macromolecular Physics, Charles University

---

This thesis compiles the publications I coauthored during my doctoral studies at University of Leipzig on the subject of optimizing thermodynamic systems, focusing on three optimization perspectives: maximum efficiency, maximum power, and maximum efficiency at given power. We considered two currently intensely studied models in finite-time thermodynamics, i.e., low-dissipation models and Brownian systems. The low-dissipation model is used to derive general bounds on the performance of real-world machines, while Brownian systems allow us to better understand the practical limits and features of small systems. First, we derived maximum efficiency at given power for various low-dissipation setups, with a particular focus on the behavior close to maximum power, which helps us to determine whether it is more beneficial to operate the system at maximum power, near maximum power or in a different regime. Then, we move to the design of maximum-efficiency and maximum-power protocols for Brownian systems under different boundary conditions. Particularly, when the constraints on control parameters are experimentally motivated, we presented a geometric method yielding maximum-efficiency and maximum-power protocols valid for systems with periodically scaled energy spectrum and otherwise arbitrary dynamics. Each chapter contains a short informal introduction to the matter as well as an outlook, pointing out the direction for our research in the future.

Contents

1 Introduction

Thermodynamic systems, characterized as collections of matter and energy undergoing processes that are governed by the laws of thermodynamics, play a fundamental role in a wide range of scientific and engineering disciplines [1, 2]. They find applications in diverse areas such as power generation [3, 4], refrigeration [5, 6], heat transfer [7, 8], etc. In recent years, optimization of thermodynamic systems has gained particular significance in light of global warming. Engineers and scientists persistently enhance system design, operation strategies, and control techniques to attain optimal performance under the constraints dictated by the laws of thermodynamics and current technology [9–11].

The second law theoretical maximum (Carnot) efficiency of thermodynamic systems can only be achieved in the quasistatic limit, where all processes are executed slowly and hence the power output is negligible compared to the maximum achievable power [12]. Real-world thermodynamic systems therefore usually operate at maximum power rather than at maximum efficiency with very limited power. The concept of maximizing power under finite-time conditions, known as efficiency at maximum power, was initially pioneered by Yvon [13], Novikov [14], Chambadal [15], and later popularized by Curzon and Ahlborn [16]. Through this optimization strategy, researchers have made significant progress in developing thermodynamic models and analyzing their performance, mainly including endoreversible [16, 17], low-dissipation [5, 18], linear irreversible [19, 20], minimally nonlinear irreversible [21–23], Brownian [24, 25], and quantum [26, 27] models.

Since it is impossible to optimize efficiency and power simultaneously, further research has focused on exploring the trade-offs between these two factors using various optimization criteria [28–30]. These include the χ criterion, which equals the product of efficiency and power and serves as a direct compromise [30, 31], the Ω criterion, which aims to balance energy benefits and losses [32, 33], and the ecological criterion, which takes into account the trade-off between power and the product of entropy production and cold reservoir temperature [34, 35]. However,

these figures of merit do not always match the engineering demand. For example, in many applications such as portable electronics or electric vehicles, power delivery needs to be stable (fixed). The optimization task of practical interest is thus to find the maximum efficiency at fixed power, revealing under which conditions this power delivery is cheapest. The research in this field can be traced back to the 1980s when Chen and Yan [36] conducted studies on endoreversible heat engines operating between two heat sources at temperatures T_h and $T_c(< T_h)$. They derived the optimal relation between efficiency and power (η and P):

$$\frac{P}{P^*} = \frac{\eta(\eta_C - \eta)}{(1 - \eta)(1 - \sqrt{1 - \eta_C})^2}, \tag{1}$$

where $\eta_C = 1 - T_c/T_h$ is Carnot efficiency and P^* is maximum power (thus $0 \leq \eta \leq \eta_C$ and $0 \leq P \leq P^*$). It implies the maximum efficiency at given power (and, equivalently, maximum power at given efficiency). Obviously, the maximum efficiency, $\eta = \eta_C$, corresponds to the reversible limit for vanishing power ($P = 0$). The efficiency at maximum power, $\eta = \eta_{CA} = 1 - \sqrt{1 - \eta_C}$, is the famous Curzon-Ahlborn efficiency [16]. This indicates that maximum efficiency at given power can be considered as a generalization of the results derived previously for the χ, Ω, and ecological criteria [30–35].

In our research, we consider two currently intensely studied models in finite-time thermodynamics, namely low-dissipation [18] and Brownian systems [24], focusing on the above three optimization perspectives (maximum efficiency, maximum power, and maximum efficiency at given power). Low-dissipation models are generally valid for slowly driven systems in contact with an equilibrium heat bath [37, 38], where the model coefficients can be calculated from the dynamical equations. The currently renewed interest in Brownian systems is mainly driven by the advancements in experimental techniques, such as optical tweezers [39], which allow a previously unprecedented control over microscopic systems. In particular, they have been recently employed to realize micrometer-sized heat engines [40, 41]. The performance of these small devices is strongly influenced by thermal fluctuations and its study gave birth to the field of stochastic thermody-

namics [42]. Interestingly, Brownian heat engines turn out to be a microscopic example of low-dissipation heat engines under certain conditions [24].

The results presented in chapters 2 and 3 are based on the publications [5–7, 9, 43] I coauthored during my doctoral studies at University of Leipzig. Specifically, in chapter 2, we derived maximum efficiency at given power for low-dissipation refrigerators [5] and heat pumps [7] as well as absorption refrigerators [6] consisting of simultaneously operating low-dissipation heat engine and refrigerator. The derived expressions imply bounds on maximum efficiency at given power for the corresponding devices, and tell us whether the machine should operate at maximum power or if it would be more beneficial to operate it in a different regime to achieve a significant increase in efficiency. Maximum efficiency at given power has been investigated for various heat engines, such as endoreversible [44], low-dissipation [45–47], quantum thermoelectric [48, 49], underdamped stochastic [25], linear irreversible [50], and minimally nonlinear irreversible systems [51]. To the best of our knowledge, however, the results for refrigerators and heat pumps were only known for endoreversible and minimally nonlinear irreversible models [44, 51, 52]. This research completed the collection of results for maximum efficiency at given power for low-dissipation models.

In chapter 3, we focus on the design of optimal protocols for Brownian systems operating at maximum efficiency or maximum power [9, 43]. Such optimization tasks, i.e., seeking the optimal time variation of control parameters, such as magnetic or electric fields, to attain a desired performance with minimum dissipation to the surroundings [24, 25, 53, 54], range from the design of a thermodynamic cycle for heat devices [42, 55] to the erasure of information in information processing devices [56–58]. In general, finding optimal finite-time protocols requires a functional optimization over all possible paths in the space of the control parameters, making it complicated and often challenging even for numerical analysis [53, 59]. This research allows us to better understand the practical limits and features of small systems. Both chapters 2 and 3 include an outlook. Finally, we conclude in chapter 4.

2 Maximum efficiency of low-dissipation systems at given power

The starting point of a low-dissipation model [18] is a Carnot engine operating reversibly. While in contact with the hot bath at temperature T_h during hot isotherm, the system accepts heat Q_h from the hot bath, resulting in the total entropy change $\Delta S_{tot,h} = -\frac{Q_h}{T_h} + \Delta S = 0$, where ΔS is the system entropy change. When coupled to the cold bath at temperature T_c during cold isotherm, the system releases heat Q_c to the cold bath, leading to the total entropy change $\Delta S_{tot,c} = \frac{Q_c}{T_c} - \Delta S = 0$. From these two equations the Carnot efficiency $\eta = 1 - \frac{Q_c}{Q_h} = 1 - \frac{T_c}{T_h}$ is recovered. Then, for finite-time Carnot cycles in the low-dissipation regime, one might expect that

$$\Delta S_{tot,i} = \frac{\Sigma_i}{t_i} + \mathcal{O}\left(\frac{1}{t_i^2}\right), \quad i = h, c, \tag{2}$$

where t_i are durations of the isotherms and Σ_i are the corresponding coefficients. As a result, the transfered heats are given by [18]

$$Q_h = T_h\left(\Delta S - \frac{\Sigma_h}{t_h}\right), \tag{3a}$$

$$Q_c = T_c\left(\Delta S + \frac{\Sigma_c}{t_c}\right). \tag{3b}$$

We stress that the low-dissipation assumption (2) is generally fulfilled in practice when the system is driven slowly [37, 38, 40, 41]. It can be described in one sentence: the total entropy production in the universe during any isotherm is inversely proportional to its duration. The low-dissipation model described by Eqs. (3a) and (3b) thus contains all models that consider first-order expansion in the velocity of the driving around a reversible process. Such systems were thoroughly studied theoretically [7, 18, 29, 33, 60–63], and the predictions are in accord with experiments [37, 40]. Additionally, low-dissipation models exactly describe some specific scenarios. Examples are Brownian heat engines under optimal time-dependent driving [24], two-stage linear irreversible heat engines working be-

tween finite-sized heat reservoirs [64], and two-state quantum systems coupled to a heat bath of bosonic oscillators [65]. Interestingly, the Brownian heat engine [24] can be arbitrarily far from equilibrium. At this point, one may notice that in the low-dissipation model we do not need to specify the system dynamics. This information is contained in the coefficients Σ_i, which tell us how the dissipation increases as the system moves away from equilibrium. For example, Σ_i is inversely proportional to the particle mobility in overdamped Brownian dynamics [5, 24] (see more details in chapter 3). We also do not need to assume that the difference between T_h and T_c is small, so all results associated with the low-dissipation model remain valid beyond the linear response regime.

One of the most influential theoretical result derived using the low-dissipation model is the efficiency at maximum power of Carnot-type low-dissipation heat engines [18]. It was obtained by utilizing Eqs. (3a) and (3b) and optimizing the output power $P = (Q_h - Q_c)/(t_h + t_c)$ with respect to the durations t_h and t_c. For symmetric dissipation ($\Sigma_h = \Sigma_c$), the resulting efficiency is the famous Curzon-Ahlborn efficiency [16]. This means that Curzon-Ahlborn efficiency is a general property of Carnot heat engines operating under the conditions of low and symmetric dissipation. Note that the durations of the adiabats have been neglected during the optimization, since they only reduce the power but do not affect the efficiency $\eta = 1 - Q_c/Q_h$. This assumption of infinitely fast adiabatic processes is frequently utilized in theory and effectively, infinitely fast adiabatic processes can be realized in experiments [41]. We use this assumption throughout this dissertation.

Low-dissipation models are equivalent to minimally nonlinear irreversible models under the tight-coupling condition [5, 21–23, 46]. However, it is an open question whether a similar equivalence exists between low-dissipation models and endoreversible models, beyond the linear response regime [66, 67]. The minimally nonlinear irreversible model generalizes the standard linear irreversible model [19], by adding a nonlinear term describing the dissipation due to the internal friction (or resistivity for thermoelectric machines [68]) [21–23]. The endoreversible models are usually phenomenological, which assume that the working medium operate

reversibly and the irreversibility is solely due to the finite-time heat transfer between the reservoirs and the working medium [16, 17].

We focus on the derivation of maximum efficiency at given power for various low-dissipation models and analyzing their behavior in proximity to or far from the maximum power. To this end, we define the relative deviation of power P from its maximal value P^* and the corresponding relative gain in efficiency [5, 6, 45, 50, 51, 69, 70]

$$\delta P = \frac{P - P^*}{P^*}, \quad \delta\eta = \frac{\eta_P - \eta_{P*}}{\eta_{P*}}, \tag{4}$$

where η_P (η_{P*}) is the corresponding efficiency at P (P^*) and thus $\delta P \in [-1, 0]$, which means that the actual power cannot surpass the maximum power. The definitions (4) usually simplify the resulting equations and allow us to obtain some explicit results. One of them is the scaling

$$\delta\eta \propto \sqrt{-\delta P} \tag{5}$$

for small value of δP, which implies a diverging slope of $\delta\eta$ at $\delta P = 0$. A system obeying the scaling (5) and working close to maximum power thus operates at considerably larger efficiency than the efficiency at maximum power η_{P*}. Consequently, it is more advantageous to operate such a system at power with slightly smaller power than the maximum power.

We note that both the diverging slope and the scaling (5) are direct consequences of the fact that the maximum power corresponds to a vanishing derivative of P with respect to the control parameter x [5, 45]. Indeed, if $\frac{\partial P}{\partial x}|_{x=x^*} = 0$, Taylor expansions of power and efficiency near x^* implies $P - P^* \approx \frac{(x-x^*)^2}{2} \frac{\partial^2 P}{\partial x^2}|_{x=x^*}$ and $\eta - \eta_{P*} \approx \frac{\partial \eta}{\partial x}|_{x=x^*}(x - x^*)$, leading to the relation (5).
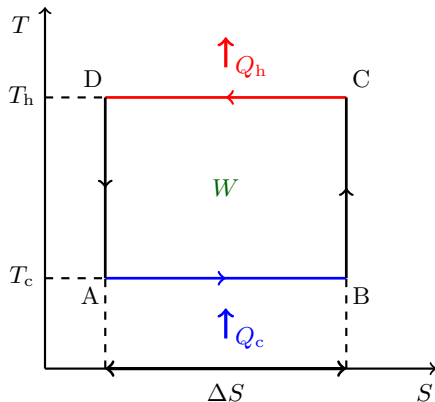
16

FIG. 1. Thermodynamic T-S (bath temperature-system entropy) diagram of the considered Carnot refrigeration cycle [5–7]. The fridge uses the input work W to extract heat Q_c from the cold bath at temperature T_c during the cold isotherm (AB, blue). The used work and the extracted heat are then dumped as heat $Q_h = Q_c + W$ into the hot bath at temperature T_h during the hot isotherm (CD, red). The input work equals the enclosed area, $Q_c = T_c \Delta S$, and $Q_h = T_h \Delta S$ only if the cycle is performed reversibly. Otherwise, the work is larger and the extracted heat smaller leading to a decreased efficiency (coefficient of performance) of the machine. The branches BC and DA (black) of the cycle are adiabats.

2.1 Interpretation of the publications

2.1.1 Low-dissipation refrigerators

Refrigerators are invaluable appliances that play a crucial role in modern-day living. Their usefulness and importance extend far beyond mere food preservation. Refrigerators keep our perishable items fresh, preventing spoilage and reducing waste. They enable us to store a wide range of food items, allowing for meal planning, convenience, and cost savings. Moreover, refrigerators promote healthier lifestyles by maintaining food safety standards, preventing bacterial growth, and preserving essential nutrients. They also facilitate the storage of medications, vaccines, and other temperature-sensitive items.

In our work [5], we considered a refrigerator, which operates along an inverse finite-time Carnot cycle consisting of two isotherms and two adiabats depicted in Fig. 1. In the low-dissipation regime, the heats exchanged by the system with the heat baths during the two isotherms are described by the revised form of Eqs. (3a)

and (3b),

$$Q_h = T_h \left(\Delta S + \frac{\Sigma_h}{t_h} \right), \tag{6a}$$

$$Q_c = T_c \left(\Delta S - \frac{\Sigma_c}{t_c} \right). \tag{6b}$$

For refrigerators, power and efficiency are called cooling power and coefficient of performance (COP). They are, respectively, defined as the heat extracted from the cold bath per cycle over the cycle duration $(t_h + t_c)$ and the extracted heat over the input work $(W = Q_h - Q_c)$:

$$P = \frac{Q_c}{t_h + t_c}, \quad \varepsilon = \frac{Q_c}{Q_h - Q_c}. \tag{7}$$

In [5], we first derived the efficiency at maximum power by optimizing P with respect to t_h and t_c, and showed that it exhibits a discontinuity at the maximally skewed irreversibility ratio $\Sigma \equiv \Sigma_h/\Sigma_c = 0$:

$$\varepsilon_-^* = 0 \quad \text{for} \quad \Sigma > 0, \tag{8a}$$

$$\varepsilon_+^* = \frac{\varepsilon_C}{2 + \varepsilon_C} \quad \text{for} \quad \Sigma = 0, \tag{8b}$$

where the Carnot COP $\varepsilon_C = T_c/(T_h - T_c)$. This discontinuity is caused by the fact that P in Eq. (7) is a monotonically decreasing function of t_h, so maximum power corresponds to the minimal allowed value of t_h, i.e., $t_h = 0$. This should be understood in the sense that the hot isotherm is much faster than the cold isotherm, $t_h \ll t_c$. Since Eqs. (8a) and (8b) are independent of Σ, they represent the lower and upper bounds on COP at maximum power of low-dissipation refrigerators. We explained why the discontinuity at $\Sigma = 0$ is not present in the optimization of power for minimally nonlinear irreversible models.

Then, we analytically derived the expression for maximum efficiency at given power, $\varepsilon^{opt} = \varepsilon^{opt}(\delta P, \Sigma, \varepsilon_C)$, by using the definitions (4). It yields the lower

$(\Sigma \to \infty)$ and upper $(\Sigma \to 0)$ bounds on the maximum COP at fixed power:

$$0 \leq \varepsilon^{opt} \leq \frac{\varepsilon_C(1 + \sqrt{-\delta P})}{2 + \varepsilon_C(1 - \sqrt{-\delta P})} \equiv \varepsilon_+^{opt}. \tag{9}$$

The upper bound ε_+^{opt} on ε^{opt} in Eq. (9) shows the relative gain in COP (4):

$$\frac{\varepsilon_+^{opt} - \varepsilon_+^*}{\varepsilon_+^*} = (1 + \varepsilon_+^*)\sqrt{-\delta P} + \mathcal{O}(\delta P), \tag{10}$$

which agrees with the scaling (5). For large irreversibility ratio Σ, this square root behavior is not valid any more and we found that the scaling reads $\propto -\delta P$. This is caused by the fact that maximum power does not correspond to a vanishing derivative of P with respect to t_h [see Eq. (8b) below]. The low-dissipation refrigerators thus exhibit different behavior close to maximum power from many models of heat engines [12, 25, 45, 48–51], where the scaling (5) holds for all parameter values. We concluded that it is beneficial to operate low-dissipation refrigerators with small Σ near maximum power, where the trade-off between power and efficiency is optimal. For large Σ , it is more advantageous to operate these machines at maximum power. Because the full expression for maximum efficiency at given power is cumbersome, we provided approximations of ε^{opt} valid for $\Sigma \to 0$ and $\Sigma \to \infty$ yielding the two different qualitative behaviors described above, and we discussed the range of validity of the approximations.

2.1.2   Low-dissipation heat pumps

Heat pumps are invaluable systems that play a crucial role in heating and cooling our environments efficiently and sustainably. They utilize the principles of thermodynamics to transfer heat from one place to another, allowing us to extract warmth from the surrounding air, ground, or water sources and deliver it where needed. With their ability to provide both heating and cooling functions, heat pumps offer year-round comfort and energy savings. By utilizing renewable energy sources, such as air or geothermal heat, they significantly reduce greenhouse gas

emissions and contribute to combating climate change. Moreover, heat pumps can be integrated with existing infrastructure, making them versatile and adaptable to various applications, including residential, commercial, and industrial settings.

In our work [7], we considered a heat pump, which operates along an inverse finite-time Carnot cycle consisting of two isotherms and two adiabats. The cycle diagram is thus the same as in Fig. 1, and the heats exchanged by the system with the heat baths during the two isotherms are still captured by Eqs. (6a) and (6b) when the heat pump can be described by the low-dissipation model. For heat pumps, power and efficiency are usually referred to as heating load and COP. They are defined as the heat transferred to the hot bath per cycle over the cycle duration $(t_h + t_c)$ and that over the input work $(W = Q_h - Q_c)$:

$$P = \frac{Q_h}{t_h + t_c}, \quad \epsilon = \frac{Q_h}{Q_h - Q_c}. \tag{11}$$

In [7], we first derived the efficiency at maximum power by optimizing P with respect to t_h and t_c, under the requirement that the device pumps heat from the cold bath to the hot one $(Q_h > Q_c > 0)$. This condition limits the allowed range of the system parameters such as the durations t_h and t_c. As a result, the maximum power diverges and the corresponding efficiency equals one (the smallest possible efficiency for heat pumps), in agreement with the results obtained using endoreversible thermodynamics [52, 71]. This regime is highly undesired, because the heat pump turns out to be a pure work-to-heat converter. Then, we analytically derived maximum efficiency at given power using Eqs. (6a) and (6b). The diverging maximum power $(P^* \to \infty)$ makes the definitions (4) inappropriate, so we instead defined the dimensionless power $\tilde{P} = \frac{\Sigma_h}{(T_h \Delta S)^2} P$. The resulting maximum efficiency at given power, $\epsilon^{opt} = \epsilon^{opt}(\tilde{P}, \Sigma, \epsilon_C)$, depends on $\tilde{P}$, Σ, and the Carnot COP for the heat pump $\epsilon_C = T_h/(T_h - T_c)$. It yields the lower $(\Sigma \to 0)$ and upper $(\Sigma \to \infty)$ bounds on the maximum efficiency:

$$1 \le \epsilon^{opt} \le \frac{(1 + \sqrt{1 + 4\tilde{P}})\epsilon_C}{2 - (1 - \sqrt{1 + 4\tilde{P}})\epsilon_C}. \tag{12}$$

20

We presented a graphical study (e.g., ϵ^{opt} varying with $\tilde{P}$ for different values of Σ) showing that the increase of efficiency with decreasing power for large value of power is slow. This implies that reasonably efficient heat pumps should operate at small value of power, which is quite different from heat engines and refrigerators that exhibit large gain in efficiency when power is slightly decreased from the maximum power [5, 45]. Finally, we compared the maximum efficiency at given power for low-dissipation heat pumps to the known results for endoreversible heat pumps [44, 52, 72]. We identified a special parameter regime when the expressions for their maximum efficiency at given power are exactly the same, and we pointed out that this agreement is unfortunately nothing more than a lucky mathematical coincidence.

2.1.3   Simultaneous absorption refrigerators

The absorption refrigerator is a remarkable cooling device that operates without the need for electricity, making it incredibly useful in various settings. Its importance lies in its ability to provide refrigeration in off-grid or remote areas where electricity is scarce or unavailable. By utilizing the principles of heat and chemical reactions, absorption refrigerators can provide reliable cooling for food, medicine, and other perishable items. This technology is especially valuable in developing regions, disaster-stricken areas, and recreational vehicles, where it ensures the preservation of essential supplies.

In our work [6], we considered absorption refrigerators consisting of a finite-time Carnot heat engine and refrigerator depicted in Fig. 2. The internal engine utilizes the temperature gradient $T_{\mathrm{h}} - T_{\mathrm{m}} > 0$ between a hot thermal reservoir and a thermal reservoir at a medium temperature to generate work. This work is then used to propel the internal refrigerator, which pumps heat from the cold thermal reservoir at temperature $T_{\mathrm{c}} < T_{\mathrm{m}}$ into the intermediate bath. As a result, the absorption refrigerator utilizes heat from the hot body to further cool the cold one. Absorption refrigerators usually operate in two ways: the internal engine and refrigerator work simultaneously or alternately [62]. Since we want to
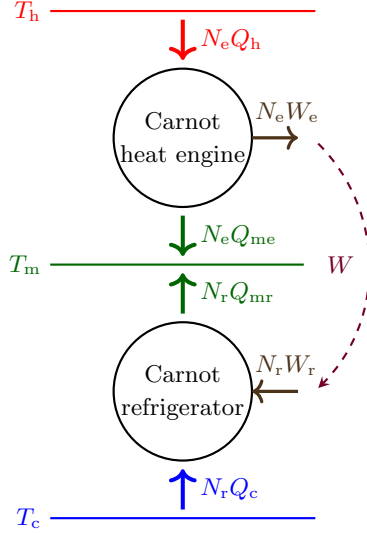
FIG. 2. Absorption refrigerators composed of an internal Carnot heat engine and Carnot refrigerator [6]. The system communicates with three heat reservoirs at temperatures $T_\mathrm{h} > T_\mathrm{m} > T_\mathrm{c}$. Both the internal engine and refrigerator use as their heat sink the reservoir at the intermediate temperature T_m. The engine in addition communicates with the hot bath at T_h and the refrigerator with the cold bath at T_c.

provide an upper bound for the maximum efficiency at given power, we adopt the former setup, because the latter one involves idle periods during the operation of the internal devices and thus has smaller maximum efficiency than the latter. However, when operating simultaneously, the internal heat engine cannot power the internal refrigerator normally because the engine generates work during half of the cycle only and accepts it during the rest. This can be solved as in usual cyclic heat engines where an external power source (or storage) is included, such that the work generated by the engine can be stored and be applied to drive the combined system during parts of the cycle when the engine accepts energy.

After one cycle of the simultaneous absorption refrigerator, both the internal engine and refrigerator return to their initial states. The cycle duration is thus given by the least common multiple of the engine and refrigeration cycles t_e and t_r. We optimized the efficiency of the absorption refrigerator with respect to t_e and t_r, and found that its maximum efficiency at given power is given by the product of those for the internal engine and refrigerator. This means that we can get the maximum efficiency at given power for this general model of simultane-

ous absorption refrigerators immediately by combining the known results for the internal engine and refrigerator. For absorption refrigerators where the internal engine and refrigerator operate alternately [62], we showed that the maximum efficiency at given power cannot be derived directly from those for the internal devices.

To obtain explicit results, we then assumed that the internal devices work in the low-dissipation regime because their maximum efficiency at given power are known [5, 45]. The derived expression for the maximum efficiency represents a (loose) upper bound for the efficiency of real-world absorption refrigerators. Again using the definitions (4), we found that a slight decrease in power of the absorption refrigerator from its maximum value leads to a large nonlinear increase in efficiency ($\delta\eta \propto \sqrt{-\delta P}$), as observed in heat engines [45], whenever the ratio of maximum powers of the internal engine and the refrigerator does not diverge. Otherwise, the increase in efficiency is linear ($\delta\eta \propto -\delta P$) as observed in refrigerators with large Σ [5]. This indicates that the efficiency of low-dissipation absorption refrigerators significantly increases when their power is slightly decreased from its maximum in all practical situations.

2.2 Outlook

As an extension, we plan to consider Carnot-type low-dissipation heat engine, refrigerator, and heat pump in the presence of heat leak and derive their maximum efficiency at given power. The heat leak implies the direct heat transfer between the reservoirs (thermal conductivity denoted by κ) and one can assume that it obeys Newton's law of cooling [73, 74],

$$Q_l = \kappa t_p (T_h - T_c). \tag{13}$$

The system then includes two most essential irreversibilities in real heat engines: dissipation and heat leak. These irreversibilities are also taken into account by steady-state irreversible heat engines such as thermoelectric devices [75]. For heat

engines, the heats exchanged between the system and the heat bath during the isotherms, Q_h and Q_c, are still captured by Eqs. (3a) and (3b). However, the total heats released by the hot bath and injected into the cold one per finite-time Carnot cycle are given by [73, 76]

$$Q_H = Q_h + Q_l, \tag{14a}$$

$$Q_C = Q_c + Q_l. \tag{14b}$$

One has to use Eqs. (14a) and (14b) to derive the maximum efficiency at given power instead of Eqs. (3a) and (3b). The same arguments should be applied to refrigerators and heat pumps. Due to the presence of heat leak, the maximum attainable efficiency is not Carnot efficiency anymore. Therefore, in addition to the regime of power close to maximum power, one should analyze the behavior near the maximum achievable efficiency. One also should investigate the influence of heat leak on this behavior.

Furthermore, one can investigate the connection among the maximum efficiency at given power for heat engines, refrigerators, and heat pumps to immediately obtain all known expressions for the maximum efficiency at given power from a single maximum efficiency at given power. This should work because refrigerators and heat pumps are essentially heat engines that run in the reverse direction. Optimizing the engine in the refrigeration mode of operation thus implies the optimization of the refrigerator and heat pump. These explains why many formulas that are quite similar occur in the derivation of maximum efficiency at given power for low-dissipation heat engines, refrigerators, and heat pumps [5, 7, 45]. For this extension, we have completed all the data processing and are writing the manuscript for publication.

As a second extension we plan to study absorption heat pumps consisting of a simultaneously operating Carnot heat engine and heat pump, which are similar to the case of absorption refrigerators [6]. This simultaneous setup would also provide larger maximum efficiency than the one where the internal heat engine and heat pump operate alternately [77]. Completely the same arguments as for

simultaneous absorption refrigerators presented in the previous subsection can be applied to the simultaneous absorption heat pump.

Third, our formulas for maximum efficiency at given power are expressed as functions of the dimensionless power, e.g., Eq. (4). The maximum efficiency can thus be further optimized with respect to the unit. For heat engines and refrigerators, a similar task of deriving maximum power at fixed maximum efficiency has been solved in Refs. [61, 78] using a geometrical approach. For low-dissipation heat pumps, such an optimization is still under investigation. Furthermore, the situation in the simultaneous absorption refrigerator is more complicated, since its maximum power depends on the maximum powers of both internal devices.

The fourth extension (and perhaps the most influential one) would be to relate the predictions of low-dissipation models to more realistic models, such as thermoradiative devices [79, 80], where we can check the validity of the assumption (2) and the generality of the obtained bounds on maximum efficiency at given power. To this end, we briefly introduce the working principles and features of thermoradiative devices in Appendix A. Thermoradiative devices [79, 80] represent a new technology that has recently emerged for electricity generation from thermal energy. In connection to this task, one should naturally also investigate the maximum efficiency at given power for thermoradiative devices, and evaluate their behavior close to maximum power and maximum efficiency.

Furthermore, we plan to investigate maximum efficiency at given power for low-dissipation systems with respect to their dynamical stability [63, 81, 82]. Finally, we plan to investigate the maximum efficiency at given power for engines working between finite-sized reservoirs [83–89] and compare the results to those derived for the low-dissipation models. For heat engines operating between two finite-sized reservoirs, the maximum efficiency at given power has been derived in Ref. [88].

Maximum efficiency of low-dissipation refrigerators at arbitrary cooling power

Viktor Holubec [1,2,*] and Zhuolin Ye[1,†]

[1]*Institut für Theoretische Physik, Universität Leipzig, Postfach 100 920, D-04009 Leipzig, Germany*
[2]*Charles University, Faculty of Mathematics and Physics, Department of Macromolecular Physics,*
V Holešovičkách 2, CZ-180 00 Praha, Czech Republic

We analytically derive maximum efficiency at given cooling power for Carnot-type low-dissipation refrigerators. The corresponding optimal cycle duration depends on a single parameter, which is a specific combination of irreversibility parameters and bath temperatures. For a slight decrease in power with respect to its maximum value, the maximum efficiency exhibits an infinitely fast nonlinear increase, which is standard in heat engines, only for a limited range of parameters. Otherwise, it increases only linearly with the slope given by ratio of irreversibility parameters. This behavior can be traced to the fact that maximum power is attained for vanishing duration of the hot isotherm. Due to the lengthiness of the full solution for the maximum efficiency, we discuss and demonstrate these results using simple approximations valid for parameters yielding the two different qualitative behaviors. We also discuss relation of our findings to those obtained for minimally nonlinear irreversible refrigerators.

I. INTRODUCTION

The laws of energy conservation and nondecrease of entropy of the universe, cornerstones of classical thermodynamics developed during 19th century, imply universal upper bounds on efficiencies of thermodynamic machines such as heat engines, heat pumps, and refrigerators [1]. They are reached by idealized machines operating under reversible conditions, with vanishing net entropy production. The advantage of these results is their generality. The disadvantages are omnipresent dissipation looses in real machines, rendering their reversible operation difficult, and even more importantly, the fact that reversible conditions correspond to practically negligible output power [2].

These issues triggered a less general, but more practical, branch of research based on various models of irreversible and/or finite-time thermodynamics, which is efficiency of thermodynamic machines at maximum power. Starting with the works on performance of nuclear power plants by Yvon, Chambadal, and Novikov [3–5] later popularized by Curzon and Ahlborn [6], this model-based research attracted a considerable attention during the last 50 years and is still lively today. Efficiency at maximum power has been studied for endoreversible [6–8], low-dissipation [9–11], linear irreversible [12–14], minimally nonlinear irreversible [15–17], quantum [18–20], and Brownian [21–23] models.

In recent years, based on the above models, yet another, another even more practice-oriented, branch of research started, optimization of efficiency at given power. For vanishing power the maximum efficiency equals the reversible limit and for maximum power efficiency at maximum power. Below we

address this task, previously solved for various heat engines [2] but only minimally nonlinear irreversible refrigerators [24,25], for Carnot-type low-dissipation refrigerators.

In Secs. II and III we introduce in detail the considered model and define variables describing its thermodynamic performance. In Sec. IV we review the corresponding result for efficiency at maximum power. Our main results on maximum efficiency at a given power are given in Sec. V. We conclude in Sec. VI. The relation between the low-dissipation and minimally nonlinear irreversible models is discussed in the Appendix.

II. MODEL AND ASSUMPTIONS

We consider a refrigerator operating along a finite-time Carnot cycle of duration t_p depicted and described in detail in Fig. 1. We assume that in the limit of infinitely slow driving, $t_\mathrm{p} \to \infty$, the fridge operates reversibly and its finite-time performance is captured by the so-called low-dissipation (LD) assumption [9]

$$Q_\mathrm{h} = T_\mathrm{h}\Delta S + \frac{\sigma_\mathrm{h}}{t_\mathrm{h}}, \qquad (1)$$

$$Q_\mathrm{c} = T_\mathrm{c}\Delta S - \frac{\sigma_\mathrm{c}}{t_\mathrm{c}}, \qquad (2)$$

for total amounts of heat interchanged with the individual reservoirs during the cycle. The ratio $\sigma_\mathrm{h}/(t_\mathrm{h}T_\mathrm{h})$ measures an excess in the total amount of entropy $Q_\mathrm{h}/T_\mathrm{h} - \Delta S$ produced during the hot isotherm due to its finite duration t_h, and similarly for $\sigma_\mathrm{c}/(t_\mathrm{c}T_\mathrm{c})$. We assume that the adiabatic branches interconnecting the isotherms are ideal and thus the net amount of entropy ΔS_tot produced per cycle is solely given by the dissipation due to the heat transferred to the two reservoirs

---

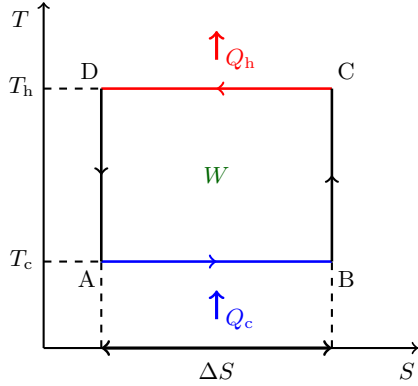*viktor.holubec@mff.cuni.cz
†zhuolinye@foxmail.com

FIG. 1. Thermodynamic T-S (bath temperature-system entropy) diagram of the considered Carnot refrigeration cycle. The fridge uses the input work W to extract heat Q_c from the cold bath at temperature T_c during the cold isotherm (AB, blue). The used work and the extracted heat are then dumped as heat $Q_h = Q_c + W$ into the hot bath at temperature T_h during the hot isotherm (CD, red). The input work equals the enclosed area, $Q_c = T_c \Delta S$, and $Q_h = T_h \Delta S$ only if the cycle is performed reversibly. Otherwise, the work is larger and the extracted heat smaller leading to a decreased efficiency (coefficient of performance) of the machine. The branches BC and DA (black) of the cycle are adiabats.

during the isotherms:

$$\Delta S_{tot} = \frac{Q_h}{T_h} - \frac{Q_c}{T_c} = \frac{\sigma_h}{t_h T_h} + \frac{\sigma_c}{t_c T_c}. \qquad (3)$$

The fridge hence operates reversibly if the isotherms are infinitely slow (and thus $t_p \to \infty$) or if the so-called irreversibility parameters σ_h and σ_c vanish.

Interestingly, this simple model, where all thermodynamically important details about the system dynamics are described by the irreversibility parameters, represents quite well two general realistic setups, justifying the considerable attention it received in recent literature [9–11,26–30]. First, Eqs. (1) and (2) can be interpreted as formal expansions of the interchanged heats in the inverse cycle duration $1/t_p$. Therefore, they should be generally valid for slowly, but not quasistatically, driven systems. Indeed, the decay of total dissipated heat with the inverse of duration was theoretically predicted for various quantum and classical setups [31–34] and observed in various experiments [35,36]. The second situation, where assumptions (1) and (2) hold for arbitrary cycle duration, is overdamped Brownian systems driven by special time-dependent protocols (usually minimizing dissipated energy during the isotherms [21,25,27,37,38]). While a similar optimization might also be performed for other systems, we are not aware of such results.

Furthermore, models of thermal machines utilizing the LD assumption can *exactly* be mapped to the minimally nonlinear irreversible (MNI) model operating under the tight coupling condition [15–17,39]. This broadly used model of irreversible thermodynamics generalizes the standard linear irreversible model [12,40] by including terms describing dissipation of the input work due to an internal friction (or, in the case of thermoelectric machines, resistivity [41]), which are proportional the irreversibility parameters. Even though this

model also can describe cyclically operating systems [42], it does not incorporate any obvious periodicity, and thus it is usually interpreted as operating in a nonequilibrium steady state. On the other hand, the LD model naturally describes machines operating cyclically. Therefore, thermal machines described by the two models are usually optimized differently. The natural control parameter for MNI models is the external force X_1, corresponding to the (scaled) input work W/T_h in the LD model, or, equivalently, the flux J_1 conjugated to X_1, which stands in the mapping to the LD model for the inverse cycle duration $1/t_p$. Since the LD models are not only optimized with respect to t_p but also with respect to distribution of this total duration among the individual branches of the cycle, the obtained optimal performance in the two models usually differs. The notable exception is bounds on performance obtained by further optimizing with respect to the irreversible parameters. Then the two optimization procedures coincide, and the results obtained within the two models agree. For more details, see the Appendix.

III. POWER AND EFFICIENCY

Central quantities describing performance of a refrigerator are its cooling power, P, and efficiency, ε, often referred to as the coefficient of performance (COP). The cooling power is defined as heat extracted from the cold bath per cycle over the cycle duration,

$$P = \frac{Q_c}{t_p} = \frac{T_c \Delta S}{t_p} - \frac{\sigma_c}{t_c t_p}, \qquad (4)$$

where we have applied the LD assumption (2). The COP measures cost of the cooling in units of input work, $W = Q_h - Q_c$, used to pump the heat from the cold bath,

$$\varepsilon = \frac{Q_c}{W} = \frac{\varepsilon_C}{1 + T_h \varepsilon_C \Delta S_{tot}/(Pt_p)}. \qquad (5)$$

A first glance at these definitions reminds us of the textbook knowledge that simultaneous optimization of power and COP is not possible (textbooks usually deal with heat engines, but the situation with refrigerators is the same). Maximum COP, $\varepsilon_C = T_c/(T_h - T_c)$, is attained under reversible conditions ($\Delta S_{tot} = 0$) when the term $T_h \varepsilon_C \Delta S_{tot}/(Pt_p)$ in the denominator of Eq. (5) vanishes. And, even though recent theoretical results on thermodynamics of small systems allowing unprecedented control of the intrinsic relaxation times show that power corresponding to ε_C can even diverge [43–46], it is doomed to be negligible compared to its maximal value [2].

In practice, we thus always have to resort to a compromise between power and COP. To this end, various *ad hoc* trade-off figures of merit of refrigerators have been proposed. Examples are the χ criterion [47–49], Ω criterion [50–52], and ecological criterion [53–55]. However, none of these tell us what we really want to know: what is the exact cost of running a refrigerator with a specific cooling power, which is usually fixed by our needs (for example, the size of the space that should be cooled). The optimization task of practical interest is thus to find the maximum COP for a given cooling power, i.e., to show under which conditions this cooling power is cheapest. With respect to heat engines, this task has already gained considerable attention in the literature [2]. Expressions for

maximum efficiency at given power were derived for quantum thermoelectric heat engines [56,57], LD heat engines [26,58], MNI heat engines [59], and a stochastic heat engine based on an uderdamped harmonic oscillator [60] and using general linear response theory [40]. With respect to refrigerators, the treasury of results for general models is not so overflowing, with a notable exception of results for MNI refrigerators [25].

Below we derive maximum COP at given power for the LD model defined above. Our bounds (22) on the maximum COP agree with those obtained by Long *et al.* [25] for MNI refrigerators. This is because, in these limiting cases, the two, generally different, optimization procedures agree. The rest of our results differ from those for MNI refrigerators quantitatively, but the most interesting qualitative features of the obtained maximum COP are preserved. Thus our discussion below might interest also readers of Ref. [25].

IV. COP AT MAXIMUM COOLING POWER

The values of cooling power accessible to a refrigerator are bounded by 0 and the maximum power, $P^\star$. A natural starting point for calculating maximum COP at fixed power is thus determination of $P^\star$ for LD refrigerators, which was done in Ref. [61]. Since peculiarities of the derivation strongly affect qualitative behavior of maximum COP at fixed power, we review it in detail.

We aim to maximize the cooling power (4) as function of the cycle duration t_p and its division among the individual branches. To this end, we assume, without loss of generality, that the sum of durations of the adiabatic branches is proportional to the total duration of the isotherms, $t_i = t_h + t_c$, so that $t_p = a t_i$ with $a \geqslant 1$. This assumption allows us to simplify the calculations, and it can easily be relaxed. Maximum power is obviously obtained for $a = a^\star = 1$ (adiabats infinitely faster than isotherms). Since the parameter a does not influence the COP (5), we keep it at this value for the rest of our discussion. Even though such infinitely fast adiabatic branches seem strange at first glance, they were realized in experiments with Brownian heat engines [62]. Together with infinitely fast adiabats an issue might arise with bringing the system far from equilibrium, thus effectively breaking the regime of validity of the LD model. However, this can be avoided by properly adjusting the value of the control parameter (for example, volume or stiffness of a potential) and temperature at the ends of the adiabatic branches [37,63]. Readers who nevertheless feel uncomfortable setting $a = 1$ can redefine the power for the rest of the paper as aP. Furthermore, we introduce the dimensionless parameter

$$\alpha = t_h/t_i \in [0, 1] \qquad (6)$$

measuring relative duration of the hot isotherm.

Maximizing the cooling power in Eq. (4) with respect to t_i gives [61]

$$t_{i,\alpha}^* = \frac{2\sigma_c}{(1-\alpha)T_c \Delta S}, \qquad (7)$$

$$P_\alpha^* = \frac{(1-\alpha)(T_c \Delta S)^2}{4\sigma_c}, \qquad (8)$$

$$\varepsilon_\alpha^* = \frac{\varepsilon_C}{2 + \varepsilon_C + \sigma \varepsilon_C (1/\alpha - 1)}, \qquad (9)$$

where we have introduced the irreversibility ratio

$$\sigma \equiv \sigma_h/\sigma_c. \qquad (10)$$

With decreasing α, the partially optimized cooling power (8) monotonously interpolates between 0 [attained for $\alpha = 1$, $t_{i,\alpha}^* = \infty$, and $\varepsilon_\alpha^* = \varepsilon_C/(2 + \varepsilon_C)$; note that this process is not reversible even though the cycle duration diverges] and its maximum, reached for $\alpha = \alpha^* = 0$ [61]. The resulting maximum power and the corresponding duration of the isothermal branches thus read

$$P^* = \frac{(T_c \Delta S)^2}{4\sigma_c}, \qquad (11)$$

$$t_i^* = \frac{2\sigma_c}{T_c \Delta S}. \qquad (12)$$

With decreasing irreversibility parameter σ_c, the maximum power and $1/t_i$ monotonously interpolate between 0 and ∞. In contrast, the COP at maximum power, ε^*, reads

$$\varepsilon_-^* = 0 \quad \text{for} \quad \sigma > 0, \qquad (13)$$

$$\varepsilon_+^* = \frac{\varepsilon_C}{2 + \varepsilon_C} \quad \text{for} \quad \sigma = 0 \qquad (14)$$

and thus it exhibits a discontinuity at $\sigma = 0$ [61], which should be understood in the sense that $\sigma_h \ll \sigma_c$. This discontinuity is caused by the requirement $\alpha^* = 0$, which should be understood in the sense that the duration of the hot isotherm is negligible compared to that of the cold one, i.e., $t_h \ll t_c$. Then the total entropy production (3) diverges unless the irreversibility parameter σ is set to zero before α.

Actually, if one does not set $\alpha = \alpha^* = 0$ exactly in the derivation, but instead considers a limiting process $\alpha \to \alpha^*$, they can get efficiencies at maximum power, ε^*, within the bounds $[\varepsilon_-^*, \varepsilon_+^*]$. For example, assuming that $\lim_{\alpha \to \alpha^*} \sigma/\alpha = k$ and thus $\sigma = k\alpha$, $k > 0$, the efficiency at maximum power reads

$$\varepsilon^* = \frac{\varepsilon_C}{2 + (1 + k)\varepsilon_C}. \qquad (15)$$

Since Eqs. (13) and (14) do not depend on σ, they represent lower and upper bounds on COP at maximum power of LD refrigerators. For MNI refrigerators, $\varepsilon_\pm^*$ describe bounds on COP at maximum power [15,25], obtained as extreme values of (9) as a function of σ. Thus the discontinuity found in the LD model, caused by optimization with respect to α, is not present in the MNI model.

In closing this section, we should discuss how reasonable taking the limit $\sigma \to 0$ is, leading to the nontrivial value ε_+^* of COP at maximum power, from a physical perspective. However, we postpone this discussion to Sec. V A and continue with optimization of COP at fixed power.

V. MAXIMUM COP AT ARBITRARY COOLING POWER

From technical reasons [2,26,27,40], it is advantageous to study the maximum COP at fixed power using the dimensionless loss in power (with respect to the maximum power),

$$\delta P \equiv \frac{P - P^*}{P^*} \in [-1, 0], \qquad (16)$$

and the dimensionless duration (of the isotherms),

$$\tau = \frac{t_{\mathrm{i}} - t_{\mathrm{i}}^*}{t_{\mathrm{i}}^*} \in [-1, \infty]. \tag{17}$$

The loss in power vanishes for $P = P^\star$ and assumes its minimum value -1 if the power P is negligible compared to $P^\star$ [2]. The definition (16) physically means that we measure energy flows in units of maximum power (11), and thus we effectively fix the value of σ_{c}. The duration τ equals -1 for $t_{\mathrm{i}} = 0$, and it is negative (positive) for $t_{\mathrm{i}} < t_{\mathrm{i}}^*$ ($t_{\mathrm{i}} > t_{\mathrm{i}}^*$). Since we are interested in maximum COP at fixed power and longer cycles in general allow for larger COPs, our intuition suggests (and the calculation below proves) that we can focus on positive values of τ only.

Fixing the cooling power (or, equivalently, δP) creates a dependence between the duration, τ, and relative duration of the hot isotherm, α. Using Eq. (4), we find that

$$\alpha = 1 + \frac{1}{(1 + \delta P)\tau^2 + 2\delta P\tau + \delta P - 1}. \tag{18}$$

Using further the definition (6), implying that $0 \leqslant \alpha \leqslant 1$, we find that the above formula makes sense only for a limited interval of τ:

$$-\frac{\sqrt{-\delta P}}{1 + \sqrt{-\delta P}} \leqslant \tau \leqslant \frac{\sqrt{-\delta P}}{1 - \sqrt{-\delta P}}. \tag{19}$$

The COP (5) in these new variables reads

$$\varepsilon = \frac{\tau^3 + A_{1,3}\tau^2 + A_{0,3}\tau + A_{0,1}}{-\tau^3 + A_{1/\varepsilon_+^*,-3}\tau^2 + B_{3,4,1}\tau + B_{1,2,-1}}, \tag{20}$$

with $A_{k,l} = (k + l\delta P)/(1 + \delta P)$ and $B_{k,l,m} = [-k(\delta P)^2 + (l/\varepsilon_{\mathrm{C}} + 1 + \sigma)\delta P + m\sigma]/(1 + \delta P)^2$, and we will now find its maximum as function of τ.

A. Bounds

For fixed τ, δP, and ε_{C}, the COP (20) is a monotonously decreasing function of σ. Analytically, this follows by noticing that $\partial\varepsilon/\partial\sigma < 0$. Intuitively, it can be understood as follows. As noted above, σ_{c} is fixed by the chosen energy unit P^*, and thus σ is solely determined by σ_{h}. COP (5) monotonously decreases with increasing entropy production ΔS_{tot}, which is, for fixed dissipation during the cold isotherm, a monotonously increasing function of σ_{h}.

The lower bound on COP is thus obtained in the limit of an infinitely irreversible hot isotherm ($\sigma = \infty$). Then $\Delta S_{\mathrm{tot}}/P$ in Eq. (5) diverges and the maximum attainable COP vanishes, regardless of values of τ and δP. Fortunately, the upper bound on COP, obtained if the hot isotherm is reversible ($\sigma = 0$), is positive. In this case, Eq. (20) can be simplified to

$$\varepsilon = \left[\frac{2(1 + \varepsilon_{\mathrm{C}})}{(1 + \tau)\varepsilon_{\mathrm{C}}(1 + \delta P)} - 1 \right]^{-1}. \tag{21}$$

For the allowed values (19) of τ, this function monotonously increases, and thus the upper bound on COP is obtained by setting $\tau = \sqrt{-\delta P}/(1 - \sqrt{-\delta P})$. In agreement with the result derived for MNI refrigerators [25], we find that the maximum

COP at fixed power, $\varepsilon^{\mathrm{opt}} = \varepsilon^{\mathrm{opt}}(\delta P)$, is bounded as

$$0 \leqslant \varepsilon^{\mathrm{opt}} \leqslant \frac{\varepsilon_{\mathrm{C}}(1 + \sqrt{-\delta P})}{2 + \varepsilon_{\mathrm{C}}(1 - \sqrt{-\delta P})} \equiv \varepsilon_+^{\mathrm{opt}}. \tag{22}$$

All known bounds on maximum efficiency at fixed power for heat engines [2,26,40,56,57,59,60] exhibit an infinite gain in efficiency (with respect to the efficiency at maximum power) when the engines operate at powers infinitely smaller than P^*, in symbols $\partial\eta^{\mathrm{opt}}/\partial\delta P|_{\delta P=0} \to \infty$. The upper bound $\varepsilon_+^{\mathrm{opt}}$ on $\varepsilon^{\mathrm{opt}}$ in Eq. (22) shows qualitatively the same large gain in COP. The corresponding relative gain in COP for small δP reads

$$\frac{\varepsilon_+^{\mathrm{opt}} - \varepsilon_+^*}{\varepsilon_+^*} = (1 + \varepsilon_+^*)\sqrt{-\delta P} + O(\delta P), \tag{23}$$

where $O(\delta P)$ denotes a correction of order δP. Thus the derivative of the relative gain with respect to δP diverges with $\delta P \to 0-$ as $1/\sqrt{-\delta P}$. This is a general behavior expected for a COP near maximum power if the latter is determined by a vanishing derivative with respect to a control parameter x [26,40,60]. Indeed, if $\partial P/\partial x|_{P=P^*} = 0$ (in the present setting, x stands for α or τ) one would expect that expansions of power and efficiency around the maximum power P^* read $\delta P \approx -x^2/c^2$ and $\varepsilon - \varepsilon^* = |a|x$, leading to the relation $\varepsilon - \varepsilon^* = |ac|\sqrt{-\delta P}$. In the present case, however, the maximum power (11) does not correspond to a a vanishing derivative with respect to α. As a result, the described "universal" behavior for LD refrigerators can be observed for small parameters σ and ε_{C} only, as suggested by behavior of bounds (22) and discussed in the following two sections.

In closing this section, let us review how (physically) reasonable the limiting values 0 and ∞ of the irreversibility ratio are, leading to the bounds (22). To this end, there is a handful of microscopic models yielding reasonable expressions for σ. For a relatively broad class of slowly driven systems (described by a generalized Markovian master equation with a symmetric protocol for hot and cold isotherms), the irreversibility ratio assumes the form $\sigma = (T_{\mathrm{h}}/T_{\mathrm{c}})^{1-\xi}$, where ξ stands for the exponent in the bath spectral density [33]. The limit $\sigma \to 0$ thus corresponds to an infinitely superohmic bath ($\xi \to \infty$), while the opposite limit $\sigma \to \infty$ is obtained for an infinitely subohmic bath ($\xi \to -\infty$). Obviously, neither of such strongly diverging spectral densities (and thus also the corresponding values of σ) make much physical sense. For overdamped Brownian dynamics with time-dependent driving optimized to minimize the dissipated work, the irreversibility ratio is given by the ratio $\sigma = \mu_{\mathrm{c}}/\mu_{\mathrm{h}}$ of mobilities [21]. Since the infinite mobility is not compatible with assumptions of overdamped dynamics [2,21,27,28,46], meaningful possibilities to reach the limiting values of σ are the vanishing mobility μ_{c} during the cold isotherm ($\sigma = \infty$) or vanishing mobility during the hot isotherm ($\sigma = 0$). Such conditions can indeed be realized. One ensuing technical problem is that with decreasing mobility the relaxation time of the system increases, and thus one has to resort to a stronger driving to get the same performance [46]. To conclude, realizing the limiting values of the irreversibility ratio exactly in the laboratory is practically impossible, but these regimes can theoretically be reasonably approximated. Nevertheless, this can
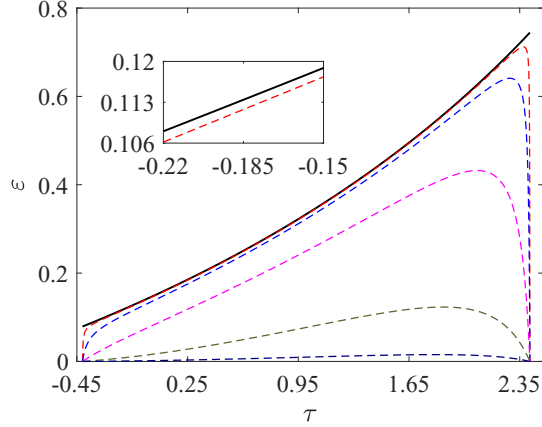
FIG. 2. COP (20) as function of τ for six values 0, 0.01, 0.1, 1, 10, and 100 of σ increasing from the top black solid line to the lowermost broken line. The inset shows that the maximum COP is attained at $\sigma = 0$. Parameters taken: $\delta P = -0.5$ and $\varepsilon_C = 1$.

be quite expensive, and thus, for real practical applications, it is important also to study the behavior of $\varepsilon^{\mathrm{opt}}$ for nonextreme values of the irreversibility ratio, which is a topic of the next section.

B. Arbitrary parameters

In Fig. 2 we show the COP (20) as a function of the duration τ for six values of the irreversibility ratio. For $\sigma = 0$, ε indeed monotonously increases. For all larger σ, it develops a peak at a position $\tau^{\mathrm{opt}} < \sqrt{-\delta P}/(1 - \sqrt{-\delta P})$, which can be determined from the condition $\partial \varepsilon / \partial \tau|_{\tau = \tau^{\mathrm{opt}}} = 0$. Explicitly, it reads

$$(\tau^{\mathrm{opt}})^4 + \tilde{A}(\tau^{\mathrm{opt}})^3 + \tilde{B}_{6+3\tilde{\sigma}, 2+2\tilde{\sigma}, -\tilde{\sigma}}(\tau^{\mathrm{opt}})^2$$
$$+ \tilde{B}_{4+3\tilde{\sigma}, -2\tilde{\sigma}, -\tilde{\sigma}}\tau^{\mathrm{opt}} + \tilde{B}_{1+\tilde{\sigma}, -2\tilde{\sigma}, 0} = 0, \qquad (24)$$

where the the coefficients $\tilde{A} = [(4 + \tilde{\sigma})\delta P + \tilde{\sigma}]/(1 + \delta P)$ and $\tilde{B}_{k,l,m} = (k\delta P^2 + l\delta P + m)/(1 + \delta P)^2$ depend on σ and ε_C only through the combination $\tilde{\sigma} = \sigma/(\frac{1}{\varepsilon_C} + 1)$. For a given loss in power, the optimal duration is thus solely determined by $\tilde{\sigma}$, which monotonously increases with both σ and ε_C.

The quartic equation (24) has four roots and can be analytically solved using Ferrari's method [64]. The physical optimal duration τ^{opt} is given by the root in the interval (19), which can be determined by inserting some specific values of δP and $\tilde{\sigma}$ into the formal expressions for the roots. Even though the ensuing expression is far too long and cumbersome to be more enlightening than a numerical solution, it can be used as a basis of various approximations explaining the qualitative behavior of τ^{opt} (or α^{opt}) and $\varepsilon^{\mathrm{opt}}$, depicted in Fig. 3.

Specifically, the maximum COP, shown in Fig. 3(a), exhibits a sharp increase with power near the maximum power only for small values of σ. In agreement with the discussion in the preceding section, the rate of this increase $-\partial \varepsilon^{\mathrm{opt}}/\partial \delta P|_{\delta P = 0}$ actually decreases with σ from ∞ (for $\sigma \to \infty$) to 0 (for $\sigma = 0$). For large values of σ, the maximum COP exhibits a fast increase (similar to that of $\varepsilon^{\mathrm{opt}}$ near $P = P^*$ for small σ) close to the vanishing power, where the COP attains
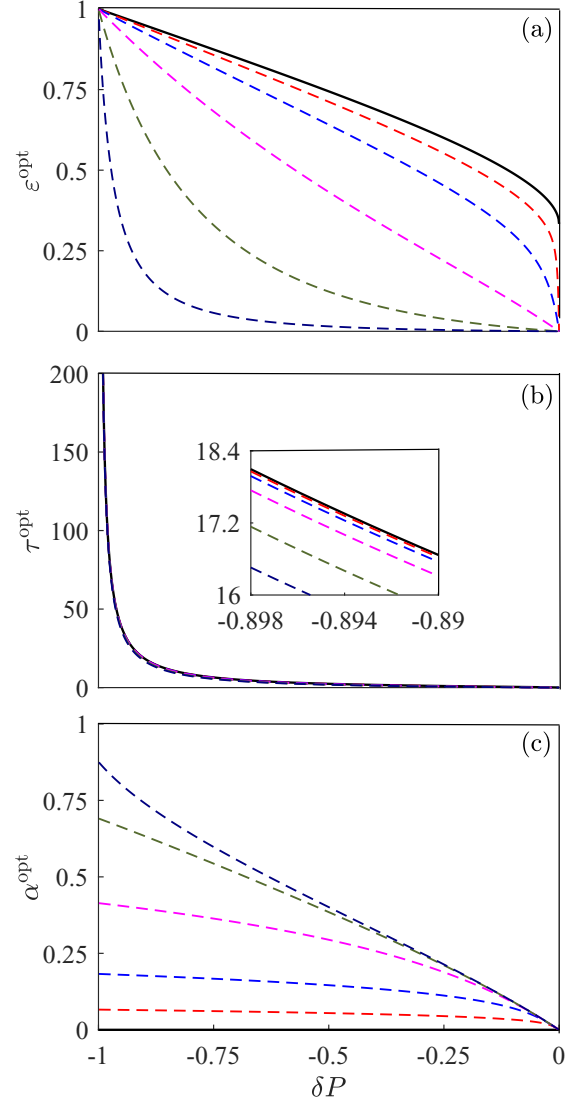
FIG. 3. (a) The optimal COP $\varepsilon^{\mathrm{opt}}$ as a function of δP for six values 0, 0.01, 0.1, 1, 10, and 100 of σ increasing from the top black solid line to the lowermost broken line. Panels (b) and (c) show the corresponding parameters τ^{opt} and α^{opt}. The inset in panel (b) magnifies the differences between the individual curves. Note the inverse ordering of the curves in panel (c). We took $\varepsilon_C = 1$.

its ultimate upper bound ε_C. While the described dependence of $\varepsilon^{\mathrm{opt}}$ on σ is significant, the optimal duration τ^{opt} in Fig. 3(b) changes with σ only slightly, always monotonously interpolating between 0 for $\delta P = 0$ and ∞ for $\delta P = -1$. This suggests that a reasonable approximation of τ^{opt} substituted for τ in Eq. (20) might lead to an excellent approximation of $\varepsilon^{\mathrm{opt}}$. The optimal relative duration of the hot isotherm shown in Fig. 3(c) is fixed by τ and δP through Eq. (18). Contrary to that of τ^{opt}, the dependence of α^{opt} on σ is significant. Let us note that a similar situation occurs also for LD heat engines [26]. To get a more analytical and quantitative grasp of the described qualitative behavior of the maximum COP, we now derive several approximate formulas valid in the two regions of σ described above.

C. Approximations

1. Small irreversibility ratio

Expanding the exact optimal duration τ^{opt} and COP ε^{opt}, obtained using Eq. (24), up to the first order in $\tilde{\sigma}$, we find that, up to a correction $O(\tilde{\sigma})$,

$$\tau^{\text{opt}} \approx \frac{\sqrt{-\delta P}}{1 - \sqrt{-\delta P}} - \frac{\sqrt{\tilde{\sigma}}}{2(-\delta P)^{1/4}}, \qquad (25)$$

$$\varepsilon^{\text{opt}} \approx \varepsilon_+^{\text{opt}} - \frac{2(1 + \varepsilon_C)(\varepsilon_+^{\text{opt}})^2 (1 - \sqrt{-\delta P})\sqrt{\tilde{\sigma}}}{\varepsilon_C(-\delta P)^{1/4}(1 + \sqrt{-\delta P})}. \qquad (26)$$

The expansion (26) explodes to $-\infty$ for $\delta P \to 0$, and thus it makes sense for reasonably large $-\delta P$ only. A similar divergence is present for all other terms in the series. This, mathematically undesirable, sharp decrease of the correction term for small $-\delta P$ describes the jump in the COP at maximum power (13)–(14) from ε_+^* for 0 for $\sigma > 0$. Note that the approximate optimal duration (25) exhibits a similar behavior.

2. Large temperature difference

The above approximation is valid for small $\tilde{\sigma}$ attained for both large temperature differences (small ε_C) and small irreversibility ratios σ. For small ε_C expression (26) can be further simplified to

$$\frac{\varepsilon^{\text{opt}}}{\varepsilon_C} = \frac{(1 + \sqrt{-\delta P})}{2} - \frac{(1 + \delta P)\tilde{\sigma}^{1/2}}{2(-\delta P)^{1/4}} + O(\varepsilon_C). \qquad (27)$$

Interestingly, the first term above is the same as that in LD [26], linear irreversible [40], and MNI [59] heat engines.

3. Large irreversibility ratio

Let us now turn to the case of large irreversibility ratio. Up to the leading order in $\tilde{\sigma}$, the solution to Eq. (24) reads

$$\tau^{\text{opt}} = -\frac{2\delta P}{1 + \delta P}. \qquad (28)$$

Interestingly, the same expression is obtained for $\tilde{\sigma} = 1$ and thus, for example, for an infinitely small temperature difference ($\varepsilon_C \to \infty$) and $\sigma = 1$. Substituting this τ^{opt} for τ in Eq. (20) leads to the expression for maximum COP at fixed power,

$$\varepsilon^{\text{opt}} \approx \frac{\delta P(1 - \delta P)\varepsilon_C}{2\delta P + (1 + \delta P)(\delta P - \sigma)\varepsilon_C}, \qquad (29)$$

which is exact for $\tilde{\sigma} = 1$ and ∞, and which can be expected to give a good approximation of ε^{opt} for all $\tilde{\sigma} \in [1, \infty]$. The expansion of Eq. (29) up to the first order in δP reads

$$\varepsilon^{\text{opt}} \approx -\frac{\delta P}{\sigma} + O(\delta P). \qquad (30)$$

4. Discussion

In agreement with results shown in Fig. 3(a), the expansions (26) and (27) clearly show that for small values of σ and/or ε_C the COP (26) exhibits a sharp nonlinear increase when the power is decreased from its maximum value. Equation (29), on the other hand, shows that, for moderate and large values of σ, this increase is linear with the slope determined by an inverse irreversibility ratio, which

is again seen in Fig. 3(a). It is noteworthy that all the above approximate results give the correct maximum COP ε_C for vanishing cooling power $\delta P = -1$.

Let us now discuss the range of validity of the above approximations more quantitatively. To this end, we define the function

$$E = \frac{1}{\varepsilon_C} \int_{-1}^{0} d(\delta P) \left| \varepsilon^{\text{opt}}(\delta P) - \varepsilon_{\text{approx}}^{\text{opt}}(\delta P) \right|, \qquad (31)$$

which measures the area in the ε^{opt}-δP plot between the true maximum COP and its individual approximations $\varepsilon_{\text{approx}}^{\text{opt}}$ given by Eqs. (26), (27), and (29).

In Fig. 4 we show only the performance of the approximations (26) and (29). Equation (27) performs slightly worse than Eq. (26) for large ε_C, but it shares the same qualitative behavior. In agreement with our vague discussion above, Fig. 4 proves that the approximation (26) works well for small $\tilde{\sigma} \gg 1$ (parameters **c** and **d**), but that it is also reasonable for small ε_C and large σ, yielding $\tilde{\sigma}$ of order 1 (**a**). For large values of the irreversibility ratio, Eq. (26) yields negative values for (almost) all δP, and thus the approximation completely fails (**b**). The approximation (29), on the other hand, performs almost perfectly for moderate and large values of $\tilde{\sigma}$ (**a** and **b**) but gives reasonable results also for small irreversibility ratios (**c** and **d**).

VI. CONCLUSION AND OUTLOOK

We have derived an exact but complicated formula for maximum COP at arbitrary power for Carnot-type low-dissipation refrigerators and also three simple approximations valid for a large part of the parameter space of the model. Based on these results, we have shown that the infinitely fast nonlinear increase in COP with decreasing power from its maximum value $P^\star$, routinely seen in heat engines [2,26,40,56,57,60], occurs in LD refrigerators only for small values of the irreversibility ratio (10) or large temperature differences (which, however, lead to small ultimate upper bounds on COP ε_C). For large irreversibility ratios, such an increase occurs only for small values of power, where the COP rapidly grows towards its maximum ε_C.

Our formulas for efficiency are functions of power measured in units of maximum power, which thus can further be optimized without affecting the efficiency corresponding to the fixed ratio $P/P^\star$. For slowly driven systems, one can straightforwardly use the results obtained in Ref. [65] for LD heat engines. For arbitrary cycle duration and a given change in the system volume (measured by the increase ΔS in system entropy during the hot isotherm), larger maximum cooling power (11) corresponds to small values of the reversibility parameter during the cold isotherm, σ_c. To conclude, an ideal LD refrigerator should be based on a working fluid with small σ_c (yielding large maximum cooling power) and even much smaller σ_h (allowing one to profit from the large gain in COP while sacrificing only a small part of the maximum power).

Our present contribution to the collection of maximum efficiencies at given power for various systems might be of immediate practical interest. Even though the used assumptions are valid only for systems under perfect experimental control such
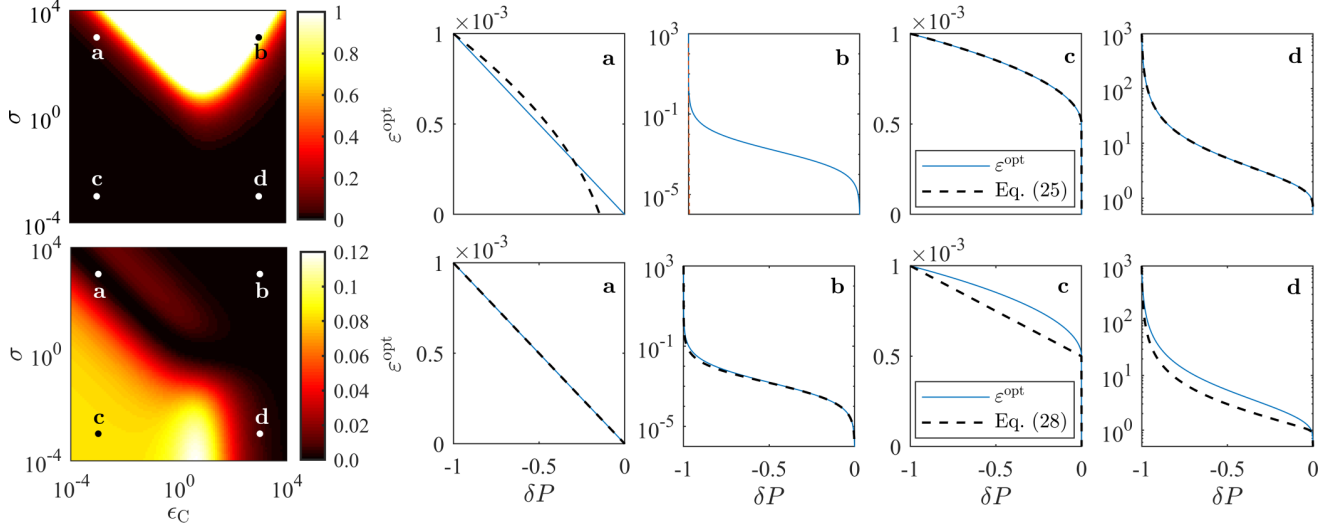
FIG. 4. Performance of the approximations (26) (top) and (29) (bottom) of the exact maximum COP. The left panels depict the error (31) (color code) as function of ε_C and σ. The remaining panels show the individual approximate functions (broken lines) and the exact $\varepsilon^{\mathrm{opt}}$ (solid lines) for the points **a**, **b**, **c**, and **d**, depicted in the leftmost figures. Their coordinates are $\mathbf{a} = (10^{-3}, 10^3)$, $\mathbf{b} = (10^3, 10^3)$, $\mathbf{c} = (10^{-3}, 10^{-3})$, and $\mathbf{d} = (10^3, 10^{-3})$. For the parameters **b**, Eq. (26) yields positive values only near the left boundary of the corresponding figure. For parameters **c** and **d** above and **a** and **b** below, the curves almost perfectly overlap.

as Brownian heat engines [21,27,35,62], taking into account additional sources of dissipation just leads to a decrease in efficiency. And thus the derived maximum efficiencies can be thought of as upper bounds on efficiencies even for relativistic settings. Furthermore, our results for refrigerators could be combined with known results for heat engines to yield maximum efficiency at fixed power for absorption refrigerators, which were studied numerically in Ref. [66]. What remains to complete the collection for LD models is a derivation of maximum efficiency at fixed power for heat pumps. Both these tasks are subjects of our present research. Furthermore, it would be interesting to investigate maximum efficiency at fixed power for LD systems with respect to their dynamical stability [10,29,30].

APPENDIX: MINIMALLY NONLINEAR IRREVERSIBLE MODEL

In this Appendix, we review in detail the mapping between the LD model and the minimally nonlinear irreversible (MNI) model [15–17]. We proceed in two steps. First, we map the average total entropy production rate

$$\frac{\Delta S_{\mathrm{tot}}}{t_p} = -\frac{Q_c}{t_p T_c} + \frac{Q_h}{t_p T_h} = \frac{1}{t_p}\frac{W}{T_h} + P\left(\frac{1}{T_h} - \frac{1}{T_c}\right) \quad (\mathrm{A1})$$

for cyclic Carnot-type refrigerators, depicted in Fig. 1, to the entropy production rate $\dot{\sigma} = J_1 X_1 + J_2 X_2$, written as a linear combination of (generalized) fluxes J_i and forces X_i, $i = 1, 2$, used in linear irreversible thermodynamics [12,40]. While there is a variety of possible choices, we employ the commonly used mapping [14,17,24] $J_1 = 1/t_p$, $X_1 = W/T_h$, and $J_2 = P$, $X_2 = 1/T_h - 1/T_c$. Consequently, the heat flux to the hot reservoir reads $Q_h/t_p = J_2 + J_1 X_1 T_h \equiv J_3$.

The MNI model assumes that the linear flux-force relation applied in linear irreversible thermodynamics is generalized as [15–17]

$$J_1 = L_{11} X_1 + L_{12} X_2, \quad (\mathrm{A2})$$

$$J_2 = L_{21} X_1 + L_{22} X_2 - \gamma_c J_1^2. \quad (\mathrm{A3})$$

Here L_{ij} $i, j = 1, 2$ denote Onsager coefficients, and the new term $-\gamma_c J_1^2$, with $\gamma_c \geqslant 0$, stands for a fraction of input power leaking into the cold bath. Physically, it describes frictional losses in mechanical machines or losses due to a finite resistivity in thermoelectric devices [41].

Using Eq. (A2), the heat fluxes from the cold bath (J_2) and to the hot bath (J_3) read

$$J_2 = \frac{L_{21}}{L_{11}} J_1 + L_{22}(1 - q^2) X_2 - \gamma_c J_1^2, \quad (\mathrm{A4})$$

$$J_3 = \frac{L_{21}}{L_{11}}\frac{T_h}{T_c} J_1 + L_{22}(1 - q^2) X_2 + \gamma_h J_1^2, \quad (\mathrm{A5})$$

where $\gamma_h J_1^2$ denotes the fraction of input power leaking into the hot reservoir. The Onsager reciprocity relations imply that the coupling strength parameter $q = L_{12}/\sqrt{L_{11}L_{22}}$ is bounded as ($|q| \leqslant 1$). As the second step in the mapping, we compare Eqs. (1) and (2) and (A4) and (A5) and try to find a mapping between the parameters. This can be done under the tight coupling condition $|q| = 1$, when the flux J_1 and the heat fluxes J_i, $i = 2, 3$ are proportional in the linear irreversible

model and efficiencies of machines based on the MNI model are largest. The result is [17]

$$
\begin{pmatrix} L_{11} & L_{12} \\ L_{21} & L_{22} \end{pmatrix} = \begin{pmatrix} \frac{T_{\mathrm{h}}}{\lambda} & \frac{T_{\mathrm{h}} T_{\mathrm{c}} \Delta S}{\lambda} \\ \frac{T_{\mathrm{h}} T_{\mathrm{c}} \Delta S}{\lambda} & \frac{T_{\mathrm{h}} (T_{\mathrm{c}} \Delta S)^2}{\lambda} \end{pmatrix}, \quad \text{(A6)}
$$

$$
\gamma_{\mathrm{h}} = \frac{\sigma_{\mathrm{h}}}{\alpha}, \quad \text{(A7)}
$$

$$
\gamma_{\mathrm{c}} = \frac{\sigma_{\mathrm{c}}}{1 - \alpha}, \quad \text{(A8)}
$$

where $\gamma \equiv \gamma_{\mathrm{h}}/\gamma_{\mathrm{c}}$ and $\lambda \equiv \sigma_{\mathrm{h}}/\alpha + \sigma_{\mathrm{c}}/(1 - \alpha)$. Let us now study the COP at maximum power of refrigerators based on the MNI model in terms of this mapping.

Assuming that we control either the flux J_1 or the corresponding thermodynamic force X_1, the maximum cooling power ensues from the formula $\partial J_2 / \partial J_1 = 0$ (or, equivalently, $\partial J_2 / \partial X_1 = 0$). We obtain the following values of model parameters at maximum cooling power [25]:

$$
\frac{1}{J_1^*} = \frac{2\gamma_{\mathrm{c}} L_{11}}{L_{21}}, \quad \text{(A9)}
$$

$$
J_2^* = \frac{L_{21}^2}{4\gamma_{\mathrm{c}} L_{11}^2}, \quad \text{(A10)}
$$

$$
\frac{J_2^*}{J_3^* - J_2^*} = \frac{\varepsilon_{\mathrm{C}}}{2 + (1 + \gamma)\varepsilon_{\mathrm{C}}}, \quad \text{(A11)}
$$

where the last expression describes the COP at maximum power. Substituting the mapping (A6)–(A8) into (A9)–(A11), we reproduce Eqs. (7)–(9) corresponding to power in the LD model optimized only with respect to the duration of the isothermal branches, t_{i}. These expressions thus still depend on the distribution of t_{i} between the two isotherms, α [16,58]. In order to get the final results (12)–(14) for COP at maximum power in the LD refrigerator, one thus just needs to further optimize the power (A9) with respect to α. This also holds for maximum COP at fixed cooling power and all other figures of merit. Indeed, substituting the mapping (A7)–(A8) into Eq. (17) in Ref. [25] for maximum COP at given power for MNI refrigerators and optimizing the resulting expression with respect to α, one obtains our results for the maximum COP at fixed power for LD refrigerators, described in Sec. V.

To conclude, LD models can exactly be mapped to MNI models with tight coupling if the latter are further optimized with respect to the additional parameter α. However, to the best of our knowledge, this possibility is usually overlooked [15–17,25]. One exception where both models always give the same results is bounds on performance, obtained by taking the limits $\sigma \to 0$ and ∞ (or, equivalently, $\gamma \to 0$ and ∞). The reason is that the dependence of the mapping on α is lost during the limiting process.

[1] H. B. Callen, *Thermodynamics and An Introduction to Thermostatistics*, 2nd ed. (Wiley, New York, 1985).

[2] V. Holubec and A. Ryabov, Diverging, but negligible power at Carnot efficiency: Theory and experiment, Phys. Rev. E **96**, 062107 (2017).

[3] J. Yvon, Saclay reactor: Acquired knowledge by two years experience in heat transfer using compressed gas, Report No. CEA-R–435, Geneva, Switzerland (IAEA, Vienna, Austria, 1955), p. 36.

[4] P. Chambadal, *Les Centrales Nucleaires* (Armand Colin, Paris, 1957).

[5] I. I. Novikov, The efficiency of atomic power stations (a review), J. Nucl. Energy (1954) **7**, 125 (1958).

[6] F. L. Curzon and B. Ahlborn, Efficiency of a Carnot engine at maximum power output, Am. J. Phys. **43**, 22 (1975).

[7] M. H. Rubin and B. Andresen, Optimal staging of endoreversible heat engines, J. Appl. Phys. **53**, 1 (1982).

[8] J. Chen and Z. Yan, Unified description of endoreversible cycles, Phys. Rev. A **39**, 4140 (1989).

[9] M. Esposito, R. Kawai, K. Lindenberg, and C. Van den Broeck, Efficiency at Maximum Power of Low-Dissipation Carnot Engines, Phys. Rev. Lett. **105**, 150603 (2010).

[10] J. Gonzalez-Ayala, J. Guo, A. Medina, J. M. M. Roco, and A. C. Hernández, Energetic Self-Optimization Induced by Stability in Low-Dissipation Heat Engines, Phys. Rev. Lett. **124**, 050603 (2020).

[11] Y. Wang, M. Li, Z. Tu, A. C. Hernández, and J. M. M. Roco, Coefficient of performance at maximum figure of merit and its bounds for low-dissipation Carnot-like refrigerators, Phys. Rev. E **86**, 011127 (2012).

[12] C. Van den Broeck, Thermodynamic Efficiency at Maximum Power, Phys. Rev. Lett. **95**, 190602 (2005).

[13] G. Benenti, K. Saito, and G. Casati, Thermodynamic Bounds on Efficiency for Systems with Broken Time-Reversal Symmetry, Phys. Rev. Lett. **106**, 230602 (2011).

[14] Y. Izumida and K. Okuda, Work Output and Efficiency at Maximum Power of Linear Irreversible Heat Engines Operating with a Finite-Sized Heat Source, Phys. Rev. Lett. **112**, 180603 (2014).

[15] Y. Izumida, K. Okuda, J. M. M. Roco, and A. C. Hernández, Heat devices in nonlinear irreversible thermodynamics, Phys. Rev. E **91**, 052140 (2015).

[16] Y. Izumida and K. Okuda, Efficiency at maximum power of minimally nonlinear irreversible heat engines, EPL **97**, 10004 (2012).

[17] Y. Izumida, K. Okuda, A. C. Hernández, and J. Roco, Coefficient of performance under optimized figure of merit in minimally nonlinear irreversible refrigerator, EPL **101**, 10005 (2013).

[18] R. Uzdin and R. Kosloff, Universal features in the efficiency at maximal work of hot quantum Otto engines, EPL **108**, 40001 (2014).

[19] O. Abah, J. Rossnagel, G. Jacob, S. Deffner, F. Schmidt-Kaler, K. Singer, and E. Lutz, Single-Ion Heat Engine at Maximum Power, Phys. Rev. Lett. **109**, 203006 (2012).

[20] J. Roßnagel, O. Abah, F. Schmidt-Kaler, K. Singer, and E. Lutz, Nanoscale Heat Engine Beyond the Carnot Limit, Phys. Rev. Lett. **112**, 030602 (2014).

[21] T. Schmiedl and U. Seifert, Efficiency at maximum power: An analytically solvable model for stochastic heat engines, EPL **81**, 20003 (2007).

[22] D. Segal, Stochastic Pumping of Heat: Approaching the Carnot Efficiency, Phys. Rev. Lett. **101**, 260601 (2008).

[23] C. Jarzynski and O. Mazonka, Feynman's ratchet and pawl: An exactly solvable model, Phys. Rev. E **59**, 6448 (1999).

[24] M. Zhang, Q. Liu, J. He, and J. Wang, Coefficient of performance and its bounds of minimally nonlinear irreversible refrigerator at arbitrary optimal value, Mod. Phys. Lett. B **32**, 1850232 (2018).

[25] R. Long, Z. Liu, and W. Liu, Performance analysis for minimally nonlinear irreversible refrigerators at finite cooling power, Phys. A: Stat. Mech. Appl. **496**, 137 (2018).

[26] V. Holubec and A. Ryabov, Maximum efficiency of low-dissipation heat engines at arbitrary power, J. Stat. Mech. (2016) 073204.

[27] V. Holubec and A. Ryabov, Efficiency at and near maximum power of low-dissipation heat engines, Phys. Rev. E **92**, 052125 (2015).

[28] V. Holubec and A. Ryabov, Erratum: Efficiency at and near maximum power of low-dissipation heat engines, Phys. Rev. E **93**, 059904(E) (2016).

[29] J. Gonzalez-Ayala, M. Santillán, I. Reyes-Ramírez, and A. Calvo-Hernández, Link between optimization and local stability of a low-dissipation heat engine: Dynamic and energetic behaviors, Phys. Rev. E **98**, 032142 (2018).

[30] J. Gonzalez-Ayala, J. Guo, A. Medina, J. M. M. Roco, and A. Calvo Hernández, Optimization induced by stability and the role of limited control near a steady state, Phys. Rev. E **100**, 062128 (2019).

[31] K. Sekimoto and S.-I. Sasa, Complementarity relation for irreversible process derived from stochastic energetics, J. Phys. Soc. Jpn. **66**, 3326 (1997).

[32] P. R. Zulkowski and M. R. DeWeese, Optimal protocols for slowly driven quantum systems, Phys. Rev. E **92**, 032113 (2015).

[33] V. Cavina, A. Mari, and V. Giovannetti, Slow Dynamics and Thermodynamics of Open Quantum Systems, Phys. Rev. Lett. **119**, 050601 (2017).

[34] V. Holubec, S. Steffenoni, G. Falasco, and K. Kroy, Active Brownian heat engines, arXiv:2001.10448 (2020).

[35] I. Martinez, É. Roldán, L. Dinis, D. Petrov, J. Parrondo, and R. A. Rica, Brownian Carnot engine, Nat. Phys. **12**, 67 (2015).

[36] Y.-H. Ma, R.-X. Zhai, C.-P. Sun, and H. Dong, Experimental validation of the $1/\tau$-scaling entropy generation in finite-time thermodynamics with dry air, arXiv:1910.13434 (2019).

[37] V. Holubec, An exactly solvable model of a stochastic heat engine: Optimization of power, power fluctuations and efficiency, J. Stat. Mech. (2014) P05022.

[38] P. Muratore-Ginanneschi and K. Schwieger, Efficient protocols for Stirling heat engines at the micro-scale, EPL **112**, 20002 (2015).

[39] I. Iyyappan and M. Ponmurugan, General relations between the power, efficiency, and dissipation for the irreversible heat engines in the nonlinear response regime, Phys. Rev. E **97**, 012141 (2018).

[40] A. Ryabov and V. Holubec, Maximum efficiency of steady-state heat engines at arbitrary power, Phys. Rev. E **93**, 050101(R) (2016).

[41] Y. Apertet, H. Ouerdane, A. Michot, C. Goupil, and P. Lecoeur, On the efficiency at maximum cooling power, EPL **103**, 40001 (2013).

[42] K. Proesmans, Y. Dreher, M. Gavrilov, J. Bechhoefer, and C. Van den Broeck, Brownian Duet: A Novel Tale of Thermodynamic Efficiency, Phys. Rev. X **6**, 041010 (2016).

[43] M. Campisi and R. Fazio, The power of a critical heat engine, Nat. Commun. **7**, 11895 (2016).

[44] M. Polettini and M. Eposito, Carnot efficiency at divergent power output, EPL **118**, 40003 (2017).

[45] P. Pietzonka and U. Seifert, Universal Trade-Off Between Power, Efficiency, and Constancy in Steady-State Heat Engines, Phys. Rev. Lett. **120**, 190602 (2018).

[46] V. Holubec and A. Ryabov, Cycling Tames Power Fluctuations Near Optimum Efficiency, Phys. Rev. Lett. **121**, 120601 (2018).

[47] C. de Tomás, A. C. Hernández, and J. M. M. Roco, Optimal low symmetric dissipation Carnot engines and refrigerators, Phys. Rev. E **85**, 010104(R) (2012).

[48] Z. Yan and J. Chen, A class of irreversible Carnot refrigeration cycles with a general heat transfer law, J. Phys. D **23**, 136 (1990).

[49] Y. Yuan, R. Wang, J. He, Y. Ma, and J. Wang, Coefficient of performance under maximum χ criterion in a two-level atomic system as a refrigerator, Phys. Rev. E **90**, 052151 (2014).

[50] A. C. Hernández, A. Medina, J. M. M. Roco, J. A. White, and S. Velasco, Unified optimization criterion for energy converters, Phys. Rev. E **63**, 037102 (2001).

[51] C. de Tomas, J. M. M. Roco, A. C. Hernández, Y. Wang, and Z. C. Tu, Low-dissipation heat devices: Unified trade-off optimization and bounds, Phys. Rev. E **87**, 012105 (2013).

[52] R. Long, Z. Liu, and W. Liu, Performance optimization of minimally nonlinear irreversible heat engines and refrigerators under a trade-off figure of merit, Phys. Rev. E **89**, 062119 (2014).

[53] F. Angulo-Brown, An ecological optimization criterion for finite-time heat engines, J. Appl. Phys. **69**, 7465 (1991).

[54] Z. Yan and L. Chen, Optimization of the rate of exergy output for an endoreversible Carnot refrigerator, J. Phys. D **29**, 3017 (1996).

[55] Y. Ust and B. Sahin, Performance optimization of irreversible refrigerators based on a new thermo-ecological criterion, Intl. J. Refrig. **30**, 527 (2007).

[56] R. S. Whitney, Most Efficient Quantum Thermoelectric at Finite Power Output, Phys. Rev. Lett. **112**, 130601 (2014).

[57] R. S. Whitney, Finding the quantum thermoelectric with maximal efficiency and minimal entropy production at given power output, Phys. Rev. B **91**, 115425 (2015).

[58] Y.-H. Ma, D. Xu, H. Dong, and C.-P. Sun, Universal constraint for efficiency and power of a low-dissipation heat engine, Phys. Rev. E **98**, 042112 (2018).

[59] R. Long and W. Liu, Efficiency and its bounds of minimally nonlinear irreversible heat engines at arbitrary power, Phys. Rev. E **94**, 052114 (2016).

[60] A. Dechant, N. Kiesel, and E. Lutz, Underdamped stochastic heat engine at maximum efficiency, EPL **119**, 50003 (2017).

[61] A. C. Hernández, A. Medina, and J. M. M. Roco, Time, entropy generation, and optimization in low-dissipation heat devices, New J. Phys. **17**, 075011 (2015).

[62] V. Blickle and C. Bechinger, Realization of a micrometre-sized stochastic heat engine, Nat. Phys. **8**, 143 (2012).

[63] K. Sekimoto, F. Takagi, and T. Hondou, Carnot's cycle for small systems: Irreversibility and cost of operations, Phys. Rev. E **62**, 7759 (2000).

[64] H. Cardano, *Artis Magnae, sive de regulis algebraicis liber unus* (Iohannem Petreium, Nuremberg, 1545).

[65] P. Abiuso and M. Perarnau-Llobet, Optimal Cycles for Low-Dissipation Heat Engines, Phys. Rev. Lett. **124**, 110606 (2020).

[66] J. Guo, H. Yang, H. Zhang, J. Gonzalez-Ayala, J. M. M. Roco, A. Medina, and A. C. Hernändez, Thermally driven refrigerators: Equivalent low-dissipation three-heat-source model and comparison with experimental and simulated results, Energy Convers. Manag. **198**, 111917 (2019).

Maximum efficiency of low-dissipation heat pumps at given heating load

Zhuolin Ye ⬛[1,*] and Viktor Holubec ⬛[2,†]

[1]*Institut für Theoretische Physik, Universität Leipzig, Postfach 100 920, D-04009 Leipzig, Germany*
[2]*Department of Macromolecular Physics, Faculty of Mathematics and Physics, Charles University,*
V Holešovičkách 2, CZ-180 00 Praha, Czech Republic

We derive an analytical expression for maximum efficiency at fixed power of heat pumps operating along a finite-time reverse Carnot cycle under the low-dissipation assumption. The result is cumbersome, but it implies simple formulas for tight upper and lower bounds on the maximum efficiency and various analytically tractable approximations. In general, our results qualitatively agree with those obtained earlier for endoreversible heat pumps. In fact, we identify a special parameter regime when the performance of the low-dissipation and endoreversible devices is the same. At maximum power, heat pumps operate as work to heat converters with efficiency 1. Expressions for maximum efficiency at given power can be helpful in the identification of more practical operation regimes.

I. INTRODUCTION

Besides the uneasy transfer to carbon-free electricity generation, e.g., by using solar, wind, water, geothermal, fission, and, soon hopefully also fusion power, a possibility to fight global warming is to use more efficient devices. To this end, practical heat engines can already operate at high efficiencies differing from the reversible efficiency by less than a factor of 2 [1]. On the other hand, most state-of-the-art heat pumps can easily decrease energy consumption for heating by a factor of 3 [2], which is still far below their second law theoretical maximum (Carnot) coefficient of performance (COP)

$$\epsilon_C = T_h/(T_h - T_c). \quad (1)$$

For example, a common situation in households with room (target) temperature $T_h \approx 293$ K and heat source temperature $T_c \approx 273$ K corresponds to $\epsilon_C \approx 14.7$, i.e., one joule of electric energy can transfer 14.7 J of heat. The recent raised interest in heat pumps [3–5] is thus fully deserved as already their implementations with current COPs might help to reduce CO_2 emissions [6,7].

It is well known that the maximum COP (1) is attained in heat pumps that operate quasistatically and, similarly as for heat engines [8], their output power (called heating load) is negligibly small. Heat pumps able to heat a household thus have to operate outside the quasistatic limit, in a regime described by finite-time thermodynamics. For heat engines and refrigerators, similar considerations lead to a thorough investigation of their efficiency at maximum power using a variety of models [9–40]. However, idealized models of heat pumps, e.g., based on the endoreversible thermodynamics [41,42], imply diverging maximum power with COP 1. At

maximum power, such heat pumps thus operate as pure work to heat converters, which is a highly undesirable operation regime.

As a result, efficiency at maximum power is for heat pumps not a useful measure of performance. A more informative figure of merit is the maximum efficiency at a given power, which generalizes various trade-off measures between power and efficiency [12,23,43–50]. Maximum efficiency at given power was thoroughly studied for various models of heat engines [30,51–58] and refrigerators [16,40,59]. However, besides numerical studies [60], the only available analytical results for heat pumps were obtained for endoreversible heat pumps [42,61,62].

In this paper, we derive the analytical expression for maximum COP at a given heating load for Carnot-type low-dissipation (LD) heat pumps. In Secs. II and III, we introduce the considered model and define the thermodynamic quantities of interest. In Sec. IV, we discuss the performance of the LD heat pumps operating at maximum power. In Sec. V, we present our main results. Specifically, the lower and upper bounds on maximum COP at a given power for LD heat pumps are derived in Sec. V A. And in Sec. V B, we derive a general expression for the maximum COP together with an analytically tractable approximation. In Sec. VI, we compare the obtained results for maximum COP of LD heat pumps to the known results for endoreversible heat pumps. We conclude in Sec. VII.

II. MODEL

Consider a heat pump operating along the finite-time reverse Carnot cycle depicted in Fig. 1. The cycle consists of two isotherms and two adiabats. During the cold isotherm, the system extracts heat Q_c from the cold bath at temperature T_c. Afterward, during the hot isotherm, it uses the input work W to pump this heat into the hot bath at temperature

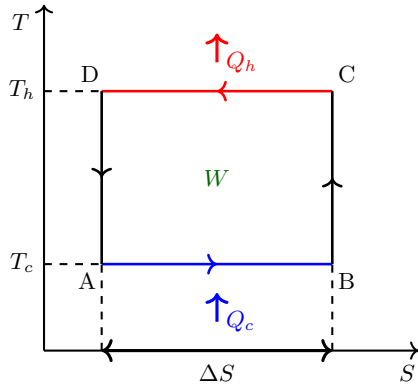*zhuolinye@foxmail.com
†viktor.holubec@mff.cuni.cz

FIG. 1. Bath temperature T-system entropy S diagram of the considered Carnot heat pump cycle. The red (blue) horizontal line denotes the hot (cold) isotherm. The black vertical lines depict the adiabats. Per cycle, the input work W is consumed to pump the heat Q_c from the cold bath at temperature T_c and deliver the heat $Q_h = Q_c + W$ into the hot bath at temperature T_h.

T_h. The resulting heat delivered per cycle into the hot bath, $Q_h = Q_c + W$, consists of the used work and the extracted heat.

In the LD regime [14,63,64], Q_i, $i = c, h$ assume the forms

$$Q_c = T_c \Delta S - \frac{\sigma_c}{t_c}, \tag{2}$$

$$Q_h = T_h \Delta S + \frac{\sigma_h}{t_h}, \tag{3}$$

where the positive irreversibility parameters σ_i depend on the details of system construction, and t_i are durations of the two isotherms. ΔS denotes the increase (decrease) in the entropy of the system during the cold (hot) isotherm. The corresponding contributions to Q_c and Q_h are reversible, i.e., they do not contribute to the total entropy produced per cycle,

$$\Delta S_{\text{tot}} = -\frac{Q_c}{T_c} + \frac{Q_h}{T_h} = \frac{\sigma_c}{t_c T_c} + \frac{\sigma_h}{t_h T_h} \geqslant 0. \tag{4}$$

ΔS_{tot} is thus solely determined by the irreversible contributions, proportional to the irreversibility parameters, and vanishes both in the quasistatic limit, $t_h \to \infty$ and $t_c \to \infty$, and in the equilibrium limit, $\sigma_c = \sigma_h = 0$. The LD forms (2) and (3) of the transferred heats can be quite generally considered as first-order expansions of the exact expressions in the inverse durations of the isotherms [63,65–69]. In addition, the LD model is exact for optimized overdamped Brownian heat engines [1,27] and other specific scenarios [66,70].

We assume that durations of the adiabatic branches are proportional to durations of the isotherms so that the cycle time is given by $t_p = a(t_h + t_c)$. Since the constant $a \geqslant 1$ only affects the heating load of the pump [see Eq. (5)], we assume in the rest of the paper that $a = 1$. This value corresponds to infinitely fast adiabats [71] and thus maximum heating load as a function of a.

III. HEATING LOAD AND COP

The performance of heat devices is described by their power, P, and efficiency, ϵ. For heat pumps, P and ϵ are called

heating load and COP [60,72]. P measures the average heat pumped into the hot bath per unit time, and ϵ shows how much work is needed to pump 1 J of heat to the hot body.

Using Eqs. (2) and (3) together with the first law of thermodynamics, $W = Q_h - Q_c$, the heating load and COP of the LD heat pump can be expressed as

$$P = \frac{Q_h}{t_p} = \frac{T_h \Delta S}{t_p} + \frac{\sigma_h}{t_h t_p}, \tag{5}$$

$$\epsilon = \frac{Q_h}{W} = \frac{\epsilon_C}{1 + T_c \epsilon_C \Delta S_{\text{tot}}/(P t_p)}. \tag{6}$$

The maximum (Carnot) COP, $\epsilon = \epsilon_C$, is attained under reversible conditions ($\Delta S_{\text{tot}} = 0$). The minimum COP, $\epsilon = 1$, describes the situation when no heat is pumped from the cold bath and thus the delivered heat, Q_h, equals the input work, W. In this regime, heat pumps are not better than work-to-heat converters, such as resistance heating wires. In the next section, we study COP at maximum heating load for LD heat pumps.

IV. COP AT MAXIMUM HEATING LOAD

Most of the available expressions for maximum efficiency at a fixed power for various models [16,30,40,51,54–59] are given as functions of the dimensionless variable P/P^*, measuring loss in power, P, with respect to the maximum power, P^*. This normalization of power usually significantly simplifies the resulting expressions. However, for endoreversible heat pumps [41,42] the maximum power diverges, suggesting that such a normalization might, in our case, not be possible. Indeed, we show below that $P^* \to \infty$ also for LD heat pumps.

To introduce a meaningful dimensionless heating load, we define the reduced heats and durations as

$$\tilde{Q}_i = \frac{Q_i}{T_h \Delta S}, \quad \tilde{t}_i = \frac{T_h \Delta S}{\sigma_h} t_i, \quad i = c, h. \tag{7}$$

Using Eqs. (2) and (3), the reduced heats read

$$\tilde{Q}_c = \frac{\epsilon_C - 1}{\epsilon_C} - \frac{1}{\sigma(1-\alpha)\tilde{t}_p}. \tag{8}$$

$$\tilde{Q}_h = 1 + \frac{1}{\alpha \tilde{t}_p}. \tag{9}$$

Here, $\sigma = \sigma_h/\sigma_c$ is the so-called irreversibility ratio, $\tilde{t}_p = \tilde{t}_h + \tilde{t}_c$ denotes the reduced cycle duration, and $\alpha \equiv t_h/t_p$ measures the allocation of the cycle duration between the two isotherms. We define the reduced heating load as the ratio of the reduced heat to the reduced cycle duration:

$$\tilde{P} = \frac{\tilde{Q}_h}{\tilde{t}_p} = \frac{1}{\tilde{t}_p} + \frac{1}{\alpha \tilde{t}_p^2} = \frac{\sigma_h}{(T_h \Delta S)^2} P. \tag{10}$$

The reduced heating load is a monotonically decreasing function of both α and $\tilde{t}_p$. The inequality $Q_h > Q_c > 0$, following from the requirement that the considered device pumps heat from the cold to the hot bath, restricts the minimal reduced cycle duration as

$$\tilde{t}_p > \frac{\epsilon_C}{\sigma(\epsilon_C - 1)(1 - \alpha)}. \tag{11}$$

The maximum reduced heating load, $\tilde{P}^*$, attained for the minimal allowed values of α and $\tilde{t}_p$,

$$\alpha^* = 0, \tag{12}$$

$$\tilde{t}_p^* = \frac{\epsilon_C}{\sigma(\epsilon_C - 1)}, \tag{13}$$

hence diverges. The corresponding COP is most easily obtained from the formula $\epsilon = \tilde{Q}_h/(\tilde{Q}_h - \tilde{Q}_c)$. Altogether, the maximum reduced heating load and the corresponding COP read

$$\tilde{P}^* = \infty, \tag{14}$$

$$\epsilon^* = 1. \tag{15}$$

This performance is achieved whenever the hot isotherm is much faster than the cold one and thus $\alpha = \alpha^* \to 0$. Noteworthy, the COP at maximum power is the smallest possible, corresponding to the negligible amount of heat pumped from the cold bath compared to the input work, $\tilde{Q}_h = \tilde{W} + \tilde{Q}_c \gg \tilde{Q}_c$. A heat pump operating at the maximum heating load thus works as an electric heater transforming work in the form of electric energy into heat. Practical heat pumps should not operate anywhere close to this regime. In the next section, we uncover more practical operation regimes of LD heat pumps by deriving their maximum COP at a given heating load.

V. MAXIMUM COP AT GIVEN HEATING LOAD

Fixing the reduced heating load in Eq. (10) creates the dependency

$$\alpha = \frac{1}{\tilde{t}_p(\tilde{P}\tilde{t}_p - 1)} \tag{16}$$

between $\alpha \in [0, 1]$ and $\tilde{t}_p$. Substituting Eq. (16) into Eqs. (8) and (9) and using the condition $\tilde{Q}_h > \tilde{Q}_c > 0$, we find the inequality

$$\tilde{t}_p > \frac{1 + \tilde{P}\tilde{t}_p^*}{2\tilde{P}} + \sqrt{\left(\frac{1 + \tilde{P}\tilde{t}_p^*}{2\tilde{P}}\right)^2 + \frac{1 - \tilde{t}_p^*}{\tilde{P}}} \equiv \tilde{t}_{p,\min}. \tag{17}$$

The minimum value of the reduced cycle duration for fixed heating load, $\tilde{t}_{p,\min}$, thus depends on the irreversibility ratio σ and the Carnot COP ϵ_C via $\tilde{t}_p^*$ in Eq. (13). For maximum and minimum values of σ, $\tilde{t}_{p,\min}$ reads

$$\tilde{t}_{p,\min} = \begin{cases} \frac{1+\sqrt{1+4\tilde{P}}}{2\tilde{P}} & \text{for} \quad \sigma \to \infty \\ \infty & \text{for} \quad \sigma \to 0. \end{cases} \tag{18}$$

The COP (6) can be written in terms of the reduced parameters introduced above as

$$\epsilon = \left[1 + \frac{\tilde{P}\tilde{t}_p - 1}{\sigma\tilde{P}\tilde{t}_p(\tilde{P}\tilde{t}_p^2 - \tilde{t}_p - 1)} - \frac{\epsilon_C - 1}{\tilde{P}\tilde{t}_p\epsilon_C}\right]^{-1}. \tag{19}$$

Below we will find its maximum as a function of $\tilde{t}_p > \tilde{t}_{p,\min}$.

A. Bounds

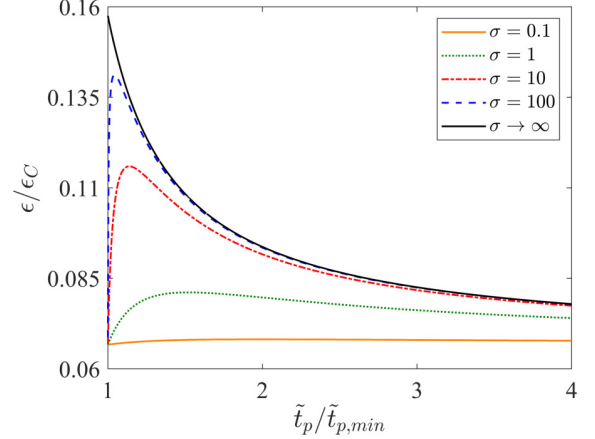First, we determine the upper and lower bounds on the maximum COP at a given heating load. Taking the derivative

FIG. 2. COP (19) as a function of $\tilde{t}_p/\tilde{t}_{p,\min}$ (17) for different values of σ, $\tilde{P} = 1$, and $\epsilon_C = 15$. The figure shows that the upper bound (21) on the optimal COP is obtained for $\sigma \to \infty$.

of ϵ (19) with respect to σ, one finds that $\partial\epsilon/\partial\sigma > 0$ and thus ϵ monotonically increases with σ. Physically, this is because the COP in Eq. (6) is for a fixed P and σ_h (fixed by our choice of time unit) a monotonically decreasing function of the entropy production, ΔS_{tot}, and thus σ_c. The lower bound on COP (19) for a fixed P is thus attained if the irreversible losses during the hot isotherm are negligible compared to those during the cold one ($\sigma = \sigma_h/\sigma_c \to 0$). The corresponding COP equals 1. Note that due to the condition (17) the reduced cycle duration $\tilde{t}_p$ in this regime diverges [cf. Eq. (18)].

The upper bound on COP (19) for a fixed P is attained if irreversible losses during the cold isotherm are negligible compared to those during the hot one ($\sigma \to \infty$). In this regime, the COP,

$$\epsilon = \left(1 - \frac{\epsilon_C - 1}{\tilde{P}\tilde{t}_p\epsilon_C}\right)^{-1}, \tag{20}$$

monotonically decreases with $\tilde{t}_p$ and thus it attains its maximum for $\tilde{t}_p = \tilde{t}_{p,\min} = (1 + \sqrt{1 + 4\tilde{P}})/(2\tilde{P})$. Altogether, the bounds on the maximum COP at given heating load, $\epsilon^{\text{opt}} = \epsilon^{\text{opt}}(\tilde{P})$, are given by

$$1 \leqslant \epsilon^{\text{opt}} \leqslant \frac{(1 + \sqrt{1 + 4\tilde{P}})\epsilon_C}{2 - (1 - \sqrt{1 + 4\tilde{P}})\epsilon_C} \equiv \epsilon_>^{\text{opt}}. \tag{21}$$

As expected, the upper bound, $\epsilon_>^{\text{opt}}$, converges to ϵ_C for $\tilde{P} \to 0$ and to 1 for $\tilde{P} \to \infty$.

B. Arbitrary parameters

Outside the limiting regimes discussed in the previous section, the optimization of COP (19) for a fixed P is more complicated. In Fig. 2, we show ϵ as a function of $\tilde{t}_p/\tilde{t}_{p,\min}$ for five values of σ. The black solid line for $\sigma \to \infty$ indeed monotonously decreases with $\tilde{t}_p$. However, for an arbitrary finite σ, the COP exhibits a global maximum for $\tilde{t}_p^{\text{opt}} > \tilde{t}_{p,\min}$. Its position follows from the condition $\partial\epsilon/\partial\tilde{t}_p|_{\tilde{t}_p=\tilde{t}_p^{\text{opt}}} = 0$, which implies the quartic equation

$$\tilde{t}_p^4 + a\tilde{t}_p^3 + b\tilde{t}_p^2 + c\tilde{t}_p + \frac{c}{2} = 0, \quad \tilde{t}_p = \tilde{t}_p^{\text{opt}}, \tag{22}$$

with the coefficients

$$\begin{pmatrix} a \\ b \\ c \end{pmatrix} = \frac{1}{\tilde{P}^2} \begin{pmatrix} -2\tilde{P} - 2\tilde{P}^2 \tilde{t}_p^* \\ 1 - 2\tilde{P} + 4\tilde{P}\tilde{t}_p^* \\ 2 - 2\tilde{t}_p^* \end{pmatrix}. \qquad (23)$$

Equation (22) has four roots which can be determined analytically using Ferrari's method. The optimal reduced cycle duration is given by the largest real-valued root:

$$\tilde{t}_p^{\text{opt}}(\tilde{P}, \tilde{t}_p^*) = -\frac{a}{4} + F + \frac{1}{2}\sqrt{-2C - 4F^2 - \frac{D}{F}}, \qquad (24)$$

where

$$A = b^2 + 3c(2 - a), \qquad (25)$$

$$B = 2b^3 - 9bc(4 + a) + \frac{27c}{2}(a^2 + 2c), \qquad (26)$$

$$C = b - \frac{3a^2}{8}, \qquad (27)$$

$$D = \frac{a^3}{8} - \frac{ab}{2} + c, \qquad (28)$$

$$E = \sqrt[3]{\frac{B + \sqrt{B^2 - 4A^3}}{2}}, \qquad (29)$$

$$F = \frac{\sqrt{3}}{6}\sqrt{\frac{A}{E} + E - 2C}. \qquad (30)$$

For a fixed $\tilde{P}$, the reduced optimal cycle duration only depends on $\tilde{t}_p^*$ in Eq. (13). Inserting $\tilde{t}_p^{\text{opt}}$ into Eq. (19) yields the maximum COP at given heating load for the LD heat pump, $\epsilon^{\text{opt}} = \epsilon^{\text{opt}}(\tilde{P}, \sigma, \epsilon_C)$.

In Fig. 3, we show ϵ^{opt}, $\tilde{t}_p^{\text{opt}}$, and $\alpha^{\text{opt}} = [\tilde{t}_p^{\text{opt}}(\tilde{P}\tilde{t}_p^{\text{opt}} - 1)]^{-1}$ [see Eq. (16)] as functions of $\tilde{P}$ for five values of σ. The exact theoretical results are depicted by solid lines. We checked that they agree within numerical precision with the optimal COP obtained by the direct numerical maximization of ϵ in Eq. (19). In agreement with the inequalities (21), ϵ^{opt} in Fig. 3(a) converges to 1 for $\tilde{P} \to \infty$ and to ϵ_C for $\tilde{P} \to 0$ (see the inset) for all σ. This panel also shows the monotonic increase of ϵ^{opt} with σ discussed in Sec. V A. The increase of the maximum COP with decreasing heating load for large $\tilde{P}$ is very slow, showing that reasonably efficient heat pumps have to operate at small values of $\tilde{P}$. In this respect, heat pumps qualitatively differ from heat engines and refrigerators, which exhibit large gains in efficiency when their power is slightly decreased from its maximum value [16,58].

The σ- dependency of $\tilde{t}_p^{\text{opt}}$ in Fig. 3(b) is significant for small values of σ but negligible for large σ. Even though the σ dependency of α^{opt} in Fig. 3(c) is always significant, the COP in Eq. (19) no longer depends on α. This suggests that we might obtain an analytically tractable approximation for ϵ^{opt}, valid for intermediate and large values of σ, by expanding $\tilde{t}_p^{\text{opt}}$ in powers of $\tilde{t}_p^* \sim 1/\sigma$. Up to the leading order in $\tilde{t}_p^*$, we find

$$\tilde{t}_p^{\text{opt}} \approx \frac{1 + \sqrt{1 + 4\tilde{P}}}{2\tilde{P}} + \frac{\sqrt{\tilde{t}_p^*}}{(1 + 4\tilde{P})^{1/4}}, \qquad (31)$$

$$\epsilon^{\text{opt}} \approx \epsilon_>^{\text{opt}} - \frac{8\tilde{P}(1 - \epsilon_C^{-1})(\epsilon_>^{\text{opt}})^2\sqrt{\tilde{t}_p^*}}{(1 + 4\tilde{P})^{1/4}(1 + \sqrt{1 + 4\tilde{P}})^2}. \qquad (32)$$
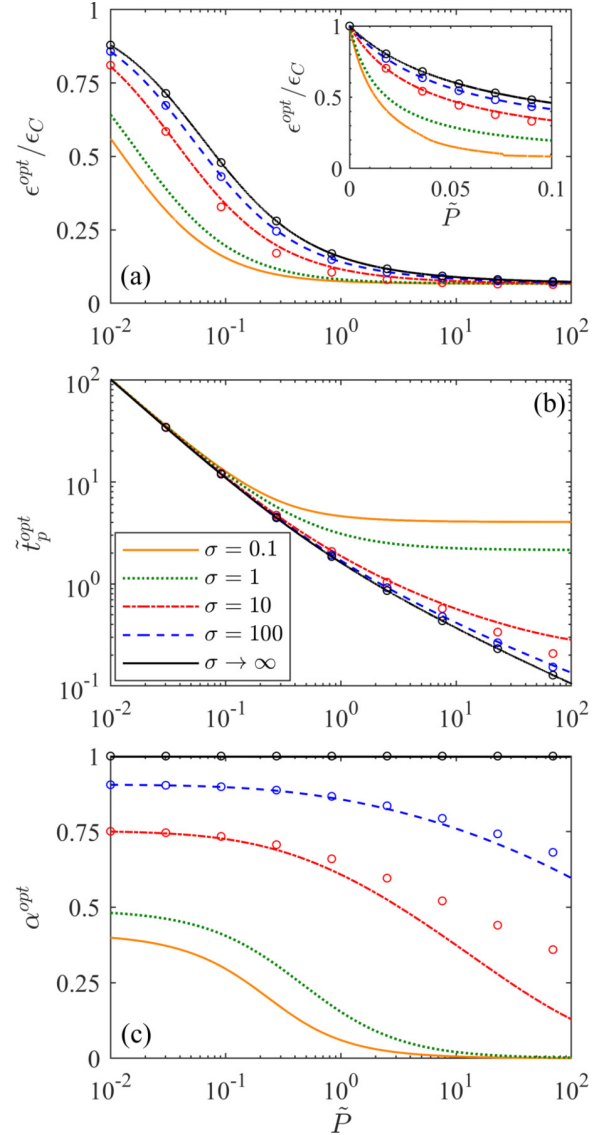

FIG. 3. The optimal COP (a), the corresponding reduced cycle duration (b), and its allocation between hot and cold isotherms (c) as a function of $\tilde{P}$ for different values of σ and $\epsilon_C = 15$. The circles follow from the approximate expressions (31) and (32). The lines were obtained using the exact result (24).

The corrections to these formulas are proportional to $\tilde{t}_p^*$. For large values of $\tilde{t}_p^*$, the approximation (32) leads to negative (thus unphysical) COP. Circles in Fig. 3 show the predictions from the approximate formulas for $\sigma > 1$, when the approximate $\epsilon^{\text{opt}} > 0$. For large values of σ (small $\tilde{t}_p^*$), the approximate (circles) and exact (lines) results indeed perfectly overlap.

VI. COMPARISON WITH ENDOREVERSIBLE HEAT PUMPS

Let us now compare the obtained results on maximum COP at a given heating load of LD heat pumps to the corresponding known results for endoreversible heat pumps [42,61,62]. The endoreversible thermodynamics assumes that the working

fluid of thermal devices operates reversibly. The only considered sources of entropy production are the finite-time heat transfers between thermal reservoirs and the working fluid [73–75]. LD models generally describe the thermodynamics of slowly driven systems [14,63,64]. On the other hand, up to a few exceptions [76–78], the endoreversible models are usually phenomenological [10,11,75,79,80].

The works [42,61] on the maximum COP at a given heating load of endoreversible heat pumps assume that the heat transfers between the working fluid and baths obey Newton's law of cooling. Denoting the temperatures of the working fluid during the hot and cold isotherms by T_{hw} and T_{cw} and the corresponding heat conductivities as κ_h and κ_c, the heats transferred during the isotherms are in this case given by

$$Q_h = \kappa_h t_h (T_{hw} - T_h), \qquad (33)$$

$$Q_c = \kappa_c t_c (T_c - T_{cw}). \qquad (34)$$

More general heat transfer laws used in Ref. [62] lead to qualitatively the same results as Newton's law of cooling, to which we stick in the following discussion.

In the endorevesible models, the COP $\varepsilon_{en} = Q_h/(Q_h - Q_c)$ is maximized with respect to the temperatures of the working fluid T_{hw} and T_{cw}. The ratio t_h/t_c of the durations of the two isotherms is determined by the endoreversibility requirement $Q_h/T_{hw} - Q_c/T_{cw} = 0$ and the total cycle duration does not influence the resulting expressions. Performing the maximization for a fixed heating load $P = Q_h/(t_h + t_c)$ with the definitions (33) and (34) yields the maximum COP [42,62]

$$\epsilon_{en}^{opt} = 1 + \frac{\epsilon_C - 1}{1 + \epsilon_C P(1 + \sqrt{r})^2/(\kappa_h T_h)}, \qquad (35)$$

where $r = \kappa_h/\kappa_c$. The maximum COP at fixed heating load thus behaves qualitatively in the same way as the corresponding result for LD heat pumps: ϵ_{en}^{opt} converges to ϵ_C for $P \to 0$ and to 1 for $P \to \infty$. However, the precise functional forms of the maximum COP for LD and endoreversible heat pumps in general differ. The exception is the parameter regime

$$\tilde{t}_p^* = 1, \quad \frac{(1 + \sqrt{r})^2}{\kappa_h} = \frac{4\sigma_h}{T_h \Delta S^2}, \qquad (36)$$

when the expressions for ϵ_{en}^{opt} and ϵ^{opt} are identical. In this regime, one can thus find an exact mapping between the LD and the endoreversible model. Note that for $\tilde{t}_p^* = 1$, Eq. (22) reduces to a quadratic equation, and Eq. (13) implies $\sigma_h/T_h = \sigma_c/T_c$.

One way to show that the two models are equivalent only in the parameter regime (36) is to compare the formulas for ϵ_{en}^{opt} and ϵ^{opt} in the limiting regimes, where they become simple. To this end, we expand the two maximum COPs as functions of the heating load close to infinite and close to vanishing P. Up to the leading order in P, the expansions read

$$\epsilon^{opt} \approx 1 + \frac{1 - \epsilon_C^{-1}}{4\tilde{t}_p^*} \frac{(T_h \Delta S)^2}{\sigma_h P}, \qquad (37)$$

$$\epsilon_{en}^{opt} \approx 1 + \frac{1 - \epsilon_C^{-1}}{(1 + \sqrt{r})^2} \frac{\kappa_h T_h}{P}, \qquad (38)$$
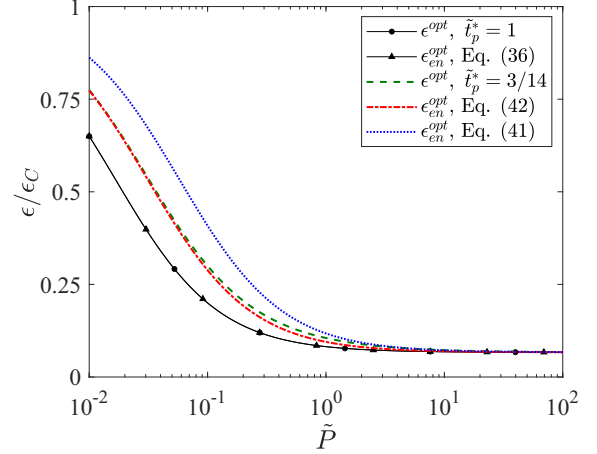

FIG. 4. The maximum COPs at fixed heating load for LD (ϵ^{opt}) and endoreversible (ϵ_{en}^{opt}) heat pumps as functions of $\tilde{P}$ for $\epsilon_C = 15$ and $\sigma_h/(T_h \Delta S)^2 = 1/(\kappa_h T_h)$. The marked black solid lines show that the condition (36) implies $\epsilon^{opt} = \epsilon_{en}^{opt}$. For the remaining lines, we set $\sigma = 5$ and thus $\tilde{t}_p^* = 3/14$. The blue dotted line corresponds to r obtained from Eq. (41). For the red dash-dotted line, we calculated r using Eq. (42).

and

$$\epsilon^{opt} \approx \epsilon_C - \epsilon_C(\epsilon_C - 1)(1 + \sqrt{\tilde{t}_p^*})^2 \frac{\sigma_h P}{(T_h \Delta S)^2}, \qquad (39)$$

$$\epsilon_{en}^{opt} \approx \epsilon_C - \epsilon_C(\epsilon_C - 1)(1 + \sqrt{r})^2 \frac{P}{\kappa_h T_h}. \qquad (40)$$

The corrections to Eqs. (37) and (38) are proportional to $1/P^2$ and those to (39) and (40) are proportional to P^2. The LD and endoreversible models for heat pumps can be mapped to each other only if the two types of expansions agree, leading to the conditions

$$\frac{(1 + \sqrt{r})^2}{\kappa_h} = \frac{\sigma_h}{T_h \Delta S^2} 4\tilde{t}_p^*, \qquad (41)$$

$$\frac{(1 + \sqrt{r})^2}{\kappa_h} = \frac{\sigma_h}{T_h \Delta S^2}(1 + \sqrt{\tilde{t}_p^*})^2. \qquad (42)$$

The first equality follows from Eqs. (37) and (38) and the second one from Eqs. (39) and (40). Requiring validity of both yields the condition (36) (see Appendix A for more details). In Fig. 4, we show ϵ^{opt} and ϵ_{en}^{opt} as functions of the reduced heating load $\tilde{P}$. The marked lines show the agreement of ϵ^{opt} and ϵ_{en}^{opt} when Eq. (36) holds and thus $\tilde{t}_p^* = 1$. The remaining lines show ϵ^{opt} (green dashed line) and ϵ_{en}^{opt} for parameters obeying solely Eq. (41) (blue dotted line) and (42) (red dash-dotted line) for $\tilde{t}_p^* = 3/14$. As expected, the green dashed line only agrees with the blue dotted line for large values of $\tilde{P}$ and with the red dash-dotted line for small values of $\tilde{P}$.

We tested that also the LD and endoreversible models for heat engines and refrigerators lead to identical results when Eq. (36) holds (data not shown). In addition, an equivalent condition was derived in the linear response regime for heat engines operating at maximum power [52,53].

VII. CONCLUSION AND OUTLOOK

Like endoreversible heat pumps, Carnot-type LD heat pumps operate at maximum power as work to heat converters such as standard electric heaters. Practical heat pumps thus should not operate in this regime. To provide a tool to decide a suitable regime of operation for a given application, we derived an analytical expression for maximum efficiency at a given heating load for LD heat pumps. In addition, we derived upper and lower bounds on this quantity. Qualitatively, our results agree with the corresponding findings obtained earlier for endoreversible heat pumps. Unlike the phenomenological endoreversible models, LD models represent a general first-order finite-time correction to the reversible operation and thus their parameters can be either calculated using a perturbation analysis or measured in experiments. Furthermore, the derived upper bound on the maximum efficiency can be considered as a loose upper bound on the efficiency of heat pumps in general. By adding the result for heat pumps to the known formulas for LD heat engines and refrigerators [16,58,59], the present paper completes the collection of results for maximum efficiency at a given power for LD thermal devices.

The presented result for maximum efficiency at a given heating load depends on the reduced heating load $\tilde{P}$ in Eq. (10). Therefore, the heating load can be further optimized for the chosen unit of energy flux without affecting the corresponding maximum efficiency. Such optimization tasks performed for LD heat engines and refrigerators are described in Refs. [81,82]. In addition, it would be interesting to investigate the operation regime of maximum efficiency at given power for LD thermal devices concerning its dynamical stability [15,83–85]. Finally, it would be worthy to investigate maximum efficiency at given power for heat devices operating between finite-sized heat sources [19,86–90] and compare the results to those derived using the idealized LD models. For heat engines working with two finite-sized reservoirs, the maximum efficiency at given power has been derived in Ref. [90].

ACKNOWLEDGMENTS

APPENDIX: HEAT FLOWS IN THE PARAMETER REGIME (36)

In this Appendix, we investigate the physical significance of the parameter regime (36), leading to the same expressions for ϵ_{en}^{opt} and ϵ^{opt} for the endoreversible and LD models. As the average heat flows Q_h/t_p are for the two models fixed to be the same value of power P, we focus on the structure of the average heat flows Q_c/t_p.

For the endoreversible heat pump, combining Eqs. (33) and (34), together with the endoreversibility condition $Q_h^{en}/T_{hw} - Q_c^{en}/T_{cw} = 0$ yields (here and below we use the superscript "en" to distinguish between the heats for the endoreversible and LD models)

$$\frac{Q_c^{en}}{t_p} = \frac{T_c P[P + \kappa_h(T_h - T_{hw})]}{rP(T_h - T_{hw}) + T_{hw}[P + \kappa_h(T_h - T_{hw})]}. \quad (A1)$$

For the LD heat pump, inserting Eq. (16) into Eq. (8) implies

$$\frac{Q_c}{t_p} = \frac{T_c T_h \Delta S^2}{\sigma_h} \frac{\tilde{P}\tilde{t}_p^2 - \tilde{t}_p(1 + \tilde{P}\tilde{t}_p^*) + \tilde{t}_p^* - 1}{\tilde{t}_p(\tilde{P}\tilde{t}_p^2 - \tilde{t}_p - 1)}. \quad (A2)$$

Imposing the condition (36) and returning to dimensional power (10), the heat flow for the LD model changes to

$$\frac{Q_c}{t_p} = \frac{4\kappa_h T_c}{(\sqrt{r} + 1)^2} \frac{P(\sqrt{r} + 1)^2(\tilde{t}_p - 1) - 4\kappa_h T_h}{P(\sqrt{r} + 1)^2 \tilde{t}_p^2 - 4\kappa_h T_h(\tilde{t}_p + 1)}. \quad (A3)$$

Interestingly, the functional forms of the heat flows (A1) and (A3) in terms of power P and the parameter to be optimized (T_{hw} for the endoreversible and $\tilde{t}_p$ for the LD model) are different, even though the analysis in the main text proves that they must be the same functions of power when T_{hw} and t_p are substituted by the values

$$T_{hw} = T_h + \frac{(1 + \sqrt{r})P}{\kappa_h}, \quad (A4)$$

$$\tilde{t}_p = 2 + \frac{4\kappa_h T_h}{(\sqrt{r} + 1)^2 P}, \quad (A5)$$

maximizing the two heat flows and thus, for fixed power, also the COP (6). The formulas for the two heat flows remain different even after the substitutions $T_{hw} = (1 + \sqrt{r})T/\kappa_h$ and $\tilde{t}_p = 2 + 4\kappa_h T_h/[(\sqrt{r} + 1)^2 T]$, which lead to expressions $\tilde{Q}_c^{en}(T, P)/t_p$ and $\tilde{Q}_c(T, P)/t_p$ exhibiting the same maximum,

$$\frac{\tilde{Q}_c^{en}}{t_p} = \frac{\tilde{Q}_c}{t_p} = \frac{\kappa_h T_c P}{\kappa_h T_h + P(1 + \sqrt{r})^2}, \quad (A6)$$

for the same value of $T = P$. The expressions $\tilde{Q}_c^{en}(T, P)/t_p$ and $\tilde{Q}_c(T, P)/t_p$ are thus different unless $T = P$. We conclude that there is no deep physical reason why the performances of the optimized endoreversible and LD models are the same in the parameter regime (36).

[1] V. Holubec and A. Ryabov, Efficiency at and near maximum power of low-dissipation heat engines, Phys. Rev. E **92**, 052125 (2015).

[2] A. Ammar, K. Sopian, M. Alghoul, B. Elhub, and A. Elbreki, Performance study on photovoltaic/thermal solar-assisted heat pump system, J. Therm. Anal. Calorim. **136**, 79 (2019).

[3] K. J. Chua, S. K. Chou, and W. Yang, Advances in heat pump systems: A review, Appl. Energy **87**, 3611 (2010).

[4] M. Mohanraj, L. Karthick, and R. Dhivagar, Performance and economic analysis of a heat pump water heater assisted regenerative solar still using latent heat storage, Appl. Therm. Eng. **196**, 117263 (2021).

[5] Y. Hu and D. P. Yuill, Effects of multiple simultaneous faults on characteristic fault detection features of a heat pump in cooling mode, Energy Build. **251**, 111355 (2021).

[6] L. Aye, R. Fuller, and A. Canal, Evaluation of a heat pump system for greenhouse heating, Int. J. Therm. Sci. **49**, 202 (2010).

[7] B. Hong and R. W. Howarth, Greenhouse gas emissions from domestic hot water: Heat pumps compared to most commonly used systems, Energy Sci. Eng. **4**, 123 (2016).

[8] V. Holubec and A. Ryabov, Diverging, but negligible power at Carnot efficiency: Theory and experiment, Phys. Rev. E **96**, 062107 (2017).

[9] J. Gordon and V. N. Orlov, Performance characteristics of endoreversible chemical engines, J. Appl. Phys. **74**, 5303 (1993).

[10] M. H. Rubin and B. Andresen, Optimal staging of endoreversible heat engines, J. Appl. Phys. **53**, 1 (1982).

[11] J. Chen and Z. Yan, Unified description of endoreversible cycles, Phys. Rev. A **39**, 4140 (1989).

[12] Y. Apertet, H. Ouerdane, A. Michot, C. Goupil, and P. Lecoeur, On the efficiency at maximum cooling power, Europhys. Lett. **103**, 40001 (2013).

[13] Y. Hu, F. Wu, Y. Ma, J. He, J. Wang, A. C. Hernández, and J. M. M. Roco, Coefficient of performance for a low-dissipation Carnot-like refrigerator with nonadiabatic dissipation, Phys. Rev. E **88**, 062115 (2013).

[14] M. Esposito, R. Kawai, K. Lindenberg, and C. Van den Broeck, Efficiency at Maximum Power of Low-Dissipation Carnot Engines, Phys. Rev. Lett. **105**, 150603 (2010).

[15] J. Gonzalez-Ayala, J. Guo, A. Medina, J. M. M. Roco, and A. C. Hernández, Energetic Self-Optimization Induced by Stability in Low-Dissipation Heat Engines, Phys. Rev. Lett. **124**, 050603 (2020).

[16] V. Holubec and Z. Ye, Maximum efficiency of low-dissipation refrigerators at arbitrary cooling power, Phys. Rev. E **101**, 052124 (2020).

[17] A. C. Hernández, A. Medina, and J. Roco, Time, entropy generation, and optimization in low-dissipation heat devices, New J. Phys. **17**, 075011 (2015).

[18] G. Benenti, K. Saito, and G. Casati, Thermodynamic Bounds on Efficiency for Systems with Broken Time-Reversal Symmetry, Phys. Rev. Lett. **106**, 230602 (2011).

[19] Y. Izumida and K. Okuda, Work Output and Efficiency at Maximum power of Linear Irreversible Heat Engines Operating with a Finite-Sized Heat Source, Phys. Rev. Lett. **112**, 180603 (2014).

[20] C. Van den Broeck, Thermodynamic Efficiency at Maximum Power, Phys. Rev. Lett. **95**, 190602 (2005).

[21] Y. Izumida, K. Okuda, J. M. M. Roco, and A. C. Hernández, Heat devices in nonlinear irreversible thermodynamics, Phys. Rev. E **91**, 052140 (2015).

[22] Y. Izumida and K. Okuda, Efficiency at maximum power of minimally nonlinear irreversible heat engines, Europhys. Lett. **97**, 10004 (2012).

[23] Y. Izumida, K. Okuda, A. C. Hernández, and J. Roco, Coefficient of performance under optimized figure of merit in minimally nonlinear irreversible refrigerator, Europhys. Lett. **101**, 10005 (2013).

[24] R. Uzdin and R. Kosloff, Universal features in the efficiency at maximal work of hot quantum Otto engines, Europhys. Lett. **108**, 40001 (2014).

[25] O. Abah, J. Rossnagel, G. Jacob, S. Deffner, F. Schmidt-Kaler, K. Singer, and E. Lutz, Single-ion Heat Engine at Maximum Power, Phys. Rev. Lett. **109**, 203006 (2012).

[26] J. Roßnagel, O. Abah, F. Schmidt-Kaler, K. Singer, and E. Lutz, Nanoscale Heat Engine beyond the Carnot Limit, Phys. Rev. Lett. **112**, 030602 (2014).

[27] T. Schmiedl and U. Seifert, Efficiency at maximum power: An analytically solvable model for stochastic heat engines, Europhys. Lett. **81**, 20003 (2007).

[28] D. Segal, Stochastic Pumping of Heat: Approaching the Carnot Efficiency, Phys. Rev. Lett. **101**, 260601 (2008).

[29] C. Jarzynski and O. Mazonka, Feynman's ratchet and pawl: An exactly solvable model, Phys. Rev. E **59**, 6448 (1999).

[30] A. Dechant, N. Kiesel, and E. Lutz, Underdamped stochastic heat engine at maximum efficiency, Europhys. Lett. **119**, 50003 (2017).

[31] V. Holubec, An exactly solvable model of a stochastic heat engine: Optimization of power, power fluctuations and efficiency, J. Stat. Mech. (2014) P05022.

[32] M. Esposito, K. Lindenberg, and C. Van den Broeck, Universality of Efficiency at Maximum Power, Phys. Rev. Lett. **102**, 130602 (2009).

[33] S. Sheng and Z. C. Tu, Weighted reciprocal of temperature, weighted thermal flux, and their applications in finite-time thermodynamics, Phys. Rev. E **89**, 012129 (2014).

[34] S. Sheng and Z. C. Tu, Constitutive relation for nonlinear response and universality of efficiency at maximum power for tight-coupling heat engines, Phys. Rev. E **91**, 022136 (2015).

[35] Z. Ye, Y. Hu, J. He, and J. Wang, Universality of maximum-work efficiency of a cyclic heat engine based on a finite system of ultracold atoms, Sci. Rep. **7**, 6289 (2017).

[36] J. Guo, J. Wang, Y. Wang, and J. Chen, Universal efficiency bounds of weak-dissipative thermodynamic cycles at the maximum power output, Phys. Rev. E **87**, 012133 (2013).

[37] M. Esposito, R. Kawai, K. Lindenberg, and C. Van den Broeck, Quantum-dot Carnot engine at maximum power, Phys. Rev. E **81**, 041106 (2010).

[38] A. E. Allahverdyan, R. S. Johal, and G. Mahler, Work extremum principle: Structure and function of quantum heat engines, Phys. Rev. E **77**, 041118 (2008).

[39] A. E. Allahverdyan, K. V. Hovhannisyan, A. V. Melkikh, and S. G. Gevorkian, Carnot Cycle at Finite Power: Attainability of Maximal Efficiency, Phys. Rev. Lett. **111**, 050601 (2013).

[40] R. Long, Z. Liu, and W. Liu, Performance analysis for minimally nonlinear irreversible refrigerators at finite cooling power, Phys. A: Stat. Mech. Appl. **496**, 137 (2018).

[41] H. S. Leff and W. D. Teeters, EER, COP, and the second law efficiency for air conditioners, Am. J. Phys. **46**, 19 (1978).

[42] C. Blanchard, Coefficient of performance for finite speed heat pump, J. Appl. Phys. **51**, 2471 (1980).

[43] Z. Yan and J. Chen, A class of irreversible Carnot refrigeration cycles with a general heat transfer law, J. Phys. D **23**, 136 (1990).

[44] C. de Tomás, A. C. Hernández, and J. M. M. Roco, Optimal low symmetric dissipation Carnot engines and refrigerators, Phys. Rev. E **85**, 010104(R) (2012).

[45] A. C. Hernández, A. Medina, J. M. M. Roco, J. A. White, and S. Velasco, Unified optimization criterion for energy converters, Phys. Rev. E **63**, 037102 (2001).

[46] F. Angulo-Brown, An ecological optimization criterion for finite-time heat engines, J. Appl. Phys. **69**, 7465 (1991).

[47] C. de Tomás, J. M. M. Roco, A. C. Hernández, Y. Wang, and Z. C. Tu, Low-dissipation heat devices: Unified trade-off optimization and bounds, Phys. Rev. E **87**, 012105 (2013).

[48] N. Sánchez-Salas, L. López-Palacios, S. Velasco, and A. Calvo Hernández, Optimization criteria, bounds, and efficiencies of heat engines, Phys. Rev. E **82**, 051101 (2010).

[49] Y. Zhang, C. Huang, G. Lin, and J. Chen, Universality of efficiency at unified trade-off optimization, Phys. Rev. E **93**, 032152 (2016).

[50] R. Long and W. Liu, Ecological optimization for general heat engines, Phys. A: Stat. Mech. Appl. **434**, 232 (2015).

[51] A. Ryabov and V. Holubec, Maximum efficiency of steady-state heat engines at arbitrary power, Phys. Rev. E **93**, 050101(R) (2016).

[52] R. S. Johal, Heat engines at optimal power: Low-dissipation versus endoreversible model, Phys. Rev. E **96**, 012151 (2017).

[53] Y. Zhang and Y. Huang, Applicability of the low-dissipation model: Carnot-like heat engines under Newton's law of cooling, Phys. Rev. E **102**, 012151 (2020).

[54] Y.-H. Ma, D. Xu, H. Dong, and C.-P. Sun, Universal constraint for efficiency and power of a low-dissipation heat engine, Phys. Rev. E **98**, 042112 (2018).

[55] R. S. Whitney, Most Efficient Quantum Thermoelectric at Finite Power Output, Phys. Rev. Lett. **112**, 130601 (2014).

[56] R. S. Whitney, Finding the quantum thermoelectric with maximal efficiency and minimal entropy production at given power output, Phys. Rev. B **91**, 115425 (2015).

[57] R. Long and W. Liu, Efficiency and its bounds of minimally nonlinear irreversible heat engines at arbitrary power, Phys. Rev. E **94**, 052114 (2016).

[58] V. Holubec and A. Ryabov, Maximum efficiency of low-dissipation heat engines at arbitrary power, J. Stat. Mech. (2016) 073204.

[59] Z. Ye and V. Holubec, Maximum efficiency of absorption refrigerators at arbitrary cooling power, Phys. Rev. E **103**, 052125 (2021).

[60] J. Guo, H. Yang, J. Gonzalez-Ayala, J. M. M. Roco, A. Medina, and A. C. Hernández, The equivalent low-dissipation combined cycle system and optimal analyses of a class of thermally driven heat pumps, Energy Convers. Manag. **220**, 113100 (2020).

[61] C.-Y. Cheng and C.-K. Chen, Performance optimization of an irreversible heat pump, J. Phys. D: Appl. Phys. **28**, 2451 (1995).

[62] W. Chen, F. Sun, S. Cheng, and L. Chen, Study on optimal performance and working temperatures of endoreversible forward and reverse Carnot cycles, Int. J. Energy Res. **19**, 751 (1995).

[63] P. Salamon, A. Nitzan, B. Andresen, and R. S. Berry, Minimum entropy production and the optimization of heat engines, Phys. Rev. A **21**, 2115 (1980).

[64] Y. C. Gerstenmaier, Irreversible entropy production in low- and high-dissipation heat engines and the problem of the Curzon-Ahlborn efficiency, Phys. Rev. E **103**, 032141 (2021).

[65] K. Sekimoto and S.-I. Sasa, Complementary relation for irreversible process derived from stochastic energetics, J. Phys. Soc. Jpn. **66**, 3326 (1997).

[66] P. R. Zulkowski and M. R. DeWeese, Optimal protocols for slowly driven quantum systems, Phys. Rev. E **92**, 032113 (2015).

[67] V. Cavina, A. Mari, and V. Giovannetti, Slow Dynamics and Thermodynamics of Open Quantum Systems, Phys. Rev. Lett. **119**, 050601 (2017).

[68] Y.-H. Ma, R.-X. Zhai, J. Chen, C. P. Sun, and H. Dong, Experimental Test of the $1/\tau$-Scaling Entropy Generation in Finite-Time Thermodynamics, Phys. Rev. Lett. **125**, 210601 (2020).

[69] V. Holubec, S. Steffenoni, G. Falasco, and K. Kroy, Active Brownian heat engines, Phys. Rev. Res. **2**, 043262 (2020).

[70] I. Iyyappan and R. S. Johal, Efficiency of a two-stage heat engine at optimal power, Europhys. Lett. **128**, 50004 (2020).

[71] V. Blickle and C. Bechinger, Realization of a micrometre-sized stochastic heat engine, Nat. Phys. **8**, 143 (2012).

[72] M. H. Ahmadi, M. A. Ahmadi, M. Mehrpooya, and M. Sameti, Thermo-ecological analysis and optimization performance of an irreversible three-heat-source absorption heat pump, Energy Convers. Manag. **90**, 175 (2015).

[73] I. I. Novikov, The efficiency of atomic power stations, J. Nucl. Energy II **7**, 125 (1958).

[74] P. Chambadal, *Les Centrales Nucléaires* (Colin, Paris, 1957), Vol. 321.

[75] F. L. Curzon and B. Ahlborn, Efficiency of a Carnot engine at maximum power output, Am. J. Phys. **43**, 22 (1975).

[76] Y. Chen, J.-F. Chen, Z. Fei, and H. Quan, A microscopic theory of Curzon-Ahlborn heat engine, arXiv:2108.04128.

[77] A. Vaudrey, P. Baucour, F. Lanzetta, and R. Glises, Detailed analysis of an endoreversible fuel cell: Maximum power and optimal operating temperature determination, Front. Heat Mass Transf. **3**, 3 (2012).

[78] Q. Bouton, J. Nettersheim, S. Burgardt, D. Adam, E. Lutz, and A. Widera, A quantum heat engine driven by atomic collisions, Nat. Commun. **12**, 2063 (2021).

[79] L. Chen and Z. Yan, The effect of heat-transfer law on performance of a two-heat-source endoreversible cycle, J. Chem. Phys. **90**, 3740 (1989).

[80] M. Huleihil and B. Andresen, Convective heat transfer law for an endoreversible engine, J. Appl. Phys. **100**, 014911 (2006).

[81] P. Abiuso and M. Perarnau-Llobet, Optimal Cycles for Low-Dissipation Heat Engines, Phys. Rev. Lett. **124**, 110606 (2020).

[82] P. Abiuso, H. J. D. Miller, M. Perarnau-Llobet, and M. Scandi, Geometric optimisation of quantum thermodynamic processes, Entropy **22**, 1076 (2020).

[83] I. Reyes-Ramírez, J. Gonzalez-Ayala, A. Calvo Hernández, and M. Santillán, Local-stability analysis of a low-dissipation heat engine working at maximum power output, Phys. Rev. E **96**, 042128 (2017).

[84] J. Gonzalez-Ayala, M. Santillán, I. Reyes-Ramírez, and A. Calvo-Hernández, Link between optimization and local stability of a low-dissipation heat engine: Dynamic and energetic behaviors, Phys. Rev. E **98**, 032142 (2018).

[85] J. Gonzalez-Ayala, A. Calvo Hernández, and J. M. M. Roco, From maximum power to a trade-off optimization of low-dissipation heat engines: Influence of control parameters and the role of entropy generation, Phys. Rev. E **95**, 022131 (2017).

[86] M. J. Ondrechen, M. H. Rubin, and Y. B. Band, The generalized Carnot cycle: A working fluid operating in finite time between finite heat sources and sinks, J. Chem. Phys. **78**, 4721 (1983).

[87] Y. Wang, Optimization in finite-reservoir finite-time thermodynamics, Phys. Rev. E **90**, 062140 (2014).

[88] Y. Wang, Optimizing work output for finite-sized heat reservoirs: Beyond linear response, Phys. Rev. E **93**, 012120 (2016).

[89] Y.-H. Ma, Effect of finite-size heat source's heat capacity on the efficiency of heat engine, Entropy **22**, 1002 (2020).

[90] H. Yuan, Y.-H. Ma, and C. Sun, Optimizing thermodynamic cycles with two finite-sized reservoirs, Phys. Rev. E **105**, L022101 (2022).

Maximum efficiency of absorption refrigerators at arbitrary cooling power

Zhuolin Ye [1,*] and Viktor Holubec[1,2,†]

[1]*Institut für Theoretische Physik, Universität Leipzig, Postfach 100 920, D-04009 Leipzig, Germany*
[2]*Charles University, Faculty of Mathematics and Physics, Department of Macromolecular Physics, V Holešovičkách 2,
CZ-180 00 Praha, Czech Republic*

We consider absorption refrigerators consisting of simultaneously operating Carnot-type heat engine and refrigerator. Their maximum efficiency at given power (MEGP) is given by the product of MEGPs for the internal engine and refrigerator. The only subtlety of the derivation lies in the fact that the maximum cooling power of the absorption refrigerator is not limited just by the maximum power of the internal refrigerator, but, due to the first law, also by that of the internal engine. As a specific example, we consider the simultaneous absorption refrigerators composed of low-dissipation (LD) heat engines and refrigerators, for which the expressions for MEGPs are known. The derived expression for maximum efficiency implies bounds on the MEGP of LD absorption refrigerators. It also implies that a slight decrease in power of the absorption refrigerator from its maximum value results in a large nonlinear increase in efficiency, observed in heat engines, whenever the ratio of maximum powers of the internal engine and the refrigerator does not diverge. Otherwise, the increase in efficiency is linear as observed in LD refrigerators. Thus, in all practical situations, the efficiency of LD absorption refrigerators significantly increases when their cooling power is slightly decreased from its maximum.

I. INTRODUCTION

The performance of heat engines, transforming heat to work, or refrigerators and heat pumps, displacing heat against a temperature gradient, is determined by two main quantities: output power and efficiency. Unfortunately, thermodynamic laws imply that they cannot be optimized simultaneously [1]. This is because the largest efficiencies correspond to reversible and thus slow processes, leading to output powers which are at best negligible fractions of the maximum power [2].

The implication for engineers, whose natural task is to develop designs that deliver a desired (fixed) power as cheaply as possible, is that their devices in general do not operate in the regimes of maximum efficiency [1,3] or maximum power [4–21], which were both thoroughly investigated theoretically in the past, but rather in the regime with maximum efficiency corresponding to the given power (MEGP). The MEGP received the attention of the theory of finite-time thermodynamic processes only recently [22–27], generalizing results obtained previously for a variety of trade-off relations between power and efficiency [28–37].

Unlike model-independent equilibrium results such that the maximum efficiency of thermal devices is the Carnot efficiency [1,3], all available results on the optimal performance of thermal devices operating with finite cycle times are based on specific model systems. Nevertheless, these models are usually constructed in an idealized fashion so that real-world devices inevitably dissipate more and thus operate at smaller efficiencies. The results for MEGP obtained in these models thus represent (loose) upper bounds on real-world efficiencies.

Specifically, the idealized models just consider inevitable energy losses imposed by the second law of thermodynamics. In particular, losses connected to heat leakages and construction imperfections are neglected. Most of the idealized models operate along a finite-time Carnot cycle composed of two adiabatic and two isothermal branches and assume that the total entropy change in the universe during each of the isotherms obeys the so-called low-dissipation (LD) assumption [7]

$$\Delta S_{\text{tot}} = \Sigma/t, \tag{1}$$

where the irreversibility parameter $\Sigma > 0$ depends on details of the system construction, and t is the duration of the isotherm. The low-dissipation assumption is not just a useful approximation allowing to derive explicit analytical results. This model exactly describes Brownian heat engines optimized with respect to output power [15,24], which can now be realized in experiments [38,39]. More generally, the LD model describes the first finite-time correction to the quasistatic dissipation, which was revealed not only in theoretical studies [40–42], but also in experiments [39,43]. Furthermore, with respect to MEGP, the LD model was shown to be equivalent to the minimally nonlinear irreversible model [14,33,44], and, for small temperature gradients, also to the linear irreversible model [26]. Regardless of the relatively simple mathematical structure of the LD models, the exact results on MEGP are so far known for LD heat engines [25] and refrigerators [44] only. Other devices such as absorption refrigerators [45] and heat pumps [46] are still investigated numerically even when formulated within the LD setting.

---
*zhuolinye@foxmail.com
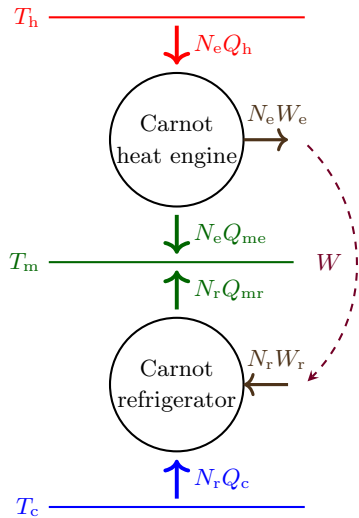†viktor.holubec@mff.cuni.cz

FIG. 1. Sketch of the CAR composed of internal Carnot heat engine and Carnot refrigerator. The overall CAR system communicates with three heat reservoirs at temperatures $T_h > T_m > T_c$. Both the internal engine and refrigerator use as their heat sink the reservoir at the intermediate temperature T_m. The engine in addition communicates with the hot bath at T_h and the refrigerator with the cold bath at T_c.

In the present paper, we consider absorption refrigerators consisting of simultaneously operating Carnot-type (internal) heat engine and refrigerator. We show how the MEGP for this general model follows from the MEGPs for the internal heat engine and refrigerator. To derive explicit results, we consider absorption refrigerators consisting of LD heat engines and refrigerators, for which expressions for MEGPs are known. The obtained MEGP represents a loose upper bound for the efficiency of real-world absorption refrigerators, which recently experienced a renewed interest of physicists due to their potential to recycle waste heat in microscopic (quantum) devices [47–52].

The rest of the paper is organized as follows. In Sec. II, we introduce the general model and derive the general results. In Sec. III, we derive the MEGP for LD absorption refrigerators and discuss its properties. We conclude in Sec. IV.

II. CARNOT ABSORPTION REFRIGERATORS

We consider absorption refrigerators consisting of a finite-time Carnot heat engine and refrigerator, which we call as Carnot absorption refrigerators (CARs). As shown in Fig. 1, the internal engine utilizes the temperature gradient $T_h - T_m > 0$ between a hot thermal reservoir and a thermal reservoir at a medium temperature to generate work. This work is then used to propel the internal refrigerator, which pumps heat from the cold thermal reservoir at temperature $T_c < T_m$ into the intermediate bath. As a result, the CAR utilizes heat from the hot body to further cool the cold one. In practice, such refrigerators are often used in cases where there is no reliable source of electricity, for example, in caravans. While described already in 1858 by Carré, absorption refrigerators now acquired renewed attention in the field of quantum thermodynamics [47–53]. This is because they seem to be promising

building blocks of quantum devices, where they should help to keep the quantum parts at very low temperatures by utilizing the junk heat produced by classical chips inevitably present in these setups.

In this work, we aim to provide an upper bound for MEGP for CARs and thus we assume that the internal engine and refrigerator work simultaneously [54]. Another possibility would be that they alternate [45]. Such CARs, however, involve during their operation idle periods of the internal devices and thus provide smaller MEGPs than the simultaneously operating setup. As we show below, the MEGP for simultaneous setups follows from MEGPs for the internal devices. In Appendix A, we discuss that for the alternating setup the optimization is actually more complicated and the knowledge of MEGPs of the internal engine and refrigerator is not sufficient for the derivation of MEGP.

A. Working cycle of simultaneous CAR

Below, we will optimize the efficiency of the CAR with respect to durations t_e and t_r of the engine and refrigeration cycles and thus we assume that they are different. The duration of one cycle of the CAR, t_s, is defined as a period after which both the internal devices attain their initial states. It is thus given by the least common multiple of t_e and t_r. We assume that such a common multiple exists and denote it as

$$N_e = t_s/t_e, \qquad (2)$$

($N_r = t_s/t_r$) the number of engine (refrigeration) cycles performed per one full CAR cycle.

Now we are ready to define the thermodynamic quantities of interest, sketched in Fig. 1. Per CAR cycle, the engine produces work $W = N_e W_e$, which is used by the refrigerator to pump heat $N_r Q_c$ from the cold bath. The output power of the engine W/t_s and the input power of the refrigerator thus reads

$$P \equiv W_e/t_e = W_r/t_r, \qquad (3)$$

where $W_r = W/N_r$ denotes the work used by the refrigerator per refrigeration cycle.

According to the first law, we have $W_e = Q_h - Q_{me}$ and $Q_c = Q_{mr} - W_r$. Here, Q_h and Q_{me} are the heats taken from the hot bath and delivered to the intermediate bath by the engine per period t_e, respectively. Similarly, Q_{mr} is heat pumped into the intermediate bath by the refrigerator per period t_r. The amount of heat extracted by the internal refrigerator from the cold bath per CAR cycle is given by $N_r Q_c$. The cooling powers of the simultaneous CAR R_s and the internal refrigerator R are thus the same and read

$$R_s = R = N_r Q_c/t_s = Q_c/t_r. \qquad (4)$$

The energy input of the CAR is $N_e Q_h$ and thus its efficiency, referred to as the coefficient of performance (COP), is given by

$$\psi = \frac{N_r Q_c}{N_e Q_h} = \frac{Q_c/t_r}{Q_h/t_e} = \varepsilon \eta. \qquad (5)$$

Here, $\eta = W_e/Q_h$ and $\varepsilon = Q_c/W_r = R/P$ denote the efficiency of the internal heat engine and refrigerator, respectively.

B. Maximum cooling power

Before we turn our attention to the MEGP for CARs, we determine the interval of allowed values of the cooling power (4). Its minimum value 0 is achieved for infinitely slow cycles. The maximum cooling power R_s^* turns out to be limited by maximum powers of both constituting devices.

The power source of the refrigerator inside the CAR is the internal heat engine and thus the maximum cooling power of the CAR cannot be larger than the maximum cooling power of the internal refrigerator without restrictions to input power R^*, i.e., $R_s^* \leqslant R^*$. Furthermore, the cooling power is related to output power of the engine by

$$P = R/\varepsilon(R). \tag{6}$$

We denote as $\bar{R}$ the maximum value of cooling power solving the equation

$$P^* = \bar{R}/\varepsilon(\bar{R}), \tag{7}$$

where P^* is the maximum power of the engine. If $\bar{R} < R^*$, the engine is not powerful enough to utilize the whole potential of the refrigerator and $R_s^* = \bar{R}$. Similarly, $\bar{R} > R^*$ means that the refrigerator is not powerful enough to use the enitre power provided by the engine and $R_s^* = R^*$. Altogether, we found that the maximum power of the CAR is given by

$$R_s^* = \min(\bar{R}, R^*). \tag{8}$$

In the next section, we finally discuss the MEGP for the simultaneous CARs.

C. MEGP for simultaneous CARs

Inserting Eq. (6) for engine output power as function of power of the refrigerator in Eq. (5), we obtain the COP of the CAR as function of R:

$$\psi(R) = \varepsilon(R)\eta\left[\frac{R}{\varepsilon(R)}\right]. \tag{9}$$

To get the MEGP for CAR, we need to optimize the right-hand side of this equation with respect to the durations of t_r and t_e for fixed R. Using Eqs. (6), (B2), and (C1), Eq. (9) can be rewritten in the form

$$\psi(R) = \frac{\eta_C \varepsilon_C}{1 + \varepsilon_C T_m \sigma / R}, \tag{10}$$

where η_C and ε_C are the Carnot efficiency of reversible Carnot heat engine and refrigerator, respectively, i.e., $\eta_C = 1 - T_m/T_h$ and $\varepsilon_C = T_c/(T_m - T_c)$, and

$$\sigma = \Delta S_{\text{tot,r}}/t_r + \Delta S_{\text{tot,e}}/t_e \tag{11}$$

is the sum of the average entropy production rates in the internal heat engine and internal refrigerator and thus the total average entropy production rate during the CAR cycle. Expressions for the total entropy changes per engine and refrigeration cycle $\Delta S_{\text{tot},r}$ and $\Delta S_{\text{tot},e}$ are given in Eqs. (B3) and (C2) in the Appendix. The maximization of COP (9) at fixed R is thus equivalent to the minimization of the average entropy production rate $\sigma = \sigma(R)$ under the same conditions.

The output power of the internal heat engine depends on the setup and performance of the refrigerator through the refrigeration power $R/\varepsilon(R)$ only. Thus, to yield the maximum value of the product in Eq. (9), $\eta[R/\varepsilon(R)]$ must attain its maximal value, $\eta^{\text{opt}}[R/\varepsilon(R)]$, corresponding to the given refrigeration power (MEGP). Furthermore, all known expressions for MEGP are decreasing functions of power [25,26,44,55,56]. Importantly, all these models neglect losses, which cannot be avoided by quasistatic operation, such as heat leakages, and thus they can saturate the Carnot bound on efficiency in the limit of vanishing power. Assuming that this idealization holds also in our present case, $\eta^{\text{opt}}[R/\varepsilon(R)]$ will be maximal if $\varepsilon(R)$ will be given by the maximum refrigerating efficiency at the given power $\varepsilon^{\text{opt}}(R)$. Altogether, the MEGP for the considered idealized CARs reads

$$\psi^{\text{opt}}(R) = \varepsilon^{\text{opt}}(R)\eta^{\text{opt}}\left[\frac{R}{\varepsilon^{\text{opt}}(R)}\right]. \tag{12}$$

The MEGP for the simultaneous CAR thus, in general, follows from the expressions for MEGPs for the internal engine and refrigerator. Let us now consider the simultaneous CAR composed of a LD heat engine and LD refrigerator [25,44]. For this specific model, we verified the validity of Eq. (12) by direct numerical maximization of Eq. (9). In the next section, we utilize the known analytical expressions for η^{opt} and ε^{opt} for this model to discuss in detail properties of the MEGP (12) for this LD CAR based on analytical grounds.

III. LOW-DISSIPATION SIMULTANEOUS CARS

Let us now consider the Carnot LD heat engine and refrigerator depicted in Fig. 2, for which the MEGPs were derived in Refs. [25] and [44], respectively. Their working cycles are composed of two isotherms realized in finite time and described by the irreversibility parameters Σ_i, $i = h, me, c, mr$. These isotherms are interconnected by infinitely fast adiabats [57].

The internal engine accepts heat

$$Q_h = T_h \Delta S_e - \frac{\Sigma_h}{t_h} \tag{13}$$

during the hot isotherm (red) of duration t_h and releases heat

$$Q_{me} = T_m \Delta S_e + \frac{\Sigma_{me}}{t_{me}} \tag{14}$$

during the isotherm corresponding to the medium temperature (green) of duration t_{me}. The terms proportional to the increase in the entropy of the working medium of the engine during the hot isotherm, ΔS_e, correspond to the reversible parts of the transferred heats. The total duration of the engine working cycle reads $t_e = t_h + t_{me}$. Similarly, the refrigerator accepts heat

$$Q_c = T_c \Delta S_r - \frac{\Sigma_c}{t_c} \tag{15}$$

during the cold isotherm (blue) of duration t_c and dumps heat

$$Q_{mr} = T_m \Delta S_r + \frac{\Sigma_{mr}}{t_{mr}} \tag{16}$$

during the intermediate isotherm (green) of duration t_{mr}. The reversible components of transferred heats are proportional to the increase in the entropy of the working medium of the
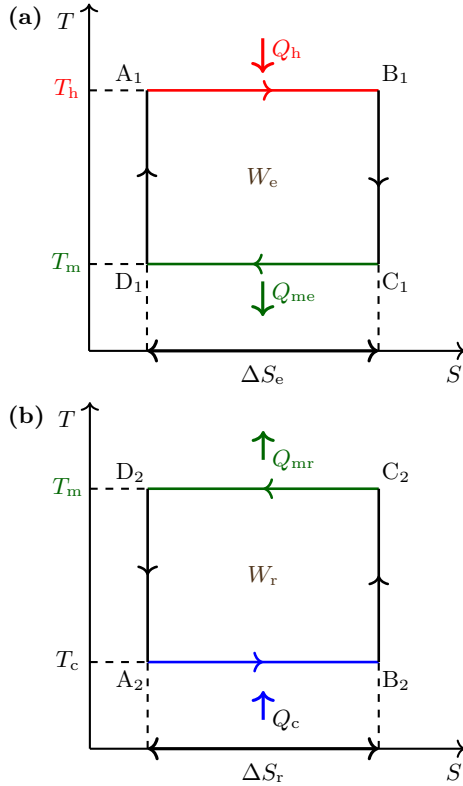
FIG. 2. Bath temperature-system entropy (T-S) diagrams of the components of the CAR depicted in Fig. 1 considered in its low-dissipation version. (a) LD Carnot heat engine and (b) LD Carnot refrigerator. The horizontal colored lines are isotherms and the vertical black lines represent adiabats. The areas enclosed of the two rectangles equal to the respective works only if the cycles are realized quasistatically.

refrigerator during the cold isotherm ΔS_r, which can be different than ΔS_e. The total duration of the refrigeration cycle is $t_r = t_c + t_{mr}$. The internal heat engine and refrigerator operate reversibly if the duration of all the isotherms diverge or if all the irreversibility parameters vanish.

Let us now consider a simultaneous CAR composed of the LD heat engine and LD refrigerator. We call it an LD simultaneous CAR. In what follows, we discuss in detail its performance in terms of MEGP.

A. MEGP

The MEGP for the LD CAR follows from Eq. (12) after inserting the expressions for MEGP of the internal LD heat engine η^{opt} and refrigerator $\varepsilon^{\mathrm{opt}}$. For the engine, we derive η^{opt} in Appendix B. Similarly to the derivation given in Ref. [25], our present approach involves an approximation in calculation of the optimal redistribution of the total cycle duration between the two isothermal branches. Nevertheless, our analytical result for η^{opt} is, within the numerical precision, indistinguishable from the corresponding result obtained by exact numerical optimization of the efficiency. For the refrigerator, we review in Appendix C the derivation of analytical expression for $\varepsilon^{\mathrm{opt}}$ from Ref. [44].

All results for MEGP available in the literature [2,24–26,44,55,56] are given as functions of the dimensionless variable

$$\delta X = \frac{X - X^*}{X^*}, \qquad (17)$$

measuring how much power is lost by operating the device at power X smaller than the maximum power X^*. In our case, we have three such variables: the loss in power of the internal engine δP; the loss in cooling power of the internal refrigerator δR; and the loss in cooling power of the CAR δR_s. In general, these variables can assume values from the interval $[-1, 0]$. The minimum is attained if the actual power is negligible compared to the maximum power and the maximum corresponds to devices operating at maximum power. However, in our specific setting where the input power of the refrigerator can be limited by the output power of the engine, the upper bound for δR reads $R_s^*/R^* - 1 \leqslant 0$.

To insert the known results for MEGP of the refrigerator and heat engine into Eq. (12), we need to express them in terms of refrigeration power R and engine output power $P = R/\varepsilon^{\mathrm{opt}}(R)$, respectively. From now on, we use the shorthand notation $\varepsilon^{\mathrm{opt}}(\delta R) \equiv \varepsilon^{\mathrm{opt}}[R(\delta R)]$, where $R(\delta R) = (1 + \delta R)R^*$, and similarly for $\eta^{\mathrm{opt}}(\delta P)$. Furthermore, to be able to discuss the MEGP of the CAR, $\psi^{\mathrm{opt}} = \varepsilon^{\mathrm{opt}}(\delta R)\eta^{\mathrm{opt}}(\delta P)$, as a function of the loss in cooling power of the CAR, we use Eqs. (6) and (17) to express δP and δR in terms of δR_s. The result is

$$\delta P = \frac{1}{\tilde{P}^*} \frac{1 + \delta R}{\varepsilon^{\mathrm{opt}}(\delta R)} - 1, \qquad (18)$$

$$\delta R = (1 + \delta R_s)\tilde{R}_s^* - 1, \qquad (19)$$

where we introduced the reduced maximum powers of the engine $\tilde{P}^* = P^*/R^*$, and the CAR, $\tilde{R}_s^* = R_s^*/R^*$, measured in units of maximum power of the internal refrigerator.

When expressed in terms of δP, the MEGP of the LD heat engine η^{opt} depends only on the ratio of the irreversibility parameters $\Sigma_e = \Sigma_h/\Sigma_{me}$, Carnot efficiency, η_C, and δP. For details, see Appendix B. Similarly, we show in Appendix C that $\varepsilon^{\mathrm{opt}}$ is only a function of $\Sigma_r = \Sigma_{mr}/\Sigma_c$, $\varepsilon_C = T_c/(T_m - T_c)$ and δR. Since the MEGP $\varepsilon^{\mathrm{opt}}(R)$ is a monotonously decreasing function of R, the ratio $R/\varepsilon^{\mathrm{opt}}(R)$ attains its maximum value for R^*. Therefore, Eqs. (7) and (8) imply that the reduced maximum power of the CAR $\tilde{R}_s^*$ is given by

$$\tilde{P}^* = \tilde{R}_s^*/\varepsilon^{\mathrm{opt}}(\tilde{R}_s^* - 1) \qquad (20)$$

if the resulting $\tilde{R}_s^*$ is smaller than 1 and by $\tilde{R}_s^* = 1$ otherwise. Hence $\tilde{R}_s^*$ is determined by Σ_r, ε_C, and $\tilde{P}^*$. Collecting all these results and inserting them into Eq. (12), we can finally write the MEGP of the LD simultaneous CAR in terms of the relative loss in its maximum cooling power δR_s. The resulting expression depends on the six parameters introduced above, namely,

$$\psi^{\mathrm{opt}} \equiv \psi^{\mathrm{opt}}(\delta R_s, \tilde{P}^*, \Sigma_e, \Sigma_r, \eta_C, \varepsilon_C). \qquad (21)$$

In the following sections, we use this expression to provide more explicit results on MEGP of CARs.

B. Bounds on MEGP

We start by deriving maximum and minimum values of the optimal COP ψ^{opt} with respect to the working medium of the CAR (or of its constituents). In the LD approximation, the detailed physics of the working medium is described by the irreversibility parameters Σ_i, $i = h, me, c, mr$ defined by Eqs. (13) to (16) [15,24,40,58,59].

The optimal COP (21) depends on irreversibility parameters through the ratios $\Sigma_e = \Sigma_h/\Sigma_{me}$ and $\Sigma_r = \Sigma_{mr}/\Sigma_c$ and the reduced maximum power of the internal engine $\tilde{P}^*$. With respect to the previous two, the optimal COP attains its minimum for $\Sigma_e \to 0$ (hot isotherm of the internal engine cycle is reversible compared to the other one) and $\Sigma_r \to \infty$ (cold isotherm of the refrigeration cycle is reversible compared to the other one). Its maximum ψ^{opt} is attained in the opposite limit $\Sigma_e \to \infty$ and $\Sigma_r \to 0$. Taking these limits into Eq. (21), we find the lower and upper bounds for the optimal COP as follows:

$$0 \leqslant \psi^{\text{opt}} \leqslant \frac{\varepsilon_C(1 + \sqrt{-\delta R})}{2 + \varepsilon_C(1 - \sqrt{-\delta R})} \frac{\eta_C(1 + \sqrt{-\delta P})}{2 - \eta_C(1 - \sqrt{-\delta P})}. \quad (22)$$

This inequality has to be further optimized with respect to the parameter $\tilde{P}^*$, which enters the upper bound through Eqs. (18) and (19) for δP and δR, respectively. Note that, due to the limits $\Sigma_e \to \infty$ and $\Sigma_r \to 0$ taken to derive the upper bound, we have to use $\varepsilon^{\text{opt}} = \varepsilon_+^{\text{opt}}$ defined in Eq. (C13) in the formula for δP. One finds that the upper bound is a monotonously decreasing function of $\tilde{P}^*$ and thus its maximum is obtained for $\tilde{P}^* = 0$. The resulting ultimate bounds on the optimal COP of the CAR at given cooling power read

$$0 \leqslant \psi^{\text{opt}} \leqslant \frac{\varepsilon_C \eta_C (1 + \sqrt{-\delta R_s})}{2 - \eta_C(1 - \sqrt{-\delta R_s})} \equiv \psi_+^{\text{opt}}(\delta R_s). \quad (23)$$

The upper bound evaluated for $\delta R_s = 0$, $\psi_+^{\text{opt}}(0) = \varepsilon_C \eta_C / (2 - \eta_C)$, denotes the upper bound for COP of the CAR at maximum cooling power.

The increase in COP gained after a slight decrease of the cooling power from its maximum value can be measured by the expression

$$\frac{\psi_+^{\text{opt}}(\delta R_s) - \psi_+^{\text{opt}}(0)}{\psi_+^{\text{opt}}(0)} = \frac{2 - 2\eta_C}{2 - \eta_C}\sqrt{-\delta R_s} + \mathcal{O}(\delta R_s). \quad (24)$$

Its derivative with respect to δR_s diverges, implying that a slight decrease of the cooling power leads to a significant gain in the upper bound on COP. Qualitatively the same behavior has generally been observed for MEGPs of various heat engines [22,23,25–27,56]. With respect to LD refrigerators, the MEGP is proportional to $\sqrt{-\delta R}$ for a limited range of parameters only and behaves as $\propto -\delta R$ otherwise [44]. In the next section, we investigate whether the increase of MEGP for the CAR behaves for small values of δR_s always like the MEGPs in heat engines [25] or if it sometimes also exhibits the linear behavior observed in refrigerators [44].

C. MEGP near maximum cooling power

Examples of parameter regimes where the MEGP for LD refrigerators exhibits the two qualitatively different behaviors are $\Sigma_r \to 0$ (square root) and $\Sigma_r \to \infty$ (linear) [44]. We thus investigate behavior of the MEGP for the CAR (21) in these two regimes using the cumbersome analytical expressions derived in Appendixes B and C.

1. $\Sigma_r \to 0$

Expanding the exact expression for ε^{opt} in Eq. (C12) up to the first order with respect to Σ_r, we obtain

$$\varepsilon^{\text{opt}} = \varepsilon_+^{\text{opt}} - \frac{2(1 + \varepsilon_C)\left(\varepsilon_+^{\text{opt}}\right)^2 (1 - \sqrt{-\delta R})\sqrt{\tilde{\Sigma}_r}}{\varepsilon_C(-\delta R)^{1/4}(1 + \sqrt{-\delta R})}, \quad (25)$$

where $\tilde{\Sigma}_r$ is defined below Eq. (C11) and $\varepsilon_+^{\text{opt}}$ in Eq. (C13). Substituting Eqs. (25) and (B14) for ε^{opt} and η^{opt} into Eq. (12) for MEGP for the CAR, expressing δP and δR in terms of δR_s using Eqs. (18) and (19), and expanding the resulting expression up to the first order in δR_s, we find

$$\psi^{\text{opt}} = r_1 + r_2\sqrt{-\delta R_s}. \quad (26)$$

The coefficients r_1 and r_2 depend, in a complicated way, on the parameters $\tilde{P}^*$, ε_C, η_C, and Σ_e. The obtained dependence of the MEGP of the CAR on the loss in cooling power might have been expected since, in this parameter regime, the behavior near maximum power of the engine and the refrigerator is the same [25,44].

2. $\Sigma_r \to \infty$

In this limit, the MEGP for LD refrigerators (C12) reads (see Eq. (29) in Ref. [44])

$$\varepsilon^{\text{opt}} \approx \frac{\delta R(1 - \delta R)\varepsilon_C}{2\delta R + (1 + \delta R)(\delta R - \Sigma_r)\varepsilon_C}. \quad (27)$$

Using a similar procedure as for obtaining Eq. (26), we find that up to the second order in δR_s

$$\psi^{\text{opt}} = g_1 + g_2\sqrt{-\delta R_s} + g_3\delta R_s, \quad (28)$$

where the coefficients g_1, g_2, and g_3 depend on $\tilde{P}^*$, ε_C, η_C, and Σ_e in a complicated way. Interestingly, for $\tilde{P}^* \to \infty$, g_2 vanishes and the increase in COP of the CAR becomes linear. As discussed at the end of the next section, for diverging $\tilde{P}^*$, the heat engine works at Carnot efficiency and the behavior of the MEGP of the CAR is solely determined by that of the refrigerator [44].

D. MEGP for arbitrary parameters

Outside the limiting parameter regimes discussed above, the full analytical expression (21) for the MEGP is too cumbersome to get an immediate insight into the behavior of ψ^{opt}. Therefore, in this section, we investigate its dependence on the model parameters graphically.

In Fig. 3, we show the reduced maximum power of the CAR $\tilde{R}_s^*$ as a function of the reduced power of the internal heat engine $\tilde{P}^*$. The larger the available input power of the refrigerator (provided by the engine) the larger the corresponding maximum cooling power of the CAR until it reaches its maximum $\tilde{R}_s^* = 1$, where the whole cooling potential of the internal refrigerator is utilized. The minimum value of the reduced power $\tilde{P}^* = 1/\varepsilon^{\text{opt}}(0)$, allowing for $\tilde{R}_s^* = 1$, follows from Eq. (20). Here, $\varepsilon^{\text{opt}}(0) = \varepsilon_{\pm}^*$ denotes the MEGP for the
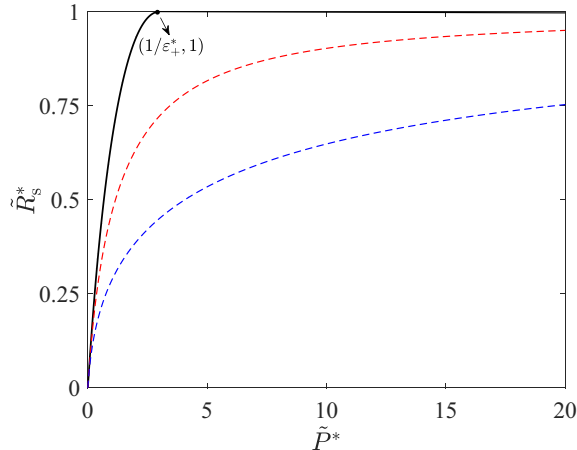
FIG. 3. The reduced maximum power of the CAR $\tilde{R}_s^*$ as a function of the reduced maximum power of the internal heat engine $\tilde{P}^*$ for three values 0, 1, and 10 of the ratio Σ_r of irreversibility parameters, which increases from the uppermost solid line to the lowermost dashed one. We take $\varepsilon_C = 1$.
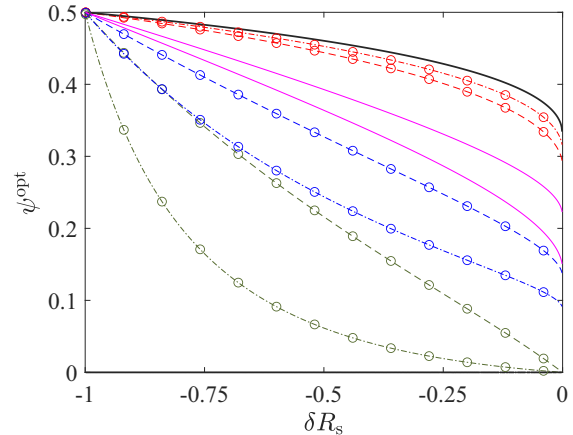

FIG. 4. The MEGP of the CAR (21) as a function of the loss in cooling power δR_s for three values 0, 1, and ∞ of the reduced maximum power of the engine $\tilde{P}^*$. The reduced power $\tilde{P}^*$ increases from the uppermost dashed line to the lowermost one with $\Sigma_r = \Sigma_e = 1$. The dot-dashed lines of the same color as the dashed ones correspond to the same $\tilde{P}^*$ and $\Sigma_r = \Sigma_e = 10$. The two pink solid lines in the middle depict the upper bound on MEGP (22) for fixed $\tilde{P}^*$ obtained for $\Sigma_r = 0$ and $\Sigma_e \to \infty$. For the top one we took $\tilde{P}^* = 1$. The bottom one corresponds to arbitrary $\tilde{P}^* \geqslant 1/\varepsilon_+^*$. The bottom and top black solid lines represent the ultimate lower ($\Sigma_r \to \infty$, $\Sigma_e = 0$, and arbitrary $\tilde{P}^*$) and upper ($\Sigma_r = 0$, $\Sigma_e \to \infty$, and $\tilde{P}^* = 0$) bounds on MEGP (23) (note that the lower bound coincides with the horizontal axis). MEGP for the CAR obtained using brute-force numerical optimization of its COP (circles) perfectly agree with the curves calculated using the analytical formula (21) (lines). Other parameters taken: $\varepsilon_C = 1$ and $\eta_C = 1/2$.

refrigerator defined in Eqs. (C5) and (C6). Hence, $\tilde{R}_s^* = 1$ for finite value ($\tilde{P}^* = 1/\varepsilon_+^*$) of the reduced power only if $\Sigma_r = 0$, i.e., when the dissipation during the hot isotherm of the refrigeration cycle becomes negligible compared to that during the cold one. For $\Sigma_r > 0$, the whole cooling potential of the internal refrigerator can be utilized only for infinite values of the reduced power $\tilde{P}^* = 1/\varepsilon_-^* \to \infty$. This is caused by the discontinuity in the ability of the refrigerator working at maximum power conditions to utilize the energy provided by the engine $\varepsilon^{\text{opt}}(0)$, which is positive for $\Sigma_r = 0$ and vanishes for $\Sigma_r > 0$ [44]. Figure 3 also shows that, for fixed $\tilde{P}^*$ and ε_C, $\tilde{R}_s^*$ decreases as the amount of energy dissipated during the hot isotherm of the refrigeration cycle increases (larger Σ_r).

In Fig. 4, we plot the MEGP for CARs (21) as a function of δR_s for different values of $\tilde{P}^*$, Σ_e, and Σ_r. The upper bounds (22) for MEGP for fixed reduced power $\tilde{P}^*$ are depicted for $\tilde{P}^* = 1$ (top pink solid line in the middle) and $\tilde{P}^* \geqslant 1/\varepsilon_+^*$ (bottom pink solid line in the middle). They indeed bound the MEGP obtained for arbitrary values of ratios of irreversibility parameters Σ_e and Σ_r, and values of $\tilde{P}^*$ larger than those chosen to plot the individual curves. The ultimate upper bound on MEGP (23) is depicted by the uppermost black solid line. According to the figure, the MEGP ψ^{opt} exhibits a fast nonlinear increase with decreasing power near $\delta R_s \to 0$ unless $\tilde{P}^* \to \infty$. Only then is this increase linear, in agreement with our discussion below Eq. (28). To check our analytical results, we also calculated the MEGP for simultaneous LD CARs by a direct brute-force numerical optimization of COP (5). The figure shows that the obtained numerical results (symbols) perfectly overlap with our analytical predictions (lines).

In Fig. 5, we show the characteristics of the heat engine and refrigerator corresponding to the MEGP of the CAR with $\Sigma_r = \Sigma_e = 1$, depicted in Fig. 4. For $\tilde{P}^* \to 0$, Eqs. (18) to (20) imply that $\delta R = -1$, $\varepsilon^{\text{opt}} = \varepsilon_C$, and $\delta P = \delta R_s$. Similarly, for $\tilde{P}^* \to \infty$ it follows that $\delta R = \delta R_s$, $\delta P = -1$, and $\eta^{\text{opt}} = \eta_C$. When the refrigerator works at the Carnot COP ε_C, the dimensionless refrigeration cycle duration τ_r^{opt} diverges and

we have $N_e/N_r \to \infty$, i.e., within one full CAR cycle, there are infinitely more engine cycles than refrigeration cycles. An opposite situation occurs when the engine works at Carnot efficiency.

IV. CONCLUSION AND OUTLOOK

We showed that the maximum efficiency at given cooling power (MEGP) for an absorption refrigerator composed of simultaneously operating Carnot-type heat engine and Carnot-type refrigerator (CAR) follows from the MEGPs for the internal heat engine and refrigerator. We applied these general findings to low-dissipation (LD) simultaneous CARs, where the internal devices work in the LD regime and the corresponding expressions for MEGPs are known [25,44]. We used the resulting cumbersome analytical formula for the MEGP for derivation of concise expressions for upper and lower bounds on the MEGP for the LD CARs. We also investigated the behavior of the MEGP close to the maximum power. Unless the ratio of maximum powers of the internal engine and the refrigerator diverges, a slight decrease in power of the LD CAR leads to a fast nonlinear increase in the MEGP generically observed in heat engines [25]. Otherwise, the increase in the MEGP is linear as can be observed in LD refrigerators [44].

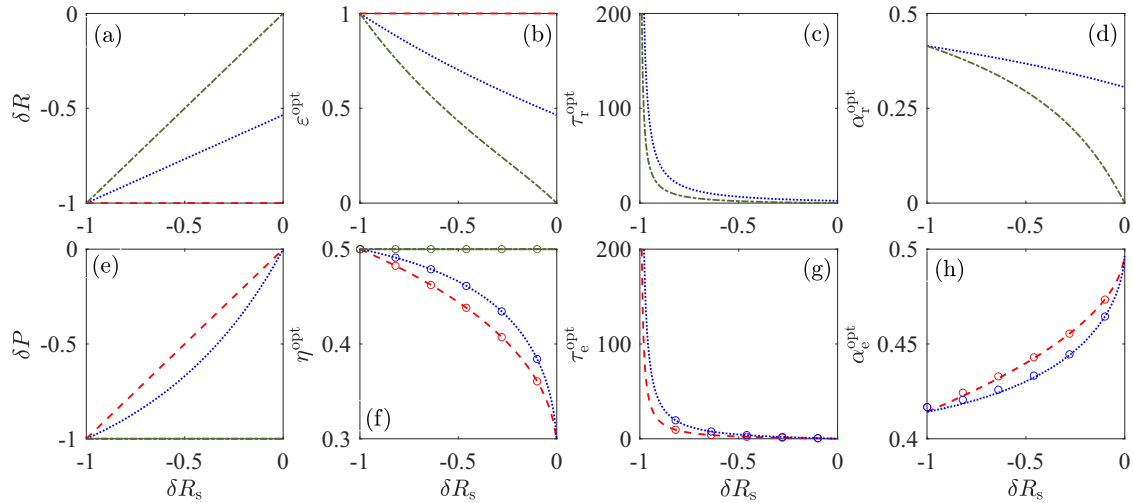In the LD approximation, the detailed dynamics of the system in question determines the so-called irreversibility

FIG. 5. Top: Characteristics of the internal refrigerator corresponding to the MEGP for the CAR depicted in Fig. 4 for $\Sigma_r = \Sigma_e = 1$ as functions of the loss in output power of the CAR, δR_s. (a) The loss in output power δR, (b) MEGP $\varepsilon^{\mathrm{opt}}$, (c) the optimal dimensionless cycle duration τ_r^{opt}, defined in Eq. (C7), and (d) the optimal relative duration of the hot isotherm α_r^{opt}, defined below Eq. (C7). Bottom: The corresponding characteristics of the internal heat engine. (e) The loss in output power δP, (f) MEGP η^{opt}, (g) the optimal dimensionless cycle duration τ_e^{opt} defined in Eq. (B8), and (h) the optimal relative duration of the hot isotherm α_e^{opt}, defined above Eq. (B1). Colors of the individual lines, marking the used value of the reduced maximum power $\tilde{P}^*$, are the same as those used in Fig. 4 (red dashed, blue dotted, green dash-dotted corresponds to reduced powers 0, 1, and ∞, respectively). The vanishing reduced power corresponds to the Carnot COP of the refrigerator $\varepsilon^{\mathrm{opt}} = \varepsilon_C$, where τ_r^{opt} diverges, and arbitrary α_r^{opt}. Panels (c) and (d) thus show no red dashed lines. Similarly, diverging $\tilde{P}^*$ corresponds to the Carnot efficiency of the engine $\eta^{\mathrm{opt}} = \eta_C$, and thus we show no green dash-dotted lines in panels (g) and (h). Even though the depicted parameters for the heat engines were obtained using the approximation (B13), they are almost indistinguishable from exact numerical results (circles). Slight deviations can be observed for α_e^{opt} only.

parameters. The MEGP for simultaneous LD CARs, derived in this paper, is as function of power measured in units of the maximum power, which depends on the irreversibility parameters. Using a specific dynamical model, the maximum power can be further optimized with respect to theses parameters, allowing to derive expressions for maximum power at fixed maximum efficiency. For LD heat engines and refrigerators, such an optimization was performed in Refs. [58,59] using the geometrical approach to thermodynamics generically valid close to equilibrium. While the dependence of maximum power on irreversibility parameters in these two settings is obvious, the situation in LD CARs is slightly different since their maximum power is controlled by both the maximum power of the internal refrigerator and that of the internal heat engine. Equations (7) and (8) suggest that the power of the CAR attains its maximum if one maximizes the COP of the internal refrigerator, its maximum power, and also the maximum power of the heat engine. However, detailed investigations in this direction will be a subject of our future work.

The presented LD model is constructed in an idealized fashion and the resulting MEGP can serve as a (loose) upper bound for real-world absorption refrigerators. Such bounds are thus nowadays available for heat engines [25], refrigerators [44], and absorption refrigerators. It remains to derive them for heat pumps, which will also be a subject of our future work. For a numerical study of the MEGP for absorption heat pumps, we refer to Ref. [46]. Furthermore, it would be interesting to investigate MEGPs for LD systems in context of the stability analysis described in Refs. [8,60–62].

Originally, the finite-time performance of heat engines was studied using the endoreversible model [63]. While efficiencies at maximum power for the endoreversible and LD models are described by similar expressions [64], to the best of our knowledge, no results for MEGP for endoreversible models are known. As a future research project, it would be also interesting to investigate to what extent the apparent equivalence between the two models holds concerning the MEGP.

APPENDIX A: MEGP FOR ALTERNATING CARS

For alternating CARs [45], the internal heat engine and refrigerator do not operate simultaneously. The duration of one cycle of the alternating CAR is thus given by the sum $t_e + t_r$ of the durations of the engine and refrigerator. According to the first law of thermodynamics, the output work of the heat engine per cycle equals to the input work of the refrigerator,

i.e., $W_e = W_r$. The power of the heat engine and the cooling power of the refrigerator then read

$$\mathcal{P} = \frac{W_e}{t_e + t_r} = \frac{P}{1 + \Lambda}, \quad (\text{A1})$$

$$\mathcal{R} = \frac{Q_c}{t_e + t_r} = \frac{R}{1 + 1/\Lambda}, \quad (\text{A2})$$

where $\Lambda \equiv t_r/t_e$ measures the ratio of durations of the two internal cycles. The first law in the form of Eq. (6) implies that these two powers are interconnected through the COP ε of the refrigerator

$$\mathcal{P} = \frac{\mathcal{R}}{\varepsilon(R)}. \quad (\text{A3})$$

Using Eqs. (A2) and (A3), the COP (5) can be rewritten as

$$\begin{aligned}
\psi(\mathcal{R}) &= \varepsilon(R)\eta(P) \\
&= \varepsilon(\mathcal{R}, \Lambda)\eta(\mathcal{P}, \Lambda) \\
&= \varepsilon(\mathcal{R}, \Lambda)\eta\left(\frac{\mathcal{R}}{\varepsilon(\mathcal{R}, \Lambda)}, \Lambda\right), \quad (\text{A4})
\end{aligned}$$

where the notation $\varepsilon(R) = \varepsilon[\mathcal{R}(1 + 1/\Lambda)] \equiv \varepsilon(\mathcal{R}, \Lambda)$ highlights that both the efficiencies now explicitly depend on the ratio of the durations of the internal cycles Λ through the definitions (A1) and (A2) of $\mathcal{R}$ and $\mathcal{P}$. Consequently, in the optimization of COP (A4) with respect to the durations of the refrigeration and engine cycles, the engine and refrigeration efficiencies cannot be optimized independently as it was done in Eq. (12). The optimization of COP for alternating CARs is thus more complicated than that for simultaneous CARs and the knowledge of MEGPs for the internal engine and refrigerator might not be sufficient for determination of MEGP for alternating CARs.

APPENDIX B: MEGP FOR LD HEAT ENGINES

In this Appendix, we derive the expression η^{opt} for MEGP for LD heat engines. The derivation is slightly different from that used in Ref. [25].

Introducing the relative duration of the hot isotherm, $\alpha_e = t_h/t_e$, in Eqs. (13) and (14), the power output and efficiency of the LD heat engine can be expressed as

$$P = \frac{W_e}{t_e} = \frac{(T_h - T_m)\Delta S_e}{t_e} - \frac{\alpha \Sigma_{me} + (1-\alpha)\Sigma_h}{\alpha(1-\alpha)t_e^2}, \quad (\text{B1})$$

$$\eta = \frac{W_e}{Q_h} = \frac{\eta_C}{1 + T_m \Delta S_{\text{tot},e}/(Pt_e)}, \quad (\text{B2})$$

where

$$\Delta S_{\text{tot},e} = -\frac{Q_h}{T_h} + \frac{Q_{me}}{T_m} = \frac{\Sigma_h}{t_h T_h} + \frac{\Sigma_{me}}{t_{me} T_m} \geqslant 0 \quad (\text{B3})$$

is the total entropy production per engine cycle.

Maximizing the power (B1) with respect to α and t_e yields [15]

$$\alpha_e^* = \frac{\sqrt{\Sigma_e}}{1 + \sqrt{\Sigma_e}}, \quad (\text{B4})$$

$$t_e^* = \frac{2(\sqrt{\Sigma_h} + \sqrt{\Sigma_{me}})^2}{T_h \eta_C \Delta S_e}, \quad (\text{B5})$$

$$P^* = \frac{1}{4}\left(\frac{T_h \eta_C \Delta S_e}{\sqrt{\Sigma_h} + \sqrt{\Sigma_{me}}}\right)^2, \quad (\text{B6})$$

$$\eta^* = \frac{\eta_C(1 + \sqrt{\Sigma_e})}{2 + \sqrt{\Sigma_e}(2 - \eta_C)}, \quad (\text{B7})$$

where $\Sigma_e = \Sigma_h/\Sigma_{me}$ is the so-called irreversibility ratio and $\eta_C = 1 - T_m/T_h$ denotes Carnot efficiency. Now we use Eqs. (B4) and (B5) to define the coordinate transformation

$$\tau_e = \frac{t_e}{t_e^*} - 1 \in [-1, \infty], \quad (\text{B8})$$

$$a = \frac{\alpha_e}{\alpha_e^*} - 1 \in \left[-1, \frac{1}{\alpha_e^*} - 1\right], \quad (\text{B9})$$

which reduces the number of variables in the problem [25]. The point of maximum power (B6) corresponds to $\delta P = 0$ (17) and $\tau_e = a = 0$. The (relative) loss in power (17) and efficiency (B2) in these new coordinates read

$$\delta P = \frac{a^2\sqrt{\Sigma_e}}{(1+a)(a\sqrt{\Sigma_e} - 1)(1 + \tau_e)^2} - \left(\frac{\tau_e}{1 + \tau_e}\right)^2, \quad (\text{B10})$$

$$\begin{aligned}
\eta &= \frac{(1 + \sqrt{\Sigma_e})\eta_C}{a\sqrt{\Sigma_e} - 1} \\
&\times \frac{2a^2\sqrt{\Sigma_e}(1 + \tau_e) + (a\sqrt{\Sigma_e} - a - 1)(1 + 2\tau_e)}{2(1+a)(1 + \sqrt{\Sigma_e})(1 + \tau_e) - \eta_C\sqrt{\Sigma_e}}.
\end{aligned} \quad (\text{B11})$$

Solving Eq. (B10) with respect to the dimensionless cycle duration τ_e, we find two roots

$$\tau_e = \frac{-\delta P}{1 + \delta P} \pm \frac{\sqrt{\delta P(1 + a - a\sqrt{\Sigma_e}) + a^2\sqrt{\Sigma_e}}}{(1 + \delta P)\sqrt{(1+a)(a\sqrt{\Sigma_e} - 1)}}. \quad (\text{B12})$$

Since longer cycles in general allow for larger efficiencies, we thus take the root with the positive sign. Substituting it into Eq. (B11), evaluating the condition $\partial\eta/\partial a|_{a=a^{\text{opt}}} = 0$ for maximum efficiency, and expanding it up to the fourth order in a, we find

$$\left.\frac{\partial\eta}{\partial a}\right|_{a=a^{\text{opt}}} = \sum_{n=0}^{4} b_n a^n + \mathcal{O}(a^5) = 0, \quad (\text{B13})$$

where the coefficients b_n are complicated functions of δP, Σ_e, and η_C. Equation (B13) for the optimal value a^{opt} of the parameter a can be solved exactly [65]. The corresponding optimal value of τ_e^{opt} follows by substituting the resulting a^{opt} for a in Eq. (B12).

Substituting the obtained expressions for a^{opt} and τ_e^{opt} for a and τ into Eq. (B11), we obtain a lengthy but manageable (e.g., by using software for symbolic manipulation such as MATHEMATICA) formula for the MEGP for LD heat engines

$$\eta^{\text{opt}} = \eta^{\text{opt}}(\delta P, \Sigma_e, \eta_C). \quad (\text{B14})$$

Even though this results was obtained using the approximation (B13), we tested that the resulting approximate MEGP (B14) and the exact MEGP obtained numerically are indistinguishable within the numerical precision (the measured absolute error is on the order of 10^{-7}). Furthermore, the expression (B14) yields exact lower ($\Sigma_e = 0$) and upper

($\Sigma_e \to \infty$) bounds on the MEGP of LD heat engines [25]

$$\frac{\eta_C}{2}(1 + \sqrt{-\delta P}) \leqslant \eta^{\text{opt}} \leqslant \frac{\eta_C(1 + \sqrt{-\delta P})}{2 - \eta_C(1 - \sqrt{-\delta P})}. \quad \text{(B15)}$$

APPENDIX C: MEGP FOR LD REFRIGERATORS

In this Appendix, we review the derivation of the expression ε^{opt} for MEGP for LD refrigerators given in Ref. [44].

The COP of the refrigerator is given by

$$\varepsilon = \frac{Q_c}{W_r} = \frac{\varepsilon_C}{1 + \varepsilon_C T_m \Delta S_{\text{tot,r}}/(Rt_r)}, \quad \text{(C1)}$$

where

$$\Delta S_{\text{tot,r}} = -\frac{Q_c}{T_c} + \frac{Q_{mr}}{T_m} = \frac{\Sigma_c}{t_c T_c} + \frac{\Sigma_{mr}}{t_{mr} T_m} \geqslant 0 \quad \text{(C2)}$$

is the total entropy production per refrigeration cycle. Substituting Eq. (15) into Eq. (4) and maximizing the resulting expression with respect to t_{mr} and t_c gives [44,66]

$$t_c^* = t_r^* = \frac{2\Sigma_c}{T_c \Delta S_r}, \quad \text{(C3)}$$

$$R^* = \frac{(T_c \Delta S_r)^2}{4\Sigma_c}. \quad \text{(C4)}$$

At maximum power conditions, the duration of the cold isotherm t_c^* thus equals the duration of the entire cycle t_r^*, which should be understood in the sense that the hot isotherm is infinitely faster than the cold one. The corresponding COP of the internal refrigerator at maximum power ε^* reads

$$\varepsilon_-^* = 0 \qquad \text{for} \quad \Sigma_r > 0, \quad \text{(C5)}$$

$$\varepsilon_+^* = \frac{\varepsilon_C}{2 + \varepsilon_C} \quad \text{for} \quad \Sigma_r = 0, \quad \text{(C6)}$$

where $\Sigma_r = \Sigma_{mr}/\Sigma_c$ is the so-called irreversibility ratio and $\varepsilon_C = T_c/(T_m - T_c)$ denotes Carnot COP. The COP at maximum power ε^* thus exhibits a discontinuity at $\Sigma_r = 0$. Using Eq. (C3), we define the dimensionless cycle duration as

$$\tau_r = \frac{t_r}{t_r^*} - 1 \in [-1, \infty]. \quad \text{(C7)}$$

Introducing further the relative duration of the hot isotherm $\alpha_r = t_{mr}/t_r$, we find from Eqs. (4), (17), and (C7) that

$$\alpha_r = 1 + \frac{1}{(1 + \delta R)\tau_r^2 + 2\delta R\tau_r + \delta R - 1}. \quad \text{(C8)}$$

Since α_r by definition satisfies $0 \leqslant \alpha_r \leqslant 1$, the above formula makes sense only if

$$-\frac{\sqrt{-\delta R}}{1 + \sqrt{-\delta R}} \leqslant \tau_r \leqslant \frac{\sqrt{-\delta R}}{1 - \sqrt{-\delta R}}. \quad \text{(C9)}$$

The COP (C1) in these new variables reads

$$\varepsilon = \frac{\tau_r^3 + A_{1,3}\tau_r^2 + A_{0,3}\tau_r + A_{0,1}}{-\tau_r^3 + A_{1/\varepsilon_+^*,-3}\tau_r^2 + B_{3,4,1}\tau_r + B_{1,2,-1}}, \quad \text{(C10)}$$

with $A_{k,l} = (k + l\delta R)/(1 + \delta R)$ and $B_{k,l,m} = [-k(\delta R)^2 + (l/\varepsilon_C + 1 + \Sigma_r)\delta R + m\Sigma_r]/(1 + \delta R)^2$. The maximum of COP (C10) can be determined by the condition $\partial\varepsilon/\partial\tau_r|_{\tau_r = \tau_r^{\text{opt}}} = 0$, which explicitly reads

$$(\tau_r^{\text{opt}})^4 + \tilde{A}(\tau_r^{\text{opt}})^3 + \tilde{B}_{6+3\tilde{\Sigma}_r,2+2\tilde{\Sigma}_r,-\tilde{\Sigma}_r}(\tau_r^{\text{opt}})^2$$
$$+ \tilde{B}_{4+3\tilde{\Sigma}_r,-2\tilde{\Sigma}_r,-\tilde{\Sigma}_r}\tau_r^{\text{opt}} + \tilde{B}_{1+\tilde{\Sigma}_r,-2\tilde{\Sigma}_r,0} = 0. \quad \text{(C11)}$$

Above, the coefficients $\tilde{A} = [(4 + \tilde{\Sigma}_r)\delta R + \tilde{\Sigma}_r]/(1 + \delta R)$ and $\tilde{B}_{k,l,m} = (k\delta R^2 + l\delta R + m)/(1 + \delta R)^2$ depend on Σ_r and ε_C only through the combination $\tilde{\Sigma}_r = \Sigma_r/(\frac{1}{\varepsilon_C} + 1)$.

The quartic equation (C11) has four roots and can be analytically solved [44,65]. The optimal dimensionless cycle duration $\tau_r^{\text{opt}} = \tau_r^{\text{opt}}(\delta R, \Sigma_r, \varepsilon_C)$ is determined by the only physically reasonable root, located in the interval (C9). Substituting it for τ in Eq. (C10), we obtain a lengthy but manageable (e.g., by using software for symbolic manipulation such as MATHEMATICA) exact expression for ε^{opt},

$$\varepsilon^{\text{opt}} = \varepsilon^{\text{opt}}(\delta R, \Sigma_r, \varepsilon_C). \quad \text{(C12)}$$

It turns out to be bounded by the inequalities

$$0 \leqslant \varepsilon^{\text{opt}} \leqslant \frac{\varepsilon_C(1 + \sqrt{-\delta R})}{2 + \varepsilon_C(1 - \sqrt{-\delta R})} \equiv \varepsilon_+^{\text{opt}}, \quad \text{(C13)}$$

where the lower bound corresponds to $\Sigma_r \to \infty$ and the upper bound to $\Sigma_r = 0$.

[1] H. B. Callen, *Thermodynamics and an Introduction to Thermostatistics*, Student Edition (Wiley India, Noida, India, 2006).

[2] V. Holubec and A. Ryabov, Diverging, but negligible power at carnot efficiency: Theory and experiment, Phys. Rev. E **96**, 062107 (2017).

[3] I. Müller, *A History of Thermodynamics: The Doctrine of Energy and Entropy* (Springer, New York, 2007).

[4] J. Yvon, Saclay reactor: Acquired knowledge by two years experience in heat transfer using compressed Gas, Tech. Rep. (CEA Saclay, Saclay, France, 1955).

[5] P. Chambadal, *Les Centrales Nucléaires*, Vol. 321 (Colin, Paris, 1957).

[6] I. I. Novikov, The efficiency of atomic power stations (a review), J. Nucl. Energy II **7**, 125 (1958).

[7] M. Esposito, R. Kawai, K. Lindenberg, and C. Van den Broeck, Efficiency at Maximum Power of Low-Dissipation Carnot Engines, Phys. Rev. Lett. **105**, 150603 (2010).

[8] J. Gonzalez-Ayala, J. Guo, A. Medina, J. M. M. Roco, and A. C. Hernández, Energetic Self-Optimization Induced by Stability in Low-Dissipation Heat Engines, Phys. Rev. Lett. **124**, 050603 (2020).

[9] Y. Wang, M. Li, Z. C. Tu, A. C. Hernández, and J. M. M. Roco, Coefficient of performance at maximum figure of merit and its

bounds for low-dissipation carnot-like refrigerators, Phys. Rev. E **86**, 011127 (2012).

[10] C. Van den Broeck, Thermodynamic Efficiency at Maximum Power, Phys. Rev. Lett. **95**, 190602 (2005).

[11] G. Benenti, K. Saito, and G. Casati, Thermodynamic Bounds on Efficiency for Systems with Broken Time-Reversal Symmetry, Phys. Rev. Lett. **106**, 230602 (2011).

[12] Y. Izumida and K. Okuda, Work Output and Efficiency at Maximum Power of Linear Irreversible Heat Engines Operating with a Finite-Sized Heat Source, Phys. Rev. Lett. **112**, 180603 (2014).

[13] Y. Izumida, K. Okuda, J. M. M. Roco, and A. C. Hernández, Heat devices in nonlinear irreversible thermodynamics, Phys. Rev. E **91**, 052140 (2015).

[14] Y. Izumida and K. Okuda, Efficiency at maximum power of minimally nonlinear irreversible heat engines, Europhys. Lett. **97**, 10004 (2012).

[15] T. Schmiedl and U. Seifert, Efficiency at maximum power: An analytically solvable model for stochastic heat engines, Europhys. Lett. **81**, 20003 (2007).

[16] D. Segal, Stochastic Pumping of Heat: Approaching the Carnot Efficiency, Phys. Rev. Lett. **101**, 260601 (2008).

[17] C. Jarzynski and O. Mazonka, Feynman's ratchet and pawl: An exactly solvable model, Phys. Rev. E **59**, 6448 (1999).

[18] M. Esposito, K. Lindenberg, and C. Van den Broeck, Universality of Efficiency at Maximum Power, Phys. Rev. Lett. **102**, 130602 (2009).

[19] M. Esposito, K. Lindenberg, and C. Van den Broeck, Thermoelectric efficiency at maximum power in a quantum dot, Europhys. Lett. **85**, 60010 (2009).

[20] M. Esposito, R. Kawai, K. Lindenberg, and C. Van den Broeck, Quantum-dot carnot engine at maximum power, Phys. Rev. E **81**, 041106 (2010).

[21] N. Nakpathomkun, H. Q. Xu, and H. Linke, Thermoelectric efficiency at maximum power in low-dimensional systems, Phys. Rev. B **82**, 235428 (2010).

[22] R. S. Whitney, Most Efficient Quantum Thermoelectric at Finite Power Output, Phys. Rev. Lett. **112**, 130601 (2014).

[23] R. S. Whitney, Finding the quantum thermoelectric with maximal efficiency and minimal entropy production at given power output, Phys. Rev. B **91**, 115425 (2015).

[24] V. Holubec and A. Ryabov, Efficiency at and near maximum power of low-dissipation heat engines, Phys. Rev. E **92**, 052125 (2015).

[25] V. Holubec and A. Ryabov, Maximum efficiency of low-dissipation heat engines at arbitrary power, J. Stat. Mech. (2016) 073204.

[26] A. Ryabov and V. Holubec, Maximum efficiency of steady-state heat engines at arbitrary power, Phys. Rev. E **93**, 050101(R) (2016).

[27] A. Dechant, N. Kiesel, and E. Lutz, Underdamped stochastic heat engine at maximum efficiency, Europhys. Lett. **119**, 50003 (2017).

[28] Y. Apertet, H. Ouerdane, A. Michot, C. Goupil, and P. Lecoeur, On the efficiency at maximum cooling power, Europhys. Lett. **103**, 40001 (2013).

[29] Z. Yan and J. Chen, A class of irreversible carnot refrigeration cycles with a general heat transfer law, J. Phys. D **23**, 136 (1990).

[30] C. de Tomás, A. C. Hernández, and J. M. M. Roco, Optimal low symmetric dissipation carnot engines and refrigerators, Phys. Rev. E **85**, 010104(R) (2012).

[31] A. C. Hernández, A. Medina, J. M. M. Roco, J. A. White, and S. Velasco, Unified optimization criterion for energy converters, Phys. Rev. E **63**, 037102 (2001).

[32] F. Angulo-Brown, An ecological optimization criterion for finite-time heat engines, J. Appl. Phys. **69**, 7465 (1991).

[33] Y. Izumida, K. Okuda, A. C. Hernández, and J. Roco, Coefficient of performance under optimized figure of merit in minimally nonlinear irreversible refrigerator, Europhys. Lett. **101**, 10005 (2013).

[34] C. de Tomas, J. M. M. Roco, A. C. Hernández, Y. Wang, and Z. C. Tu, Low-dissipation heat devices: Unified trade-off optimization and bounds, Phys. Rev. E **87**, 012105 (2013).

[35] N. Sánchez-Salas, L. López-Palacios, S. Velasco, and A. Calvo Hernández, Optimization criteria, bounds, and efficiencies of heat engines, Phys. Rev. E **82**, 051101 (2010).

[36] Y. Zhang, C. Huang, G. Lin, and J. Chen, Universality of efficiency at unified trade-off optimization, Phys. Rev. E **93**, 032152 (2016).

[37] R. Long and W. Liu, Ecological optimization for general heat engines, Phys. A: Stat. Mech. Appl. **434**, 232 (2015).

[38] V. Blickle and C. Bechinger, Realization of a micrometre-sized stochastic heat engine, Nat. Phys. **8**, 143 (2012).

[39] I. A. Martínez, É. Roldán, L. Dinis, D. Petrov, J. M. Parrondo, and R. A. Rica, Brownian carnot engine, Nat. Phys. **12**, 67 (2016).

[40] K. Sekimoto and S.-I. Sasa, Complementarity relation for irreversible process derived from stochastic energetics, J. Phys. Soc. Jpn. **66**, 3326 (1997).

[41] P. R. Zulkowski and M. R. DeWeese, Optimal protocols for slowly driven quantum systems, Phys. Rev. E **92**, 032113 (2015).

[42] V. Cavina, A. Mari, and V. Giovannetti, Slow Dynamics and Thermodynamics of Open Quantum Systems, Phys. Rev. Lett. **119**, 050601 (2017).

[43] Y.-H. Ma, R.-X. Zhai, J. Chen, C. P. Sun, and H. Dong, Experimental Test of the $1/\tau$-Scaling Entropy Generation in Finite-Time Thermodynamics, Phys. Rev. Lett. **125**, 210601 (2020).

[44] V. Holubec and Z. Ye, Maximum efficiency of low-dissipation refrigerators at arbitrary cooling power, Phys. Rev. E **101**, 052124 (2020).

[45] J. Guo, H. Yang, H. Zhang, J. Gonzalez-Ayala, J. Roco, A. Medina, and A. C. Hernández, Thermally driven refrigerators: Equivalent low-dissipation three-heat-source model and comparison with experimental and simulated results, Energy Convers. Manag. **198**, 111917 (2019).

[46] J. Guo, H. Yang, J. Gonzalez-Ayala, J. Roco, A. Medina, and A. C. Hernández, The equivalent low-dissipation combined cycle system and optimal analyses of a class of thermally driven heat pumps, Energy Convers. Manag. **220**, 113100 (2020).

[47] A. Levy and R. Kosloff, Quantum Absorption Refrigerator, Phys. Rev. Lett. **108**, 070604 (2012).

[48] L. A. Correa, J. P. Palao, G. Adesso, and D. Alonso, Performance bound for quantum absorption refrigerators, Phys. Rev. E **87**, 042131 (2013).

[49] L. A. Correa, J. P. Palao, D. Alonso, and G. Adesso, Quantum-enhanced absorption refrigerators, Sci. Rep. **4**, 3949 (2014).

[50] J. B. Brask and N. Brunner, Small quantum absorption refrigerator in the transient regime: Time scales, enhanced cooling, and entanglement, Phys. Rev. E **92**, 062101 (2015).

[51] J. O. González, J. P. Palao, and D. Alonso, Relation between topology and heat currents in multilevel absorption machines, New J. Phys. **19**, 113037 (2017).

[52] V. Holubec and T. Novotný, Effects of noise-induced coherence on the fluctuations of current in quantum absorption refrigerators, J. Chem. Phys. **151**, 044108 (2019).

[53] G. Maslennikov, S. Ding, R. Hablützel, J. Gan, A. Roulet, S. Nimmrichter, J. Dai, V. Scarani, and D. Matsukevich, Quantum absorption refrigerator with trapped ions, Nat. Commun. **10**, 202 (2019).

[54] One might argue that, when operating simultaneously, the internal heat engine cannot power the internal refrigerator because the engine generates work during half of the cycle only and accepts it during the rest. However, already the realization of a cyclically operating heat engine requires the existence of a work source, where the work generated by the engine is stored and which is used to propel the engine during parts of the cycle where it accepts energy. The same work source can power the simultaneous CAR. In practice, the energy transfer to/from the work source could lead to additional losses decreasing the performance of the CAR. Since our aim here is to provide an upper bound on efficiency, we neglect such losses. Furthermore, we are interested only on second law limitations on the performance of the CAR working under idealistic conditions (no heat leakages, no losses during work-to-work conversion) and thus the practical implementation of the work source is irrelevant for our analysis.

[55] R. Long, Z. Liu, and W. Liu, Performance analysis for minimally nonlinear irreversible refrigerators at finite cooling power, Phys. A: Stat. Mech. Appl. **496**, 137 (2018).

[56] R. Long and W. Liu, Efficiency and its bounds of minimally nonlinear irreversible heat engines at arbitrary power, Phys. Rev. E **94**, 052114 (2016).

[57] Adiabatic processes are described by vanishing average heat flux into the system and can be realized either by disconnecting the system from the thermal environment or by changing the control parameters in such a way that the average heat flux vanishes [39,67]. A fast adiabat is effectively an example of the first case since the heat does not have enough time to enter the system, see Ref. [38] for an experimental realization of such branches in an over-damped Brownian setup. In general, fast changes of control parameters can bring the system far from equilibrium. In the overdamped description, this can be avoided by suitably tuning the jump in potential and temperature [15,24]. However, in the underdamped regime this is in general not possible and one has to employ adiabatic branches with finite duration. In our present analysis, this would lead to a decrease in output power of all the considered devices.

[58] P. Abiuso and M. Perarnau-Llobet, Optimal Cycles for Low-Dissipation Heat Engines, Phys. Rev. Lett. **124**, 110606 (2020).

[59] P. Abiuso, H. J. D. Miller, M. Perarnau-Llobet, and M. Scandi, Geometric optimisation of quantum thermodynamic processes, Entropy **22**, 1076 (2020).

[60] I. Reyes-Ramírez, J. Gonzalez-Ayala, A. Calvo Hernández, and M. Santillán, Local-stability analysis of a low-dissipation heat engine working at maximum power output, Phys. Rev. E **96**, 042128 (2017).

[61] J. Gonzalez-Ayala, M. Santillán, I. Reyes-Ramírez, and A. Calvo-Hernández, Link between optimization and local stability of a low-dissipation heat engine: Dynamic and energetic behaviors, Phys. Rev. E **98**, 032142 (2018).

[62] J. Gonzalez-Ayala, J. Guo, A. Medina, J. M. M. Roco, and A. Calvo Hernández, Optimization induced by stability and the role of limited control near a steady state, Phys. Rev. E **100**, 062128 (2019).

[63] F. L. Curzon and B. Ahlborn, Efficiency of a carnot engine at maximum power output, Am. J. Phys. **43**, 22 (1975).

[64] Z.-C. Tu, Recent advance on the efficiency at maximum power of heat engines, Chin. Phys. B **21**, 020513 (2012).

[65] M. Abramowitz and I. A. Stegun, *Handbook of Mathematical Functions with Formulas, Graphs, and Mathematical Tables*, Vol. 55 (Dover, New York, 1964).

[66] A. C. Hernández, A. Medina, and J. Roco, Time, entropy generation, and optimization in low-dissipation heat devices, New J. Phys. **17**, 075011 (2015).

[67] I. A. Martínez, E. Roldán, L. Dinis, D. Petrov, and R. A. Rica, Adiabatic Processes Realized with a Trapped Brownian Particle, Phys. Rev. Lett. **114**, 120601 (2015).

3   Optimal protocols for Brownian systems

Brownian motion can be traced to the observations by Robert Brown in 1827. While examining pollen grains suspended in water under a microscope, Brown made an intriguing observation. He noticed that the particles displayed erratic and jiggling movements, which seemed to occur spontaneously and independently of external forces or deliberate motion. His observations sparked scientific interest and triggered further investigations into the phenomenon. Initially, there were various speculations about the cause of this random motion, including theories involving electric or magnetic interactions. The true theoretical explanation for Brownian motion was provided by Albert Einstein in 1905 [90], who formulated a mathematical model that described Brownian motion as the result of random collisions between particles and fluid molecules. Einstein's work on Brownian motion played a crucial role in confirming the existence of atoms and molecules, which was still debated at the time. Furthermore, his theoretical framework provided a quantitative understanding of the random behavior observed in Brownian motion, validating the molecular kinetic theory. Since then, Brownian motion has become an important concept in physics, mathematics, and other scientific disciplines. It serves as a fundamental example of stochastic processes in areas such as statistical physics, biology, and economics.

A useful tool to model Brownian motion is the Langevin equation that describes the motion of a particle in a fluid under the influence of both deterministic and random forces

$$\underbrace{m\ddot{x}}_{\text{inertial force}} = -\underbrace{\nabla V(x)}_{\text{potential force}} - \underbrace{\gamma\dot{x}}_{\text{viscous force}} + \underbrace{\sqrt{2\gamma k_B T}\eta(t)}_{\text{random force}}, \tag{15}$$

where V is the external potential, m (x) is the mass (position) of the particle, t is time, γ is the friction coefficient that accounts for the damping effect of the fluid, T is temperature, k_B is Boltzmann's constant, and $\eta(t)$ represents a delta-correlated stationary Gaussian process with zero-mean, i.e., $\langle\eta(t)\rangle = 0$ and $\langle\eta(t)\eta(t')\rangle = \delta(t - t')$, which means that it has zero average and vanishing correlations at

different times. The Langevin equation (15) is a stochastic version of Newton's second law of motion, where the random force term accounts for the random, unpredictable forces acting on the particle due to the thermal motion of the fluid molecules. The inertial force, known as inertial resistance or inertial effect, is a force that arises from the Brownian particle's tendency to resist changes in its state of motion. It is related to Newton's first law of motion, which states that an object at rest will remain at rest, and an object in motion will continue in motion with the same velocity unless acted upon by an external force. The viscous force, known as viscous drag or simply viscosity, is a type of resistance that opposes the motion of the Brownian particle through the fluid.

Typically, the Langevin equation (15) is investigated in two regimes: the overdamped regime and the underdamped regime. The difference between over-damped and underdamped Brownian motion lies in the relative strengths of the damping and inertial forces acting on the particle. In overdamped regime, the damping force dominates over the inertial force, which means that the particle experiences strong resistance from the surroundings, causing it to move slowly and gradually approach a steady state. The particle thus quickly reaches equilibrium without exhibiting significant oscillations or fluctuations. On the other hand, underdamped regimes occurs when the inertial force is comparable or stronger than the damping force. In this case, the particle experiences less resistance from the medium and is more affected by the inertia. The particle moves rapidly, exhibiting oscillatory behavior and undergoing periodic fluctuations around the equilibrium position. The inertia of the particle allows it to move more freely. In the overdamped limit, the inertial force term is so much smaller than the other three that it can be eliminated adiabatically from the the full inertial Langevin equation (15),

$$\underbrace{\gamma\dot{x}}_{\text{viscous force}} = -\underbrace{\nabla V(x)}_{\text{potential force}} + \underbrace{\sqrt{2\gamma k_B T}\eta(t)}_{\text{random force}}, \qquad (16)$$

Motivated by the improvements in micromanipulation, e.g., optical tweezers, which allows building engines based on a single particle, and the desire to bet-ter understand the performance of thermodynamic systems on the microscale,
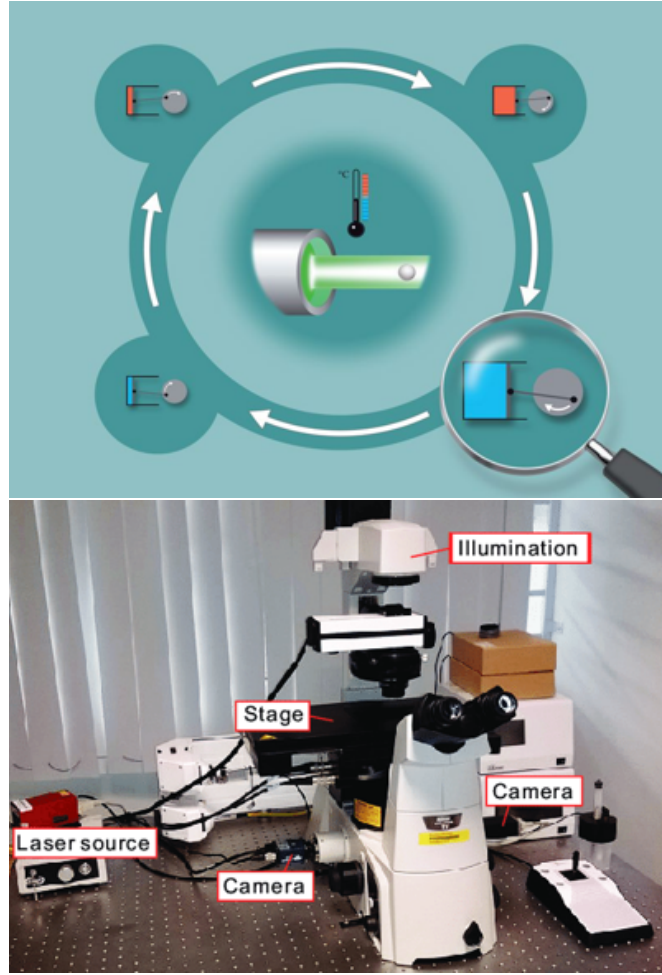
FIG. 3. Top: engines based on a single particle [41]. Bottom: real equipment of optical tweezers.

researchers started to derive finite-time optimal protocols. Optical tweezers (originally called single-beam gradient force trap) are scientific instruments that use a highly focused laser beam to hold and move microscopic and sub-microscopic objects like atoms, nanoparticles and droplets, in a manner similar to tweezers, as shown in Fig. 3. If the object is held in air or vacuum without additional support, it can be called optical levitation. Most of available experimental setups with optical tweezers are designed to control colloids in water. These systems are well described by the overdamped Langevin dynamics (16). Motivated by these experiments, Schmiedel and Seifert [24, 53] derived optimal protocols for engines based on a colloidal particle embedded in water (acting as the heat bath).

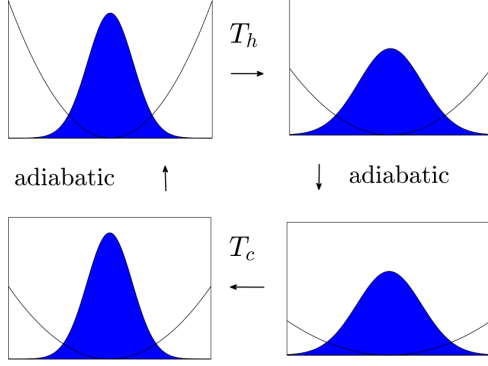Let us now briefly review the paradigmatic model of stochastic thermody-

FIG. 4. The operational cycle of heat engines based on a particle diffusing in a time-dependent potential [12, 24]. The filled blue curve represents the probability density for the position of the particle. The black parabola stands for the potential at the beginning of the individual branches.

namics developed by Schmiedel and Seifert [24]. In their work, they derived the maximum-power protocol of a Carnot-type engine based on an overdamped Brownian particle diffusing in a harmonic potential, $V(x) = \lambda(t)x^2/2$, where $\lambda(t)$ is the stiffness describing the strength of the potential that can be controlled experimentally. The system dynamics is described by Eq. (16). Denoting as $\sigma(t) \equiv \langle x^2(t) \rangle$ the position variance of the particle, one get its time evolution from (16),

$$\dot{\sigma} = -2\mu\lambda\sigma + 2\mu T, \tag{17}$$

where $\mu = 1/\gamma$ is the mobility of the particle. Note that the Langevin equation can be reformulated as the Fokker–Planck equation that governs the probability distribution of the position of the particle, from which we can also obtain the equation of motion (17) in Ref. [24]. The optimization is performed in two steps. First, fixing the time intervals of the isotherms of the cycle $t_i \leq t \leq t_f$, they optimize the work done during the two isotherms assuming fixed initial (σ_i) and final (σ_f) position variances

$$
\begin{aligned}
W[\lambda(t)] &= \int_{t_i}^{t_f} dt \dot{\lambda} \frac{\sigma}{2} \\
&= \frac{1}{4\mu} \int_{t_i}^{t_f} dt \frac{\dot{\sigma}^2}{\sigma} - \frac{1}{2}[\ln \sigma]|_{t_i}^{t_f} + \frac{1}{2}[\lambda \sigma]|_{t_i}^{t_f}
\end{aligned} \tag{18}
$$

59

This allows to find the optimal periodic response of the system $[\sigma^*(t)]$ during the cycle, which in turn leads to the corresponding optimal protocol $[\lambda^*(t)]$ via (17). The resulting optimal protocol $\lambda^*(t)$ involves discontinuities at the beginning and at the end of the isotherms, which can be considered as two infinitely fast adiabatic branches. The transferred heats between the system and the reservoirs during the two optimized isotherms read

$$Q_h = T_h \left[\frac{1}{2} \ln \frac{\sigma_f}{\sigma_i} - \frac{(\sigma_f - \sigma_i)^2}{\mu T_h t_h} \right], \tag{19a}$$

$$Q_c = T_c \left[\frac{1}{2} \ln \frac{\sigma_f}{\sigma_i} + \frac{(\sigma_f - \sigma_i)^2}{\mu T_c t_c} \right], \tag{19b}$$

which agree with Eqs.(3a) and (3b). This means that the Brownian heat engine is a microscopic example of the low-dissipation model. We reiterate that the Brownian heat engine can be arbitrarily far from equilibrium. Finally, Schmiedel and Seifert [24] optimized the power $P = (Q_h - Q_c)/(t_h + t_c)$ by using Eqs. (19a) and (19b) with respect to the durations t_h and t_c.

We stress that during the optimization the boundary values σ_i and σ_f are fixed. This condition was adopted in most of the subsequent work [25, 91, 92]. However, as we can see from Eq. (17), modulating the stiffness $\lambda(t)$ defines the evolution of the response $\sigma(t)$. Conversely, a given response trajectory $\sigma(t)$ is translated to the initial control $\lambda(t)$. This implies that fixing the boundary values of $\sigma(t)$ (constrained response) is non-trivially related to fixing the boundary values of $\lambda(t)$ (constrained control). In what follows, we show that the results of optimization strongly depend on where the boundary conditions are imposed [9, 10, 43, 93]. From an experimental point of view, one should thus better impose known and equipment-motivated constrains on the control variable $\lambda(t)$. Below we first derive optimal protocols for finite-time heat engines under constrained control. Then, we show how to generalize the results of [24] to the multidimensional case, perhaps with a limited control over some of the degrees of freedom.

3.1 Interpretation of the publications

3.1.1 Constrained control

In this work [9], we considered a finite-time stochastic heat engine described by a periodically scaled Hamiltonian with the scaling parameter λ

$$H(x,t) = \lambda(t)f(x), \tag{20}$$

where $f(x)$ represents an arbitrary function of the system degrees of freedom x. This class of Hamiltonian generalizes the well-known "breathing" parabola model [24] for a Brownian particle subject to the harmonic potential $H(x,t) = \lambda(t)x^2/2$ [thus $f(x) = x^2/2$]. Furthermore, it includes semiclassical two-level (or multilevel) systems with controlled gaps between the individual energy levels [94] and quantum spins, where the control parameter is an externally controlled magnetic field [95]. We assume that the system is coupled to a reservoir at temperature $T(t)$ with the same period t_p as $\lambda(t)$. Motivated by experimental praxis, our control parameters are thus $\lambda(t)$ and $T(t)$ fulfilling

$$\lambda(t) \in [\lambda_-, \lambda_+], \quad T(t) \in [T_-, T_+], \tag{21}$$

and we aim to find the optimal time variation for them yielding maximum efficiency and maximum power.

Denoting as $\sigma(t) \equiv \langle f[x(t)] \rangle$ the average response of the system, the maximum-efficiency protocol can be evaluated in the $\lambda - \sigma$ diagram shown in Fig. 5. The starting point is the definitions of work and heat in stochastic thermodynamics. Per cycle, the engine transforms the fraction

$$\eta = \frac{W_{\text{out}}}{Q_{\text{in}}} = 1 - \frac{Q_{\text{out}}}{Q_{\text{in}}} \tag{22}$$

of the heat

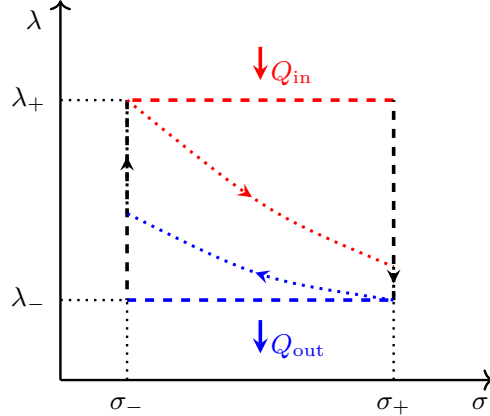$$Q_{\text{in}} = \int_0^{t_p} \lambda(t)\theta[d\sigma(t)]d\sigma(t) \tag{23}$$

FIG. 5. The maximum-efficiency protocol under the constraints (21) (dashed line) compared to a suboptimal cycle (dotted line) [9].

from the heat source into output work

$$W_{\text{out}} = - \int_0^{t_{\text{p}}} \sigma(t) d\lambda(t), \tag{24}$$

and dumps the remaining heat $Q_{\text{out}} = Q_{\text{in}} - W_{\text{out}} = \int_0^{t_{\text{p}}} \lambda(t)\theta[-d\sigma(t)]d\sigma(t)$ into the heat sink (The Heaviside step function $\theta(\bullet) = 1$ when the heat flows on average into the system, i.e., $d\sigma > 0$). Maximizing η (22) is equivalent to minimizing the ratio $Q_{\text{out}}/Q_{\text{in}}$. From the definitions of Q_{in} and Q_{out}, it is not very difficult to find that this corresponds to the rectangle in Fig. 5. This means that the optimal variation of $\lambda(t)$ is piecewise constant. We noted that a similar optimization problem is often solved in classical thermodynamics showing that the maximum efficiency of an equilibrium cycle under the constraint $T(t) \in [T_-, T_+]$ on the bath temperature is the Carnot efficiency. However, in our case, the system can be arbitrarily far from equilibrium. Unlike the piecewise constant variation of $\lambda(t)$ yielding the maximum efficiency, the variation of $T(t)$ corresponding to maximum efficiency in our work [9] has more freedom. Actually, we provided basic conditions that $T(t)$ should follow guaranteeing the proper operation of the engine. However, we adhered to the piecewise constant variation of $T(t)$, because it yields the maximum output work. Altogether, the maximum-efficiency finite-time cycle under the constraints (21) is both Carnot [piecewise constant $T(t)$] and Otto [piecewise constant $\lambda(t)$] cycles. Furthermore, when the variation of λ is small

62

and the system is close to equilibrium at the ends of the isotherms, we provided a similar geometric proof showing that the maximum-efficiency protocol (piecewise constant variation of both λ and T) also yields maximum output power. Finally, we provided numerical evidence supporting our results by using an overdamped Brownian heat engine described by Eqs. (16) and (17) [24].

We stress that our results of maximum-efficiency and maximum-power protocols are valid for arbitrary dynamics. This means that they can be applied to anything driven cyclically and described by the factorized structure of the Hamiltonian (20). However, they in general cannot be applied to molecular motors operating in steady state (thus not driven cyclically). Furthermore, macroscopic systems are usually described by much more complicated Hamiltonians. More importantly, for macroscopic systems one usually cannot control the full Hamiltonian but rather some collective degree of freedom such as volume or pressure. Nevertheless, our results might apply for these systems if macroscopic internal energy would have functional form of our Hamiltonian (20).

3.1.2 Constrained response

In this work [43], we imposed the boundary conditions on the system state $\sigma(t)$, as done in Ref. [24, 53]. However, we generalized the derivation to the multidimensional case. To this end, we considered a system of N overdamped Brownian particles described by the position vector $\boldsymbol{x}$ and mutually interacting via the time-dependent potential

$$V(\boldsymbol{x}, t) = \frac{1}{2}\boldsymbol{x}^{\mathsf{T}}\lambda(t)\boldsymbol{x} \ . \tag{25}$$

Each particle $i = 1, \ldots, N$ might have a different number of degrees of freedom d_i, i.e. $\boldsymbol{x} \in \mathbb{R}^M$, where $M = \sum_{i=1}^{N} d_i$. The potential (25) accounts for both self-energy of the individual particles and interactions between the particles. The stiffness matrix $\lambda \geq 0$ is symmetric. Assuming that all the particles have the same friction

coefficient γ, the system dynamics obeys the set of Langevin equations [96]

$$\gamma \dot{\boldsymbol{x}} = -\lambda \boldsymbol{x} + \sqrt{2\gamma k_B T}\boldsymbol{\eta} \,, \tag{26}$$

where the Gaussian noise $\boldsymbol{\eta}$ obeys $\langle \boldsymbol{\eta} \rangle = 0$. Its components $\langle \eta_i(t)\eta_j(t') \rangle = \delta_{ij}\delta(t - t')$, and T is the temperature of the thermal environment, which we assume is constant. The time evolution of the covariance matrix $\sigma(t) = \langle \boldsymbol{x}\boldsymbol{x}^\mathsf{T} \rangle (t)$ can be obtained from Eq. (26) and reads $\dot{\Sigma} = \langle \boldsymbol{x}\dot{\boldsymbol{x}}^\mathsf{T} \rangle + \langle \dot{\boldsymbol{x}}\boldsymbol{x}^\mathsf{T} \rangle$

$$\dot{\sigma}(t) = -\lambda(t)\sigma(t) - \sigma(t)\lambda(t) + 2T \,, \tag{27}$$

where $\dot{\sigma} = \langle \boldsymbol{x}\dot{\boldsymbol{x}}^\mathsf{T} \rangle + \langle \dot{\boldsymbol{x}}\boldsymbol{x}^\mathsf{T} \rangle$. Following Refs. [24, 53], we expressed the work input of a finite time transformation of duration τ by using (27) as

$$\begin{aligned} W &= \frac{1}{2} \int_0^\tau dt \; \mathrm{Tr}[\dot{\lambda}\sigma] \\ &= \frac{1}{2}\mathrm{Tr}[\lambda\sigma]\Big|_0^\tau - \frac{T}{2}\log\det\sigma\Big|_0^\tau + \frac{1}{2}\int_0^\tau dt \; \mathrm{Tr}\left[\int_0^\infty d\nu \; e^{-\nu\sigma}\dot{\sigma}e^{-\nu\sigma}\dot{\sigma}\right]. \end{aligned} \tag{28}$$

This allowed us to find the optimal variation of the covariance matrix $[\sigma^*(t)]$ and thus the corresponding optimal protocol $[\lambda^*(t)]$ via Eq. (27).

Then, we further generalized the paradigmatic case of the potential (25) to a more general case of the quadratic potential with time-dependent center $\boldsymbol{z}(t)$, i.e. $V(\boldsymbol{x}, t) = \frac{1}{2}[\boldsymbol{x} - \boldsymbol{z}(t)]\lambda(t)[\boldsymbol{x} - \boldsymbol{z}(t)]$. We illustrated our findings and highlighted the distinction between partial and global control by performing an analysis on a system involving two interacting particles and a particle confined in a 2-dimensional squeezing potential, each subject to different control limitations. Here partial control means that only some of the elements of the matrix λ and the vector $\boldsymbol{z}$ can be controlled. This is a frequently encountered scenario in experimental studies involving complex many-body systems.

3.2 Outlook

As a natural extension of our work, we plan to investigate optimal performance of underdamped Brownian heat engines under constrained control, i.e., fixing the boundary values of the experimentally motivated parameters instead of the system state. We plan to find the corresponding maximum-efficiency and maximum-power protocols, and compare the performance to the known results in the situation when boundary conditions are imposed on the system state [25] and also to our results obtained using the 'overdmaped' (without kinetic energy) Hamiltonian (20). We also plan to generalize the harmonic potential (20) to more complicated forms, study the optimal performance under constrained control, and compare the obtained results to those under constrained response.

Optimal finite-time heat engines under constrained control

Zhuolin Ye [1,*] Federico Cerisola,[2,3] Paolo Abiuso [4,5] Janet Anders [3,6] Martí Perarnau-Llobet [5] and Viktor Holubec [7,†]

[1]*Institut für Theoretische Physik, Universität Leipzig, Postfach 100 920, D-04009 Leipzig, Germany*
[2]*Department of Materials, University of Oxford, Parks Road, Oxford OX1 3PH, United Kingdom*
[3]*Department of Physics and Astronomy, University of Exeter, Stocker Road, Exeter EX4 4QL, United Kingdom*
[4]*ICFO-Institut de Ciències Fotòniques, The Barcelona Institute of Science and Technology, 08860 Castelldefels (Barcelona), Spain*
[5]*Department of Applied Physics, University of Geneva, 1211 Geneva, Switzerland*
[6]*Institut für Physik und Astronomie, University of Potsdam, 14476 Potsdam, Germany*
[7]*Department of Macromolecular Physics, Faculty of Mathematics and Physics, Charles University, V Holešovičkách 2, CZ-180 00 Praha, Czech Republic*

We optimize finite-time stochastic heat engines with a periodically scaled Hamiltonian under experimentally motivated constraints on the bath temperature T and the scaling parameter λ. We present a general geometric proof that maximum-efficiency protocols for T and λ are piecewise constant, alternating between the maximum and minimum allowed values. When λ is restricted to a small range and the system is close to equilibrium at the ends of the isotherms, a similar argument shows that this protocol also maximizes output power. These results are valid for arbitrary dynamics. We illustrate them for an overdamped Brownian heat engine, which can experimentally be realized using optical tweezers with stiffness λ.

I. INTRODUCTION

The unprecedented improvement in experimental control over microscopic Brownian [1] and quantum systems [2–4] has induced a revolution in the study of heat engines [5,6]. It aims to generalize equilibrium and finite-time thermodynamics [7–15] to the nanoscale, where thermal and quantum fluctuations render thermodynamic variables such as work and heat stochastic [16]. Intense effort is devoted to uncover optimal performance of stochastic heat engines [16–41]. However, optimal control protocols are only known under approximations of fast [34–36] or slow [28,37–41] driving, or for specific microscopic models: engines based on overdamped Brownian particles in harmonic [24] or log-harmonic [42] potential, and underdamped harmonic Brownian heat engines [43]. Furthermore, most of these exact results are obtained under constraints on the state of the working medium [44], instead of experimentally motivated constraints on the control parameters [45,46]. An exception is Ref. [47], showing that reaching maximum efficiency of slowly driven cyclic heat engines requires control over the scaling of the full Hamiltonian to avoid heat leakages.

In this paper, we optimize finite-time thermodynamic cycles under constraints on control parameters such as trap stiffness of optical tweezers λ and bath temperature T. We show that, different from constraining the response such as the width σ of the phase distribution, constraining the control allows for surprisingly simple and general derivation of maximum-efficiency and maximum-power protocols. Besides other stark differences, for constrained control of Brownian heat engines, these protocols significantly outperform the protocol optimized for power and efficiency under constraints on σ [24].

The paper is organized as follows. In Sec. II, we introduce the considered setup with a periodically scaled Hamiltonian under experimentally motivated constraints. In Sec. III, we derive the corresponding maximum-efficiency protocol. In Sec. IV, we prove that the maximum-efficiency protocol yields, under certain conditions, also maximum output power. In Sec. V, we present a case study of optimization of power and efficiency for constrained control by considering a specific overdamped Brownian heat engine. Besides illustrating the general results derived in Secs. III and IV, we provide numerical evidence that the maximum-power protocol is, in this case, piecewise linear. We conclude in Sec. VI.

*zhuolinye@foxmail.com
†viktor.holubec@mff.cuni.cz

II. SETUP

Following Ref. [47], we assume that the Hamiltonian of the system that serves as a working medium of the stochastic heat engine is of the form

$$H(x,t) = \lambda(t)f(x), \qquad (1)$$

where the control parameter $\lambda(t)$ periodically expands and shrinks the energy spectrum in time, and $f(x)$ is an arbitrary function of the system degrees of freedom x such that the equilibrium partition function $Z(t) = \int dx \exp[-H(x,t)/(k_B T)]$ is finite for all $k_B T \geqslant 0$ (k_B denotes the Boltzmann constant). This class of Hamiltonians generalizes the well-known "breathing" parabola model [24] for an overdamped particle trapped in a parametrically driven harmonic potential. It also includes semiclassical two-level (or multilevel) systems with controlled gaps between the individual energy levels [16], and quantum spins, where the control parameter is an externally controlled magnetic field [17].

We connect the system to a heat bath and periodically alter its temperature $T(t)$ with the same finite period t_p as $\lambda(t)$. The parameters under experimental control are thus $\lambda(t)$ and $T(t)$ and our aim is to find optimal t_p-periodic protocols for them under the experimentally motivated constraints [48]

$$\lambda(t) \in [\lambda_-, \lambda_+], \quad T(t) \in [T_-, T_+]. \tag{2}$$

III. MAXIMUM-EFFICIENCY PROTOCOL

Our first main result is a general geometric proof that the maximum-efficiency finite-time cycle under the constraints (2) is a Carnot-Otto cycle composed of two isotherms/isochores interconnected by two adiabats. The maximum-efficiency protocol $\{T(t), \lambda(t)\}$ is thus piecewise constant:

$$\{T(t), \lambda(t)\}_\eta = \begin{cases} \{T_+, \lambda_+\}, & 0 < t < t_+, \\ \{T_-, \lambda_-\}, & t_+ < t < t_p. \end{cases} \tag{3}$$

And the maximum efficiency is given by

$$\eta = 1 - \frac{\lambda_-}{\lambda_+}. \tag{4}$$

The proof relies just on the definition of heat and it is thus independent of the details of the system dynamics, including the times t_+ and t_p. It holds both for situations when the heat bath is memoryless (Markovian) and non-Markovian. The nonequilibrium dynamics of the system communicating with a Markovian bath can be described by Fokker-Planck or master equations for the probability density for x [49]. Except for a few exactly solvable settings [16,49], these equations are usually hard to solve analytically for non-quasi-static time-dependent protocols. However, in the non-Markovian case, a corresponding closed deterministic description might not be available at all [50]. Then one has to resort to stochastic descriptions, such as a generalized Langevin equation, making even a numerical optimization challenging. The derivation also holds in situations with a nonequilibrium bath, such as in recently intensely studied cyclic active Brownian heat engines [51–54].

Let us now derive Eqs. (3) and (4). Under reasonable assumptions, any periodic variation of the control parameters eventually induces a periodic average response of the system, $\sigma(t) = \langle f[x(t)] \rangle$. This ensemble average is a functional of $T(t)$ and $\lambda(t)$ specified by dynamical equations of the system. Due to the factorized structure of the Hamiltonian (1), the average internal energy of the system $\langle H(x,t) \rangle$ is given by $\lambda(t)\sigma(t)$. Decomposing its infinitesimal change into a component corresponding to the external variation of the control λ
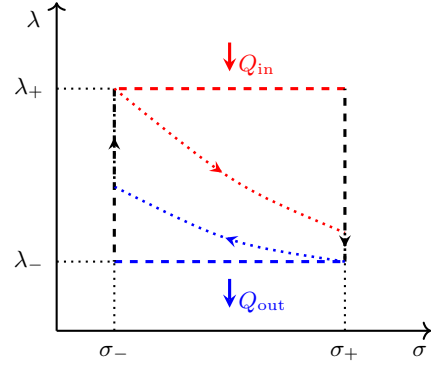

FIG. 1. The maximum-efficiency protocol (3) under the constraints in Eq. (2) (dashed line) compared to a suboptimal cycle (dotted line).

(work) and the rest (heat) [5,6], it follows that output work and input heat increments are given by $\dj W_{out}(t) = -\sigma(t)d\lambda(t)$ and $\dj Q(t) = \lambda(t)d\sigma(t)$, respectively. Per cycle, the engine transforms the fraction

$$\eta = \frac{W_{out}}{Q_{in}} = 1 - \frac{Q_{out}}{Q_{in}} \tag{5}$$

of the heat

$$Q_{in} = \int_0^{t_p} \lambda(t)\theta[d\sigma(t)]d\sigma(t) \tag{6}$$

from the heat source into output work

$$W_{out} = -\int_0^{t_p} \sigma(t)d\lambda(t), \tag{7}$$

and dumps the remaining heat $Q_{out} = Q_{in} - W_{out} = \int_0^{t_p} \lambda(t)\theta[-d\sigma(t)]d\sigma(t)$ into the heat sink. [The Heaviside step function $\theta(\bullet) = 1$ when the heat flows on average into the system, i.e., $d\sigma > 0$.]

Consider now the λ-σ diagram of the cycle depicted in Fig. 1. We seek the shape of the cycle which yields maximum efficiency η under the constraints (2).[1] The cycle must run clockwise to secure that $Q_{in} > Q_{out}$. Next, we note that maximizing η amounts to minimizing the ratio Q_{out}/Q_{in}. For given boundary values $\sigma_\pm$ of σ, this is obviously achieved by setting $\lambda = \lambda_+$ when $d\sigma > 0$ and $\lambda = \lambda_-$ when $d\sigma < 0$. In such a case, $Q_{in} = \lambda_+ \Delta\sigma$, $Q_{out} = \lambda_- \Delta\sigma$, and the efficiency is given by Eq. (4). The increase in the system response $\Delta\sigma = \sigma_+ - \sigma_-$, which can be a complicated functional of the protocol $\{T(t), \lambda(t)\}$, canceled out. Equation (4) is thus valid for arbitrary $\sigma_\pm$, and it represents the maximum efficiency of a heat engine based on Hamiltonian (1) under the constraints (2). The corresponding maximum-efficiency protocol for λ forms a rectangle ranging from λ_- to λ_+ in the λ-σ diagram regardless the cycle duration and dynamical equations of the

---

[1]A similar optimization problem is often solved in courses on classical thermodynamics to show that maximum efficiency of an equilibrium cycle under the constraint $T(t) \in [T_-, T_+]$ on the bath temperature is the Carnot efficiency. However, in our case, the system can be arbitrarily far from equilibrium.

system. The only constraint on these control parameters is that the cycle runs in the λ-σ diagram clockwise.

When not driven, a system out of equilibrium relaxes towards the equilibrium state corresponding to the instantaneous values of the fixed control parameters. For cyclically varied control parameters, the system can no longer relax to equilibrium and its nonequilibrium state "lags behind" the quasistatic cycle specified by the instantaneous values of the control parameters. In our setting, $\sigma(t)$ lags behind $\sigma^{\mathrm{eq}}(t) = \int dx f(x) \exp\{-\lambda(t) f(x)/[k_{\mathrm{B}} T(t)]\}/Z(t)$. In Appendix B 1, we show that $\sigma^{\mathrm{eq}}(t)$ is a monotonically increasing function of T/λ. Denoting as t_+ the duration of the $\lambda = \lambda_+$ branch, clockwise cycles with $\Delta\sigma > 0$ are thus obtained for temperature protocols $T(t)$ which obey (i) $\dot{T}(t) \geqslant 0$ when $\lambda = \lambda_+$, (ii) $\dot{T}(t) \leqslant 0$ when $\lambda = \lambda_-$, and (iii) $T(t_{+-})/\lambda_+ > T(t_{\mathrm{p}-})/\lambda_-$, where $T(t-) \equiv \lim_{\epsilon \to 0} T(t - |\epsilon|)$. The last condition implies that the maximum efficiency (4) obeys the standard second-law inequality $\eta \leqslant 1 - T(t_{\mathrm{p}-})/T(t_{+-}) \leqslant 1 - T_-/T_+$. It saturates for the "compression ratio" $\lambda_-/\lambda_+ = T_-/T_+$. Even for a finite cycle time t_{p}, output power, in this case, vanishes because $\sigma^{\mathrm{eq}}(t)$ becomes constant, yielding an infinitesimal quasistatic cycle with a vanishing output work. In the maximum-efficiency protocol (3), we use the specific protocol for $T(t)$ that maximizes the upper bound on η. In Appendix B 1, we argue that this temperature protocol also maximizes the output work of the engine regardless of $\lambda(t)$ because it yields the largest temperate differences between the bath and the system when they exchange heat. However, we reiterate that the maximum efficiency (4) can be achieved for an arbitrary protocol for $T(t)$ that obeys the above conditions (i)-(iii). This freedom in $T(t)$ can be exploited in setups where precise control of the bath (effective) temperature is difficult, such as in active Brownian heat engines [52].

The adiabatic branches connecting the isotherms in the protocol (3) can be realised using several qualitatively different approaches [31]. (i) One can disconnect the system from the heat bath, which might be impractical for microscopic engines. (ii) One may keep the system in thermal contact with the bath and vary the control parameters T and λ in such a way that the response σ does not change [55]. This approach allows circumventing some of the shortcomings of overdamped thermodynamics [56], where the heat fluxes through the momentum degrees of freedom are neglected. (iii) One can realize the adiabatic branches by changing the control parameters much faster than the relaxation time of the response σ [57]. In the specific maximum-efficiency protocol (3), we employ the last possibility. It minimizes the cycle time t_{p} and thus maximize the output power $P \equiv W_{\mathrm{out}}/t_{\mathrm{p}}$. Besides, it allows for a direct comparison with the maximum-efficiency protocols derived for Brownian heat engines under constraints on σ [24]. However, other realisations of the adiabatic branches yield the same maximum efficiency (4). We reiterate that also the choice of the durations t_+ and $t_{\mathrm{p}} - t_+$ of the isotherms in (3) do not affect the maximum η.

IV. MAXIMUM-POWER PROTOCOL

If the durations of the isotherms are long enough compared to the relaxation time of the system, i.e., $\Delta\sigma$ is close to its equilibrium value, and the compression ratio λ_-/λ_+ is large,

the maximum-efficiency protocol (3) also yields maximum output work W_{out} (7) and power

$$P = \frac{W_{\mathrm{out}}}{t_{\mathrm{p}}} \qquad (8)$$

under the constrained control (2). This is our second result. To prove it, consider the generally unreachable geometric loose upper bound on the output work $\max W_{\mathrm{out}} = \Delta\lambda \max \Delta\sigma^{\mathrm{eq}} = (\lambda_+ - \lambda_-)[\sigma^{\mathrm{eq}}(T_+/\lambda_-) - \sigma^{\mathrm{eq}}(T_-/\lambda_+)]$, which follows from the broadly valid assumption $\max \Delta\sigma < \max \Delta\sigma^{\mathrm{eq}}$ and the insight that W_{out} is given by the area enclosed by the cycle in the λ-σ diagram. Expanding $\max W_{\mathrm{out}}$ in $\Delta\lambda$ yields $\max W_{\mathrm{out}} = \Delta\lambda[\sigma^{\mathrm{eq}}(T_+/\lambda_+) - \sigma^{\mathrm{eq}}(T_-/\lambda_-)] + \mathcal{O}(\Delta\lambda^2)$. Up to the leading order in $\Delta\lambda$ and under the condition that the system has relaxed at the ends of the two isotherms to equilibrium, this upper bound is saturated by the protocol (3), which completes the proof. We note that (i) the condition $\Delta\sigma = \Delta\sigma^{\mathrm{eq}}$ does not mean that the cycle is slow as the system has to be close to equilibrium at the ends of the two isotherms only and can be arbitrarily far from equilibrium otherwise. (ii) This condition allows one to analytically calculate the whole probability distribution for the output work regardless of additional details of the system dynamics [16,58]. Interestingly, for semiclassical systems, piecewise constant protocols with two or more branches also maximize output power when the cycle time is much shorter than the system relaxation time [34,35,59].

Beyond these regimes, W_{out} and P strongly depend on all details of the dynamics through $\sigma(t)$ and cycle time t_{p}. While W_{out} and P are still optimized by the temperature protocol and the choice of fast adiabats in (3), optimal protocols for $\lambda(t)$ under the constraints (2) are no longer piecewise constant and they have to be identified for each system separately. Similarly to the derivation of maximum-efficiency and maximum-power protocols under constraints on the system state [24,42–44], this often involves functional optimization or extensive numerical work which are both nontrivial tasks.

In the next section, we illustrate the main features of maximum-efficiency and maximum-power protocols under constrained control on an engine based on an overdamped Brownian particle in a harmonic potential. This model describes experimental realizations of microscopic heat engines using optical tweezers [57,60,61]. Besides, the corresponding maximum-efficiency and maximum-power protocols under the constrained response are known [24], allowing for a direct comparison with our results obtained under constrained control.

V. CASE STUDY: OVERDAMPED BROWNIAN HEAT ENGINE

Let us now consider the specific Brownian heat engine based on an overdamped particle with mobility μ diffusing in a controlled harmonic potential. The Hamiltonian (1) now reads $H(x, t) = \lambda(t) x^2/2$, with x the position of the particle. The response of the system $\sigma(t) = \langle x^2/2 \rangle$ is proportional to the position variance and it obeys the first-order differential equation [16,24,62]

$$d\sigma(t)/dt = -2\mu\lambda(t)\sigma(t) + \mu k_{\mathrm{B}} T(t). \qquad (9)$$

TABLE I. Considered classes of protocols with free parameters a, b, c, d to be determined by the optimization (protocols λ_{pwc} and λ_{S} have only two free parameters). The protocols are in general discontinuous at times t_+ and t_{p}. The piecewise constant protocol $\lambda_{\text{pwc}}(t)$ is a variant of the maximum-efficiency protocol $\lambda_\eta(t)$ (3), where $\lambda_{\text{pwc}}(t)$ does not have to reach the boundary values λ_- and λ_+. The piecewise linear protocol $\lambda_{\text{pwl}}(t)$ has zero curvature. The protocol $\lambda_{\text{slow}}(t)$ minimizes the irreversible losses during isothermal branches under close-to-equilibrium conditions. Such protocols can be derived for Brownian heat engines with Hamiltonians of the form $\lambda(t)x^n/n$ (for details, see Appendix C). The protocol $\lambda_{\text{S}}(t)$ maximizes both power and efficiency under the constraint that $\sigma(0) = \sigma(t_{\text{p}}) \equiv a$ and $\sigma(t_+) \equiv b$ [24]. The corresponding response $\sigma_{\text{S}}(t)$ is given by Eq. (D2). For $b = d = 0$, λ_{pwl} and λ_{slow} reduce to λ_{pwc}.

	$\lambda_{\text{pwc}}(t)$	$\lambda_{\text{pwl}}(t)$	$\lambda_{\text{slow}}(t)$	$\lambda_{\text{S}}(t)$
$t < t_+$	a	$a + bt$	$\dfrac{a}{(1+bt)^2}$	$\dfrac{T_+}{2\sigma_{\text{S}}(a,b,t)} - \dfrac{\sqrt{b}-\sqrt{a}}{\mu t_+ \sqrt{\sigma_{\text{S}}(a,b,t)}}$
$t > t_+$	c	$c + dt$	$\dfrac{c}{(1+dt)^2}$	$\dfrac{T_-}{2\sigma_{\text{S}}(a,b,t)} + \dfrac{\sqrt{b}-\sqrt{a}}{\mu t_- \sqrt{\sigma_{\text{S}}(a,b,t)}}$

In Sec. III, we proved that the maximum-efficiency protocol under the constraints (2) should, in this case, be the protocol (3). In this section, we illustrate this results by direct numerical optimization. In addition, we ask which protocol for λ yields the largest output power under the constraints (2). Even though the model (9) is exactly solvable [16], the corresponding optimal $\lambda(t)$ has to be found numerically, e.g., by the method in Ref. [63]. To keep the optimization transparent, we instead consider the specific set of families of protocols for the isothermal strokes in Table I and numerically optimize over their free parameters. When such classes are chosen suitably, the resulting suboptimal performance will be close to the global optimum [64,65]. Besides, we use the protocol for temperature and adiabatic branches from Eq. (3), and fix the durations of the two isotherms and thus t_{p}. The durations can be further optimized once the optimal variation of λ is known. The solutions to Eq. (9) can involve exponentials of very large or small numbers, which can lead to numerical instabilities inducing large losses of precision, and thus they have to be treated with care. To secure that our solutions are always precise enough, we have solved Eq. (9) in our analysis also numerically.

For the protocols in Table I and the temperature protocol in Eq. (3), we thus numerically optimized the efficiency (5) and output power (8) as functions of the parameters $\{a, b, c, d\}$ under constraints on $\lambda(t)$. For constrained response $\sigma(t)$, we additionally verified in Appendix D that the protocol λ_{S} obtained from Ref. [24] indeed yields both the maximum power and maximum efficiency.

The results of optimizing efficiency under the constrained control are depicted in Fig. 2. For all of the trial protocols from Table I except for λ_{S} the optimal values of parameters b and d were 0. All these protocols thus collapsed to the piecewise constant maximum-efficiency protocol λ_η (3), illustrating our general theoretical result. Notably, the efficiency achieved by the maximum-efficiency protocol is significantly larger than that provided by usage of the protocol λ_{S}, which gives maximum efficiency under constrained response.
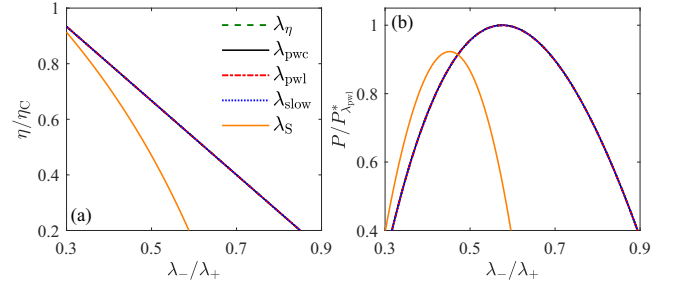

FIG. 2. Numerical optimization of the efficiency of the Brownian heat engine under constrained control verifies that the maximum-efficiency protocol is given by Eq. (3). (a) Maximum efficiency and (b) the corresponding power (in units of the ultimate maximum power $P^*_{\lambda_{\text{pwl}}}$ for λ_{pwl}) as functions of λ_-/λ_+. All protocols except for λ_{S} perfectly overlap. Parameters used are $t_+ = t_- = 1$, $k_{\text{B}}T_+ = 1$, $k_{\text{B}}T_- = 0.25$ (thus Carnot efficiency $\eta_{\text{C}} \equiv 1 - T_-/T_+ = 0.75$), $\lambda_+ = 0.5$, and $\mu = 1$.

Main results of the optimization of output power under the constrained control are summarized in Fig. 3. (i) With increasing minimum compression ratio λ_-/λ_+ allowed by the constraints (2), maximum power for all considered protocols in (a) is first constant and then, at an optimal compression ratio r^*, decreases. The decreasing part corresponds to protocols which span between the allowed boundary values, i.e., $\max \lambda(t) = \lambda(0+) = \lambda_+$ and $\min \lambda(t) = \lambda(t_++) = \lambda_-$. At the plateau, the boundary values of the protocols are chosen within the bounds (2) to keep the optimal compression ratio r^*. (ii) Values of maximum power obtained for the protocols which have enough free parameters are indistinguishable within our numerical precision. As the corresponding optimized protocols seem to have minimum possible curvature $\ddot\lambda(t)$, we conclude that the maximum-power protocol is λ_{pwl}. (iii) Only the protocol λ_{S}, optimized for constrained response σ, yields notably smaller power than other protocols. (iv) In agreement with our above discussion, for large enough values of $\lambda_-/\lambda_+ \geqslant 0.59$, the optimized parameters for protocols λ_{pwc}, λ_{pwl}, and λ_{slow} are $b = d = 0$, $a = \lambda_+$, and $c = \lambda_-$, reducing them to λ_η (3). (v) The maximum powers for the protocols λ_η and λ_{pwl} differ just by 1%.

In Fig. 4, we further show that the relative difference in maximum power for λ_{pwl} and λ_η is small for a broad range of values of T_-/T_+ and t_-/t_+. From panels (c)–(f) we conclude that the optimal ratio t_-/t_+ is between 1 and 2, which is in agreement with the results of Appendix B 2 b [see Eq. (B19) below]. Thus, for branch durations that optimize output power, the relative difference δP in (a) is always below 12%, decreasing with the temperature ratio. These results indicate that when one can optimize W_{out} and P over λ_-, the maximum-efficiency protocol (3) often yields almost the maximum power.

The optimization over λ_- is natural for experimental platforms with limitations on the maximum strength of the potential only. The maximum power regime of the maximum-efficiency protocol (3) can be, to a large extend, investigated analytically. First, assuming again that durations of the isotherms are long enough that the system is close to equilibrium at times t_+ and t_{p}, we have $W_{\text{out}} =$
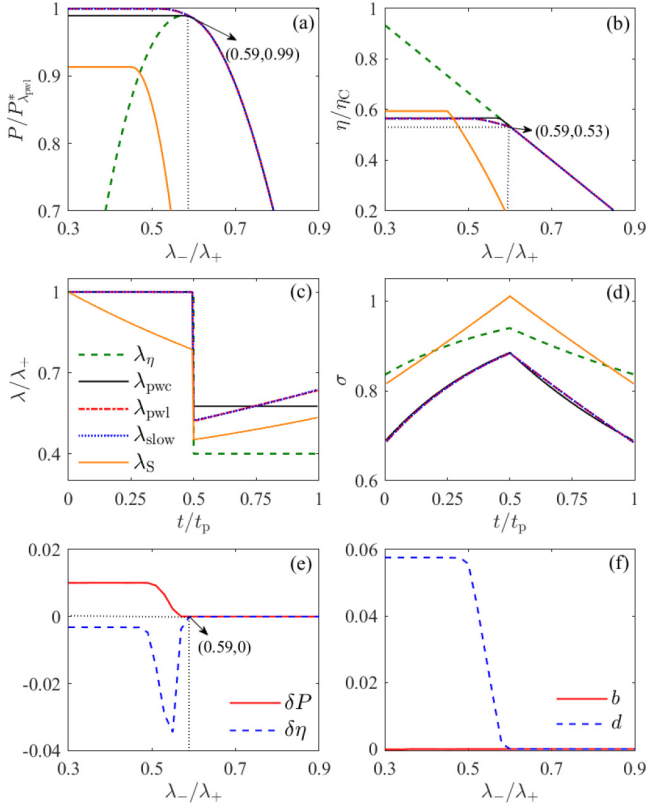
FIG. 3. Numerical optimization of the output power of the Brownian heat engine illustrates that the maximum-efficiency protocol λ_η (3) also yields maximum power when the compression ratio λ_-/λ_+ is large and the durations $t_+ = t_- = 1$ of the two isotherms are comparable to the relaxation times $1/(2\mu\lambda_\pm)$ for σ. (a) Powers (in units of the ultimate maximum power $P^*_{\lambda_{\text{pwl}}}$ for λ_{pwl}) and (b) the corresponding efficiencies obtained using λ_η (3) and the protocols in Table I. For $\lambda_-/\lambda_+ \geqslant 0.59$ all protocols except for λ_{S} coincide. (c) and (d) show the protocols and the resulting response for $\lambda_-/\lambda_+ = 0.4$. (e) The relative differences $\delta X = (X_{\lambda_{\text{pwl}}} - X_{\lambda_{\text{pwc}}})/X_{\lambda_{\text{pwl}}}$ of power $(X = P)$ and efficiency $(X = \eta)$ for λ_{pwl} and λ_{pwc}. (f) The optimal values of parameters b and d for λ_{pwl}. We used the same parameters as in Fig. 2.

$(\lambda_+ - \lambda_-)[\sigma^{\text{eq}}(T_+/\lambda_+) - \sigma^{\text{eq}}(T_-/\lambda_-)]$. For $f(x) = |x|^n$ in Eq. (1), we then find that the optimal compression ratio is $\lambda_-/\lambda_+ = \sqrt{T_-/T_+}$, which leads to the output work $W_{\text{out}} = k_{\text{B}}T_+(2\eta_{\text{CA}} - \eta_{\text{C}})/n$ and Curzon-Ahlborn efficiency $\eta = \eta_{\text{CA}} = 1 - \sqrt{T_-/T_+}$ (see Appendix B 2 a for details). For other than power-law Hamiltonians, the efficiency at maximum power can differ from η_{CA} but it can still be determined numerically regardless details of dynamical equations for the system (for details, see Appendix B 2 a). Relaxing the assumption of slow (but not quasistatic) isotherms, the optimization of W_{out} with respect to λ_- requires specification of the dynamics. In Fig. 5, we show that the efficiency at maximum power of the Brownian heat engine described by Eq. (9) and driven by the maximum-efficiency protocol (3) is bounded between the Curzon-Ahlborn efficiency, achieved for slow isotherms, and the efficiency $2 - \sqrt{4 - 2\eta_{\text{C}}} < \eta_{\text{CA}}$, reached in the limit $t_{\text{p}} \to 0$.

In closing this section, we summarize the strong effects of the constraints (constrained control versus constrained response [24]). First, constraining the control allowed us to derive much more generally valid results than constraining the response. Second, for the constrained response, the power and efficiency can be optimized simultaneously, whereas for the constrained control this is, in general, not possible. Third, the resulting functional forms of the optimal protocols and the corresponding optimal performance strongly differ. Fourth, the change of boundary conditions alters the optimal allocation of cycle duration between hot and cold isotherms, t_+/t_-, as we show below Eq. (B19) in the Appendix.

VI. CONCLUSION

We have optimized the thermodynamic performance of finite-time overdamped stochastic heat engines under the constraint that control parameters, such as potential strength or bath temperature, can be varied only over a limited range. This optimization problem is experimentally motivated and differs from previously studied optimization studies performed with constraints on the system's state. We have found that, for working fluids described by the experimentally most common "breathing" Hamiltonians proportional to a control parameter, the maximum efficiency is reached by piecewise constant modulation of the control parameters, independently of the detailed dynamics of the system. When the control parameter can only be changed over a small range and the system is close to equilibrium at the ends of the isotherms, the maximum-efficiency protocol also yields maximum output power. But outside this regime, the maximization of power requires specifying the dynamical equations of the working fluid. For engines based on an overdamped Brownian particle trapped in a harmonic potential, we numerically found that the maximum-power protocol is linear. Nevertheless, the global maxima of the maximum-power and maximum-efficiency protocols are in this setting close, suggesting that the maximum-efficiency protocol provides a reasonable estimate of the output power.

The main strength of the presented derivations of the maximum-efficiency and maximum-power protocols under constrained control is their simplicity and unprecedented generality. Their possible extension to more complicated Hamiltonians is sketched in Appendix A. While more general extensions remain to be explored in future work, the validity of our results for Brownian heat engines is already of experimental relevance. These engines are often realized using optical tweezers with strict bounds on the trap stiffness λ: too small λ leads to losing the Brownian particle while too large λ can induce its overheating. Interestingly, the achievable trap stiffnesses are well above 10^{-6} N/m [31]. For spherical Brownian particles with the radius of 10^{-6} m in water, the Stokes law predicts the mobility of $\mu \approx 0.5 \times 10^8$ m/Ns, leading to the relaxation time $1/(2\mu\lambda)$ of the response σ on the order of 10^{-2} s. The assumption that the durations of the isotherms are longer than the response relaxation time, used in our derivation of the maximum-power protocol, is thus, in this setup, natural. Besides, we believe that extensions of our results can find applications in more involved optimization tasks, e.g., performed using machine learning algorithms [66,67] or geometric methods [68,69], as well as in quantum setups [39,70,71].
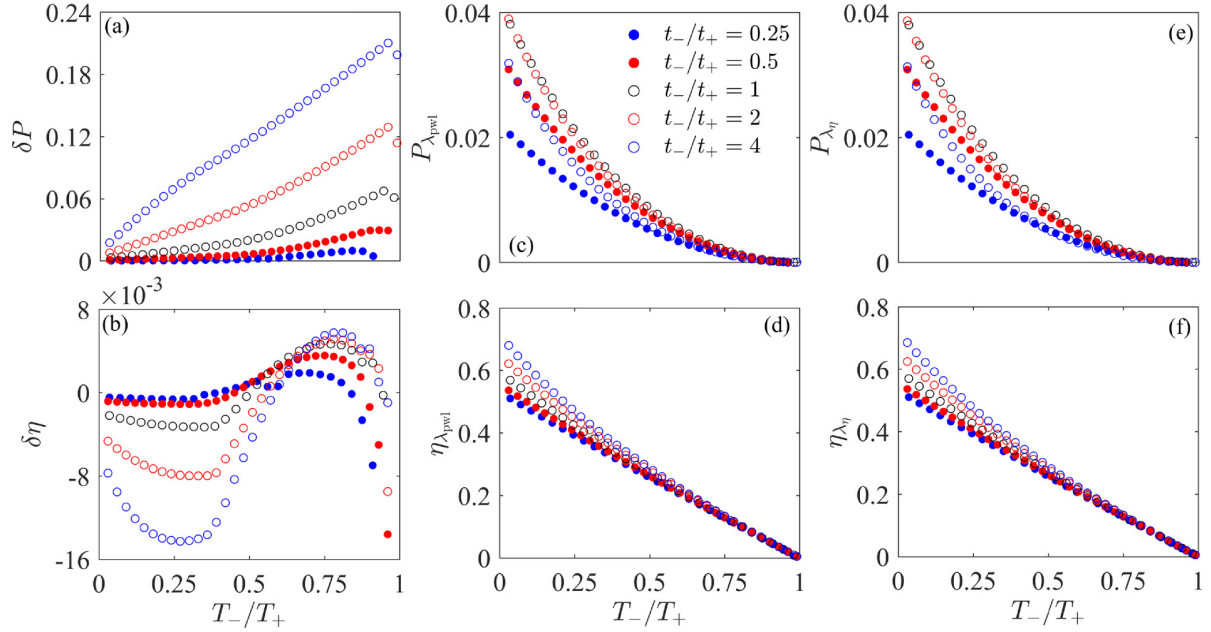
FIG. 4. The relative differences $\delta X = (X_{\lambda_{\mathrm{pwl}}} - X_{\lambda_\eta})/X_{\lambda_{\mathrm{pwl}}}$ of (a) maximum power ($X = P$) optimized with respect to λ_- and (b) the corresponding efficiency ($X = \eta$) for the linear protocol λ_{pwl} and the maximum-efficiency protocol (3) for different values of T_-/T_+ and t_-/t_+. (c)–(f) show the corresponding values of maximum power and efficiency. The piecewise constant protocol λ_{pwc} and the maximum-efficiency protocol λ_η (3) are in this case equal. We used the same parameters as in Fig. 2.
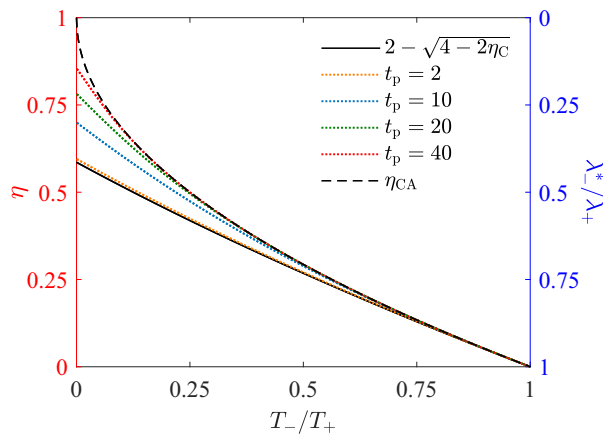
FIG. 5. Efficiency at maximum output power (η, red axis) and the corresponding optimal compression ratio (λ_-^*/λ_+, blue axis) for the maximum-efficiency protocol (3) as functions of the temperature ratio T_-/T_+ for six values of cycle duration t_{p} (colored curves) and $t_- = t_+$. The cycle time, t_{p}, is measured in units of the system relaxation time during the hot isotherm. The corresponding ratio during the cold isotherm reads $t_{\mathrm{p}} \lambda_-^*/\lambda_+$. We used the same parameters as in Fig. 2.

APPENDIX A: MAXIMUM-EFFICIENCY PROTOCOL FOR MULTITERM HAMILTONIANS

Consider a heat engine with a working fluid described by the Hamiltonian

$$H(x, t) = \sum_i \lambda_i(t) f_i(x) \qquad (A1)$$

with control parameters $\lambda_i(t)$, $i = 1, \ldots, N$. As in the main text, we now aim to derive the finite-time protocol for the constrained control parameters, $\lambda_i(t) \in (\lambda_i^-, \lambda_i^+)$, which would yield maximum efficiency of the engine. It will turn out that if the compression ratios λ_i^-/λ_i^+ for all the control parameters equal, the geometric argument from the main text still applies.

The heat increment is for the Hamiltonian (A1) given by $đQ = \sum_i \lambda_i(t) d\sigma_i(t)$ with the response functions $\sigma_i(t) = \langle f_i(x) \rangle$. For arbitrary fixed maximum changes $\Delta\sigma_i$ in the response functions during the cycle, geometric upper and lower bounds on Q_{in} and Q_{out} and thus on efficiency are achieved by clockwise rectangular cycles in the individual λ_i-σ_i diagrams. These hypothetical cycles yield the following geometric upper

bound on efficiency:

$$\eta = 1 - \frac{Q_{\text{out}}}{Q_{\text{in}}} \leqslant 1 - \frac{\sum_i \Delta\sigma_i \lambda_i^-}{\sum_i \Delta\sigma_i \lambda_i^+}. \qquad \text{(A2)}$$

We use the term "geometric" to stress that this bound follows from the analysis of the cycle in the λ-σ diagram, without considering the relation between the protocol $[\lambda_1(t), \ldots, \lambda_N(t)]$ and the response $[\sigma_1(t), \ldots, \sigma_N(t)]$ imposed by dynamical equations of the working fluid. This means that the given set of $\Delta\sigma_i$ might not be achievable by the piecewise constant protocol and thus the bound in (A2) is loose. Furthermore, we seek an optimal protocol constrained just by the conditions on λ_i, and the upper bound in (A2) in general strongly depends on the fixed values of $\Delta\sigma_i$. For the single-term Hamiltonian $H(x,t) = \lambda(t)f(x)$ used in the main text, this has not been an issue because then $\Delta\sigma$ in the nominator and denominator in (A2) cancel out and the upper bound becomes independent of the details of the dynamics. The optimal protocol for efficiency is then the piecewise constant protocol for $\lambda(t)$ because it saturates the geometric upper bound. To sum up, the bound in (A2) allows one to derive the maximum-efficiency protocol only if it happens to be independent of $\Delta\sigma_i$. In the opposite case, the optimal protocol cannot be determined without considering the dynamical equations and performing the corresponding functional optimization.

Let us now investigate when the upper bound in (A2) becomes independent of the system response, $\Delta\sigma_i$. Defining the set of "probabilities" $p_i = \Delta\sigma_i \lambda_i^+ / \sum_i \Delta\sigma_i \lambda_i^+$, the ratio in the upper bound in (A2) can be rewritten as the average

$$\frac{\sum_i \Delta\sigma_i \lambda_i^-}{\sum_i \Delta\sigma_i \lambda_i^+} = \sum_i p_i \frac{\lambda_i^-}{\lambda_i^+}. \qquad \text{(A3)}$$

This expression becomes independent of σ_i only if all the compression ratios λ_i^-/λ_i^+ are equal. In such a case, the maximum-efficiency protocol is thus a piecewise constant protocol for each of λ_i and yields the efficiency

$$\eta = 1 - \lambda_i^-/\lambda_i^+. \qquad \text{(A4)}$$

Besides this result, the probabilistic interpretation (A3) of the upper bound in (A2) also yields the dynamics independent (but in general loose) *upper bound* on efficiency,

$$\eta \leqslant 1 - \min_i \frac{\lambda_i^-}{\lambda_i^+}. \qquad \text{(A5)}$$

To close this section, we note that a piecewise constant protocol for λ_i will always yield the efficiency $1 - (\sum_i \Delta\sigma_i \lambda_i^-)/(\sum_i \Delta\sigma_i \lambda_i^+)$, with values of $\Delta\sigma_i$ induced by the dynamical equations of the system. Within the class of piecewise constant protocols, the upper bound (A5) is then tight if the constraints on all the control parameters λ_i allow to achieve the minimum compression ratio $\min_i \frac{\lambda_i^-}{\lambda_i^+}$. Furthermore, for such protocols, Eq. (A3) also implies the *lower bound* on the efficiency,

$$\eta \geqslant 1 - \max_i \frac{\lambda_i^-}{\lambda_i^+}, \qquad \text{(A6)}$$

which is always tight.

APPENDIX B: PROPERTIES OF MAXIMUM-EFFICIENCY PROTOCOL

In this section, we provide further details concerning the maximum-efficiency protocol for the Hamiltonian, $H(x,t) = \lambda(t)f(x)$, discussed in the main text. First, we argue that the maximum-efficiency protocol that yields maximum output work for the given piecewise constant $\lambda(t)$ requires piecewise constant variation of temperature. Then, we investigate output power of the maximum-efficiency protocol as a function of the lower bound on the control parameter $\lambda(t)$.

1. Temperature protocol

In the main text, we have shown that the maximum-efficiency protocol for the control parameter $\lambda(t)$ is piecewise constant and the corresponding efficiency $\eta = 1 - \lambda_-/\lambda_+$. The only condition on the temperature protocol was that the cycle is performed clockwise in the λ-σ diagram. Nevertheless, in order to allow the engine to operate at Carnot efficiency and to maximize its output work, we have chosen the protocol (3).

For this choice of $T(t)$, the working medium of the engine operates with the largest possible temperature gradient during the whole cycle. This maximizes the heat flux through the engine, which can be utilized to yield the maximum amount of work $W_{\text{out}} = \eta Q_{\text{in}}$. Besides, the engine efficiency η is also known to increase with the bath temperature difference [see also Figs. 4(c)–4(f)].

Let us now provide an alternative and more technical argument that the choice of $T(t)$ in Eq. (3) maximizes the output work. We restrict this argument to the maximum-efficiency protocol for λ in Eq. (3). However, generalizations to other protocols are straightforward. The main idea is that connecting the system to the hottest possible bath when $\dot\sigma > 0$ and to the coldest possible bath when $\dot\sigma < 0$ maximizes the extent of the cycle in the σ direction in the σ-λ diagram and thus also W_{out}.

For the protocol (3), the output work is given by

$$W_{\text{out}} = \Delta\lambda \Delta\sigma, \qquad \text{(B1)}$$

with $\Delta\lambda = \lambda_+ - \lambda_-$ and the maximum change in the response parameter during the cycle $\Delta\sigma = \sigma_+ - \sigma_-$. To maximize W_{out}, we thus need to maximize $\Delta\sigma$. To this end, it is reasonable to assume that

$$\Delta\sigma \leqslant \Delta\sigma^{\text{eq}}, \qquad \text{(B2)}$$

where $\Delta\sigma^{\text{eq}} = \max\sigma^{\text{eq}} - \min\sigma^{\text{eq}}$ is the maximum change in the response parameter σ during the cycle with isochoric branches (constant λ) longer than the system relaxation time. This assumption is in particular valid for arbitrary overdamped dynamics, where σ always converges to its equilibrium value (k_B denotes the Boltzmann constant)

$$\sigma^{\text{eq}}(t) = \sum_x f(x) \frac{\exp\{-\lambda(t)f(x)/[k_B T(t)]\}}{\sum_x \exp\{-\lambda(t)f(x)/[k_B T(t)]\}}, \qquad \text{(B3)}$$

corresponding to the instantaneous values of the control parameters $\{T(t), \lambda(t)\}$. Noticing that $\sigma^{\text{eq}}(t) = U(t)/\lambda(t)$, where $U(t) = \langle H(x,t) \rangle$ is the thermodynamic internal energy

of the system, the positivity of heat capacity

$$C_v = \frac{\partial U}{\partial T} = \frac{\partial \sigma^{eq}}{\partial (T/\lambda)} > 0 \qquad (B4)$$

implies that σ^{eq} is a monotonously increasing function of the ratio T/λ.

From Fig. 1 in the main text, it follows that $\max \sigma^{eq}$ and $\min \sigma^{eq}$ are the values of σ^{eq} at the ends of the isochores with $\lambda = \lambda_+$ and $\lambda = \lambda_-$, respectively. The upper bound on $\Delta\sigma$ is thus given by

$$\max \sigma^{eq} - \min \sigma^{eq} = \sigma^{eq}(T_+/\lambda_+) - \sigma^{eq}(T_-/\lambda_-). \quad (B5)$$

It is attained for slow isochores when $T = T_+$ for $\lambda = \lambda_+$ and $T = T_-$ for $\lambda = \lambda_-$. As long as $\dot{\sigma}^{eq} > 0$ for $\lambda = \lambda_+$ and $\dot{\sigma}^{eq} < 0$ for $\lambda = \lambda_-$ (so that the used definitions of input and output heat hold), details of the temperature protocol during the isochores in this limit do not alter the value of $\Delta\sigma^{eq}$ and thus $W_{out} = \Delta\lambda\Delta\sigma^{eq}$. However, these details become important for finite-time cycles.

A typical dynamical equation for an overdamped degree of freedom has the form

$$\dot{\sigma}(t) = t_R^{-1}[\sigma^{eq} - \sigma(t)]. \qquad (B6)$$

For constant values of control parameters $T(t)$ and $\lambda(t)$, which enter the relaxation time t_R and the equilibrium state $\sigma^{eq}(t)$ defined in Eq. (B3), this equation describes an exponential relaxation of σ to σ^{eq} (for a specific example, see Sec. B 2 b). For a cyclic variation of the control parameters, σ lags behind σ^{eq} [72]. More precisely, $\sigma \leqslant \sigma^{eq}$ and $\dot{\sigma} \geqslant 0$ for $\lambda = \lambda_+$, when σ^{eq} increases to $\max \sigma^{eq}$, and $\sigma \geqslant \sigma^{eq}$ and $\dot{\sigma} \leqslant 0$ for $\lambda = \lambda_-$, when σ^{eq} decreases to $\min \sigma^{eq}$. The change in the response $\Delta\sigma = \int_0^{t_+} \dot{\sigma} \, dt = -\int_{t_+}^{t_p} \dot{\sigma} \, dt$ and thus it can be maximized by maximizing (minimizing) the instantaneous rate of change of the response, $\dot{\sigma}$, during the first (second) isochore. From Eq. (B6), it follows that this is achieved by setting $\sigma^{eq} = \max \sigma^{eq}$ during the fist isochore and $\sigma^{eq} = \min \sigma^{eq}$ during the second one. Altogether, this suggests that the piecewise constant temperature protocol in Eq. (3) yields maximum $\Delta\sigma$ and thus output work W_{out} (B1) for arbitrary cycle duration.

2. Efficiency at maximum power

Let us now turn to the task of maximizing the output work $W_{out} = (\lambda_+ - \lambda_-)\Delta\sigma$ with respect to λ_-. Analytical results can be obtained in the limits of slow and fast isotherms.

a. Slow isotherms

When the duration of the isotherms is longer than the relaxation time of the response σ, one can approximate σ_+ and σ_- in $\Delta\sigma$ by their equilibrium values. Using Eq. (B1), the output work then reads

$$W_{out} = \Delta\lambda\Delta\sigma^{eq}. \qquad (B7)$$

Equation (B4) implies that the partial derivative of σ^{eq} with respect to the control parameter λ (T is constant) is given by

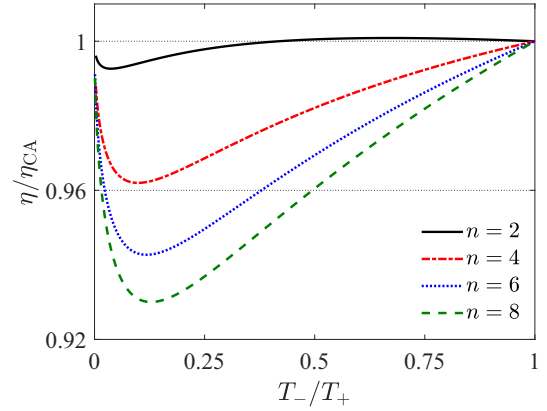$$\frac{\partial}{\partial\lambda}\sigma^{eq}(T/\lambda) = -\frac{T}{\lambda^2}C_v. \qquad (B8)$$

FIG. 6. Efficiency at maximum output work obtained using the Hamiltonian $H = \lambda(t)(|x|^n/n - \ln|x|)$ as a function of T_-/T_+. Parameters used are $k_B T_+ = 1$ and $\lambda_+ = 0.5$.

The condition on the extreme of W_{out} (B7) with respect to λ_- thus reads

$$\frac{\partial W_{out}}{\partial\lambda_-} = (\lambda_+ - \lambda_-)\frac{T_-}{\lambda_-^2}C_v(T_-/\lambda_-) - \frac{U(T_+/\lambda_+)}{\lambda_+}$$
$$+ \frac{U(T_-/\lambda_-)}{\lambda_-} = 0, \qquad (B9)$$

where we additionally used the relation $\sigma^{eq} = U/\lambda$ between σ^{eq} and the internal energy U.

For power law Hamiltonians of the form $H = \lambda|x|^n/n$ where $C_v = k_B/n$ and $U = k_B T/n$, this equation can be solved explicitly. The resulting optimal compression ratio is given by $\lambda_-/\lambda_+ = \sqrt{T_-/T_+}$. The corresponding efficiency at the maximum output work is given by the Curzohn-Ahlborn efficiency,

$$\eta = 1 - \frac{\lambda_-}{\lambda_+} = 1 - \sqrt{\frac{T_-}{T_+}} \equiv \eta_{CA}, \qquad (B10)$$

and the maximum output work is (Carnot efficiency $\eta_C = 1 - T_-/T_+$)

$$W_{out} = \frac{k_B T_+}{n}(2\eta_{CA} - \eta_C). \qquad (B11)$$

Let us now consider the asymmetric Hamiltonian $H = \lambda(t)(|x|^n/n - \ln|x|)$. In this case, the internal energy and heat capacity are given by

$$U = \frac{k_B T + \lambda[1 + \ln\frac{\lambda}{nk_B T} - \psi^{(0)}(\frac{\lambda + k_B T}{nk_B T})]}{n}, \quad (B12)$$

$$C_v = \frac{nk_B T(k_B T - \lambda) + \lambda^2\psi^{(1)}(\frac{\lambda + k_B T}{nk_B T})}{n^2 k_B^2 T^2}, \quad (B13)$$

where $\psi^{(m)}(z)$ denotes the polygamma function of order m. In this case, Eq. (B9) is transcendental and we solved it numerically. In Fig. 6, we show the resulting efficiency at the maximum output work as a function of T_-/T_+. Even though the resulting efficiency is still close to η_{CA}, it can be both slightly larger and smaller than that.

b. Fast isotherms

Let us now assume that the duration of the isothermal branches are much shorter than the system relaxation time. In such a case, the work optimization cannot be done without specifying the dynamical equation for the response σ. To this end, we assume that it obeys the overdamped equation (B6) with the equilibrium value σ^{eq} and relaxation time t_R determined by the values of the control parameters $\{T(t), \lambda(t)\}$ at time t. The most prominent examples of systems described by this formula are a two-level system [35] and an overdamped particle trapped in a harmonic potential [24].

Solving Eq. (B6) for the maximum-efficiency protocol (3), we find that

$$
\sigma(t) = \begin{cases}
\sigma_0 e^{-\frac{t}{t_R^+}} + \sigma_{\mathrm{eq}}^+ \left(1 - e^{-\frac{t}{t_R^+}}\right), & 0 < t < t_+, \\
\sigma_1 e^{-\frac{t-t_+}{t_R^-}} + \sigma_{\mathrm{eq}}^- \left(1 - e^{-\frac{t-t_+}{t_R^-}}\right), & t_+ < t < t_{\mathrm{p}},
\end{cases}
\tag{B14}
$$

where $\sigma_0 \equiv \sigma(0)$ and $\sigma_1 \equiv \sigma(t_+)$ are determined by the condition that $\sigma(t)$ must be a continuous function of time. The variables corresponding to the first (second) isotherm are denoted by max (min). It turns out that

$$
\Delta \sigma = \sigma_+ - \sigma_- = \sigma_1 - \sigma_0
$$

$$
= \Delta \sigma^{\mathrm{eq}} \frac{\sinh\left(t_+/t_R^+\right)\sinh\left(t_-/t_R^-\right)}{\sinh\left(t_+/t_R^+ + t_-/t_R^-\right)} \leqslant \Delta \sigma^{\mathrm{eq}}.
\tag{B15}
$$

Substituting this result into the expression for the output work (B1) and expanding the result up to the leading order in the ratios of duration of the individual isotherms to the corresponding relaxation times, t_+/t_R^+ and t_-/t_R^-, we find that

$$
W_{\mathrm{out}} = \Delta \lambda \, \Delta \sigma^{\mathrm{eq}} \frac{\frac{t_+ t_-}{t_R^+ t_R^-}}{\frac{t_+}{t_R^+} + \frac{t_-}{t_R^-}}.
\tag{B16}
$$

To maximize the output work, we need to choose a specific model to determine the dependence of the equilibrium values of response and relaxation times on the control parameters. To this end, we consider the paradigmatic model of stochastic thermodynamics, $\dot{\sigma}(t) = -2 \mu \lambda(t) \sigma(t) + \mu k_B T$, describing an overdamped Brownian particle with mobility μ in a harmonic trap [24,62]. In this case, $\sigma^{\mathrm{eq}} = T/(2\mu\lambda)$ and $t_R = 1/(2\mu\lambda)$, and the maximum output work (B16) is produced for

$$
\frac{\lambda_-}{\lambda_+} = \sqrt{(\alpha + 1)(\alpha + 1 - \eta_C)} - \alpha,
\tag{B17}
$$

where $\alpha \equiv t_+/t_-$. The corresponding efficiency reads

$$
\eta = 1 - \frac{\lambda_-}{\lambda_+} = \alpha + 1 - \sqrt{(\alpha + 1)(\alpha + 1 - \eta_C)},
\tag{B18}
$$

which reduces to η_{CA} for $\alpha \to 0$ and $\eta_C/2$ for $\alpha \to \infty$. Assuming that $\alpha = 1$ ($t_+ = t_-$), Eq. (B18) is given by the formula

$$
\eta = 2 - \sqrt{4 - 2\eta_C} = \frac{\eta_C}{2} + \frac{\eta_C^2}{16} + \mathcal{O}\left(\eta_C^3\right)
\tag{B19}
$$

used in the main text. The corresponding expansion for the Curzohn-Ahlborn efficiency, $\eta_{CA} \approx \frac{\eta_C}{2} + \frac{2\eta_C^2}{16}$, has an identical linear term and a twice larger quadratic term.

Last but not least, with respect to α, the output power $W_{\mathrm{out}}/t_{\mathrm{p}}$ using Eq. (B16) develops a peak at $\alpha = \alpha^* = \sqrt{\frac{\lambda_-}{\lambda_+}} < 1$. This also contradicts the situation with constrained σ, where maximum power is attained when the durations of the isotherms are equal ($\alpha = \alpha^* = 1$) [24].

APPENDIX C: OPTIMAL DRIVING FOR SYSTEMS CLOSE TO EQUILIBRIUM

In this Appendix, we consider optimization of a slowly driven heat engine based on an overdamped Brownian particle trapped in the power-law potential $H = \lambda(t)x^n/n$ with $n = 2, 4, \ldots$. We use the temperature protocol from Eq. (3) and impose fixed values of the response σ (or, in the slow driving limit equivalently also the control λ) at the ends of the two isotherms. Dynamics of the particle position is described by the Langevin equation

$$
\dot{x} = -\mu\lambda(t)x^{n-1} + \sqrt{2D(t)}\xi(t),
\tag{C1}
$$

where $D(t) = \mu k_B T(t)$ denotes the diffusion coefficient. From Eq. (C1) and its formal solution

$$
x(t) = -\mu \int dt\, \lambda(t)x^{n-1}(t) + \sqrt{2D(t)} \int dt\, \xi(t),
\tag{C2}
$$

we find that $\langle x(t)\xi(t)\rangle = \sqrt{D/2}$ and thus

$$
\frac{d}{dt}\langle x^2(t)\rangle = -2\mu\lambda(t)\langle x^n(t)\rangle + 2D.
\tag{C3}
$$

Let us now assume that the control parameters $\{T(t), \lambda(t)\}$ vary slowly with respect to the relaxation time of the system, such that, during the limit cycle, the system is always close to equilibrium, and solve this equation up to the first order in $\dot{\lambda}(t)$. To this end, we consider the ansatz $\langle x^2(t)\rangle = \langle x^2(t)\rangle_0$ and $\langle x^n(t)\rangle = \langle x^n(t)\rangle_0 + \langle x^n(t)\rangle_{\dot{\lambda}}$, where

$$
\langle x^m(t)\rangle_0 = \int_{-\infty}^{\infty} dx\, x^m \frac{\exp\left(-\mu\frac{\lambda x^n}{nD}\right)}{Z},
\tag{C4}
$$

with the partition function $Z = 2[nD/\mu\lambda(t)]^{1/n}\Gamma(1 + 1/n)$, is the value of the moment $\langle x^m(t)\rangle$ corresponding to the infinitely slow driving, and $\langle x^n(t)\rangle_{\dot{\lambda}}$ is the correction proportional to $\dot{\lambda}$. We find that

$$
\langle x^n(t)\rangle_0 = \frac{D(t)}{\mu\lambda(t)},
\tag{C5}
$$

$$
\langle x^2(t)\rangle_0 = \left[\frac{nD(t)}{\mu\lambda(t)}\right]^{2/n} \frac{\Gamma(3/n)}{\Gamma(1/n)},
\tag{C6}
$$

and

$$
\langle x^n(t)\rangle_{\dot{\lambda}} = -\frac{1}{2\mu\lambda(t)} \frac{d}{dt}\langle x^2(t)\rangle_0.
\tag{C7}
$$

We reiterate that this solution is valid only for protocols $\{T(t), \lambda(t)\}$ which are changing slowly with respect to the relaxation time of the system so that the system is, during the whole cycle, close to equilibrium. However, as we know from the previous discussion, both the piecewise constant

maximum-efficiency protocol for constrained control and the optimal protocol (D1) for the constrained response contain discontinuities, where $\{T(t), \lambda(t)\}$ changes abruptly. To be able to use the slow driving approximation for the derivation of optimal cyclic protocols, we thus need to additionally assume that during these jumps the system is not driven far from equilibrium. To this end, we assume that the ratio $\lambda(t)/T(t)$ in the Boltzmann factor is during the jumps at the ends of the isotherms constant. This additional assumption fixes the state of the system σ at the ends of the isotherms and thus the present optimization scheme is only suitable for the optimization under the constrained response. Let us now proceed with the optimization.

Work done on the system during the time interval $t_i \leqslant t \leqslant t_f$ for the given Hamiltonian reads

$$W = \frac{1}{n} \int_{t_i}^{t_f} dt\, \dot{\lambda}(t) \langle x^n(t) \rangle \equiv W(t_i, t_f). \quad (C8)$$

Having fixed the state of the system at the ends of the isotherms, it is enough to maximize the work during these branches. For an isothermal process, the work Eq. (C8) can be written as $W = \Delta F + W_{irr}$, where the first term, denoting the nonequilibrium free energy difference [24], comes from $\langle x^n(t) \rangle_0$, and the second term reads

$$W_{irr} = \frac{1}{n} \int_{t_i}^{t_f} dt\, \dot{\lambda}(t) \langle x^n(t) \rangle_{\dot{\lambda}} = \frac{1}{n^2 \mu}\left(\frac{nD}{\mu}\right)^{2/n}$$

$$\times \frac{\Gamma(3/n)}{\Gamma(1/n)} \int_{t_i}^{t_f} dt\, \dot{\lambda}(t)^2 \lambda(t)^{-2(1+n)/n}. \quad (C9)$$

As ΔF is fixed by the imposed boundary conditions on the state of the system σ, to maximize the output work $-W$ means to minimize the irreversible work W_{irr} as a functional of $\lambda(t)$. This leads to the Euler-Lagrange equation

$$\ddot{\lambda}(t)\lambda(t) - \frac{1+n}{n}\dot{\lambda}(t)^2 = 0, \quad (C10)$$

which has the general solution

$$\lambda_{slow}(t) = \frac{a}{(1+bt)^n}. \quad (C11)$$

We thus come to an interesting conclusion that the optimal slow protocol for the constrained response scales with the same exponent as the potential. The values of a and b can be expressed in terms of the boundary conditions for $\lambda_{slow}(t)$, i.e., $\lambda_{slow}(t_i) \equiv \lambda_i$ and $\lambda_{slow}(t_f) \equiv \lambda_f$. The optimal slow protocol (C11) then reads

$$\lambda_{slow}(t) = \frac{\lambda(t_i)}{\left[1 + \left(\sqrt[n]{\frac{\lambda(t_i)}{\lambda(t_f)}} - 1\right)\frac{t-t_i}{t_f-t_i}\right]^n}. \quad (C12)$$

And the corresponding irreversible work and input work are given by

$$W_{irr} = \frac{\frac{\Gamma(3/n)}{\Gamma(1/n)}\left[\frac{nD}{\mu\lambda_i}\right]^{2/n}\left(\sqrt[n]{\frac{\lambda_i}{\lambda_f}}-1\right)^2}{\mu(t_f-t_i)}, \quad (C13)$$

$$W = \frac{\frac{\Gamma(3/n)}{\Gamma(1/n)}\left[\frac{nD}{\mu\lambda_i}\right]^{2/n}\left(\sqrt[n]{\frac{\lambda_i}{\lambda_f}}-1\right)^2}{\mu(t_f-t_i)} - \frac{D}{n\mu}\ln\frac{\lambda_i}{\lambda_f}. \quad (C14)$$

These results are valid for the individual isothermal branches of the cycle. Importantly, the obtained optimized values of
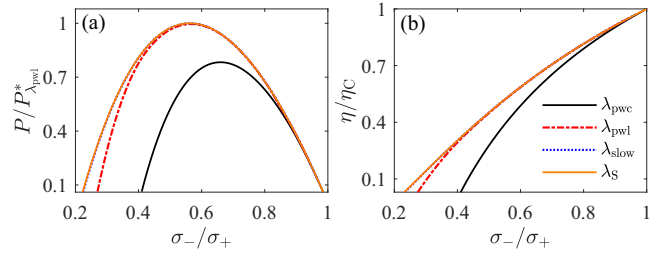

FIG. 7. Optimal performance for fixed boundary values of the response: $\sigma_- \equiv \sigma(0) = \sigma(t_p)$ and $\sigma_+ \equiv \sigma(t_+) = 0.5$. (a) Maximum power (in units of the ultimate maximum power $P^*_{\lambda_{pwl}}$ for λ_{pwl}) and (b) maximum efficiency as functions of σ_-/σ_+. Lines corresponding to λ_S (orange solid) and λ_{slow} (blue dotted) perfectly overlap. The maximum-efficiency protocol (3) and the piecewise constant protocol λ_{pwc} are in this case equal. We used the same parameters as in Fig. 2.

the irreversible work are correct up to the order $1/(t_f - t_i)$, which is their exact dependence on the process duration [24]. These results are thus exact even though they were obtained from the approximate optimal protocol. According to Refs. [24,73], these irreversible works determine the optimal performance of the engine under the constrains on σ, i.e., they give the maximum output work $W_{out} = -W(0, t_+) - W(t_+, t_p)$ and efficiency $\eta = W_{out}/[T_h \Delta S - W_{irr}(0, t_+)]$ (ΔS is the increase in entropy of the system during the hot isotherm). Also this performance is thus from the approximate analysis based on the slow driving obtained exactly.

APPENDIX D: CONSTRAINED RESPONSE

To test our numerical procedure, in this Appendix we check numerically that the protocol λ_S obtained from Ref. [24] is indeed optimal for both power and efficiency under the constraints on σ. When the values of the response (position variance) σ at the ends of the two isotherms are fixed, i.e., $\sigma_- \equiv \sigma(0) = \sigma(t_p)$ and $\sigma_+ \equiv \sigma(t_+)$, the protocol which yields both maximum efficiency and power reads [24]

$$\lambda_S = \begin{cases} \dfrac{T_+}{2\sigma_S} - \dfrac{\sqrt{\sigma_+} - \sqrt{\sigma_-}}{\mu t_+ \sqrt{\sigma_S}}, & 0 < t < t_+, \\[2ex] \dfrac{T_-}{2\sigma_S} + \dfrac{\sqrt{\sigma_+} - \sqrt{\sigma_-}}{\mu t_- \sqrt{\sigma_S}}, & t_+ < t < t_p, \end{cases} \quad (D1)$$

with

$$\sigma_S = \begin{cases} \dfrac{\sigma_-}{2}\left[1 + \left(\sqrt{\dfrac{\sigma_+}{\sigma_-}} - 1\right)\dfrac{t}{t_+}\right]^2, & 0 < t < t_+, \\[2ex] \dfrac{\sigma_+}{2}\left[1 + \left(\sqrt{\dfrac{\sigma_-}{\sigma_+}} - 1\right)\dfrac{t-t_+}{t_-}\right]^2, & t_+ < t < t_p. \end{cases} \quad (D2)$$

However, this protocol is no longer optimal when one imposes just maximum and minimum values on the response, i.e., $\sigma(t) \in [\sigma_-, \sigma_+]$. Then, our analysis shows that the maximum-efficiency and maximum-power protocol is still of the above form, but with $\sigma_- < \sigma(0) = \sigma(t_p) < \sigma(t_+) < \sigma_+$.

In Fig. 7, we show the maximum power (a) and maximum efficiency (b) for the trial protocols under the constraint $\sigma_- \equiv \sigma(0) = \sigma(t_p)$ and $\sigma_+ \equiv \sigma(t_+)$. As expected, power and

efficiency corresponding to the protocol λ_S are largest from all the protocols. In particular, the figure demonstrates that the linear protocol, which was found to maximize output power for constrained λ, yields smaller output power than λ_S. And the piecewise constant protocol yields smaller efficiency than λ_S. Nevertheless, it is interesting to note that the performance

of the protocol $\lambda_{slow}(t)$, which optimizes both output power and efficiency for slow driving (see Sec. C for details), is for the chosen parameters indistinguishable from that of λ_S. This means that the chosen cycle is slow enough. Finally, for small enough cycles (small σ_-/σ_+) performances of all the protocols are equal.

---

[1] G. Pesce, P. H. Jones, O. M. Maragò, and G. Volpe, Optical tweezers: theory and practice, Eur. Phys. J. Plus **135**, 949 (2020).

[2] D. J. Wineland, Nobel lecture: Superposition, entanglement, and raising Schrödinger's cat, Rev. Mod. Phys. **85**, 1103 (2013).

[3] S. Haroche, Nobel lecture: Controlling photons in a box and exploring the quantum to classical boundary, Rev. Mod. Phys. **85**, 1083 (2013).

[4] N. M. Myers, O. Abah, and S. Deffner, Quantum thermodynamic devices: from theoretical proposals to experimental reality, AVS Quantum Sci. **4**, 027101 (2022).

[5] K. Sekimoto, *Stochastic Energetics*, Lecture Notes in Physics Vol. 799 (Springer, Berlin, 2010).

[6] U. Seifert, Stochastic thermodynamics, fluctuation theorems and molecular machines, Rep. Prog. Phys. **75**, 126001 (2012).

[7] F. L. Curzon and B. Ahlborn, Efficiency of a Carnot engine at maximum power output, Am. J. Phys. **43**, 22 (1975).

[8] M. H. Rubin, Optimal configuration of a class of irreversible heat engines. I, Phys. Rev. A **19**, 1272 (1979).

[9] P. Salamon, A. Nitzan, B. Andresen, and R. S. Berry, Minimum entropy production and the optimization of heat engines, Phys. Rev. A **21**, 2115 (1980).

[10] B. Andresen, R. S. Berry, M. J. Ondrechen, and P. Salamon, Thermodynamics for processes in finite time, Acc. Chem. Res. **17**, 266 (1984).

[11] B. Andresen, P. Salamon, and R. S. Berry, Thermodynamics in finite time, Phys. Today **37**(9), 62 (1984).

[12] M. Mozurkewich and R. S. Berry, Finite-time thermodynamics: Engine performance improved by optimized piston motion, Proc. Natl. Acad. Sci. USA **78**, 1986 (1981).

[13] C. Van den Broeck, Thermodynamic Efficiency at Maximum Power, Phys. Rev. Lett. **95**, 190602 (2005).

[14] B. Jiménez de Cisneros and A. C. Hernández, Collective Working Regimes for Coupled Heat Engines, Phys. Rev. Lett. **98**, 130602 (2007).

[15] K. H. Hoffmann, An introduction to endoreversible thermodynamics, AAPP Phys. Math. Nat. Sci. **86**, 1 (2008).

[16] V. Holubec and A. Ryabov, Fluctuations in heat engines, J. Phys. A: Math. Theor. **55**, 013001 (2022).

[17] E. Geva and R. Kosloff, A quantum-mechanical heat engine operating in finite time. a model consisting of spin-1/2 systems as the working fluid, J. Chem. Phys. **96**, 3054 (1992).

[18] A. Parmeggiani, F. Jülicher, A. Ajdari, and J. Prost, Energy transduction of isothermal ratchets: Generic aspects and specific examples close to and far from equilibrium, Phys. Rev. E **60**, 2127 (1999).

[19] T. Hondou and K. Sekimoto, Unattainability of Carnot efficiency in the Brownian heat engine, Phys. Rev. E **62**, 6021 (2000).

[20] T. Feldmann and R. Kosloff, Performance of discrete heat engines and heat pumps in finite time, Phys. Rev. E **61**, 4774 (2000).

[21] R. D. Astumian and P. Hänggi, Brownian motors, Phys. Today **55**(11), 33 (2002).

[22] J. M. R. Parrondo and B. J. de Cisneros, Energetics of brownian motors: a review, Appl. Phys. A **75**, 179 (2002).

[23] P. Reimann, Brownian motors: noisy transport far from equilibrium, Phys. Rep. **361**, 57 (2002).

[24] T. Schmiedl and U. Seifert, Efficiency at maximum power: An analytically solvable model for stochastic heat engines, Europhys. Lett. **81**, 20003 (2008).

[25] Z. C. Tu, Efficiency at maximum power of Feynman's ratchet as a heat engine, J. Phys. A: Math. Theor. **41**, 312003 (2008).

[26] M. Esposito, K. Lindenberg, and C. Van den Broeck, Universality of Efficiency at Maximum Power, Phys. Rev. Lett. **102**, 130602 (2009).

[27] M. Esposito, K. Lindenberg, and C. V. den Broeck, Thermoelectric efficiency at maximum power in a quantum dot, Europhys. Lett. **85**, 60010 (2009).

[28] M. Esposito, R. Kawai, K. Lindenberg, and C. Van den Broeck, Efficiency at Maximum Power of Low-Dissipation Carnot Engines, Phys. Rev. Lett. **105**, 150603 (2010).

[29] O. Abah, J. Roßnagel, G. Jacob, S. Deffner, F. Schmidt-Kaler, K. Singer, and E. Lutz, Single-Ion Heat Engine at Maximum Power, Phys. Rev. Lett. **109**, 203006 (2012).

[30] O. Raz, Y. Subaşı, and R. Pugatch, Geometric Heat Engines Featuring Power that Grows with Efficiency, Phys. Rev. Lett. **116**, 160601 (2016).

[31] V. Holubec and A. Ryabov, Cycling Tames Power Fluctuations near Optimum Efficiency, Phys. Rev. Lett. **121**, 120601 (2018).

[32] K. Brandner and K. Saito, Thermodynamic Geometry of Microscopic Heat Engines, Phys. Rev. Lett. **124**, 040602 (2020).

[33] P. Terrén Alonso, P. Abiuso, M. Perarnau-Llobet, and L. Arrachea, Geometric optimization of nonequilibrium adiabatic thermal machines and implementation in a qubit system, PRX Quantum **3**, 010326 (2022).

[34] V. Cavina, P. A. Erdman, P. Abiuso, L. Tolomeo, and V. Giovannetti, Maximum-power heat engines and refrigerators in the fast-driving regime, Phys. Rev. A **104**, 032226 (2021).

[35] P. A. Erdman, V. Cavina, R. Fazio, F. Taddei, and V. Giovannetti, Maximum power and corresponding efficiency for two-level heat engines and refrigerators: optimality of fast cycles, New J. Phys. **21**, 103049 (2019).

[36] A. Das and V. Mukherjee, Quantum-enhanced finite-time Otto cycle, Phys. Rev. Res. **2**, 033083 (2020).

[37] P. Abiuso and M. Perarnau-Llobet, Optimal Cycles for Low-Dissipation Heat Engines, Phys. Rev. Lett. **124**, 110606 (2020).

[38] T. E. Humphrey, R. Newbury, R. P. Taylor, and H. Linke, Reversible Quantum Brownian Heat Engines for Electrons, Phys. Rev. Lett. **89**, 116801 (2002).

[39] P. Abiuso, H. J. Miller, M. Perarnau-Llobet, and M. Scandi, Geometric optimisation of quantum thermodynamic processes, Entropy **22**, 1076 (2020).

[40] H. J. D. Miller, M. H. Mohammady, M. Perarnau-Llobet, and G. Guarnieri, Thermodynamic Uncertainty Relation in Slowly Driven Quantum Heat Engines, Phys. Rev. Lett. **126**, 210603 (2021).

[41] V. Cavina, A. Mari, and V. Giovannetti, Slow Dynamics and Thermodynamics of Open Quantum Systems, Phys. Rev. Lett. **119**, 050601 (2017).

[42] V. Holubec, An exactly solvable model of a stochastic heat engine: optimization of power, power fluctuations and efficiency, J. Stat. Mech. Theory Exp. **2014**, P05022.

[43] A. Dechant, N. Kiesel, and E. Lutz, Underdamped stochastic heat engine at maximum efficiency, Europhys. Lett. **119**, 50003 (2017).

[44] Y. Zhang, Optimization of stochastic thermodynamic machines, J. Stat. Phys. **178**, 1336 (2020).

[45] P. Abiuso, V. Holubec, J. Anders, Z. Ye, F. Cerisola, and M. Perarnau-Llobet, Thermodynamics and optimal protocols of multidimensional quadratic Brownian systems, J. Phys. Commun. **6**, 063001 (2022).

[46] A. Zhong and M. R. DeWeese, Limited-control optimal protocols arbitrarily far from equilibrium, Phys. Rev. E **106**, 044135 (2022).

[47] M. Bauer, K. Brandner, and U. Seifert, Optimal performance of periodically driven, stochastic heat engines under limited control, Phys. Rev. E **93**, 042112 (2016).

[48] C. A. Plata, D. Guéry-Odelin, E. Trizac, and A. Prados, Optimal work in a harmonic trap with bounded stiffness, Phys. Rev. E **99**, 012140 (2019).

[49] H. Risken, Fokker-planck equation, in *The Fokker-Planck Equation: Methods of Solution and Applications* (Springer, 1996), pp. 63–95.

[50] V. Holubec, A. Ryabov, S. A. M. Loos, and K. Kroy, Equilibrium stochastic delay processes, New J. Phys. **24**, 023021 (2022).

[51] S. Krishnamurthy, S. Ghosh, D. Chatterji, R. Ganapathy, and A. K. Sood, A micrometre-sized heat engine operating between bacterial reservoirs, Nat. Phys. **12**, 1134 (2016).

[52] V. Holubec, S. Steffenoni, G. Falasco, and K. Kroy, Active Brownian heat engines, Phys. Rev. Res. **2**, 043262 (2020).

[53] A. Kumari, P. S. Pal, A. Saha, and S. Lahiri, Stochastic heat engine using an active particle, Phys. Rev. E **101**, 032109 (2020).

[54] G. Gronchi and A. Puglisi, Optimization of an active heat engine, Phys. Rev. E **103**, 052134 (2021).

[55] I. A. Martínez, E. Roldán, L. Dinis, D. Petrov, and R. A. Rica, Adiabatic Processes Realized with a Trapped Brownian Particle, Phys. Rev. Lett. **114**, 120601 (2015).

[56] D. Arold, A. Dechant, and E. Lutz, Heat leakage in overdamped harmonic systems, Phys. Rev. E **97**, 022131 (2018).

[57] V. Blickle and C. Bechinger, Realization of a micrometre-sized stochastic heat engine, Nat. Phys. **8**, 143 (2012).

[58] V. Holubec and A. Ryabov, Diverging, but negligible power at carnot efficiency: Theory and experiment, Phys. Rev. E **96**, 062107 (2017).

[59] V. Cavina, A. Mari, A. Carlini, and V. Giovannetti, Optimal thermodynamic control in open quantum systems, Phys. Rev. A **98**, 012139 (2018).

[60] I. A. Martínez, É. Roldán, L. Dinis, D. Petrov, J. M. R. Parrondo, and R. A. Rica, Brownian carnot engine, Nat. Phys. **12**, 67 (2016).

[61] I. A. Martínez, É. Roldán, L. Dinis, and R. A. Rica, Colloidal heat engines: a review, Soft Matter **13**, 22 (2017).

[62] T. Schmiedl and U. Seifert, Optimal Finite-Time Processes In Stochastic Thermodynamics, Phys. Rev. Lett. **98**, 108301 (2007).

[63] H. Then and A. Engel, Computing the optimal protocol for finite-time processes in stochastic thermodynamics, Phys. Rev. E **77**, 041105 (2008).

[64] V. Holubec and A. Ryabov, Efficiency at and near maximum power of low-dissipation heat engines, Phys. Rev. E **92**, 052125 (2015).

[65] T. R. Gingrich, G. M. Rotskoff, G. E. Crooks, and P. L. Geissler, Near-optimal protocols in complex nonequilibrium transformations, Proc. Natl. Acad. Sci. USA **113**, 10263 (2016).

[66] P. A. Erdman and F. Noé, Identifying optimal cycles in quantum thermal machines with reinforcement-learning, NPJ Quantum Inf. **8**, 1 (2022).

[67] I. Khait, J. Carrasquilla, and D. Segal, Optimal control of quantum thermal machines using machine learning, Phys. Rev. Res. **4**, L012029 (2022).

[68] A. Dechant and Y. Sakurai, Thermodynamic interpretation of Wasserstein distance, arXiv:1912.08405.

[69] T. Van Vu and Y. Hasegawa, Geometrical Bounds of the Irreversibility in Markovian Systems, Phys. Rev. Lett. **126**, 010601 (2021).

[70] M. Carrega, L. M. Cangemi, G. De Filippis, V. Cataudella, G. Benenti, and M. Sassetti, Engineering dynamical couplings for quantum thermodynamic tasks, PRX Quantum **3**, 010323 (2022).

[71] N. Pancotti, M. Scandi, M. T. Mitchison, and M. Perarnau-Llobet, Speed-Ups to Isothermality: Enhanced Quantum Thermal Machines through Control of the System-Bath Coupling, Phys. Rev. X **10**, 031015 (2020).

[72] V. Holubec, *Non-equilibrium Energy Transformation Processes: Theoretical Description at the Level of Molecular Structures*, Springer Theses (Springer International, Cham, 2014).

[73] V. Holubec and A. Ryabov, Maximum efficiency of low-dissipation heat engines at arbitrary power, J. Stat. Mech. Theory Exp. (2016) 073204.

Journal of Physics Communications

Thermodynamics and optimal protocols of multidimensional quadratic Brownian systems

Paolo Abiuso[1,2] ⓘ, Viktor Holubec[3] ⓘ, Janet Anders[4,5], Zhuolin Ye[6], Federico Cerisola[4,7] and Martí Perarnau-Llobet[2] ⓘ

1   ICFO-Institut de Ciències Fotòniques, The Barcelona Institute of Science and Technology, 08860 Castelldefels (Barcelona), Spain
2   Department of Applied Physics, University of Geneva, 1211 Geneva, Switzerland
3   Charles University, Faculty of Mathematics and Physics, Department of Macromolecular Physics, V Holešovičkách 2, CZ-180 00 Praha, Czech Republic
4   Department of Physics and Astronomy, University of Exeter, Stocker Road, Exeter EX4 4QL, United Kingdom
5   Institut für Physik und Astronomie, University of Potsdam, 14476 Potsdam, Germany
6   Institut für Theoretische Physik, Universität Leipzig, Postfach 100 920, D-04009 Leipzig, Germany
7   Department of Materials, University of Oxford, Parks Road, Oxford OX1 3PH, United Kingdom

E-mail: paolo.abiuso@icfo.eu

Abstract

We characterize finite-time thermodynamic processes of multidimensional quadratic overdamped systems. Analytic expressions are provided for heat, work, and dissipation for any evolution of the system covariance matrix. The Bures-Wasserstein metric between covariance matrices naturally emerges as the local quantifier of dissipation. General principles of how to apply these geometric tools to identify optimal protocols are discussed. Focusing on the relevant slow-driving limit, we show how these results can be used to analyze cases in which the experimental control over the system is partial.

1. Introduction

The minimisation of dissipation is a central goal in finite-time thermodynamics [1–3]. In most applications, one is interested in finding the optimal time variation of some control parameters, e.g., magnetic or electric fields, in order to achieve a desired task while minimising the amount of energy dissipated to the environment. Such tasks could range from the design of a cycle for a thermal engine [4, 5] to the erasure of information in an information processing device [6–8]. Finding optimal protocols in finite time is however often a very challenging task, as it requires a functional optimisation over all possible paths in the control parameter space, as well as a perfect understanding of the non-equilibrium dynamics resulting from such control. In the regime of small mesoscopic systems, remarkable progress on this topic has been achieved in the last decades with the development of the field of stochastic thermodynamics [4, 9–14]. Optimal drivings are nowadays known for overdamped [15–20] and underdamped systems [21–23], as well as driven single-level quantum dots [24]. However, such explicit solutions only exist for one-dimensional systems and are, in general, computationally hard to scale up.

Other solutions are known for situations in which the control parameter varies *slowly* compared to the system relaxation time, as the optimisation admits a geometric formulation [25–32] and the problem considerably simplifies. Indeed, the space of control parameters can be endowed with a Riemannian metric in such a way that geodesic paths correspond to minimally dissipative thermodynamic processes. While the geodesic equations might be hard to solve, the important realisation is that the number of coupled equations is given by the number of control parameters, and independent of the size of the system of interest (by comparison, a full out-of-equilibrium solution of the dynamics needs a number of equations that scales exponentially with the number of components of the system). This has enabled finding optimal driving protocols in such regime for complex systems such as a two dimensional Ising model [33, 34], nanomagnets [35], and quantum spin chains [36]. Optimal protocols for different classes of slowly driven heat engines have also been developed by such a

geometric approach [32, 37–44]. Besides the slow driving regime, the optimization problem can also be simplified in the opposite, *fast-driving*, regime [45–48].

Beyond the slow or fast driving limits, a general connection has been established between optimal transport and minimally-dissipative thermodynamic protocols in the overdamped limit [49, 50]. This connection was recently exploited to show that the minimal dissipation in any process governed by a Langevin equation is directly related to the L^2-Wasserstein distance between initial and final states [51, 52] (see also [53–55]). However in general full control on the system's Hamiltonian is needed to saturate this bound. To address the relevant case of partial experimental control, one therefore requires a different approach, that is able to quantify dissipation on non-optimal trajectories.

In this paper, we study thermodynamic transformations for many-body quadratic overdamped systems. We derive general expressions for the flux of work and heat, and we show that the dissipation is governed by the Bures-Wasserstein (BW) distance between covariance matrices, which coincides with the L^2-Wasserstein distance between Gaussian distributions of [51–55]. Our derivation allows for a direct generalisation of the well-known single-body case, studied by Schmiedl and Seifert for a single-particle overdamped system [15], as well as new insights on the form of optimal drivings. In particular, we provide an integral analytic expression for the dissipation valid for *any response trajectory* of the system, not necessarily minimally dissipating. This also naturally enables the study of *partial control*. That is, the situation where the limited number of control parameters does not allow for exploring the whole space of states, so that the fundamental lower bounds of [49, 51] might not be reachable. This is a common scenario in complex systems, where experimentally only a few degrees of freedom are controllable. In order to illustrate the applicability of our results, and to show the difference between partial and global control, we analyse a system of two interacting particles and a particle confined in a 2-dimensional squeezing potential with different control limitations.

2. Model: Many-body overdamped spring

We consider a system of N overdamped Brownian particles described by the position vector $\boldsymbol{x}$ and mutually interacting via the time-dependent potential

$$V(\boldsymbol{x}, t) = \frac{1}{2}\boldsymbol{x}^\top K(t)\boldsymbol{x}, \tag{1}$$

or, equivalently, via the force field $F(\boldsymbol{x}) = -\nabla V(\boldsymbol{x}) = -K\boldsymbol{x}$ (when possible, we omit writing the time argument from now on). Each particle $i = 1,\ldots,N$ might have a different number of degrees of freedom d_i, i.e., $\boldsymbol{x} \in \mathbb{R}^M$, where $M = \sum_{i=1}^{N} d_i$. The potential (1) accounts for both self-energy of the individual particles and interactions between the particles. The stiffness matrix K is symmetric and positive definite $K \geqslant 0$ (that is, the potential is confining). Assuming that all the particles have the same friction coefficient γ, the system dynamics obeys the set of Langevin equations [56]

$$\gamma\dot{\boldsymbol{x}} = -K\boldsymbol{x} + \sqrt{2\gamma k_B T}\,\boldsymbol{\eta}, \tag{2}$$

where the Gaussian noise $\boldsymbol{\eta}$ obeys $\langle \boldsymbol{\eta} \rangle = 0$, its components $\langle \eta_i(t)\eta_j(t') \rangle = \delta_{ij}\delta(t - t')$, and T is the temperature of the thermal environment, which we assume is fixed throughout (isothermal). From now on, we will use natural units in which $\gamma = 1$, $k_B = 1$. For the general case in which different particles have different friction coefficients, see section 4.

Departing from an arbitrary normalized initial distribution, the state of the system at time t is represented by a Gaussian probability density function (PDF) [56][8].

$$p(\boldsymbol{x}, t) = \frac{1}{\sqrt{(2\pi)^N \det \Sigma}} \exp\left(-\frac{\boldsymbol{x}^\top \Sigma^{-1}(t)\boldsymbol{x}}{2}\right). \tag{3}$$

Here $\Sigma(t) = \langle \boldsymbol{x}\boldsymbol{x}^\top \rangle(t)$ denotes the covariance matrix at time t. The PDF (3) has zero mean $\langle \boldsymbol{x} \rangle(t) = 0$ (see section 4 and appendix B for the more general case).

The distribution $p(\boldsymbol{x}, t)$ is therefore defined by its covariance matrix, whose dynamics $\dot{\Sigma} = \langle \boldsymbol{x}\dot{\boldsymbol{x}}^\top \rangle + \langle \dot{\boldsymbol{x}}\boldsymbol{x}^\top \rangle$ can be obtained from equation (2) and reads [56]

$$\dot{\Sigma}(t) = -K(t)\Sigma(t) - \Sigma(t)K(t) + 2T, \tag{4}$$

where implicitly $T = T\mathbb{1}$. In case the response dynamics $\Sigma(t)$ is given, and one wants to drive the potential $K(t)$ accordingly (i.e., $K(t)$ is the control protocol generating the response dynamics $\Sigma(t)$), the above equation has to be solved for $K(t)$. This is a standard Lyapunov equation that is commonly used in the context of quantum

---

[8] The PDF describing the state under the dynamics (2) is always Gaussian given Gaussian initial conditions, or after an initial transient (of order $\gamma/|K|$) [56] which is negligible for standard time-asymptotic cycling scenarios, or in the regime of slow driving.

metrology (see e.g., [57]), having solution

$$K = \int_0^\infty d\nu \; e^{-\nu\Sigma}(2T - \dot{\Sigma})e^{-\nu\Sigma} = T\Sigma^{-1} - \int_0^\infty d\nu \; e^{-\nu\Sigma}\dot{\Sigma}e^{-\nu\Sigma}. \tag{5}$$

Notice that instantaneous quenches of $K(t)$ can be added at the beginning and at the end of the protocol, without affecting the dynamics of $\Sigma(t)$. For example, to end the transformation in equilibrium, one can add a final quench to $K = T\Sigma^{-1}$.

Remark. We stress here that the explicit evaluation of equation (5) can be performed analytically. To be consistent with the notation, throughout the text we use the operator $\mathcal{I}(A, B) = \int_0^\infty d\nu \; e^{-\nu A}Be^{-\nu A}$ expressed in its integral matrix form; at the same time, in the basis that diagonalizes A, i.e., $A_{ij} = \delta_{ij}a_i$, the components of this operator can be easily expressed as $\mathcal{I}(A, B)_{ij} = \frac{B_{ij}}{a_i + a_j}$.

3. Thermodynamics of quadratic systems

The average energy of a system described by a multidimensional probability distribution (3) in the potential (1) reads

$$E(t) = \int d\boldsymbol{x} \; p(\boldsymbol{x}, t)V(\boldsymbol{x}, t) = \sum_{ij}\frac{1}{2}K_{ij}(t)\langle x_i x_j\rangle(t) = \frac{\text{Tr}[K(t)\Sigma(t)]}{2}, \tag{6}$$

where $\text{Tr}[AB] = \sum_{ij} A_{ij}B_{ji}$. The variation of energy is split canonically in a work contribution, originating in the variation of the external potential, and a heat contribution, stemming from the evolution of the system induced by the dissipative environment [4, 58]. I.e. the work (W) and heat (Q) fluxes entering the system are defined as

$$\dot{W} = \frac{\text{Tr}[\dot{K}\Sigma]}{2}, \quad \dot{Q} = \frac{\text{Tr}[K\dot{\Sigma}]}{2}. \tag{7}$$

In a similar fashion to the seminal work by Schmiedl and Seifert [15] we can write the work input of a finite time transformation of duration τ as

$$\begin{aligned}
W &= \frac{1}{2}\int_0^\tau dt \; \text{Tr}[\dot{K}\Sigma] \\
&= \frac{1}{2}\text{Tr}[K\Sigma]\Big|_0^\tau - \frac{T}{2}\text{logdet}\Sigma\Big|_0^\tau + \frac{1}{2}\int_0^\tau dt \; \text{Tr}\left[\int_0^\infty d\nu \; e^{-\nu\Sigma}\dot{\Sigma}e^{-\nu\Sigma}\dot{\Sigma}\right],
\end{aligned} \tag{8}$$

where in the second equality we integrated by parts and used equation (5). In the following we will indicate as $\mathcal{Q}(\tau) - \mathcal{Q}(0) := \Delta\mathcal{Q}$ the variation of any quantity $\mathcal{Q}$ during a transformation. Given that $\frac{1}{2}\text{logdet}\Sigma\big|_0^\tau = -\int d\boldsymbol{x} \, p \ln p \big|_0^\tau = \Delta S$ is the variation of Von Neumann entropy of the system (3), it is possible to rewrite equation (8) as

$$W - (\Delta E - T\Delta S) = \frac{1}{2}\int_0^\tau dt \; \text{Tr}\left[\int_0^\infty d\nu \; e^{-\nu\Sigma}\dot{\Sigma}e^{-\nu\Sigma}\dot{\Sigma}\right] \equiv W_{\text{irr}}. \tag{9}$$

This expression identifies the dissipated work, W_{irr}, of an arbitrary response trajectory $\Sigma(t)$. This is our first main result. The above derivation represents a natural multidimensional generalisation of the one-dimensional result of [15].

The irreversible work (9) turns out to be the integral in time of a quadratic form that coincides with the Bures-Wasserstein (BW) metric on positive-definite matrices [59, 60]. That is $W_{\text{irr}} = \int_0^\tau dt \; g_\Sigma(\dot{\Sigma}, \dot{\Sigma})$, where

$$g_\Sigma(A, B) = \frac{1}{2}\int_0^\infty d\nu \; \text{Tr}[e^{-\nu\Sigma}Ae^{-\nu\Sigma}B], \tag{10}$$

$$g_\Sigma(d\Sigma, d\Sigma) \equiv D_{\text{BW}}(\Sigma, \Sigma + d\Sigma)^2, \tag{11}$$

with the latter being the infinitesimal BW squared distance. This metric has been intensely studied as it appears in problems of statistical inference and metrology in quantum information [57, 59, 61, 62], as well as in the theory of optimal transport [60, 63].

For fixed endpoints, the lower bound for W_{irr} is obtained for the response trajectory $\bar{\Sigma}(t)$ that minimizes the integral of the quadratic form in equation (9). That is

$$W_{\text{irr}} \geqslant \frac{D_{\text{BW}}(\Sigma_1, \Sigma_2)^2}{\tau}, \tag{12}$$

where the BW-geodesic length between the initial and final points $\Sigma(0) = \Sigma_1, \Sigma(\tau) = \Sigma_2$, is given by (see appendix A, or [59, 60])

$$D_{\mathrm{BW}}(\Sigma_1, \Sigma_2)^2 \equiv \mathrm{Tr}[\Sigma_1] + \mathrm{Tr}[\Sigma_2] - 2\,\mathrm{Tr}[\sqrt{\sqrt{\Sigma_1}\,\Sigma_2\,\sqrt{\Sigma_1}}\,]. \tag{13}$$

The corresponding geodesic, i.e., the minimally dissipating response trajectory, is given by (cf appendix A)

$$\bar{\Sigma}(s\tau) = (1-s)^2\Sigma_1 + s^2\Sigma_2 + s(1-s)(\sqrt{\Sigma_1\Sigma_2} + \sqrt{\Sigma_2\Sigma_1}), \tag{14}$$

with $s = t/\tau$ and thus $0 \leqslant s \leqslant 1$ independently on the total duration t of the protocol.

The appearance of the distance (13) in (12) is no coincidence: it was realised recently [51, 52] that the optimal transport problem is connected to the irreversible entropy production in diffusive dynamics, and its value is minimized by the L^2-Wasserstein distance between the initial and final distributions [49, 51, 52, 64]. In the case of Gaussian distributions, the L^2-Wasserstein distance coincides with the above BW distance between the covariance matrices (13).

Besides it being straightforward, one key advantage of our derivation is that expression (9) is valid for *any* response trajectory and allows to compute W_{irr} also when the transformation does not saturate the lower bound (12). In particular, it can be used for the realistic case of partial experimental control, when the system is constrained to explore only a subset of the distributions space (see the following paragraph and examples in section 5).

3.1. Total control versus partial control

In experiments, the system is typically controlled by varying $K(t)$. The optimal control parameter protocol $\bar{K}$ corresponding to the geodesic (14) is determined by substituting $\bar{\Sigma}$ into (5). Perfect implementation of $\bar{K}$ would then saturate the minimal dissipation bound (13). However, this assumes that $\bar{K}$ is experimentally feasible. This might not be the case in general. Performing the minimization over a restricted region of control parameters limits the system response to a submanifold of allowed states. In general, this results in a case-dependent minimum value strictly larger than the global minimum, $W_{\mathrm{irr}} > D_{\mathrm{BW}}^2/\tau$, e.g., see Example 5.1 below.

In other cases, the initial and final point of the transformation might not even be fixed (e.g., when optimizing the strokes of a thermal cycle to increase its performance as a heat engine). To show the consequences of fixed/unfixed boundary states $\Sigma(0)$ and $\Sigma(\tau)$, consider that the variation $\dot{\Sigma} = \dot{\Sigma}_d + \dot{\Sigma}_r$ can be divided into a diagonal contribution and a non-diagonal, *rotating* contribution. That is, given the covariance matrix expressed in its diagonal basis $\Sigma = \sum_i \omega_i |i\rangle\langle i|$, the diagonal part of its variation is $\dot{\Sigma}_d = \sum_i \dot{\omega}_i |i\rangle\langle i|$ and the rotating part is $\dot{\Sigma}_r = \sum_i \omega_i(|\dot{i}\rangle\langle i| + |i\rangle\langle\dot{i}|)$. From equations (9) and (10) we know that $\dot{W}_{\mathrm{irr}} = g_\Sigma(\dot{\Sigma}, \dot{\Sigma})$. It is easy to check that $g_\Sigma(\dot{\Sigma}_d, \dot{\Sigma}_r) = 0$ which implies that the irreversible work naturally decouples into a diagonal and a rotating contribution:

$$\dot{W}_{\mathrm{irr}} = g_\Sigma(\dot{\Sigma}_d, \dot{\Sigma}_d) + g_\Sigma(\dot{\Sigma}_r, \dot{\Sigma}_r) \equiv \dot{W}_{\mathrm{irr}}^{(d)} + \dot{W}_{\mathrm{irr}}^{(r)}. \tag{15}$$

Both $\dot{W}_{\mathrm{irr}}^{(d)}$ and $\dot{W}_{\mathrm{irr}}^{(r)}$ are positive, which means that the dissipation generated in a non-commuting transformation for Σ ($\dot{W}_{\mathrm{irr}}^{(r)} > 0$) is always larger than the commuting case ($\dot{W}_{\mathrm{irr}}^{(r)} = 0$). (A similar phenomenon occurs for quantum systems, described by their density matrices [32]). At the same time, for any transformation $\Sigma(t) = \sum_i \omega_i(t)|i(t)\rangle\langle i(t)|$, the change in system entropy $\propto \Delta[\mathrm{logdet}\Sigma]$ and energy $\propto \Delta[\mathrm{Tr}[K\Sigma]]$ can also be achieved by a similar transformation $\Sigma^*(t) = \sum_i \omega_i(t)|i(0)\rangle\langle i(0)|$ (where $\omega_i(t)$ varies with time as in $\Sigma(t)$, while the basis is fixed) in which the covariance matrix commutes with itself at all times $[\Sigma^*(t), \Sigma^*(t')] = 0$, and $W_{\mathrm{irr}}^{(r)} = 0$. Moreover, it is easy to verify that such transformation has the same value of $\dot{W}_{\mathrm{irr}}^{(d)}$, which leads to the following observation:

Observation 1. If the restrictions on the control parameters $K(t)$ allow and $[\Sigma(0), \Sigma(\tau)] = 0$, rotation of the covariance matrix should be avoided in order to minimize dissipation.

In fact, it is clear that the BW-geodesic (14) is diagonal in the same basis at all times, if and only if $[\Sigma(0), \Sigma(\tau)] = 0$. If that is not the case, one cannot use $\Sigma^*(t)$ to reduce the dissipation, unless the endpoint of the trajectory is itself unconstrained. In the fully commuting case, it is easy to see that equations (6)–(9) simplify and we recover (K being diagonal in the same basis of Σ, with eigenvalues k_i)

$$E = \frac{1}{2}\sum_i k_i\omega_i, \qquad \Delta S = \frac{1}{2}\sum_i \Delta[\log\omega_i],$$

$$W_{\mathrm{irr}} = \int_0^\tau dt \sum_i \frac{1}{4}\frac{\dot{\omega}_i^2}{\omega_i} \geqslant \frac{1}{\tau}\sum_i (\sqrt{\omega_i(\tau)} - \sqrt{\omega_i(0)})^2. \tag{16}$$

When reduced to a single mode, this is exactly the result found by Schmiedl and Seifert in [15], which we thus see being *extensive in the eigenmodes* ω_i of Σ: that is, all the modes $\{\omega_i, k_i\}$ can be treated as effectively independent in the commuting case. As an instance of a transformation with fixed boundaries that force non-commutation, see Example 5.2.

As mentioned above, controlling the potential (1) in time defines the evolution of the state via the dynamical equation (4). Conversely, a given response trajectory $\Sigma(t)$ is translated to its generating control $K(t)$ through equation (5). This means that fixing the boundary values of Σ is non-trivially related to fixing boundary controls. The results of optimisation thus strongly depend on the imposed constraints [65, 66, 67]. At the same time, for the purpose of typical applications to isothermal processes (cf section 5), in which the goal is to minimize work dissipation, we can consider the *slow-driving* limit of the dynamics [68]. In this limit the potential $K(t)$ is modified slowly, more precisely we assume $\dot{K} \sim 1/\tau$ with τ much larger than the relaxation timescale of the system $\tau \gg \gamma/|K|$, and it is sufficient to solve the dynamical equation (4) up to the first order in $1/\tau$. The zeroth order corresponds to the quasistatic limit $\tau \to \infty$. This allows to expand any state-dependent quantity $\mathcal{Q}$ around its equilibrium value $\mathcal{Q}^{(0)}$, keeping only the leading correction term $\mathcal{Q}^{(1)} \sim \mathcal{O}(1/\tau)$. In our specific setting, the covariance matrix can be expanded as

$$\Sigma(t) = \Sigma^{(0)}(t) + \Sigma^{(1)}(t) + \mathcal{O}(1/\tau^2) \tag{17}$$

with $\Sigma^{(0)} = TK^{-1}$ and $\Sigma^{(1)} = -T\int_0^\infty d\nu\, e^{-\nu/K}\frac{d}{dt}(K^{-1})e^{-\nu/K}$ (cf equations (4) and (5)). However, the irreversible work (9) is already of order $\mathcal{O}(1/\tau)$. To express the dissipation in the slow regime, it is therefore sufficient to substitute $\Sigma^{(0)}$ in (9). In other words, we observe that

Observation 2. In the slow-driving limit, controlling the inverse stiffness matrix $TK^{-1}(t)$ of the potential is equivalent to directly steering the covariance matrix $\Sigma(t)$. The irreversible work in the slow-driving limit therefore reads

$$W_{\text{irr}}^{\text{slow}} = \frac{T}{2}\int_0^\tau dt\, g_{K^{-1}}\left(\frac{d}{dt}(K^{-1}), \frac{d}{dt}(K^{-1})\right). \tag{18}$$

4. Generalizations

In the previous section, we have focused on the paradigmatic case of the potential (1) and density distributions (3) centered around $\boldsymbol{x} = 0$, and a particle-independent friction coefficient. Nevertheless, the obtained results are fully extendable also when removing such assumptions.

First, in appendix B we solve the general case of a quadratic potential with time-dependent center $\boldsymbol{z}(t)$, i.e., $V(\boldsymbol{x}, t) = \frac{1}{2}(\boldsymbol{x} - \boldsymbol{z}(t))K(t)(\boldsymbol{x} - \boldsymbol{z}(t))$. As the system is in general driven out of equilibrium, the center of the potential does not necessarily coincide with the average particle position, $\langle \boldsymbol{x} \rangle \equiv \boldsymbol{\xi}(t) \neq \boldsymbol{z}(t)$, and the irreversible work gains an additional contribution (see details in appendix B). Focusing on the limit of slow driving, it can be expressed as

$$W_{\text{irr}}^{\text{slow}} = \int_0^\tau dt\, (|\dot{\boldsymbol{\xi}}|^2 + g_\Sigma(\dot{\Sigma}, \dot{\Sigma})). \tag{19}$$

Similarly to (13), the lower bound for $W_{\text{irr}}^{\text{slow}}$ is in this case

$$W_{\text{irr}}^{\text{slow}} \geqslant \frac{1}{\tau}(|\boldsymbol{\xi}_1 - \boldsymbol{\xi}_2|^2 + D_{BW}(\Sigma_1, \Sigma_2)^2). \tag{20}$$

Observations 1 and 2 from section 3 remain valid: if possible, rotations of the covariance matrix thus should be avoided; the state variables in the expression (19) can be substituted by their equilibrium values $(\boldsymbol{\xi}, \Sigma) = (\boldsymbol{z}, TK^{-1})$. Moreover, in the same limit, $\boldsymbol{\xi}(t) - \boldsymbol{z}(t) \sim \mathcal{O}(\tau^{-1})$ while the associated correction to quasistatic ΔE and ΔS is negligible $\mathcal{O}(\tau^{-2})$ (cf appendix B). This implies that moving the trap $\dot{\boldsymbol{\xi}} \neq 0$ only contributes to the dissipation (20) and should therefore be avoided when possible, in the same spirit as Observation 1.

Second, we comment on the generalization to systems where different particles have different friction coefficients γ_i. In such a case, the Langevin equations (2) become, in components,
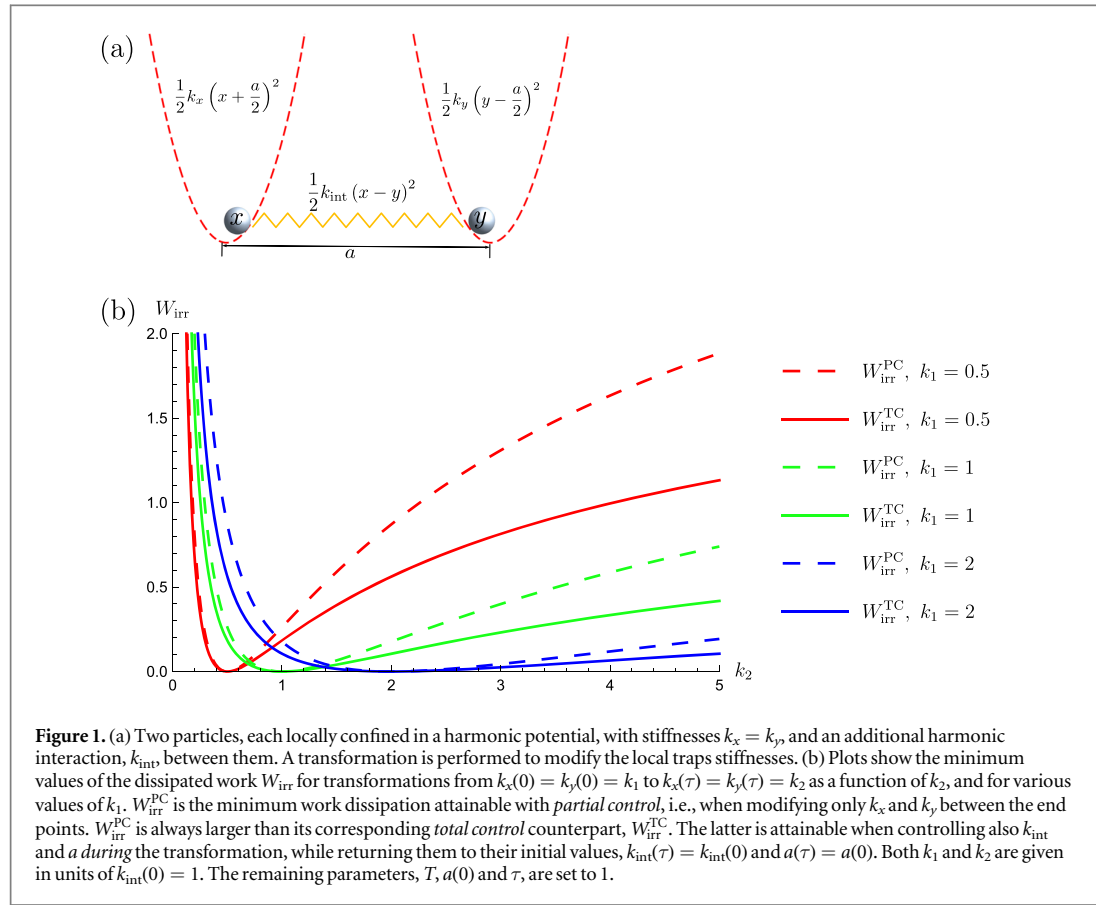
$$\gamma_i \dot{x}_i = -\sum_j K_{ij}x_j + \sqrt{2\gamma_i k_B T}\,\eta_i. \tag{21}$$

Notice that some of the γ_i might refer to different degrees of freedom of the same particle. The white noises η_i are mutually uncorrelated. We define $y_i \equiv \sqrt{\gamma_i}x_i$ and rewrite the Langevin equations as

$$\dot{\boldsymbol{y}} = -K'\boldsymbol{y} + \sqrt{2k_B T}\,\boldsymbol{\eta}, \tag{22}$$

where the transformed stiffness matrix $K'_{ij} = \frac{K_{ij}}{\sqrt{\gamma_i \gamma_j}}$ is still symmetric and positive definite. At the same time, the covariance matrix of the $\boldsymbol{y}$ variable, $\Sigma' = \langle \boldsymbol{y}\boldsymbol{y}^\top \rangle$, satisfies $\Sigma'_{ij} = \sqrt{\gamma_i}\Sigma_{ij}\sqrt{\gamma_i}$. Finally the energy of the system is given by

$$E = \frac{1}{2}\text{Tr}[\Sigma K] = \frac{1}{2}\text{Tr}[\Sigma' K'], \tag{23}$$

Figure 1. (a) Two particles, each locally confined in a harmonic potential, with stiffnesses $k_x = k_y$, and an additional harmonic interaction, k_{int}, between them. A transformation is performed to modify the local traps stiffnesses. (b) Plots show the minimum values of the dissipated work W_{irr} for transformations from $k_x(0) = k_y(0) = k_1$ to $k_x(\tau) = k_y(\tau) = k_2$ as a function of k_2, and for various values of k_1. W_{irr}^{PC} is the minimum work dissipation attainable with *partial control*, i.e., when modifying only k_x and k_y between the end points. W_{irr}^{PC} is always larger than its corresponding *total control* counterpart, W_{irr}^{TC}. The latter is attainable when controlling also k_{int} and a *during* the transformation, while returning them to their initial values, $k_{int}(\tau) = k_{int}(0)$ and $a(\tau) = a(0)$. Both k_1 and k_2 are given in units of $k_{int}(0) = 1$. The remaining parameters, T, $a(0)$ and τ, are set to 1.

and similarly $\dot{Q} = \frac{1}{2}\mathrm{Tr}[\dot{\Sigma}'K']$ and $\dot{W} = \frac{1}{2}\mathrm{Tr}[\Sigma'\dot{K}']$. Given the formal equivalence between equations (2), (6), (7) and (22), (23) above, we see that the problem is equivalently mapped to the case with fixed $\gamma_i = \gamma$, $\forall i$.

Finally, throughout the paper we assumed a fixed temperature T. At the same time, the expressions for energy (6), heat and work (7), as well as $\Delta S = \frac{1}{2}\Delta\mathrm{logdet}\Sigma$ do not intrinsically depend on the temperature T. We can therefore relax such assumption and admit a time-dependent temperature $T(t)$ [69, 70]. In such case the definition of irreversible work becomes

$$W_{irr} = W - \left(\Delta E - \int_0^\tau dt\ T\dot{S}\right) = -Q + \int_0^\tau dt\ T\dot{S} = \int_0^\tau dt\ T\dot{S}_{irr}, \qquad (24)$$

$\dot{S}_{irr}$ being the irreversible entropy production. From the derivation in section 3 we get the same expression $W_{irr} = \frac{1}{2}\int_0^\tau dt\ g_\Sigma(\dot{\Sigma}, \dot{\Sigma})$, as well as the validity of all the above observations and generalizations.

5. Applications

Here, we present two examples of application of the formalism, results and observations introduced above.

5.1. Interacting particles in double trap

First, we show how partial control over a system can substantially increase the amount of dissipation when compared to the optimal geodesics transformation. Consider the case of two particles on a line, *Romeo and Juliet*, who are constrained to be located at two different places, separated by a distance a. That is, Romeo (Juliet) is at position x (y) and subject to a confining harmonic potential of strength k_x (k_y) centered at $\frac{a}{2}\left(-\frac{a}{2}\right)$. At the same time, the two particles feel a harmonic attraction of strength k_{int}. The complete system is described by the potential (cf figure 1)

$$V = \frac{1}{2}k_x\left(x - \frac{a}{2}\right)^2 + \frac{1}{2}k_y\left(y + \frac{a}{2}\right)^2 + \frac{1}{2}k_{int}(x - y)^2, \qquad (25)$$

For two colloidal particles, such an interaction can be realized using optical tweezers [71] or an effective potential induced by feedback control [72]. Besides, it qualitatively mimics the interaction of trapped active particles studied in [72] or in a similar model [73].

Now imagine that an experimenter can operate a transformation of the Hamiltonian parameters with the goal to increase the strength of the local traps, but with a minimal energetic cost. That is, the boundaries of the transformation are $k_x(0) = k_y(0) < k_x(\tau) = k_y(\tau)$ while $a(0) = a(\tau)$ and $k_{\text{int}}(0) = k_{\text{int}}(\tau)$. We want to know the minimum dissipation that an experimenter can achieve for such a transformation. In the appendix C.1, we derive and compare the minimum dissipation protocols in the slow-driving limit for two paradigmatic cases: *i) partial control* in which the experimenter can only tune the values of k_x and k_y (while a and k_{int} are both constant), *ii) total control* in which the experimenter can control k_{int} and a as well. The comparison among the two situations is presented in figure 1. As expected, the dissipation under partial control, $W_{\text{irr}}^{\text{PC}}$, is always larger than that for total control, $W_{\text{irr}}^{\text{TC}}$. In particular we observe that having the possibility of controlling all the parameters of the potential (25) allows, in general, substantial savings of up to $\simeq 50\%$ of energy dissipation with respect to simply tuning the stiffnesses $k_{x,y}$.

5.2. Rotating a 2-dimensional squeezed potential

As a second example, we consider the rotation of a two-dimensional Gaussian system in the xy plane. Specifically, we consider a Gaussian PDF with a non-isotropic covariance matrix of the position coordinates $\{x, y\}$

$$\begin{pmatrix} \Sigma = \langle x^2 \rangle & \langle xy \rangle \\ \langle xy \rangle & \langle y^2 \rangle \end{pmatrix}, \tag{26}$$

which is squeezed with the major axis and the x-axis forming an angle θ in the xy plane. Denoting the eigenvalues of Σ as ω_a and ω_b, it can be written in the form

$$\Sigma_{\theta,\omega_a,\omega_b} = \begin{pmatrix} \cos^2(\theta)\omega_a + \sin^2(\theta)\omega_b & \sin(\theta)\cos(\theta)(\omega_a - \omega_b) \\ \sin(\theta)\cos(\theta)(\omega_a - \omega_b) & \sin^2(\theta)\omega_a + \cos^2(\theta)\omega_b \end{pmatrix}. \tag{27}$$

Our goal is to find a minimum-dissipation protocol that would overall rotate the system in the xy plane, by an angle $\delta\theta = \frac{\pi}{4}$. We thus consider protocols starting at $\Sigma(0) = \Sigma_{0,\omega_a,\omega_b}$ and ending at $\Sigma(\tau) = \Sigma_{\frac{\pi}{4},\omega_a,\omega_b}$ (cf figure 2), and compare three strategies for accomplishing this task: (i) Uniform rotation trajectory: the experimenter simply rotates the system, i.e., fixes the variances $\omega_{a,b}$ in Σ and increases θ; (ii) Pseudo-commutative trajectory: the experimenter tunes $\omega_{a,b}$ to the same value at an intermediate time, thus making the distribution isotropic. Afterwards, they re-stretch the distribution in the desired direction. Such protocol satisfies $[\dot{\Sigma}(t), \Sigma(t)] = 0 \ \forall \ t$ (notice however $[\Sigma(0), \Sigma(\tau)] \neq 0$, which implies Observation 1 cannot be applied in this case). The intermediate point can be chosen optimally to minimize the dissipation; (iii) Optimal protocol: the experimenter is able to control the system such that it follows the BW-geodesic $\bar{\Sigma}(t)$ in (14) between $\Sigma_{0,\omega_a,\omega_b}$ and $\Sigma_{\frac{\pi}{4},\omega_a,\omega_b}$. Details of the calculations for each of the trajectories are given in appendix C.3 and the results are depicted in figure 2. We find that the pseudo-commutative strategy is strongly non-optimal, and dissipates at least twice as much as the geodesics trajectory. Notice that this is not in contradiction to Observation 1, as non-commuting boundary condition induce, in general, non-commuting optimal trajectories. At the same time we see that the uniform rotation of the system Σ is close to the optimal (geodesic) trajectory in terms of dissipation, while being simpler to implement (it corresponds to a rotation of the experimental apparatus with fixed traps' strength). Finally, no timescale approximation was used in this case, but we notice that in the slow-driving limit the above strategies are equivalently translated to the stiffness matrix $K = T\Sigma^{-1}$ (cf Observation 2).

6. Discussion

In this paper, we have studied the work, heat exchange, and irreversible work dissipation of overdamped multidimensional classical systems. These may have an arbitrary number of degrees of freedom and are confined by harmonic potentials whose parameters can be partially or totally controlled. Such systems are described by multidimensional Gaussian probability distributions [56]. For uniform friction and non-moving trap centers, we have derived a general analytic expression (9) for the irreversible work (proportional to the entropy production when the temperature is fixed). This expression is valid for any response trajectory, and allows geometric optimisation based on the Bures-Wasserstein metric for positive matrices. We also discussed straightforward generalizations of these results to non-uniform friction values and nontrivial trap center dynamics. Given that in the slow-driving limit there is a one-to-one mapping between the set of reachable states Σ and the set of reachable controls K, this further allows optimization of control protocols that incorporate experimental constraints, i.e., partial control. Finally, we described general design principles for optimal
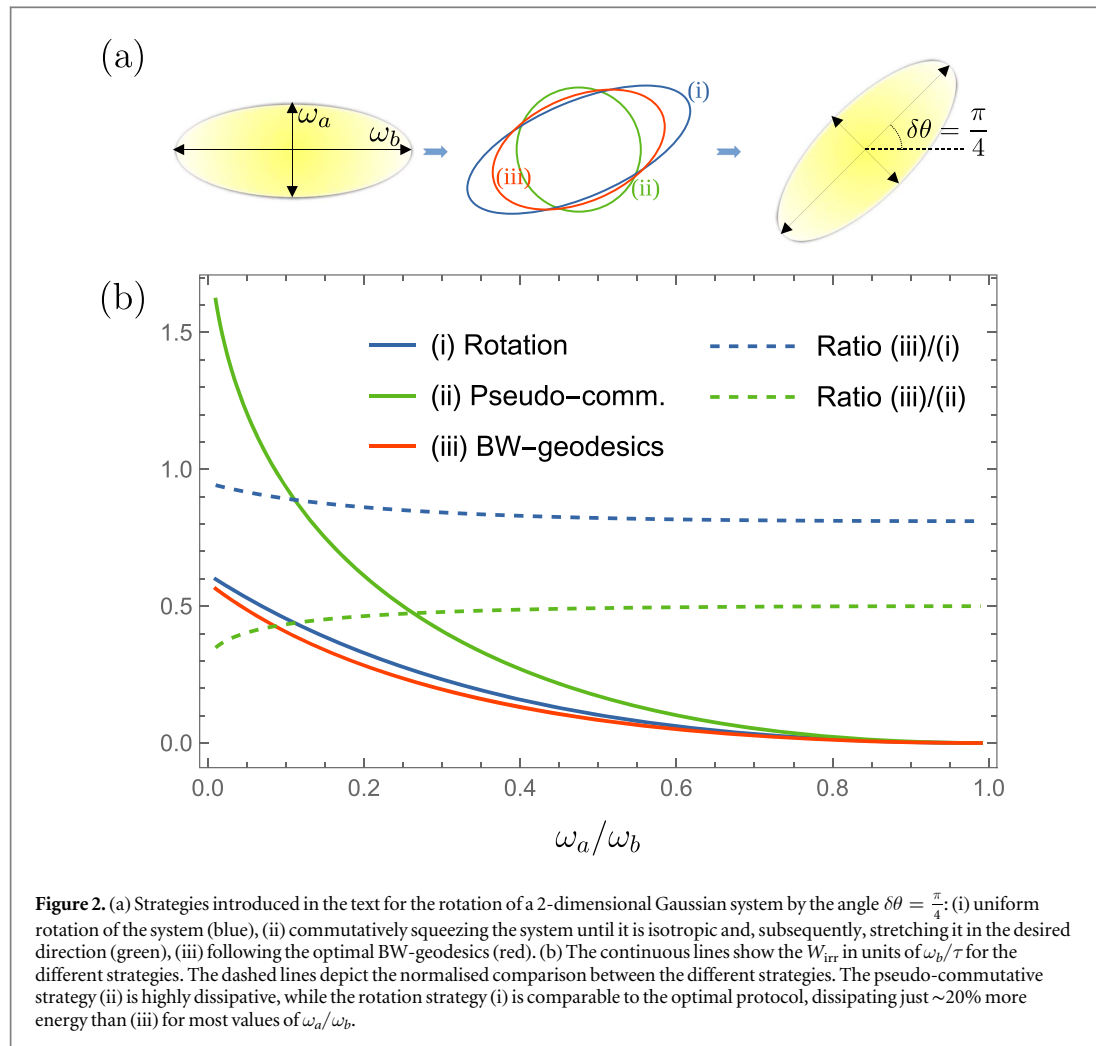
Figure 2. (a) Strategies introduced in the text for the rotation of a 2-dimensional Gaussian system by the angle $\delta\theta = \frac{\pi}{4}$: (i) uniform rotation of the system (blue), (ii) commutatively squeezing the system until it is isotropic and, subsequently, stretching it in the desired direction (green), (iii) following the optimal BW-geodesics (red). (b) The continuous lines show the W_{irr} in units of ω_b/τ for the different strategies. The dashed lines depict the normalised comparison between the different strategies. The pseudo-commutative strategy (ii) is highly dissipative, while the rotation strategy (i) is comparable to the optimal protocol, dissipating just $\sim$20% more energy than (iii) for most values of ω_a/ω_b.

parameter protocols that minimise dissipation and illustrated them for two examples, increasing local confinement of two interacting particles and rotating a squeezed potential.

The obtained results point towards the manageable optimization of control protocols in experimental systems with many degrees of freedom [72, 73, 75–77], and they can be directly applied to optical tweezers setups and electric circuits [71, 78, 79], that wish to minimise dissipation by choosing optimised control parameter protocols. Moreover, our findings can be readily applied to the case of engines and refrigerators described in the low-dissipation regime, characterized by the $1/\tau$ scaling of dissipation [15, 32, 80–83]. Further extensions include the analysis of underdamped classical systems, as well as that of quantum Gaussian systems.

Acknowledgments

Data availability statement

All data that support the findings of this study are included within the article (and any supplementary files).

Appendix A. On the Bures-Wasserstein distance

The Bures-Wasserstein (BW) distance can be defined between positive semidefinite matrices $\Sigma \geqslant 0$, and its infinitesimal value is given by the metrics g_Σ

$$D_{\mathrm{BW}}(\Sigma, \Sigma + d\Sigma)^2 = g_\Sigma(d\Sigma, d\Sigma) = \frac{1}{2}\int_0^\infty d\nu \ \mathrm{Tr}[e^{-\nu\Sigma}d\Sigma e^{-\nu\Sigma}d\Sigma]. \tag{A.1}$$

When applied to complex positive matrices of unit trace (that is, *states* in the field of quantum information), such metric represents a fundamental quantifier in problems of quantum statistical inference and metrology [57, 59, 61, 62]. At the same time it has its own relevance as a distance quantifier between positive real matrices or multivariate distributions, in the context of optimal transport theory [60, 63]. The integrated geodesics length between two points Σ_1 and Σ_2, if no constraints are imposed on the trace of the matrices, reads

$$D_{\mathrm{BW}}(\Sigma_1, \Sigma_2) = \sqrt{\mathrm{Tr}[\Sigma_1] + \mathrm{Tr}[\Sigma_2] - 2\,\mathrm{Tr}[\sqrt{\sqrt{\Sigma_1}\Sigma_2\sqrt{\Sigma_1}}\,]} \tag{A.2}$$

and the corresponding geodesics is

$$\Sigma(t) = (1 - t)^2\Sigma_1 + t^2\Sigma_2 + t(1 - t)(\sqrt{\Sigma_1\Sigma_2} + \sqrt{\Sigma_2\Sigma_1}) \tag{A.3}$$

where the square root

$$\sqrt{\Sigma_1\Sigma_2} = \Sigma_1^{\frac{1}{2}}(\Sigma_1^{\frac{1}{2}}\Sigma_2\Sigma_1^{\frac{1}{2}})^{\frac{1}{2}}\Sigma_1^{-\frac{1}{2}} \tag{A.4}$$

is the only matrix R satisfying $R^2 = \Sigma_1\Sigma_2$ and having a positive spectrum (cf [60]).

Appendix B. General case and slow-driving solution

Here we consider the case in which also the first moment of the quadratic potential can be driven. We assume [56] that the state is Gaussian with covariance matrix $\Sigma(t)$ and first moments $\boldsymbol{\xi}(t)$ (we avoid expliciting time when possible)

$$p(\boldsymbol{x}, t) = \frac{1}{\sqrt{(2\pi)^N \det\Sigma}}\exp\left(-\frac{(\boldsymbol{x} - \boldsymbol{\xi})^\top\Sigma^{-1}(\boldsymbol{x} - \boldsymbol{\xi}))}{2}\right), \tag{B.1}$$

while the potential is

$$V(\boldsymbol{x}, t) = \frac{1}{2}(\boldsymbol{x} - \boldsymbol{z}(t))K(t)(\boldsymbol{x} - \boldsymbol{z}(t)), \tag{B.2}$$

with $\boldsymbol{\xi} \neq \boldsymbol{z}$ in general. The energy of the system is therefore

$$\begin{aligned} E(t) &= \int d\boldsymbol{x}\ p(\boldsymbol{x}, t)V(\boldsymbol{x}, t) \\ &= \frac{1}{2}\mathrm{Tr}[\Sigma K] + \frac{1}{2}(\boldsymbol{\xi} - \boldsymbol{z})K(\boldsymbol{\xi} - \boldsymbol{z}) = \frac{1}{2}\mathrm{Tr}[\Sigma_z K], \end{aligned} \tag{B.3}$$

where Σ_z is the covariance matrix *centered in* $\boldsymbol{z}$, that is

$$\Sigma_z = \langle(\boldsymbol{x} - \boldsymbol{z})(\boldsymbol{x} - \boldsymbol{z})^\top\rangle = \Sigma + (\boldsymbol{\xi} - \boldsymbol{z})(\boldsymbol{\xi} - \boldsymbol{z})^\top. \tag{B.4}$$

The Langevin equation (2) becomes accordingly $\dot{\boldsymbol{x}} = -K(\boldsymbol{x} - \boldsymbol{z}) + \sqrt{2T}\boldsymbol{\eta}$ in natural units, which is translated on the Gaussian moments as

$$\dot{\boldsymbol{\xi}} = -K(\boldsymbol{\xi} - \boldsymbol{z}), \tag{B.5}$$

$$\partial_t\Sigma_z = -K\Sigma_z - \Sigma_z K + 2T, \tag{B.6}$$

where the partial derivative in time is due to the fact that Σ_z depends as well on $\boldsymbol{z}$, i.e.

$$\dot{\Sigma}_z = \partial_t\Sigma_z - \dot{\boldsymbol{z}}(\boldsymbol{\xi} - \boldsymbol{z})^\top - (\boldsymbol{\xi} - \boldsymbol{z})\dot{\boldsymbol{z}}^\top. \tag{B.7}$$

The work and heat can be computed by simply taking the derivative w.r.t. the driving parameters $K, \boldsymbol{z}$ (for the work), and the dynamical parameters $\Sigma, \boldsymbol{\xi}$ (for the heat), i.e.

$$W = \frac{1}{2}\int_0^\tau dt \, (\mathrm{Tr}[\dot{K}\Sigma_z] + \partial_z \mathrm{Tr}[K\Sigma_z]\dot{z})$$

$$= \frac{1}{2}\mathrm{Tr}[K\Sigma_z]\Big|_0^\tau - \frac{1}{2}\int_0^\tau dt \, (\mathrm{Tr}[K\dot{\Sigma}_z] - \partial_z \mathrm{Tr}[K\Sigma_z]\dot{z})$$

$$= \frac{1}{2}\mathrm{Tr}[K\Sigma_z]\Big|_0^\tau - \frac{1}{2}\int_0^\tau dt \, \mathrm{Tr}[K\partial_t\Sigma_z]. \tag{B.8}$$

Using the same steps as in the main text (integration by parts and equation (B.6)), this expression translates to

$$W = \frac{1}{2}\mathrm{Tr}[K\Sigma_z]\Big|_0^\tau + \frac{T}{2}\int_0^\tau dt \, \mathrm{Tr}[\Sigma_z^{-1}\partial_t\Sigma_z]$$

$$- \frac{1}{2}\int_0^\tau dt \, \mathrm{Tr}\left[\int_0^\infty d\nu \, e^{-\nu\Sigma_z}\partial_t\Sigma_z e^{-\nu\Sigma_z}\partial_t\Sigma_z\right], \tag{B.9}$$

which can be rewritten as

$$W - \Delta E - \frac{T}{2}\Delta \det \Sigma_z$$

$$= \frac{T}{2}\int_0^\tau dt \, \mathrm{Tr}[\Sigma_z^{-1}(\dot{\Sigma}_z - \partial_t\Sigma_z)] + \int_0^\tau dt \, g_{\Sigma_z}(\partial_t\Sigma_z, \partial_t\Sigma_z), \tag{B.10}$$

with the BW metrics (10) g. Notice that in general $\frac{1}{2}\Delta \det \Sigma_z \neq \frac{1}{2}\Delta \det \Sigma = \Delta S$ and therefore the expression above cannot be identified as the irreversible work. At the same time, minimizing dissipation requires using finite time protocols in which the system ends in equilibrium with the thermal bath, so that no dissipation follows the end of the protocol. This is automatically satisfied in the case of slow-protocols (see below). For general transformations, it is sufficient to add a final quench of the controls, $(K(\tau), z(\tau)) = (T\Sigma_z^{-1}(\tau), \xi(\tau))$. The condition $\xi(\tau) = z(\tau)$ is sufficient to rewrite (B.10) as

$$W_{\mathrm{irr}} = \frac{T}{2}\int_0^\tau dt \, \mathrm{Tr}[\Sigma_z^{-1}(\dot{\Sigma}_z - \partial_t\Sigma_z)] + \int_0^\tau dt \, g_{\Sigma_z}(\partial_t\Sigma_z, \partial_t\Sigma_z), \tag{B.11}$$

which can be computed explicitly using $\partial_t\Sigma_z - \dot{\Sigma}_z = \dot{z}(\xi - z)^\top + (\xi - z)\dot{z}^\top$.

B.1. The slow case

In the slow-driving regime a first order expansion is performed around $\frac{1}{\tau} \simeq 0$ [68]. For example in the quasistatic limit of $\tau \to \infty$ the solution for the dynamics (B.5, B.6) is clearly $\xi^{(0)} = z$ and $\Sigma_z^{(0)} = \Sigma^{(0)} = TK^{-1}$. The finite time expansion leads to

$$\xi = \xi^{(0)} + \xi^{(1)} + \xi^{(2)} + \ldots \quad + \xi^{(i)} \sim \mathcal{O}(\tau^{-i})$$

$$\xi^{(0)} = z, \quad \xi^{(1)} = -K^{-1}\dot{z}. \tag{B.12}$$

As $\xi - z = -K^{-1}\dot{z} + \mathcal{O}(\tau^{-2})$, we also get

$$\Sigma_z = \Sigma + \dot{z}K^{-2}\dot{z}^\top + \mathcal{O}(\tau^{-3}), \tag{B.13}$$

$$\dot{\Sigma}_z - \partial_t\Sigma_z = \{\dot{z}z^\top, K^{-1}\} + \mathcal{O}(\tau^{-3}) = \{\dot{\xi}\dot{\xi}^\top, K^{-1}\} + \mathcal{O}(\tau^{-3}). \tag{B.14}$$

Using the above expressions, the irreversible work reads

$$W_{\mathrm{irr}} = \int_0^\tau dt \, (|\dot{\xi}|^2 + g_\Sigma(\dot{\Sigma}, \dot{\Sigma})) + \mathcal{O}(\tau^{-2}) \tag{B.15}$$

$$= \int_0^\tau dt \, (|\dot{z}|^2 + Tg_{K^{-1}}(\dot{K^{-1}}, \dot{K^{-1}})) + \mathcal{O}(\tau^{-2}). \tag{B.16}$$

Appendix C. Detailed and solved examples

C.1. Double trap

Consider the potential

$$V = \frac{1}{2}k_x\left(x - \frac{a}{2}\right)^2 + \frac{1}{2}k_y\left(y + \frac{a}{2}\right)^2 + \frac{1}{2}k_{int}(x - y)^2, \tag{C.1}$$

which can be rewritten in matrix form as

$$V = \frac{1}{2}(x - a)^\top K(x - a) + \frac{1}{2}x^\top K_{\mathrm{int}}x \tag{C.2}$$

with

$$x = \begin{pmatrix} x \\ y \end{pmatrix}, \quad a = \begin{pmatrix} a/2 \\ -a/2 \end{pmatrix}, \quad K = \begin{pmatrix} k_x & 0 \\ 0 & k_y \end{pmatrix}, \quad K_{\text{int}} = \begin{pmatrix} k_{\text{int}} & -k_{\text{int}} \\ -k_{\text{int}} & k_{\text{int}} \end{pmatrix}. \tag{C.3}$$

To use equation (19), we rewrite the potential in the 'canonical form'

$$V = \frac{1}{2}(x - a')^{\top}(K + K_{\text{int}})(x - a')$$
$$- \frac{1}{2}a'^{\top}(K + K_{\text{int}})a' + \frac{1}{2}a^{\top}Ka, \tag{C.4}$$

where

$$a' = (K + K_{\text{int}})^{-1}Ka \tag{C.5}$$

is the effective center of the potential. The scalar $-\frac{1}{2}a'^{\top}(K + K_{\text{int}})a' + \frac{1}{2}a^{\top}Ka$ is just a global shift in energy that does not depend on the dynamics of the system and vanishes for cyclic protocols.

C.2. Confining the particles—Irreversibility parameter

We compute the irreversible work using the slow-driving approximation equation (19), in which the center of the distribution can be substituted by the center of the potential, and the covariance matrix can be substituted by the inverse stiffness matrix (cf appendix B), leading to

$$W_{\text{irr}} = \int_0^{\tau} dt \, (|\dot{a}'|^2 + g_{\Sigma}(\dot{\Sigma}, \dot{\Sigma})) \quad \text{with} \quad \Sigma = T(K + K_{\text{int}})^{-1}. \tag{C.6}$$

Suppose the experimenter wants increase the strength of the local traps to increase the confinement of the two particles. The endpoint of the transformation will therefore be

$$a(0) = a(\tau), \quad k_{\text{int}}(0) = k_{\text{int}}(\tau), \quad k_x(0) = k_y(0) < k_x(\tau) = k_y(\tau). \tag{C.7}$$

We notice that due to the symmetry of the potential at the boundary, the eigenvectors of $K + K_{\text{int}}$ are always $(1, 1)$ and $(1, -1)$, independently of the values of k_{int} and $k_x = k_y$. That is, $[(K + K_{\text{int}})(0), (K + K_{\text{int}})(\tau)] = 0$ and we can therefore assume that it commutes with itself at all times (cf Observation 1). In such case, the contribution of $g_{\Sigma}(\dot{\Sigma}, \dot{\Sigma})$ to W_{irr} simplifies to (cf equation (16))

$$g_{\Sigma}(\dot{\Sigma}, \dot{\Sigma}) = \frac{1}{2}\int_0^{\tau} dt \, \text{Tr}\left[\int_0^{\infty} d\nu \, e^{-\nu\Sigma}\dot{\Sigma}e^{-\nu\Sigma}\dot{\Sigma}\right] = \frac{1}{4}\left(\frac{\dot{\omega}_1^2}{\omega_1} + \frac{\dot{\omega}_2^2}{\omega_2}\right), \tag{C.8}$$

where ω_i are the eigenvalues of $\Sigma = T(K + K_{\text{int}})^{-1}$, which are easily computed. In particular given $k_x = k_y \equiv k$ we have

$$\omega_1 = \frac{T}{k}, \quad \omega_2 = \frac{T}{k + 2k_{\text{int}}}, \tag{C.9}$$

and therefore

$$g_{\Sigma}(\dot{\Sigma}, \dot{\Sigma}) = \frac{T}{4}\left(\frac{\dot{k}^2}{k^3} + \frac{(\dot{k} + 2\dot{k}_{\text{int}})^2}{(k + 2k_{\text{int}})^3}\right). \tag{C.10}$$

The contribution $|\dot{a}'|^2$ to W_{irr} follows from equation (C.5):

$$a' = \frac{k}{k + 2k_{\text{int}}}\frac{a}{2}\begin{pmatrix} 1 \\ -1 \end{pmatrix} \tag{C.11}$$

$$|\dot{a}'|^2 = 2a^2\left(\frac{k}{k + 2k_{\text{int}}}\right)^4\left(\frac{d}{dt}\left(\frac{k_{\text{int}}}{k}\right)\right)^2 + \frac{\dot{a}^2}{2}\left(\frac{k}{k + 2k_{\text{int}}}\right)^2. \tag{C.12}$$

The associated dissipation of the transformation can be computed from the expressions above for any slow transformation. We now consider the *partial control* (PC) case in which the distance a and interaction strength k_{int} is fixed, and the experimenter can only control the local stiffnesses $k_x = k_y \equiv k$. Substituting (C.10) and (C.12) with $\dot{a} = \dot{k}_{\text{int}} = 0$, the irreversible work (C.6) then specifies to

$$\dot{W}_{\text{irr}} = \frac{T}{4}\left(\frac{1}{k^3} + \frac{1}{(k + 2k_{\text{int}})^3}\right)\dot{k}^2 + 2a^2\frac{k_{\text{int}}^2}{(k + 2k_{\text{int}})^4}\dot{k}^2. \tag{C.13}$$

For fixed boundary values of k, it can be proven using the Cauchy-Schwarz inequality that the dissipation with partial control (C.13) is lower-bounded by

$$W_{\text{irr}}^{\text{PC}} \geqslant \frac{1}{\tau} \left(\int_{k_1}^{k_2} dk \ \sqrt{\frac{T}{4}\left(\frac{1}{k^3} + \frac{1}{(k+2k_{\text{int}})^3}\right) + 2a^2 \frac{k_{\text{int}}^2}{(k+2k_{\text{int}})^4}} \right)^2. \tag{C.14}$$

By comparison, in the case of *total control* (TC), the bound for the dissipation is given by (20), which, in our case, reads

$$W_{\text{irr}}^{\text{TC}} \geqslant \frac{1}{\tau}(|\boldsymbol{a}_1' - \boldsymbol{a}_2'|^2 + D_{\text{BW}}(\Sigma_1, \Sigma_2)^2), \quad \text{with} \tag{C.15}$$

$$|\boldsymbol{a}_1' - \boldsymbol{a}_2'|^2 = \frac{a^2}{2}\left(\frac{k_1}{k_1 + 2k_{\text{int}}} - \frac{k_2}{k_2 + 2k_{\text{int}}}\right)^2, \tag{C.16}$$

$$\frac{D_{\text{BW}}(\Sigma_1, \Sigma_2)^2}{T} = \left(\frac{1}{\sqrt{k_1}} - \frac{1}{\sqrt{k_2}}\right)^2 + \left(\frac{1}{\sqrt{k_1 + 2k_{\text{int}}}} - \frac{1}{\sqrt{k_2 + 2k_{\text{int}}}}\right)^2. \tag{C.17}$$

C.3. Rotating a 2-dimensional system

In this section, we consider the rotation of a covariance matrix Σ in 2 dimensions by an angle $\theta = \frac{\pi}{4}$. We thus impose the boundary conditions

$$\Sigma_{\text{in}} = \begin{pmatrix} \omega_a & 0 \\ 0 & \omega_b \end{pmatrix}, \quad \Sigma_{\text{fin}} = \frac{1}{2}\begin{pmatrix} \omega_a + \omega_b & \omega_a - \omega_b \\ \omega_a - \omega_b & \omega_a + \omega_b \end{pmatrix}. \tag{C.18}$$

And we minimize the irreversible work (9) according to three possible strategies.

C.3.1. Simple rotation protocol. First, we consider the transformation from Σ_{in} to Σ_{fin} to be performed by uniformly rotating the experimental apparatus, without modifying the squeezing $\{\omega_a, \omega_b\}$ of the distribution. This corresponds to an angle-parametrized protocol

$$\Sigma_\theta = \begin{pmatrix} \cos^2(\theta)\omega_a + \sin^2(\theta)\omega_b & \sin(\theta)\cos(\theta)(\omega_a - \omega_b) \\ \sin(\theta)\cos(\theta)(\omega_a - \omega_b) & \sin^2(\theta)\omega_a + \cos^2(\theta)\omega_b \end{pmatrix} \tag{C.19}$$

starting at $\Sigma_0 \equiv \Sigma_{\text{in}}$ and ending at $\Sigma_{\frac{\pi}{4}} \equiv \Sigma_{\text{fin}}$. The irreversible work production (9) is in this case given by $W_{\text{irr}} = \frac{1}{2}\int_0^\tau dt \ \text{Tr}\left[\int_0^\infty d\nu \ e^{-\nu\Sigma}\dot{\Sigma}e^{-\nu\Sigma}\dot{\Sigma}\right]$. Given the rotational symmetry of the problem, it is obvious that the optimal rotation of the system will have a constant speed $\dot{\theta}$. Thus the integrand

$$\dot{W}_{\text{irr}} = \frac{1}{2}\text{Tr}\left[\int_0^\infty d\nu \ e^{-\nu\Sigma}\dot{\Sigma}e^{-\nu\Sigma}\dot{\Sigma}\right] \tag{C.20}$$

will be constant in time and can be computed, e.g., for $\theta = 0$, which yields

$$\Sigma = \begin{pmatrix} \omega_a & 0 \\ 0 & \omega_b \end{pmatrix}, \quad \dot{\Sigma} = \dot{\theta}\begin{pmatrix} 0 & \omega_a - \omega_b \\ \omega_a - \omega_b & 0 \end{pmatrix}. \tag{C.21}$$

Now we use the fact that the operator $\mathcal{I}(A, B) = \int_0^\infty d\nu \ e^{-\nu A}Be^{-\nu A}$ can be easily expressed in components as $\mathcal{I}(A, B)_{ij} = \frac{B_{ij}}{a_i + a_j}$, in the basis that diagonalizes A, i.e., $A_{ij} = \delta_{ij}a_i$. We therefore get

$$\int_0^\infty d\nu \ e^{-\nu\Sigma}\dot{\Sigma}e^{-\nu\Sigma} = \dot{\theta}\frac{\omega_a - \omega_b}{\omega_a + \omega_b}\begin{pmatrix} 0 & 1 \\ 1 & 0 \end{pmatrix}, \tag{C.22}$$

from which it is easy to compute the value of (C.20):

$$\dot{W}_{\text{irr}} = \dot{\theta}^2\frac{(\omega_a - \omega_b)^2}{\omega_a + \omega_b}. \tag{C.23}$$

The minimum value of $W_{\text{irr}} = \int_0^\tau \dot{W}_{\text{irr}}$ for the uniform rotation over the total angle $\Delta\theta = \frac{\pi}{4}$ is thus given by

$$W_{\text{irr}} = \frac{1}{\tau}\frac{\pi^2}{16}\frac{(\omega_a - \omega_b)^2}{\omega_a + \omega_b}. \tag{C.24}$$

C.3.2. Pseudo-commutative protocol. One possible way to interpolate between Σ_{in} and Σ_{fin} (C.18) is to change the values of $\omega_{a,b}$ to reach an intermediate symmetric covariance matrix

$$\Sigma_{\text{intermediate}} = \begin{pmatrix} \omega_c & 0 \\ 0 & \omega_c \end{pmatrix}, \tag{C.25}$$

which is proportional to the identity matrix, and later 're-stretch it' in the $\pi/4$ direction in the same way. Such protocol is *locally commutative* at all times, in the sense that $[\Sigma(t), \dot{\Sigma}(t)] = 0 \ \forall t$, although the final and initial covariance matrices do not commute. The total irreversible work for such a strategy is clearly twice the

irreversible work obtained for the transformation $\Sigma_{\text{in}} \to \Sigma_{\text{intermediate}}$, in a time $\tau/2$. We therefore get, using the commutative result (16),

$$W_{\text{irr}} = \frac{4}{\tau}((\sqrt{\omega_a} - \sqrt{\omega_c})^2 + (\sqrt{\omega_b} - \sqrt{\omega_c})^2). \tag{C.26}$$

ω_c is a free parameter of the described protocol, which can be chosen to minimize W_{irr}. The optimal choice is $\omega_c = \left(\frac{\sqrt{\omega_a} + \sqrt{\omega_b}}{2}\right)^2$, leading to the minimum dissipation for pseudo-commutative protocols

$$W_{\text{irr}} = \frac{2}{\tau}(\sqrt{\omega_a} - \sqrt{\omega_b})^2. \tag{C.27}$$

C.4. Optimal protocol

The minimal value of dissipation for any protocol between Σ_{in} and Σ_{fin} is given by the main lower bound (12), which is saturated when performing the BW-geodesics (14). In our case, we obtain

$$\frac{D_{\text{BW}}(\Sigma_{\text{in}}, \Sigma_{\text{fin}})^2}{\tau} = \frac{1}{\tau}(\text{Tr}[\Sigma_{\text{in}}] + \text{Tr}[\Sigma_{\text{fin}}] - 2\,\text{Tr}[\sqrt{\sqrt{\Sigma_{\text{in}}}\,\Sigma_{\text{fin}}\,\sqrt{\Sigma_{\text{in}}}}\,])$$
$$= \frac{1}{\tau}(2(\omega_a + \omega_b) - \sqrt{2}\sqrt{2(\omega_a + \omega_b)^2 - (\omega_a - \omega_b)^2}). \tag{C.28}$$

ORCID iDs

Paolo Abiuso ⑩ https://orcid.org/0000-0001-5019-7823
Viktor Holubec ⑩ https://orcid.org/0000-0002-6576-1316
Martí Perarnau-Llobet ⑩ https://orcid.org/0000-0002-4658-0632

References

[1] Andresen B, Salamon P and Berry R S 1984 Thermodynamics in finite time *Physics Today* **37** 62–70
[2] Andresen B, Berry R S, Ondrechen M J and Salamon P 1984 Thermodynamics for processes in finite time *Acc. Chem. Res.* **17** 266–71
[3] Deffner S and Bonança M V S 2020 Thermodynamic control—an old paradigm with new applications *EPL* **131** 20001
[4] Seifert U 2012 Stochastic thermodynamics, fluctuation theorems and molecular machines *Rep. Prog. Phys.* **75** 126001
[5] Myers N M, Abah O and Deffner S 2022 Quantum thermodynamic devices: from theoretical proposals to experimental reality *AVS Quantum Sci.* **4** 027101
[6] Zulkowski P R and DeWeese M R 2014 Optimal finite-time erasure of a classical bit *Phys. Rev.* E **89** 052140
[7] Proesmans K, Ehrich J and Bechhoefer J 2020 Finite-time landauer principle *Phys. Rev. Lett.* **125** 100602
[8] Zhen Y-Z, Egloff D, Modi K and Dahlsten O 2021 Universal bound on energy cost of bit reset in finite time *Phys. Rev. Lett.* **127** 190602
[9] Jarzynski C 1997 Nonequilibrium equality for free energy differences *Phys. Rev. Lett.* **78** 2690
[10] Sekimoto K 1998 L equation and thermodynamics *Prog. Theor. Phys. Suppl.* **130** 17–27
[11] Crooks G E 1999 Entropy production fluctuation theorem and the nonequilibrium work relation for free energy differences *Phys. Rev.* E **60** 2721
[12] Seifert U 2005 Entropy production along a stochastic trajectory and an integral fluctuation theorem *Phys. Rev. Lett.* **95** 040602
[13] Jarzynski C 2011 Equalities and inequalities: Irreversibility and the second law of thermodynamics at the nanoscale *Annu. Rev. Condens. Matter Phys.* **2** 329–51
[14] Miller H J D and Anders J 2017 Entropy production and time asymmetry in the presence of strong interactions *Phys. Rev.* E **95** 062123
[15] Schmiedl T and Seifert U 2007 Optimal finite-time processes in stochastic thermodynamics *Phys. Rev. Lett.* **98** 108301
[16] Schmiedl T and Seifert U 2007 Efficiency at maximum power: An analytically solvable model for stochastic heat engines *EPL (Europhysics Letters)* **81** 20003
[17] Holubec V 2014 An exactly solvable model of a stochastic heat engine: optimization of power, power fluctuations and efficiency *J. Stat. Mech: Theory Exp.* **2014** P05022
[18] Plata C A, Guéry-Odelin D, Trizac E and Prados A 2019 Optimal work in a harmonic trap with bounded stiffness *Phys. Rev.* E **99** 012140
[19] Zhang Y 2020 Optimization of stochastic thermodynamic machines *J. Stat. Phys.* **178** 1336–53
[20] Miangolarra O M, Taghvaei A, Fu R, Yo Chen and Georgiou T T 2021 Energy harvesting from anisotropic fluctuations *Phys. Rev.* E **104** 044101
[21] Gomez-Marin A, Schmiedl T and Seifert U 2008 Optimal protocols for minimal work processes in underdamped stochastic thermodynamics *J. Chem. Phys.* **129** 024114
[22] Dechant A, Kiesel N and Lutz E 2017 Underdamped stochastic heat engine at maximum efficiency *EPL* **119** 50003
[23] Miangolarra O M, Fu R, Taghvaei A, Chen Y and Georgiou T T 2021 Underdamped stochastic thermodynamic engines in contact with a heat bath with arbitrary temperature profile *Phys. Rev.* E **103** 062103
[24] Esposito M, Kawai R, Lindenberg K and Van den Broeck C 2010 Finite-time Thermodynamics for A Single-Level Quantum Dot *EPL* **89** 20003
[25] Ruppeiner G 1995 Riemannian geometry in thermodynamic fluctuation theory *Rev. Mod. Phys.* **67** 605–59
[26] Salamon P and Berry R S 1983 Thermodynamic length and dissipated availability *Phys. Rev. Lett.* **51** 1127–30
[27] Nulton J, Salamon P, Andresen B and Anmin Q 1985 Quasistatic processes as step equilibrations *J. Chem. Phys.* **83** 334–8
[28] Crooks G E 2007 Measuring thermodynamic length *Phys. Rev. Lett.* **99** 100602
[29] Sivak D A and Crooks G E 2012 Thermodynamic metrics and optimal paths *Phys. Rev. Lett.* **108** 190602
[30] Zulkowski P R, Sivak D A, Crooks G E and DeWeese M R 2012 Geometry of thermodynamic control *Phys. Rev.* E **86** 041148

[31] Bonança M V S and Deffner S 2014 Optimal driving of isothermal processes close to equilibrium *J. Chem. Phys.* **140** 244119

[32] Abiuso P, Miller H J D, Perarnau-Llobet M and Scandi M 2020 Geometric optimisation of quantum thermodynamic processes *Entropy* **22** 1076

[33] Rotskoff G M and Crooks G E 2015 Optimal control in nonequilibrium systems: Dynamic riemannian geometry of the ising model *Phys. Rev. E* **92** 060102

[34] Gingrich T R, Rotskoff G M, Crooks G E and Geissler P L 2016 Near-optimal protocols in complex nonequilibrium transformations *PNAS* **113** 10263–8

[35] Rotskoff G M, Crooks G E and Vanden-Eijnden E 2017 Geometric approach to optimal nonequilibrium control: Minimizing dissipation in nanomagnetic spin systems *Phys. Rev. E* **95** 012148

[36] Scandi M and Perarnau-Llobet M 2019 Thermodynamic length in open quantum systems *Quantum* **3** 197

[37] Abiuso P and Perarnau-Llobet M 2020 Optimal cycles for low-dissipation heat engines *Phys. Rev. Lett.* **124** 110606

[38] Brandner K and Saito K 2020 Thermodynamic geometry of microscopic heat engines *Phys. Rev. Lett.* **124** 040602

[39] Miller H J D and Mehboudi M 2020 Geometry of work fluctuations versus efficiency in microscopic thermal machines *Phys. Rev. Lett.* **125** 260602

[40] Bhandari B, Alonso P T, Taddei F, von Oppen F, Fazio R and Arrachea L 2020 Geometric properties of adiabatic quantum thermal machines *Phys. Rev. B* **102** 155407

[41] Terrén Alonso P, Abiuso P, Perarnau-Llobet M and Arrachea L 2022 Geometric optimization of nonequilibrium adiabatic thermal machines and implementation in a qubit system *PRX Quantum* **3** 010326

[42] Frim A G and DeWeese M R 2021 Optimal finite-time brownian carnot engine arXiv:2107.05673

[43] Frim A G and DeWeese M R 2021 A geometric bound on the efficiency of irreversible thermodynamic cycles arXiv:2112.10797

[44] Eglinton J and Brandner K 2022 Geometric bounds on the power of adiabatic thermal machines arXiv:2202.08759

[45] Cavina V, Erdman P A, Abiuso P, Tolomeo L and Giovannetti V 2021 Maximum-power heat engines and refrigerators in the fast-driving regime *Phys. Rev. A* **104** 032226

[46] Erdman P A, Cavina V, Fazio R, Taddei F and Giovannetti V 2019 Maximum power and corresponding efficiency for two-level heat engines and refrigerators: optimality of fast cycles *New J. Phys.* **21** 103049

[47] Das A and Mukherjee V 2020 Quantum-enhanced finite-time otto cycle *Phys. Rev. Research* **2** 033083

[48] Blaber S, Louwerse M D and Sivak D A 2021 Steps minimize dissipation in rapidly driven stochastic systems *Phys. Rev. E* **104** L022101

[49] Aurell E, Mejía-Monasterio C and Muratore-Ginanneschi P 2011 Optimal protocols and optimal transport in stochastic thermodynamics *Phys. Rev. Lett.* **106** 250601

[50] Aurell E, Gawedzki K, Mejía-Monasterio C, Mohayaee R and Muratore-Ginanneschi P 2012 Refined second law of thermodynamics for fast random processes *J. Stat. Phys.* **147** 487–505

[51] Dechant A and Sakurai Y 2019 Thermodynamic interpretation of wasserstein distance arXiv:1912.08405

[52] Chen Y, Georgiou T T and Tannenbaum A 2019 Stochastic control and nonequilibrium thermodynamics: Fundamental limits *IEEE Trans. Autom. Control* **65** 2979–91

[53] Van Vu T and Hasegawa Y 2021 Geometrical bounds of the irreversibility in markovian systems *Phys. Rev. Lett.* **126** 010601

[54] Nakazato M and Ito S 2021 Geometrical aspects of entropy production in stochastic thermodynamics based on wasserstein distance *Phys. Rev. Research* **3** 043093

[55] Dechant A 2021 Minimum entropy production, detailed balance and wasserstein distance for continuous-time markov processes arXiv:2110.01141

[56] Risken H 1996 Fokker-planck equation *In The Fokker-Planck Equation* (Berlin: Springer) pp 63–95

[57] Paris M G A 2009 Quantum estimation for quantum technology *International Journal of Quantum Information* **7** 125–37

[58] Sekimoto K 2010 *Stochastic Energetics* vol 799 (Berlin: Springer)

[59] Bengtsson I and Życzkowski K 2017 *Geometry of Quantum States: An Introduction To Quantum Entanglement* (Cambridge: Cambridge University Press)

[60] Bhatia R, Jain T and Lim Y 2019 On the bures-wasserstein distance between positive definite matrices *Expositiones Mathematicae* **37** 165–91

[61] Wootters W K 1981 Statistical distance and hilbert space *Phys. Rev. D* **23** 357

[62] Braunstein S L and Caves C M 1994 Statistical distance and the geometry of quantum states *Phys. Rev. Lett.* **72** 3439

[63] Olkin I and Pukelsheim F 1982 The distance between two random vectors with given dispersion matrices *Linear Algebr. Appl.* **48** 257–63

[64] Nakazato M and Ito S 2021 Geometrical aspects of entropy production in stochastic thermodynamics based on wasserstein distance *Phys. Rev. Research* **3** 043093

[65] Bauer M, Brandner K and Seifert U 2016 Optimal performance of periodically driven, stochastic heat engines under limited control *Phys. Rev. E* **93** 042112

[66] Ye Z, Cerisola F, Abiuso P, Anders J, Perarnau-Llobet M and Holubec V 2022 Optimal finite-time heat engines under constrained control arXiv:2202.12953

[67] Zhong A and DeWeese M R 2022 Limited-control optimal protocols arbitrarily far from equilibrium arXiv:2205.08662

[68] Cavina V, Mari A and Giovannetti V 2017 Slow dynamics and thermodynamics of open quantum systems *Phys. Rev. Lett.* **119** 050601

[69] Brandner K, Saito K and Seifert U 2015 Thermodynamics of micro-and nano-systems driven by periodic temperature variations *Phys. Rev. X* **5** 031019

[70] Brandner K and Seifert U 2016 Periodic thermodynamics of open quantum systems *Phys. Rev. E* **93** 062134

[71] Jones P H, Maragò O M and Volpe G 2015 *Optical Tweezers: Principles and Applications* (Cambridge: Cambridge University Press)

[72] Khadka U, Holubec V, Yang H and Cichos F 2018 Active particles bound by information flows *Nat. Commun.* **9** 3864

[73] Krishnamurthy S, Ganapathy R and Sood A K 2021 Synergistic action in colloidal heat engines coupled by non-conservative flows arXiv:2101.07015

[74] Mamede I N, Harunari P E, Akasaki B A N, Proesmans K and Fiore C E 2022 Obtaining efficient thermal engines from interacting brownian particles under time-periodic drivings *Phys. Rev. E* **105** 024106

[75] Hucul D, Yeo M, Olmschenk S, Monroe C, Hensinger W K and Rabchuk J 2008 On the transport of atomic ions in linear and multidimensional ion trap arrays *Quantum Information & Computation* **8** 501–78

[76] Renaut C, Cluzel B, Dellinger J, Lalouat L, Picard E, Peyrade D, Hadji E and De Fornel F 2013 On chip shapeable optical tweezers *Sci. Rep.* **3** 1–4

[77] Mayer D, Schmidt F, Haupt S, Bouton Q, Adam D, Lausch T, Lutz E and Widera A 2020 Nonequilibrium thermodynamics and optimal cooling of a dilute atomic gas *Phys. Rev. Research* **2** 023245

[78] Ciliberto S 2017 Experiments in stochastic thermodynamics: Short history and perspectives *Phys. Rev.* X **7** 021051

[79] Gao D, Ding W, Nieto-Vesperinas M, Ding X, Rahman M, Zhang T, Lim C and Qiu C-W 2017 Optical manipulation from the microscale to the nanoscale: fundamentals, advances and prospects *Light: Science & Applications* **6** e17039

[80] Esposito M, Kawai R, Lindenberg K and Van den Broeck C 2010 Efficiency at maximum power of low-dissipation carnot engines *Phys. Rev. Lett.* **105** 150603

[81] Martínez I A, Roldán É, Dinis L, Petrov D, Parrondo J M R and Rica R A 2015 Brownian carnot engine *Nat. Phys.* **12** 67–70

[82] Ma Y, Xu D, Dong H and Sun C-P 2018 Universal constraint for efficiency and power of a low-dissipation heat engine *Phys. Rev.* E **9** 042112

[83] Ye Z and Holubec V 2021 Maximum efficiency of absorption refrigerators at arbitrary cooling power *Phys. Rev.* E **103** 052125

4 Conclusion

We derived maximum efficiency at given power for low-dissipation refrigerators and heat pumps as well as absorption refrigerators consisting of simultaneous operating low-dissipation heat engines and refrigerators in Refs. [5–7]. We provided simple analytical upper and lower bounds on this quantity. For low-dissipation refrigerators [5], we showed that the infinitely fast nonlinear increase in efficiency with decreasing power from the maximum power, routinely occurred in heat engines [25, 44–51], can be observed for small irreversibility ratio only. For large irreversibility ratio, the increase in efficiency is linear. Thus, low-dissipation refrigerators are for small irreversibility ratio more beneficial to operate near maximum power than at maximum power to achieve considerably larger efficiency compared to the efficiency at maximum power. Otherwise, they are more advantageous to operate at maximum power. For low-dissipation heat pumps [7], the increase in efficiency with decreasing power for large value of power is slow. Reasonably efficient heat pumps thus should operate far from the maximum power, which is different from heat engines [45] and refrigerators [5]. We identified a special parameter regime when the expressions for maximum efficiency at given power for low-dissipation heat pumps and endoreversible heat pumps [44, 52, 72] agree. We pointed out that, at maximum power, the low-dissipation heat pump operates as a pure work-to-heat converter. The corresponding power diverges and the efficiency is the smallest possible (one). For absorption refrigerators [6], we showed how their maximum efficiency at given power follows from those for the internal engine and refrigerator. When the internal engine and refrigerator are low dissipation, we analytically showed that a slight decrease in power of the absorption refrigerator from its maximum value leads to a large nonlinear increase in efficiency, as observed in heat engines [45], whenever the ratio of maximum powers of the internal engine and refrigerator does not diverge. Otherwise, the increase in efficiency is linear as observed in refrigerators with large irreversibility ratio [5]. Thus, in all practical situations, the efficiency of absorption refrigerators significantly increases when their power is slightly decreased from its maximum. We

concluded that it is more beneficial to operate actual absorption refrigerators near maximum power than at maximum power, so that the corresponding efficiency is much enhanced compared to the efficiency at maximum power.

We designed optimal finite-time protocols for Brownian systems under different boundary conditions in Refs. [9, 43]. We showed that the results of optimization strongly depend on which boundary conditions are imposed. For experimentally motivated constraints on control parameters, we derived optimal protocols for finite-time heat engines under constrained control [9]. When the constraints are imposed on the system response, we showed how to generalize the paradigmatic model [24] in stochastic thermodynamics to the multidimensional case [43], perhaps with a limited control over some of the degrees of freedom.

Appendix A Thermoradiative devices

Thermoradiative devices, theoretically studied by Strandberg [79] and later experimentally realized by Santhanam and Fan [80], represent a new technology that has recently emerged for electricity generation from thermal energy. The electric current in these devices is driven by the difference in the chemical potential for electron populations above and below a bandgap ($E_G = E_C - E_V$) (for more details see Fig. 6). The difference in chemical potential ($\mu = E_{fe} - E_{fh} < 0$) arises due to an asymmetry in the excitation and deexcitation processes of electrons across the bandgap, exhibiting certain similarities to traditional thermophotovoltaic cells [97–100]. Nevertheless, there are some differences in their working principles, even though both of them are composed of p-n junctions: As shown in Fig. 7, while thermophotovoltaic cells accept thermal radiation from a higher-temperature source than the cell itself, thermoradiative cells, on the other hand, operate at elevated temperatures and release a net outflow of photons to colder surroundings, causing the generated bias and thus electric current in the opposite direction.
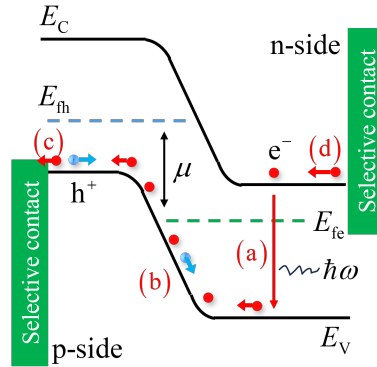

FIG. 6. A possible route for an electron going through the thermoradiative device [79]. (a) An electron-hole pair recombines radiatively over the bandgap $E_G = E_C - E_V$, where E_C is the bottom level of the conduction band and E_V is the top level of the valance band. (b) The electron increases its energy by thermal excitations due to redistribution of the electron population when electrons leave the device. (c) Electron extraction to an external circuit via a metallic contact, leaving a hole behind. (d) The electron completes the loop when it is reinserted to the conduction band of the device.

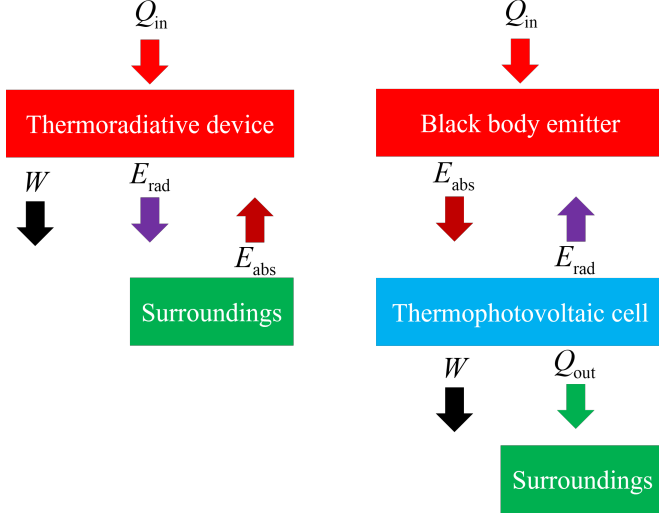A thermoradiative device is a special type of heat engine and thus it allows to

FIG. 7. For thermoradiative devices, heat Q_{in} and radiative energy E_{abs} is supplied, while work W is produced and radiative energy E_{rad} is emitted. On the contrary, a thermophotovoltaic cell accepts radiative energy E_{abs} from a heated body while generating work W and emitting radiative energy E_{rad}. In general, heat must be removed from the thermophotovoltaic cell to prevent its temperature from rising (Q_{out}) [79].

attain the Carnot efficiency at vanishing power. This can be understood as follows. The current density and the energy flux density released by the thermoradiative device are represented by [79, 101–103]

$$J/e = \dot{N}(T_{\text{A}}, 0) - \dot{N}(T_{\text{D}}, \mu_{\text{D}}), \tag{29}$$

$$\dot{Q}_{\text{out}} = \dot{E}(T_{\text{D}}, \mu_{\text{D}}) - \dot{E}(T_{\text{A}}, 0), \tag{30}$$

where

$$\dot{N}(T, \mu) = \frac{2\pi}{c^2 h^3} \int_{E_{\text{G}}}^{\infty} d\varepsilon \frac{\varepsilon^2}{e^{(\varepsilon - \mu)/k_{\text{B}}T} - 1}, \tag{31}$$

$$\dot{E}(T, \mu) = \frac{2\pi}{c^2 h^3} \int_{E_{\text{G}}}^{\infty} d\varepsilon \frac{\varepsilon^3}{e^{(\varepsilon - \mu)/k_{\text{B}}T} - 1}. \tag{32}$$

Here $\dot{N}(T, \mu)$ is the flux density of photons with energy $\varepsilon \in [E_{\text{G}}, \infty]$ incoming to the thermoradiative device from the surroundings ($T = T_{\text{A}}$, $\mu = 0$) and that radiated by the thermoradiative device to the surroundings ($T = T_{\text{D}}$, $\mu = \mu_{\text{D}}$), and $\dot{E}(T, \mu)$ is the corresponding energy flux density. e, c, h, k_{B}, E_{G}, T, and μ denote, respectively, the elementary charge, speed of light, Plank constant, Boltzmann

constant, bandgap, temperature, and chemical potential difference. The device voltage and the chemical potential difference are related by $V = \mu_D/e$, and thus the output power density and efficiency are expressed as [79]

$$P = JV = \mu_D[\dot{N}(T_A, 0) - \dot{N}(T_D, \mu_D)], \tag{33}$$

$$\eta = \frac{P}{P + \dot{Q}_{out}} = \left[1 - \frac{1}{\mu_D}\frac{\dot{E}(T_A, 0) - \dot{E}(T_D, \mu_D)}{\dot{N}(T_A, 0) - \dot{N}(T_D, \mu_D)}\right]^{-1}. \tag{34}$$

For large bandgap E_G such that $\varepsilon - \mu \gg k_B T$, we obtain $\exp[(\varepsilon - \mu)/k_B T] - 1 \approx \exp[(\varepsilon - \mu)/k_B T]$. Then Eqs. (31) and (32) become simple,

$$\dot{N}(T, \mu) \approx \frac{2\pi k_B T}{c^2 h^3} E_G^2 \exp\left[\frac{\mu - E_G}{k_B T}\right], \tag{35}$$

$$\dot{E}(T, \mu) \approx \frac{2\pi k_B T}{c^2 h^3} E_G^3 \exp\left[\frac{\mu - E_G}{k_B T}\right]. \tag{36}$$

Using the approximations (35) and (36), one readily obtains that vanishing output power density in Eq. (33) corresponds to

$$\mu_D = E_G\left(1 - \frac{T_D}{T_A}\right), \tag{37}$$

and thus the efficiency (34) approaches the Carnot efficiency

$$\eta \approx \frac{\mu_D}{\mu_D - E_G} = 1 - \frac{T_A}{T_D}. \tag{38}$$

This is natural because a larger bandgap E_G means that only electrons with higher energy can deexcite across the bandgap. The limited number of transitioned electrons allows the electron population in each band to converge to Fermi–Dirac statistic (equilibrium), and thus the efficiency reaches the Carnot efficiency, as dictated by equilibrium thermodynamics.

[1] V. V. Sychev, *Complex thermodynamic systems* (Springer Science & Business Media, 2013).

[2] M. Chandrashekar and F. Wong, Thermodynamic systems analysis—i. a graph-theoretic approach, Energy **7**, 539 (1982).

[3] J. Roßnagel, O. Abah, F. Schmidt-Kaler, K. Singer, and E. Lutz, Nanoscale heat engine beyond the carnot limit, Phys. Rev. Lett. **112**, 030602 (2014).

[4] O. Abah, J. Roßnagel, G. Jacob, S. Deffner, F. Schmidt-Kaler, K. Singer, and E. Lutz, Single-ion heat engine at maximum power, Phys. Rev. Lett. **109**, 203006 (2012).

[5] V. Holubec and Z. Ye, Maximum efficiency of low-dissipation refrigerators at arbitrary cooling power, Phys. Rev. E **101**, 052124 (2020).

[6] Z. Ye and V. Holubec, Maximum efficiency of absorption refrigerators at arbitrary cooling power, Phys. Rev. E **103**, 052125 (2021).

[7] Z. Ye and V. Holubec, Maximum efficiency of low-dissipation heat pumps at given heating load, Phys. Rev. E **105**, 024139 (2022).

[8] K. J. Chua, S. K. Chou, and W. Yang, Advances in heat pump systems: A review, Applied energy **87**, 3611 (2010).

[9] Z. Ye, F. Cerisola, P. Abiuso, J. Anders, M. Perarnau-Llobet, and V. Holubec, Optimal finite-time heat engines under constrained control, Phys. Rev. Res. **4**, 043130 (2022).

[10] M. Bauer, K. Brandner, and U. Seifert, Optimal performance of periodically driven, stochastic heat engines under limited control, Phys. Rev. E **93**, 042112 (2016).

[11] C. A. Plata, D. Guéry-Odelin, E. Trizac, and A. Prados, Optimal work in a harmonic trap with bounded stiffness, Phys. Rev. E **99**, 012140 (2019).

[12] V. Holubec and A. Ryabov, Diverging, but negligible power at carnot efficiency: Theory and experiment, Phys. Rev. E **96**, 062107 (2017).

[13] J. Yvon, The saclay reactor: two years experience on heat transfer by means of a

compressed gas, in *Proceedings of the International Conference on Peaceful Uses of Atomic Energy* (Geneva, 1955) p. 387.

[14] I. I. Novikov, The efficiency of atomic power stations, J. Nucl. Energy II **7**, 125 (1958).

[15] P. Chambadal, *Les centrales nucléaires*, Vol. 321 (Colin, 1957).

[16] F. L. Curzon and B. Ahlborn, Efficiency of a carnot engine at maximum power output, American Journal of Physics **43**, 22 (1975).

[17] M. H. Rubin and B. Andresen, Optimal staging of endoreversible heat engines, Journal of Applied Physics **53**, 1 (1982).

[18] M. Esposito, R. Kawai, K. Lindenberg, and C. Van den Broeck, Efficiency at maximum power of low-dissipation carnot engines, Phys. Rev. Lett. **105**, 150603 (2010).

[19] C. Van den Broeck, Thermodynamic efficiency at maximum power, Phys. Rev. Lett. **95**, 190602 (2005).

[20] G. Benenti, K. Saito, and G. Casati, Thermodynamic bounds on efficiency for systems with broken time-reversal symmetry, Phys. Rev. Lett. **106**, 230602 (2011).

[21] Y. Izumida, K. Okuda, J. M. M. Roco, and A. C. Hernández, Heat devices in nonlinear irreversible thermodynamics, Phys. Rev. E **91**, 052140 (2015).

[22] Y. Izumida and K. Okuda, Efficiency at maximum power of minimally nonlinear irreversible heat engines, Europhysics Letters **97**, 10004 (2012).

[23] Y. Izumida, K. Okuda, A. C. Hernández, and J. Roco, Coefficient of performance under optimized figure of merit in minimally nonlinear irreversible refrigerator, EPL (Europhysics Letters) **101**, 10005 (2013).

[24] T. Schmiedl and U. Seifert, Efficiency at maximum power: An analytically solvable model for stochastic heat engines, Europhysics letters **81**, 20003 (2007).

[25] A. Dechant, N. Kiesel, and E. Lutz, Underdamped stochastic heat engine at maximum efficiency, Europhysics Letters **119**, 50003 (2017).

[26] R. Uzdin and R. Kosloff, Universal features in the efficiency at maximal work of hot quantum otto engines, Europhysics Letters **108**, 40001 (2014).

[27] J. Wang, Z. Ye, Y. Lai, W. Li, and J. He, Efficiency at maximum power of a

quantum heat engine based on two coupled oscillators, Phys. Rev. E **91**, 062134 (2015).

[28] R. Long, Z. Liu, and W. Liu, Performance optimization of minimally nonlinear irreversible heat engines and refrigerators under a trade-off figure of merit, Phys. Rev. E **89**, 062119 (2014).

[29] Y. Wang, M. Li, Z. C. Tu, A. C. Hernández, and J. M. M. Roco, Coefficient of performance at maximum figure of merit and its bounds for low-dissipation carnot-like refrigerators, Phys. Rev. E **86**, 011127 (2012).

[30] Y. Yuan, R. Wang, J. He, Y. Ma, and J. Wang, Coefficient of performance under maximum χ criterion in a two-level atomic system as a refrigerator, Phys. Rev. E **90**, 052151 (2014).

[31] C. de Tomás, A. C. Hernández, and J. M. M. Roco, Optimal low symmetric dissipation carnot engines and refrigerators, Phys. Rev. E **85**, 010104 (2012).

[32] A. C. Hernández, A. Medina, J. M. M. Roco, J. A. White, and S. Velasco, Unified optimization criterion for energy converters, Phys. Rev. E **63**, 037102 (2001).

[33] C. de Tomas, J. M. M. Roco, A. C. Hernández, Y. Wang, and Z. C. Tu, Low-dissipation heat devices: Unified trade-off optimization and bounds, Phys. Rev. E **87**, 012105 (2013).

[34] F. Angulo-Brown, An ecological optimization criterion for finite-time heat engines, Journal of Applied Physics **69**, 7465 (1991).

[35] Y. Ust and B. Sahin, Performance optimization of irreversible refrigerators based on a new thermo-ecological criterion, International Journal of Refrigeration **30**, 527 (2007).

[36] L. Chen and Z. Yan, The effect of heat-transfer law on performance of a two-heat-source endoreversible cycle, The Journal of Chemical Physics **90**, 3740 (1989).

[37] Y.-H. Ma, R.-X. Zhai, J. Chen, C. P. Sun, and H. Dong, Experimental test of the $1/\tau$-scaling entropy generation in finite-time thermodynamics, Phys. Rev. Lett. **125**, 210601 (2020).

[38] P. Salamon, A. Nitzan, B. Andresen, and R. S. Berry, Minimum entropy production and the optimization of heat engines, Phys. Rev. A **21**, 2115 (1980).

[39] J. R. Moffitt, Y. R. Chemla, S. B. Smith, and C. Bustamante, Recent advances in optical tweezers, Annu. Rev. Biochem. **77**, 205 (2008).

[40] I. A. Martínez, É. Roldán, L. Dinis, D. Petrov, J. M. Parrondo, and R. A. Rica, Brownian carnot engine, Nature physics **12**, 67 (2016).

[41] V. Blickle and C. Bechinger, Realization of a micrometre-sized stochastic heat engine, Nature Physics **8**, 143 (2012).

[42] U. Seifert, Stochastic thermodynamics, fluctuation theorems and molecular machines, Reports on progress in physics **75**, 126001 (2012).

[43] P. Abiuso, V. Holubec, J. Anders, Z. Ye, F. Cerisola, and M. Perarnau-Llobet, Thermodynamics and optimal protocols of multidimensional quadratic brownian systems, Journal of Physics Communications **6**, 063001 (2022).

[44] W. Chen, F. Sun, S. Cheng, and L. Chen, Study on optimal performance and working temperatures of endoreversible forward and reverse carnot cycles, International journal of energy research **19**, 751 (1995).

[45] V. Holubec and A. Ryabov, Maximum efficiency of low-dissipation heat engines at arbitrary power, Journal of Statistical Mechanics: Theory and Experiment **2016**, 073204 (2016).

[46] Y.-H. Ma, D. Xu, H. Dong, and C.-P. Sun, Universal constraint for efficiency and power of a low-dissipation heat engine, Phys. Rev. E **98**, 042112 (2018).

[47] X.-H. Zhao, Z.-N. Gong, and Z. C. Tu, Low-dissipation engines: Microscopic construction via shortcuts to adiabaticity and isothermality, the optimal relation between power and efficiency, Phys. Rev. E **106**, 064117 (2022).

[48] R. S. Whitney, Most efficient quantum thermoelectric at finite power output, Phys. Rev. Lett. **112**, 130601 (2014).

[49] R. S. Whitney, Finding the quantum thermoelectric with maximal efficiency and minimal entropy production at given power output, Phys. Rev. B **91**, 115425 (2015).

[50] A. Ryabov and V. Holubec, Maximum efficiency of steady-state heat engines at arbitrary power, Phys. Rev. E **93**, 050101 (2016).

[51] R. Long and W. Liu, Efficiency and its bounds of minimally nonlinear irreversible

heat engines at arbitrary power, Phys. Rev. E **94**, 052114 (2016).

[52] C. Blanchard, Coefficient of performance for finite speed heat pump, Journal of Applied Physics **51**, 2471 (1980).

[53] T. Schmiedl and U. Seifert, Optimal finite-time processes in stochastic thermodynamics, Phys. Rev. Lett. **98**, 108301 (2007).

[54] O. Movilla Miangolarra, R. Fu, A. Taghvaei, Y. Chen, and T. T. Georgiou, Underdamped stochastic thermodynamic engines in contact with a heat bath with arbitrary temperature profile, Phys. Rev. E **103**, 062103 (2021).

[55] N. M. Myers, O. Abah, and S. Deffner, Quantum thermodynamic devices: From theoretical proposals to experimental reality, AVS Quantum Science **4**, 027101 (2022).

[56] Y.-Z. Zhen, D. Egloff, K. Modi, and O. Dahlsten, Universal bound on energy cost of bit reset in finite time, Phys. Rev. Lett. **127**, 190602 (2021).

[57] K. Proesmans, J. Ehrich, and J. Bechhoefer, Finite-time landauer principle, Phys. Rev. Lett. **125**, 100602 (2020).

[58] P. R. Zulkowski and M. R. DeWeese, Optimal finite-time erasure of a classical bit, Phys. Rev. E **89**, 052140 (2014).

[59] H. Then and A. Engel, Computing the optimal protocol for finite-time processes in stochastic thermodynamics, Phys. Rev. E **77**, 041105 (2008).

[60] Y. Hu, F. Wu, Y. Ma, J. He, J. Wang, A. C. Hernández, and J. M. M. Roco, Coefficient of performance for a low-dissipation carnot-like refrigerator with nonadiabatic dissipation, Phys. Rev. E **88**, 062115 (2013).

[61] P. Abiuso and M. Perarnau-Llobet, Optimal cycles for low-dissipation heat engines, Phys. Rev. Lett. **124**, 110606 (2020).

[62] J. Guo, H. Yang, H. Zhang, J. Gonzalez-Ayala, J. Roco, A. Medina, and A. C. Hernández, Thermally driven refrigerators: Equivalent low-dissipation three-heat-source model and comparison with experimental and simulated results, Energy Conversion and Management **198**, 111917 (2019).

[63] J. Gonzalez-Ayala, J. Guo, A. Medina, J. M. M. Roco, and A. C. Hernández, Energetic self-optimization induced by stability in low-dissipation heat engines,

Phys. Rev. Lett. **124**, 050603 (2020).

[64] I. Iyyappan and R. S. Johal, Efficiency of a two-stage heat engine at optimal power, Europhysics Letters **128**, 50004 (2020).

[65] P. R. Zulkowski and M. R. DeWeese, Optimal protocols for slowly driven quantum systems, Phys. Rev. E **92**, 032113 (2015).

[66] R. S. Johal, Heat engines at optimal power: Low-dissipation versus endoreversible model, Phys. Rev. E **96**, 012151 (2017).

[67] Y. Zhang and Y. Huang, Applicability of the low-dissipation model: Carnot-like heat engines under newton's law of cooling, Phys. Rev. E **102**, 012151 (2020).

[68] Y. Apertet, H. Ouerdane, A. Michot, C. Goupil, and P. Lecoeur, On the efficiency at maximum cooling power, Europhysics Letters **103**, 40001 (2013).

[69] V. Holubec and A. Ryabov, Efficiency at and near maximum power of low-dissipation heat engines, Phys. Rev. E **92**, 052125 (2015).

[70] R. Long, Z. Liu, and W. Liu, Performance analysis for minimally nonlinear irreversible refrigerators at finite cooling power, Physica A: Statistical Mechanics and its Applications **496**, 137 (2018).

[71] H. S. Leff and W. D. Teeters, Eer, cop, and the second law efficiency for air conditioners, American Journal of Physics **46**, 19 (1978).

[72] C.-Y. Cheng and C.-K. Chen, Performance optimization of an irreversible heat pump, Journal of Physics D: Applied Physics **28**, 2451 (1995).

[73] J. Chen, The maximum power output and maximum efficiency of an irreversible carnot heat engine, Journal of Physics D: Applied Physics **27**, 1144 (1994).

[74] J. Gonzalez-Ayala, A. Medina, J. M. M. Roco, and A. C. Hernández, Entropy generation and unified optimization of carnot-like and low-dissipation refrigerators, Phys. Rev. E **97**, 022139 (2018).

[75] Y. Apertet, H. Ouerdane, O. Glavatskaya, C. Goupil, and P. Lecoeur, Optimal working conditions for thermoelectric generators with realistic thermal coupling, Europhysics Letters **97**, 28001 (2012).

[76] L. Chen, F. Sun, and C. Wu, Influence of internal heat leak on the power versus efficiency characteristics of heat engines, Energy conversion and management **38**,

1501 (1997).

[77] J. Guo, H. Yang, J. Gonzalez-Ayala, J. Roco, A. Medina, and A. C. Hernández, The equivalent low-dissipation combined cycle system and optimal analyses of a class of thermally driven heat pumps, Energy Conversion and Management **220**, 113100 (2020).

[78] P. Abiuso, H. J. Miller, M. Perarnau-Llobet, and M. Scandi, Geometric optimisation of quantum thermodynamic processes, Entropy **22**, 1076 (2020).

[79] R. Strandberg, Theoretical efficiency limits for thermoradiative energy conversion, Journal of Applied Physics **117**, 055105 (2015).

[80] P. Santhanam and S. Fan, Thermal-to-electrical energy conversion by diodes under negative illumination, Phys. Rev. B **93**, 161410 (2016).

[81] J. Gonzalez-Ayala, J. Guo, A. Medina, J. M. M. Roco, and A. Calvo Hernández, Optimization induced by stability and the role of limited control near a steady state, Phys. Rev. E **100**, 062128 (2019).

[82] J. Gonzalez-Ayala, M. Santillán, I. Reyes-Ramírez, and A. Calvo-Hernández, Link between optimization and local stability of a low-dissipation heat engine: Dynamic and energetic behaviors, Phys. Rev. E **98**, 032142 (2018).

[83] Y. Izumida and K. Okuda, Work output and efficiency at maximum power of linear irreversible heat engines operating with a finite-sized heat source, Phys. Rev. Lett. **112**, 180603 (2014).

[84] M. J. Ondrechen, M. H. Rubin, and Y. B. Band, The generalized carnot cycle: A working fluid operating in finite time between finite heat sources and sinks, The Journal of Chemical Physics **78**, 4721 (1983).

[85] J. Chen and Z. Yan, Unified description of endoreversible cycles, Phys. Rev. A **39**, 4140 (1989).

[86] Y. Wang, Optimization in finite-reservoir finite-time thermodynamics, Phys. Rev. E **90**, 062140 (2014).

[87] Y. Wang, Optimizing work output for finite-sized heat reservoirs: Beyond linear response, Phys. Rev. E **93**, 012120 (2016).

[88] H. Yuan, Y.-H. Ma, and C. P. Sun, Optimizing thermodynamic cycles with two

finite-sized reservoirs, Phys. Rev. E **105**, L022101 (2022).

[89] Y.-H. Ma, Effect of finite-size heat source's heat capacity on the efficiency of heat engine, Entropy **22**, 1002 (2020).

[90] A. Einstein, Über die von der molekularkinetischen theorie der wärme geforderte bewegung von in ruhenden flüssigkeiten suspendierten teilchen, Annalen der physik **4** (1905).

[91] V. Holubec, An exactly solvable model of a stochastic heat engine: optimization of power, power fluctuations and efficiency, Journal of Statistical Mechanics: Theory and Experiment **2014**, P05022 (2014).

[92] A. Gomez-Marin, T. Schmiedl, and U. Seifert, Optimal protocols for minimal work processes in underdamped stochastic thermodynamics, The Journal of chemical physics **129**, 024114 (2008).

[93] A. Zhong and M. R. DeWeese, Limited-control optimal protocols arbitrarily far from equilibrium, Phys. Rev. E **106**, 044135 (2022).

[94] V. Holubec and A. Ryabov, Fluctuations in heat engines, Journal of Physics A: Mathematical and Theoretical **55**, 013001 (2021).

[95] E. Geva and R. Kosloff, A quantum-mechanical heat engine operating in finite time. a model consisting of spin-1/2 systems as the working fluid, The Journal of chemical physics **96**, 3054 (1992).

[96] H. Risken and H. Risken, *Fokker-planck equation* (Springer, 1996).

[97] C. Lin, B. Wang, K. H. Teo, and Z. Zhang, Performance comparison between photovoltaic and thermoradiative devices, Journal of Applied Physics **122**, 243103 (2017).

[98] D. Fan, T. Burger, S. McSherry, B. Lee, A. Lenert, and S. R. Forrest, Near-perfect photon utilization in an air-bridge thermophotovoltaic cell, Nature **586**, 237 (2020).

[99] T. J. Coutts, An overview of thermophotovoltaic generation of electricity, Solar energy materials and solar cells **66**, 443 (2001).

[100] C. Zhang, Z. Liao, L. Tang, Z. Liu, R. Huo, Z. Wang, and K. Qiu, A comparatively experimental study on the temperature-dependent performance of thermophoto-

voltaic cells, Applied Physics Letters **114**, 193902 (2019).

[101] Z. Ye, X. Zhang, W. Li, G. Su, and J. Chen, Optimum operation states and parametric selection criteria of a high temperature fuel cell-thermoradiative cell system, Energy conversion and management **173**, 470 (2018).

[102] A. Luque and A. Martí, Increasing the efficiency of ideal solar cells by photon induced transitions at intermediate levels, Phys. Rev. Lett. **78**, 5014 (1997).

[103] Z. Ye, W. Peng, S. Su, and J. Chen, Intermediate band thermoradiative cells, IEEE Transactions on Electron Devices **65**, 5428 (2018).

Curriculum Vitae

First name: Zhuolin   Surname: Ye

Gender: male   Date of birth: June 29, 1994

Nationality: Chinese   Email: zhuolinye@foxmail.com

Education

2012.09-2016.07	Nanchang University	Undergraduate
	Major: Optical Information Science and Technology	
	Thesis: A Universal Expression for the Efficiency of an Irreversible Heat Engine	
	Supervisor: Prof. Dr. Jianhui Wang	
2016.09-2019.07	Xiamen University	Master
	Major: Condensed Matter Physics	
	Thesis: Investigation on the Performance Characteristics of Thermoradiative Cells and Their Coupling Systems (**Excellent Master Thesis** of Fujian Province 2019)	
	Supervisor: Prof. Dr. Jincan Chen	
2016.12-present	University of Leipzig	PhD
	Major: Condensed matter theory	
	Thesis: Optimization of thermodynamic systems	
	Supervisor: Prof. Dr. Klaus Kroy & Dr. Viktor Holubec	

Awards

The Third Prize of **BuildMoNa-Awards** 2023

Chinese Government Scholarship for Postgraduates 2019

Academic experience

- Oral report "*Optimal finite-time heat engines under constrained control*" in 15th BuildMoNa Annual Conference 2023.

- Oral report "*Maximum efficiency of low-dissipation refrigerators at arbitrary cooling power*" in 14th BuildMoNa Annual Conference 2022.

- Reviewer for **Physical Review Letters**, **New Journal of Physics**, **Energy Conversion and Management**, Journal of Physics Communications, Entropy, ChemEngineering, Molecules, and Energies.

- International collaboration with scientists from University of Oxford, University of Exeter, and University of Geneva [9, 43].

List of Publications

1. **Z. Ye***, F. Cerisola, P. Abiuso, J. Anders, M. Perarnau-Llobet, and V. Holubec*, Optimal finite-time heat engines under constrained control, Physical Review Research 4, 043130 (2022) [9].

2. **Z. Ye*** and V. Holubec*, Maximum efficiency of low-dissipation heat pumps at given heating load, Physical Review E 105, 024139 (2022) [7].

3. **Z. Ye*** and V. Holubec*, Maximum efficiency of absorption refrigerators at arbitrary cooling power, Physical Review E 103, 052125 (2021) [6].

4. V. Holubec* and **Z. Ye***, Maximum efficiency of low-dissipation refrigerators at arbitrary cooling power, Physical Review E 101, 052124 (2020) [5].

5. P. Abiuso*, V. Holubec, J. Anders, **Z. Ye**, F. Cerisola, and M. Perarnau-Llobet, Thermodynamics and optimal protocols of multidimensional quadratic Brownian systems, Journal of Physics Communications 6, 063001 (2022) [43].

6. Y. Hu, V. Holubec, J. Chen, B. Liu, J. Liu, Q. Wu, and **Z. Ye***, Conversion of low-grade heat from molten carbonate fuel cells to electricity by thermoradiative devices with optimized transport properties (Submitted to *Energy Conversion and Management*).

7. Y. Hu, V. Holubec, B. Liu, J. Liu, Q. Wu, and **Z. Ye***, Solar-powered thermoradiative devices with modeled transport properties (Finished writing).

8. **Z. Ye*** and V. Holubec*, Optimal trade-off between power and efficiency for leaky low-dissipation heat devices (Writing).

Author contributions

This thesis compiles the publications [5–7, 9, 43] I coauthored during my doctoral studies at University of Leipzig. Among them, [5–7] are completed only under the guidance of my supervisor Dr. Viktor Holubec, while [9, 43] additionally originate from the international collaboration with scientists from University of Oxford, University of Exeter, and University of Geneva.

In [5], I learned about the derivation of maximum efficiency at given power for the first time. After long discussions with Viktor, I derived the efficiency at maximum power and maximum efficiency at given power for low-dissipation refrigerators. Taking advice from Viktor, I defined a reasonable function measuring the validity of the approximations of the maximum efficiency at fixed power. I also performed a comparative analysis of low-dissipation refrigerators and minimally nonlinear irreversible refrigerators, showing that these two kinds of models indeed agree under the tight-coupling condition. In [6], I learned from Viktor that the maximum efficiency at given power for simultaneous absorption refrigerators follow from those for the internal devices. Then I specially derived the maximum efficiency at given power for simultaneous absorption refrigerators when the internal devices are low dissipation, and evaluated under which parameter regimes the system is more beneficial to operate close to maximum power than at maximum power. I also contributed to the explanation on why the knowledge of maximum efficiency at given power of the internal engine and refrigerator is not sufficient for the derivation of maximum efficiency at given power for alternating absorption refrigerators. All numerical simulations are completed by me. During this work [6], I had enlightening discussions with Prof. Dr. Jincan Chen regarding three-heat-source refrigeration cycles. The idea of [7] was proposed by me, and I found that the maximum-power regime of low-dissipation heat pumps is highly undesirable. I analytically derived the maximum efficiency at given power for low-dissipation heat pumps, and identified a parameter regime when the performances of low-dissipation heat pumps and endoreversible heat pumps agree. Later this parameter regime was refined by Viktor using a fairer comparative analysis. All

numerical simulations are completed by me.

During the international collaboration on [9], I actively participated in regular weekly meetings, where I reported my progress. My contributions included the derivation of efficiency at maximum power induced by the maximum-efficiency piecewise constant protocol and of the optimal protocol applicable near equilibrium, as well as conducting all numerical simulations. As for the international collaboration on [43], I played a supportive role, actively providing feedback in the weekly meetings and checking the validity of the analytical results.

Acknowledgments

It is incredible how fast time has gone by. It feels like I blinked and suddenly found myself at the end of my academic journey, ready to graduate. In the past four years, I embarked on a journey abroad that has been filled with countless new experiences, and I am filled with curiosity and gratitude.

First and foremost, I am immensely grateful to my two supervisors, Prof. Dr. Klaus Kroy and Dr. Viktor Holubec, for their invaluable guidance and support throughout my doctoral journey. Klaus provided me with a good research environment, answered many of my questions, and belongs to a member of my Thesis Advisory Committee. Viktor not only has important guidance to me academically, but also tries his best to help me in life. When I first arrived in Germany, he drove me to buy daily necessities and gave me a quilt. Afterwards, he treated me to the first meal, gave me the router and helped me debug it. I was very moved at that time. Furthermore, despite being very busy, he always patiently answers my questions. I love my time with Klaus and Viktor. I sincerely hope to have the opportunity to listen to their guidance again in the future.

Then I would like to thank another two members of my Thesis Advisory Committee, Prof. Dr. Jürgen Vollmer and Prof. Dr. Frank Cichos, for listening to my imperfect reports and giving valuable suggestions in their busy schedule. I acknowledge Martí Perarnau-Llobet, Janet Anders, Paolo Abiuso, and Federico Cerisola for the cooperation with them on the topic of designing optimal protocols in finite-time thermodynamics. I sincerely thank my colleagues, in particular, Sven Auschra, Pin-Chuan Chen, Xiaoya Su, and Daniel Geiss, for the help they provide me in study and life. Morever, Sven was the one who picked me up from Leipzig airport when I first came to Germany. I thank my friends Weihao Zhou and Yong Yan as well as the President of the Leipzig Student Union, Zhiyuan Luo, for providing me friendly and interesting conditions during my life. I also feel obliged to thank my two supervisors at the undergraduate and master stages, Prof. Dr. Jianhui Wang and Prof. Dr. Jincan Chen, as well as my brother Zhimin Yang in studies, for their help in my application for the National Youth Fund.

I want to say thank you and sorry to Yingying Hu for engaging in a four-year long-distance relationship with me. The bittersweet moments and challenges within this experience are known only to ourselves. At the same time, I also want to say thanks and sorry to my family. They raised me and provided unconditional support, but I was not physically present with them throughout the year, and I pursued my studies until almost reaching the age of thirty, without contributing any income to the family. I still find it hard to comprehend that my beloved mother passed away the year I went abroad, and I often sense her presence by my side, accompanying me. I regret my past immaturity that frequently caused her frustration. Today, have I become the person you hoped I would be?